Reactions with Gallium Methylene

DISSERTATION

der Mathematisch-Naturwissenschaftlichen Fakultät

der Eberhard Karls Universität Tübingen

zur Erlangung des Grades eines

Doktors der Naturwissenschaften

(Dr. rer. nat.)

vorgelegt von

M. Sc. Georgios Spiridopoulos

aus Reutlingen

Tübingen

2022

Gedruckt mit Genehmigung der Mathematisch-Naturwissenschaftlichen Fakultät der Eberhard Karls Universität Tübingen.

Tag der mündlichen Qualifikation: 16.12.2022

Dekan: Prof. Dr. Thilo Stehle

1. Berichterstatter: Prof. Dr. Reiner Anwander

2. Berichterstatter: Prof. Dr. Doris Kunz

Reactions with Gallium Methylene

Georgios Spiridopoulos
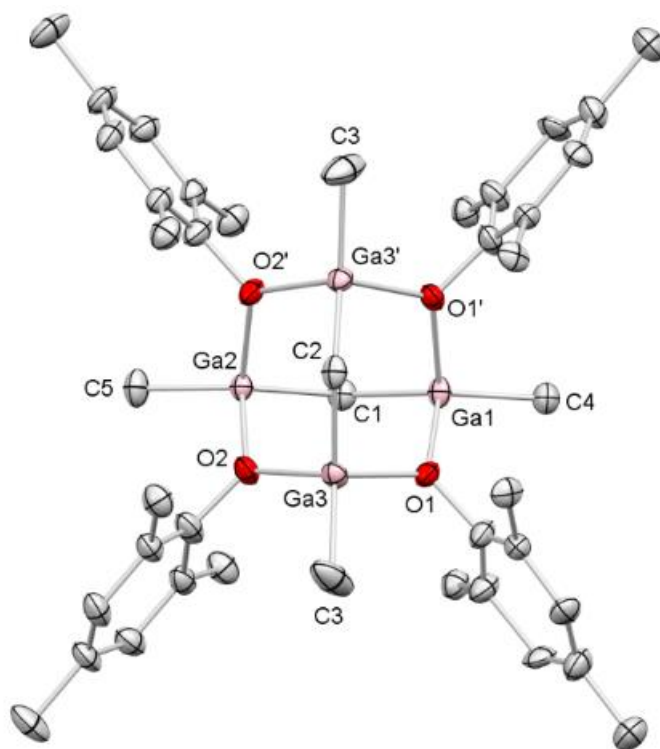
Preface

The following PhD thesis consists of the reactivity of main group methylidene complexes towards different alcohols, primary amines, thiophenols and donor molecules, a summary of the main results, the original scientific papers and unpublished results. This work has been carried out in Tübingen at the Institut für Anorganische Chemie of the Eberhard Karls Universität Tübingen in Germany over the period from February 2019 to January 2022 under the supervision of Prof. Dr. Reiner Anwander. The research has been funded by the Deutsche Forschungsgemeinschaft (DFG).

Acknowledgements

stand. Hervorheben möchte ich auch noch meine Freundin **Yvonne Scharf**, welche mich insbesondere während der Promotionszeit unterstützte und mir den Rücken freihielt.

Contents

Abbreviations

do	donor
DRIFT	Diffuse Reflectance Infrared Fourier Transform
EA	Elemental Analysis
e.g.	exempli gratia
Et	Ethyl
et. al	*et alii* or *et aliae*
HMBC	Heteronuclear Multiple Bond Correlation
HSQC	Heteronuclear Single Quantum Coherence
IR	Infrared
NMR	Nuclear Magnetic Resonance
Py	Pyridin
rt	Ambient temperature
SBA	Santa Barbara Amorphous
TMA	Trimethylaluminum
TMEDA	Tetramethylenediamine
TMG	Trimethylgallium
THF	Tetrahydrofuran

Summary

Reports of main-group methylene complexes are severely limited in the literature. In earlier studies, the $[Mg(CH)_2]_n$ and $[Li_2CH_2]_n$ was synthesized by Karl Ziegler in 1955. It took another 64 years until Martin Bonath succeeded in synthesizing and characterizing a homoleptic gallium methylene in 2019.

The focus of this work is the synthesis and characterization of new main-group metal methylene compounds as well as the derivatization of $[Ga_8(CH_2)_{12}]$. In transition-metal methylene chemistry as well as in rare-earth metal methylene chemistry, a large number of synthesis protocols already exist for the preparation of further metal methylene derivatives. First, analogous to the synthesis of $[Ga_8(CH_2)_{12}]$, the corresponding rare-earth metallocene precursor $[Cp^*_2Lu(AlMe_4)]$ was used to synthesize an aluminum methyl methylene. From this, a mixed metal methylene cluster with the molecular formula $[Cp^*_4Lu_2Al_{10}(\mu\text{-}CH_2)_{12}(CH_3)_8]$ was obtained. Subsequently, the Lewis acid $AlMe_3$ was added to both, $[Ga_8(CH_2)_{12}]$ and the Tebbe reagent $[Cp_2Ti(CH_2)(Cl)Al(CH_3)_2]$. The individual reactions led to the successful synthesis of methylaluminomethylene with the molecular formula $[(CH_3)Al(CH_2)]_{12}$. More in-depth NMR spectroscopic studies revealed the decomposition of the Al_{12} cluster into smaller fragments with coordinated solvent and bridging methylene units. In further reactivity reactions, the methylene unit was successfully transferred to ketones like benzophenone.

Inspired by the successful reaction of gallium methylene $[Ga_8(CH_2)_{12}]$ with $AlMe_3$ to methylaluminomethylene, gallium methylene was further reacted with various substituted phenols, anilines and thiophenols in a protonolysis reaction. The complexes obtained followed the general structural motif $[Ga_4(\mu_2\text{-}CH_2)_2(CH_3)_4(\mu_2\text{-}XAr)_4]$ with bridging methylene units. By means of incomplete protonolysis reaction due to the increasing steric demand of phenols, a pentametallic gallium methylene aryloxide complex with the molecular formula $[Ga_5(\mu_2\text{-}CH_2)_6(OC_6H_4tBu2\text{-}2,6)_3]$ was formed.

The successful protonolysis of $[Ga_8(CH_2)_{12}]$ and the extensive studies on $GaMe_3$ on various mesoporous silicate support materials led to the assumption that the $[Ga_8(CH_2)_{12}]$ is a suitable substrate for grafting reactions. The reaction of gallium methylene with mesoporous materials SBA-15$_{500}$ (large pores) and MCM-41$_{500}$ (small pores) resulted in various hybrid materials with high metal content. The hybrid materials obtained exhibited dimeric structures on the surface and formed intact bridging methylene units. Further, the hybrid materials could be successfully used as methylene transfer reagents using benzophenone.

Zusammenfassung

Berichte über Hauptgruppenmethylen Komplexe sind in der Literatur stark limitiert. In früheren Studien wurde das $[Mg(CH)_2]$ und $[Li_2CH_2]_n$ von Karl Ziegler im Jahr 1955 synthetisiert. Erst nach weiteren 64 Jahren gelang es Martin Bonath im Jahr 2019 ein homoleptisches Gallium Methylene zu synthetisieren und charakterisieren.

Der Fokus dieser Arbeit liegt in der Synthese und Charakterisierung neuer Hauptgruppenmetallmethylen-Verbindungen sowie der Derivatisierung des $[Ga_8(CH_2)_{12}]$. In der Nebengruppenmetallmethylen-Chemie als auch in der Seltenerdmetallmethylen-Chemie existiert bereits eine Vielzahl an Syntheseprotokollen für die Darstellung weiterer Metall-Methylen-Derivate. Zunächst wurde analog zur Synthese von $[Ga_8(CH_2)_{12}]$ der entsprechende Seltenerdmetallocen-Vorläufer $[Cp^*_2Lu(AlMe_4)]$ zur Synthese eines Aluminium-Methyl-Methylens herangezogen. Daraus konnte ein gemischter Metall-Methylene-Cluster mit der Summenformel $[Cp^*_4Lu_2Al_{10}(\mu\text{-}CH_2)_{12}(CH_3)_8]$ erhalten werden. Nachfolgend wurde sowohl dem $[Ga_8(CH_2)_{12}]$ als auch dem Tebbe-Reagenz $[Cp_2Ti(CH_2)(Cl)Al(CH_3)_2]$ die Lewis-Säure $AlMe_3$ zugesetzt. Die einzelnen Reaktionen führten zur erfolgreichen Synthese des Aluminium-Methyl-Methylen mit der Summenformel $[Al_{12}(CH_2)_{12}(CH_3)_{12}]$. Tiefgreifendere NMR-spektroskopische Untersuchungen zeigten die Zerlegung des Al_{12}-Clusters in kleinere Fragmente mit koordiniertem Lösemittel und verbrückenden Methyleneinheiten. In weiterführenden Reaktivitätsreaktionen konnte die Methyleneinheit erfolgreich auf Ketone übertragen werden.

Inspiriert durch die erfolgreiche Umsetzung des Galliummethylens $[Ga_8(CH_2)_{12}]$ mit $AlMe_3$ wurde dieses mit verschiedenen substituierten Phenolen, Anilinen und Thiophenolen in einer Protonolyse umgesetzt. Die erhaltenen Komplexe folgten dem allgemeinen Strukturmotiv $[Ga_4(\mu_2\text{-}CH_2)_2(CH_3)_4(\mu_2\text{-}XAr)_4]$ mit verbückenden Methyleneinheiten. Mittels unvollständiger Protonolyse aufgrund des zunehmenden sterischen Anspruchs der Phenole, bildete sich ein fünfkerner Galliummethylenaryloxid-Komplex mit der Summenformel $[Ga_5(\mu_2\text{-}CH_2)_6(OC_6H_4tBu_2\text{-}2,6)_3]$.

Die erfolgreiche Protonolyse des $[Ga_8(CH_2)_{12}]$ und die umfangreichen Studien zu $GaMe_3$ auf verschiedenen mesoporösen Silikat-Trägermaterialien führten zur Annahme, dass das $[Ga_8(CH_2)_{12}]$ hierfür ein geeignetes Substrat darstellt. Die Umsetzung von Galliummethylen mit mesoporösen Materialien SBA-15$_{500}$ (große Poren) und MCM-41$_{500}$ (kleine Poren) ergab verschiedene Hybridmaterialien mit hohem Metallgehalt. Die erhaltenen Hybridmaterialien zeigten dimere Strukturen an der Oberfläche und bilden intakte verbrückende Methyleneinheiten. Weiter konnten die Hybridmaterialien erfolgreich als Methylen-Transferreagenzien am Beispiel von Benzophenon eingesetzt werden.

Publications

Publications incorporated into this thesis

Paper I $[(CH_3)Al(CH_2)]_{12}$: Methylaluminomethylene (MAM-12)

G. Spiridopoulos, M. Kramer, F. Kracht, C. Maichle-Mössmer, R. Anwander

Chem. Eur. J. **2022**, 28, e202200823

DOI : **https://doi.org/10.1002/chem.202200823**

Paper II   Gallium Methylene in the Pocket

G. Spiridopoulos, M. Bonath, C. Maichle-Mössmer , R. Anwander

Organometallics, **2022**, 41, 2854-2861

DOI : **https://doi.org/10.1021/acs.organomet.2c00391**

Manuscript   Homoleptic $Ga_8(CH_2)_{12}$ and $GaMe_3$ grafting onto Mesoporous Silica MCM-41_{500} and SBA.15_{500}

G. Spiridopoulos, Y. Liang, R. Anwander

Publications with minor contributions

Paper IV   C-H Bond Activation and Isoprene Polymerization Studies Applying Pentamethylcyclopentadienyl-Supported Rare-Earth-Metal Bis(Tetramethylaluminate) and Dimethyl Complexes

C. O. Hollfelder, M. Zimmermann-Meermann, G. Spiridopoulos, D. Werner, K. W. Törnroos, C. Maichle-Mössmer, R. Anwander

Molecules **2019**, *24*, 3703

DOI: 10.3390/molecules24203703

Poster presentations

Poster I   Gallium Methylene in the Pocket

G. Spiridopoulos, C. Maichle-Mössmer, R. Anwander

Anwander Group, *Poster Session*, Tübingen, Germany, *October 4-6*, **2021**.

Poster II   C–H Bond Activation by Rare-Earth-Metallocene Alkylaluminates

G. Spiridopoulos, M. Bonath, C. Maichle-Mössmer, R. Anwander

XXX Tage der Seltenen Erden – Terrae Rarae , Montpellier, France, *September 22-24*, **2021**.

Personal Contribution

Paper I: $[CH_3)Al(CH_2)]_{12}$: Methylaluminomethylene (MAM-12)

All reactions and analyses described were planned and conducted by myself. Analyses include one-dimensional (^1H, $^{13}C\{^1H\}$) NMR spectroscopy and DRIFT spectroscopy. DOSY experiments were performed with the support of Dr. Markus Kramer. Manuscript writing was also done by me.

Elemental analyses were performed by Wolfgang Bock. X-ray diffraction were performed by Dr. Cäcilia Maichle-Mössmer.

Paper II: Galliummethylene in the Pocket

All reactions and analyses described were planned and conducted by myself. Analyses include one-dimensional (^1H, $^{13}C\{^1H\}$) NMR spectroscopic methods, and DRIFT spectroscopy. Manuscript writing was also done by myself.

Elemental analyses were performed by Wolfgang Bock. Single crystal X-ray diffraction were performed by Dr. Cäcilia Maichle-Mössmer.

Manuscript: Homoleptic $Ga_8(CH_2)_{12}$ and $GaMe_3$ grafting onto Mesoporous Silica MCM-41_{500} and SBA-15_{500}

All reactions and analyses described were planned and conducted by myself (except synthesis of SBA-15_{500} and MCM-41_{500} were performed by Dr. Yucang Liang). Analyses include physisorption, one-dimensional (^1H) NMR spectroscopic methods and DRIFT. Manuscript writing was also done by me. The ^{13}C-CP MAS measurements were done by Dr. Klaus Eichele.

Elemental analyses were performed by Wolfgang Bock, Single crystal X-ray diffraction were performed by Dr. Cäcilia Maichle-Mössmer

Paper IV: C-H Bond Activation and Isoprene Polymerization Studies Applying Pentamethylcyclopentadienyl-Supported Rare-Earth-Metal Bis(Tetramethylaluminate) and Dimethyl Complexes

In this publication, two reactions were conducted by myself.

Objective of this Thesis

The main emphasis of this thesis is to study the reactivity of the homoleptic $[Ga_8(CH_2)_{12}]$ complex toward different Brønsted acidic compounds like alcohols, primary amines, thiophenols, donors and the synthesis of other main group methylidenes.

Chapter A gives an historical overview of the synthesis and reactivity of different transition and main group metal methylenes.

Chapter B contains a summary of the main results of this thesis and is divided into two parts:

- Aluminomethylene
- Reactivity of Gallium Methylene

In **Chapter C** unpublished results, which are not part of a publication or manuscript, are presented. This contains further reactivity of $[Ga_8(CH_2)_{12}]$ and alternative approaches to gallium methylene.

Chapter E is a compilation of publications.

A

Metal-Methylene

Chemistry

Historical Overview of Metal Alkylidenes

First reports of synthesized carbenes date back to 1915 when TSCHUGAJEFF and SHANAWY-GRIGORJEWA synthesized the first platinum carbene without knowing the structure.[1] The structural elucidation of this compound has remained elusive until the 1970s. The group of ENEMARK was able to elucidate the exact molecular structure of **1** (Figure 1) and correct is with the findings from 1915.[2]

1

Figure 1. First Pt carbene species.[1-2]

Many years after this unrecognized seminal discovery, ZIEGLER reported on the synthesis of s block methylidenes [Li$_2$CH$_2$]$_n$ (**2**) and [MgCH$_2$]$_n$ (**3**) (Scheme 1). The resulting brown pyrophoric powders are presumably polymeric.[3]

Scheme 1. Synthesis of pyrophoric [Li$_2$(CH$_2$)]$_n$ (**2**) and [MgCH$_2$]$_n$ (**3**)

Interestingly, Ziegler's work received little attention despite the patenting and the use in industrial applications, for example, the reactivity towards dihalogenido alkyls.[4] Several years later, after renewed interest and new findings from LAGOW and KAWA in the polymeric

compounds **2** and **3**,[5-7] STUCKY succeeded in determining the solid-state structure of the deuterated compound $[Li_2CD_2]_n$.[8] Two years after the groundbreaking discovery of the Fischer carbenes by Nobel prize winner E. O. FISCHER,[9] LEHMKUHL and SCHÄFER reported on the isolation and characterization of methylene bis(aluminum dichloride) (**4**) (Scheme 2) in yields of 40%.[10]
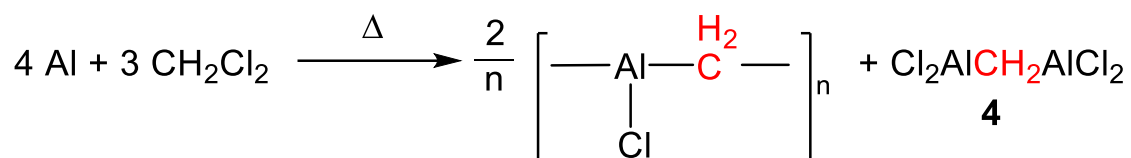
Scheme 2. Synthesis of methylene bis(aluminium dichloride) **4**.

Unfortunately, the X-ray structure of compound **4** has not yet been determined. Analogous to compound **4**, the presumably isostructural compound $[Br_2AlCH_2AlBr_2]$ (**5**) with bromine instead of chlorine was obtained by the group of MOTTUS by an electrochemical-chemical method.[11] The interest in an aluminum methylene was considerably high. In addition to the pyrolysis of $LiCH_3$ and $Mg(CH_3)_2$ ZIEGLER also attempted the pyrolysis of $Al(CH_3)_3$ (TMA), but the isolation of putative aluminum methylene remained elusive. In 1968, SINN succeeded in synthesizing a poly(aluminum-methyl-methylene) (**6**) starting from Cp_2TiCl_2 with an 100-fold excess of $Al(CH_3)_3$ (Scheme 3)[12]
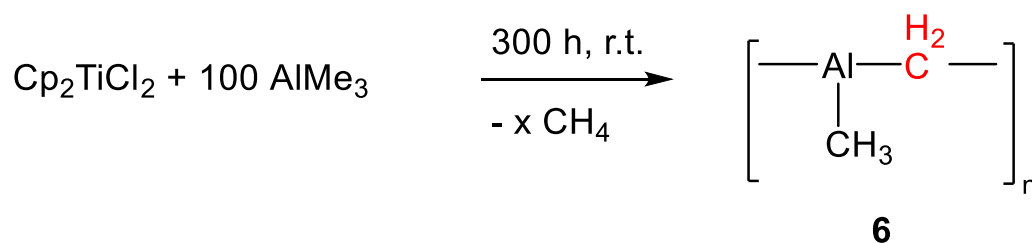
Scheme 3. Synthesis of polymeric methyl-methylene-aluminium **6**.

It is remarkable that the putative intermediate is most likely the TEBBE reagent, which was published and elucidated in 1978.[13] In 1974, SCHROCK reported on the first synthesis of an high oxidation state (in this case d^0) metal-alkylidene complex by α-hydrogen abstraction to produce $[(Me_3CCH_2)_3Ta=CHCMe_3]$ (**7**) (Scheme 4, approach I).[14] With this discovery (ten years after the groundbreaking development of the FISCHER carbenes) and the subsequent definition of the SCHROCK alkylidene chemistry, Richard Schrock received the Nobel Prize (for the superior findings in metathesis reactions) in 2005. This intramolecular α-hydrogen

abstraction has since been used to prepare many different Ta (and Nb) neopentylidene and benzylidene complexes.[15-18] Further studies of SCHROCK on the stabilization of Ta methyl complexes by sterically more demanding ligands like cyclopentadienyl (Cp = C_5H_5) finally yielded a "tantalum ylide" $[Cp_2Ta(CH_2)(CH_3)]$ (**9**) (Scheme 4, approach II).[19]
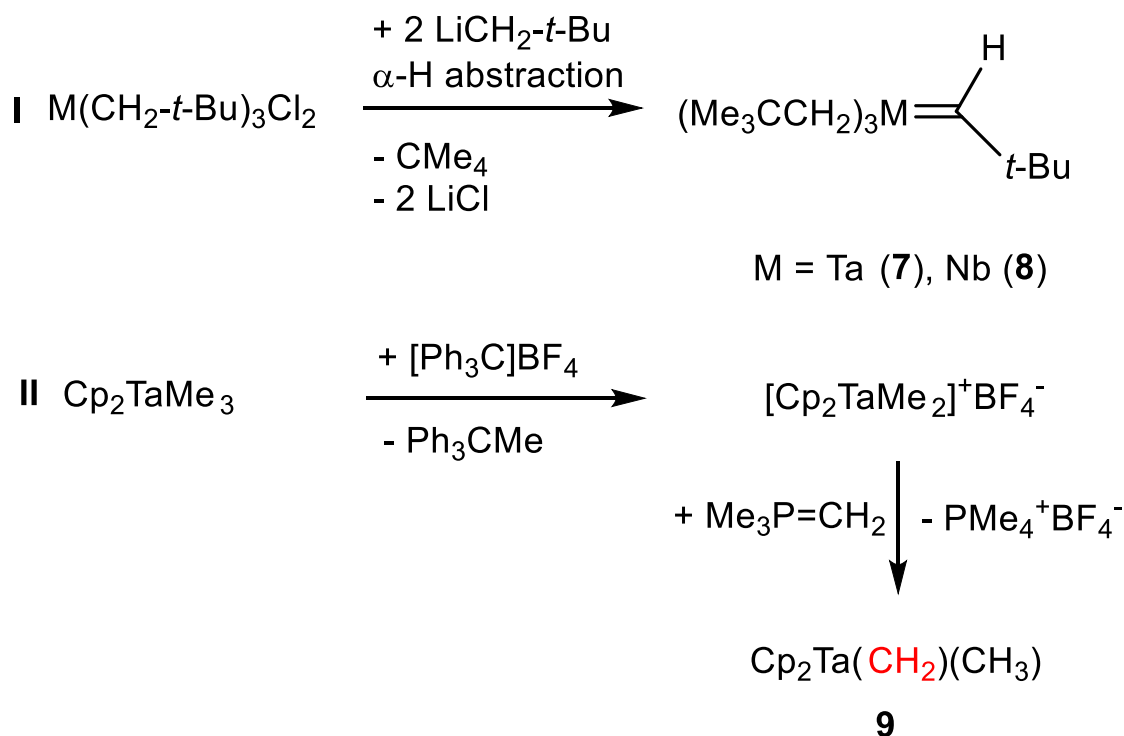
Scheme 4. Different synthesis approaches to metal alkylidenes.[19]

The methylidene complex **9** was isolated and characterized. In the same year 1975, HERRMANN also succeeded in synthesizing a dinuclear manganese complex with a bridging methylene unit and marked also a milestone in the field of transition-metal methylene chemistry.[20]
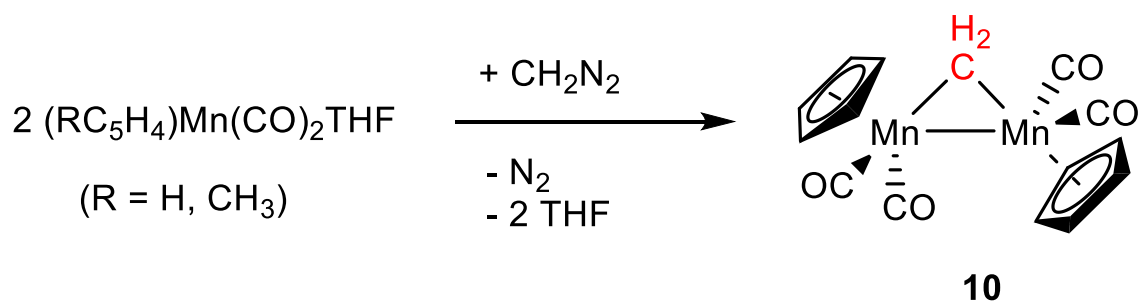
Scheme 5. Synthesis of Herrmann's bridging methylene manganese complex **10**.[20]

Over the years, the library of Schrock methylene complexes has grown tremendously. Here, this type of complexes has spread over the transition metals to afford Ti^{IV}, Zr^{IV}, Hf^{IV}, V^V, Nb^V,

Ta^V, Cr^{VI}, Mo^{VI}, W^{VI}, Re^{VII} and Mn^{II} alkylidene complexes (for example $[(\eta^5\text{-}C_5H_4R)_2Ti(CHCMe_3)(PMe_3)]$ (R = H, Me)).[21-25] Apart from the α-hydrogen abstraction, di- and polyalkyls of early transition metals that are not in the highest oxidation state typically d^1 metals (Ti^{III}, Zr^{III}, V^{IV} and Nb^{IV}), can be oxidized to alkylidene complexes by Ag^I salts or I_2.[26] The TEBBE reagent is a well established SCHROCK type methylene with applications on the laboratory scale and in the chemical industry. BRESLOW, NEWBURG and NATTA noted that the reaction of titanocenes with organoaluminum promote the homogenous polymerization of ethylene whereby bimetallic Cp₂Ti/Al based complexes are the catalytic active species here[27-28] It was not until the characterization of such titanocene hydride complexes and the investigations of KAMINSKY in 1975[29] that TEBBE was able to synthesize and characterize the archetypal TEBBE reagent $[Cp_2Ti(\mu_2\text{–}CH_2)(\mu_2\text{–}Cl)Al(CH_3)_2]$ (**11**) in the year 1978 with the simple and straightforward reaction of $[Cp_2TiCl_2]$ and two equivalents of $AlMe_3$. TEBBE's reagent can also be synthesized by means of $[Cp_2Ti(CH_3)_2]$ and one equivalent of $Al(CH_3)_2Cl$ (Scheme 6)).[13]
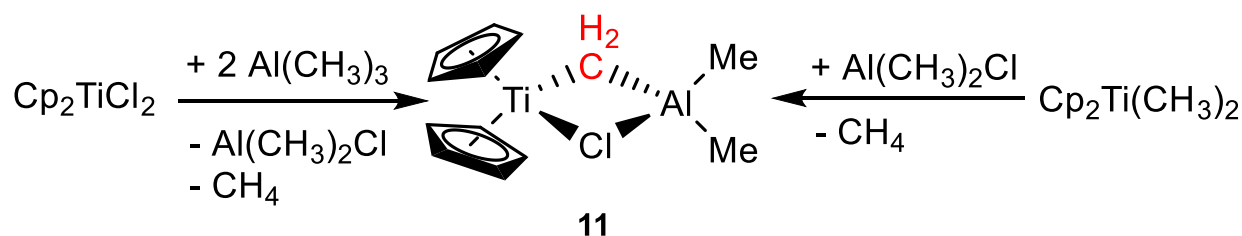
Scheme 6. Synthesis pathway of Tebbe's reagent **11**.[13]

The incredible range of alkylidene complexes is described further in this section. Various theoretical calculations and matrix isolations studies proved that the principles or the orbital theories on the bonding situation of transition-metal methylenes cannot be adopted to the s-block metals or in general the main-group metals.[30-31] In the late 1970s, methylene chemistry also expanded into rare-earth metals which was slightly surprising. As mentioned earlier, the bonding situation of transition-metals also cannot be transferred to rare-earth metals. (rare-earth metals cannot stabilize a carbonic unit (CR_2^{2-}) by back donation and have predominantly ionic bonds). Because most of the lanthanides are in the +III oxidation state (Ln^{III}), an orbital mismatch of the f-element metal center and the carbon atom of the methylene occurs. The resulting bonding of the metal center to the methylene unit is mainly defined by electrostatic and steric factors.[32-34]

Despite the theoretical calculations, SCHUMANN reported in the late 1970s on the synthesis of the first lutetium and erbium alkylidenes *via* a silane elimination $[Li(do)_x][Ln(CH_2SiMe_3)_2(CHSiMe_3)]_n$ (**12**) (do = donor, Ln = rare-earth metal). Unfortunately, an X-ray structure does not exist. The proposed structure was confirmed by spectroscopic methods and elemental analysis.[35] Despite the great efforts, it took about 30 years until CAVELL succeded in the year 2000 to fully characterize the first rare-earth metal alkylidene with a pincer-like structure (Scheme 7, **13**).[36] At this point it should be noted that in the further elaboration pincer-type alkylidenes will not be discussed further.
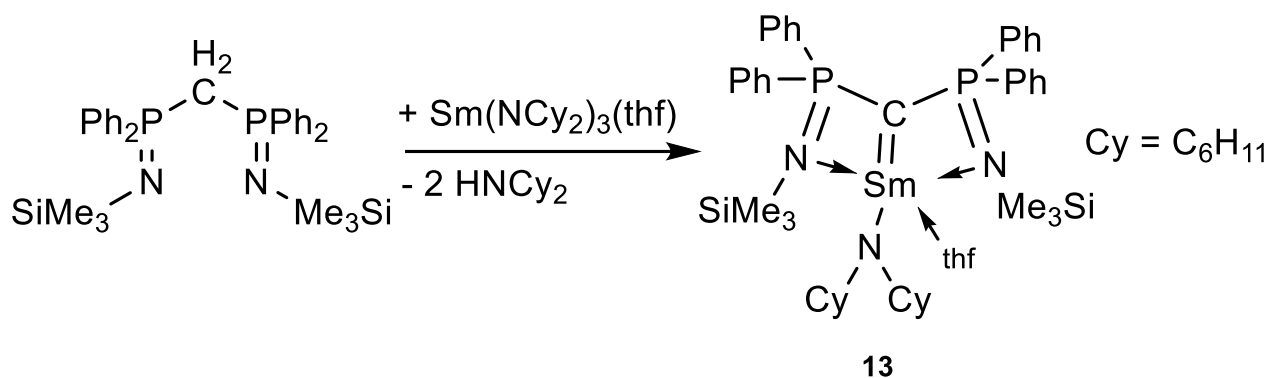
Scheme 7. Synthesis of first rare-earth alkylidene complex **13**.

Based on this discovery, the interest of such rare-earth metal alkylidene has further increased. Many different molecules containing Sm and Tm were synthesized.[37-38] It should be noted, that in 2006 our group successfully synthesized and structurally characterized a trimetallic rare-earth metal methylene complex $[Cp*_3Ln_3(\mu-Cl)_3(\mu_3-Cl)(\mu_3-CH_2)(thf)_3]$ (**14**) (Ln = Y, La) by reacting Cp-stabilized heterobimetallic $[Cp*Ln(AlMe_4)_xCl_y]_z$ (Ln = Y: z = 2, y = x; Ln = La: z = 6, y = 2x) precursor with thf as a donor to induce the C–H-bond activation (Scheme 8).[39]
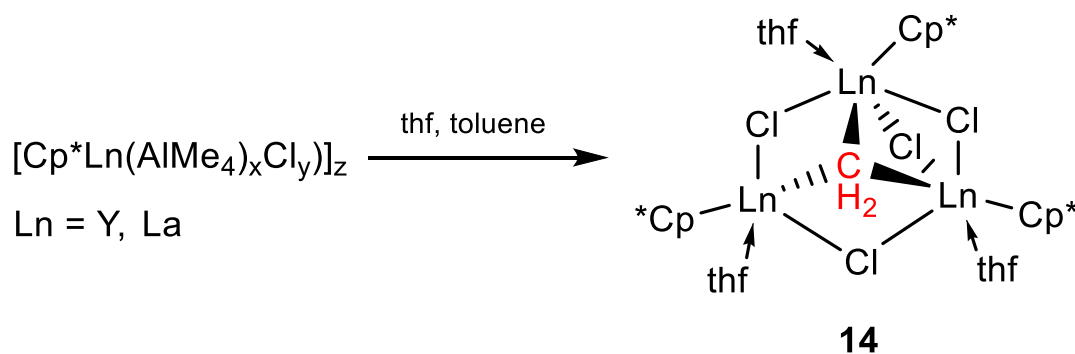
Scheme 8. Synthesis pathway of trimetallic rare-earth metal methylene compound **14**.

The chemistry of main-group metal alkylidenes has remained elusive despite the rapid growth in the number of transition-metal alkylidenes. Due to MOTTUS successful synthesis of [Br$_2$AlCH$_2$AlBr$_2$] (**5**), the question arose whether this is also possible for higher homologues (e.g. In). Furthermore, in 1985 the research group of TUCK succeeded in the synthesis and X-ray crystal structure determination of an isostructural indium alkylidene complex [Cl$_2$InCH$_2$InCl$_2$(TMEDA)$_2$] (**15**) (TMEDA = *N,N,N',N'*-tetramethylethanediamine) and [Cl(Br)InCH$_2$InCl$_2$(TMEDA)$_2$] (**16**) via the reaction of InCl$_3$ and InX (X = Cl, Br) in a mixture of dichloromethane/TMEDA/toluene.[40]
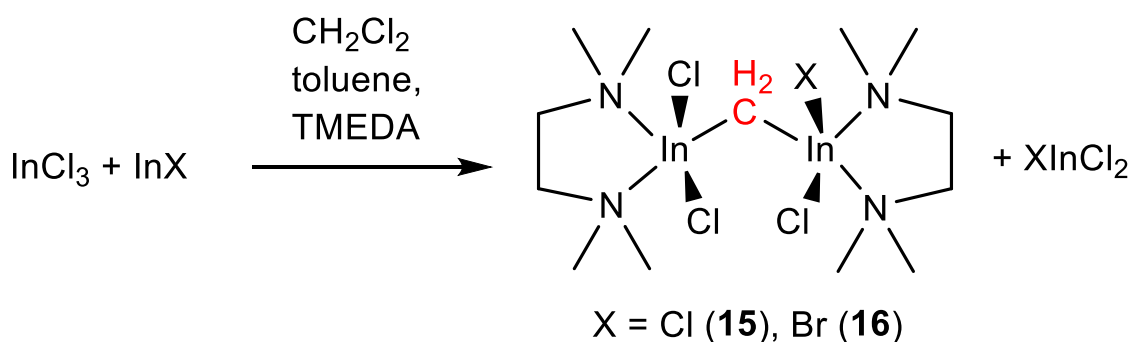
Scheme 9. Synthesis of indium methylidene complexes **15** and **16**.

Molecules like compound **15** and **16** are well known.[41] For example, it has been demonstrated that [IZnCH$_2$I]is a methylene transfer reagent.[41-42] However, the reports that deal with main group metal compounds with bridging methylidenes are relatively scarce. Experiments with aluminum alkyls and salt compounds like lithium-methyl and lithium-ethyl yielded unidentified compounds.[43] Hereby other alkylaluminum compounds and polymeric methylidene species were suggested.[43] Another few years have passed until in 1990 the group of UHL was able to synthesize and determine the crystal structure of methylene bis(aluminum dialkyl) [R$_2$Al–CH$_2$–AlR$_2$] (**17**) (R = CH(SiMe$_3$)$_2$) via a salt metathesis reaction of four equivalents bis(trimethylsilyl)methyl lithium with one equivalent of [Cl$_2$Al–CH$_2$–AlCl$_2$] (Scheme 10).[44]
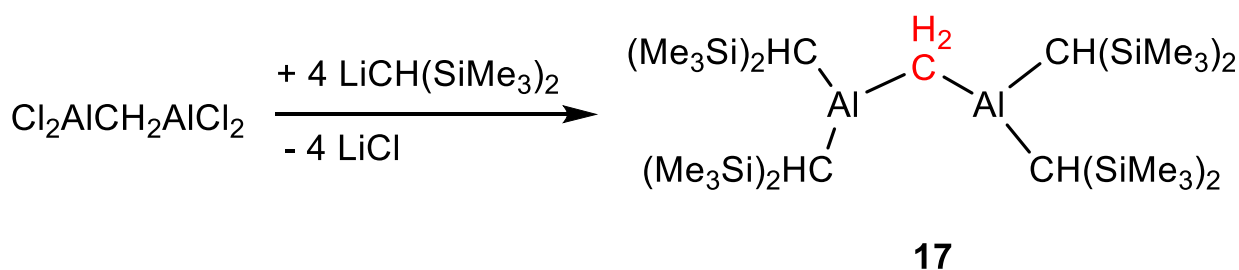
Scheme 10. Synthesis of methylene bis(aluminum dialkyl) **17**.

Due to the facile handling and synthesis of such [Cl$_2$Al–CH$_2$–AlCl$_2$] precursors and the ease of synthesis of compound **17**, additional molecules like R$_2$Al–CH$_2$–AlR$_2$ were synthesized [R = N(SiMe$_3$)$_2$ (**18**),[45] R = N(CMe$_2$–CH$_2$)$_2$CH$_2$ (**19**)[45]]. Furthermore, the mixed derivative with the formula [R(Cl)Al–CH$_2$–AlR(Cl)] (R = CH(SiMe$_3$)$_2$, **20**) was obtained by a salt metathesis reaction.[46] In an attempt to use less demanding ligands, only alkylaluminum (AlR$_3$) compounds and unidentified products were obtained.[43] This molecular structure with two aluminum and a bridging methylidene unit is also suitable to act as chelating Lewis acid in the presence of an additional base (e.g. TMEDA). Hereby, mono-adducts with several structural motifs were obtained such as [Li(base)$_n$][**17**(X)] (X= NO$_2$ (**21**),[47] NO$_3$ (**22**),[47] N$_3$ (**23**),[48] CH$_3$CO$_2$ (**24**)[48] and Me$_2$PCHPMe$_2$ (**25**)[49]) and [Li(base)$_n$][**17**(X*)] (X* = H (**26**),[50] CH$_2$-t-Bu (**27**),[51] Me (**28**),[52] n-Bu (**29**),[52] C≡C-SiMe$_3$ (**30**),[52] C≡C-t-Bu (**31**),[52] C≡C-Ph (**32**)[52] and C≡C-PPh$_2$ (**33**).[52] Moreover, using a more demanding lithium aryl yielded complex [Li(base)$_n$][**17**(X)] (X = aryl = C$_6$H$_2$(2,4,6-i-Pr)$_3$, **34**), featuring the same structural motif.[53] Despite the successful and great results of UHL, the number of main group metal alkylidenes remained relatively moderate. The structural motif presented by UHL and TUCK with the bridging methylidene unit is omnipresent in the structurally characterized main group metal methylidenes. STUCKY'S elucidation in 1990 provided the largest contribution to a homoleptic main group metal methylidene.[8] Given the first characterized homoleptic lithium methylidene, 29 years have passed untill 2019 BONATH from our group synthesized and fully characterized a homoleptic gallium methylidene [Ga$_8$(CH$_2$)$_{12}$] (**35**) (Scheme 11)[54] with utilization of rare-earth metal complexeses ([Ln(C$_5$Me$_5$)$_2$CH$_3$] (Ln = Lu) complexes have demonstrated similar C–H reactivities in the past.).[55-56] By reacting [(C$_5$Me$_5$)$_2$Ln{(μ-Me)$_2$GaMe$_2$}] (Ln = Y, Lu) with an eightfold excess of GaMe$_3$ at 130 °C provided access to a yellow precipitate, which was indentified as the homoleptic complex **35**. Noteworthy, the isolated intermediate **37** gives insight into the mechanism of formation of methylidenes and especially the formation of gallium methylidene. The equilibrium of [Ga$_8$(CH$_2$)$_{12}$] in thf forces the molecule to a six membered cluster [Ga$_6$(μ-CH$_2$)$_9$(thf)$_6$] (**36**).

$Cp^*_2Ln(\{\mu\text{-Me}\}_2GaMe_2$

$\xrightarrow[\text{- 4 CH}_4]{\text{+ exc. GaMe}_3}$

$Ga_8(CH_2)_{12}$

35

Ln = Y, Lu

6 GaMe$_3$

+ exc. GaMe$_3$

- 4 CH$_4$

+ thf

$[Cp^*_2Ln_3(\{\mu_3\text{-Me}\}_6Ga_9(\mu\text{-Me}_2)_9]$

37

$Ga_6(CH_2)_9(thf)_6$

36
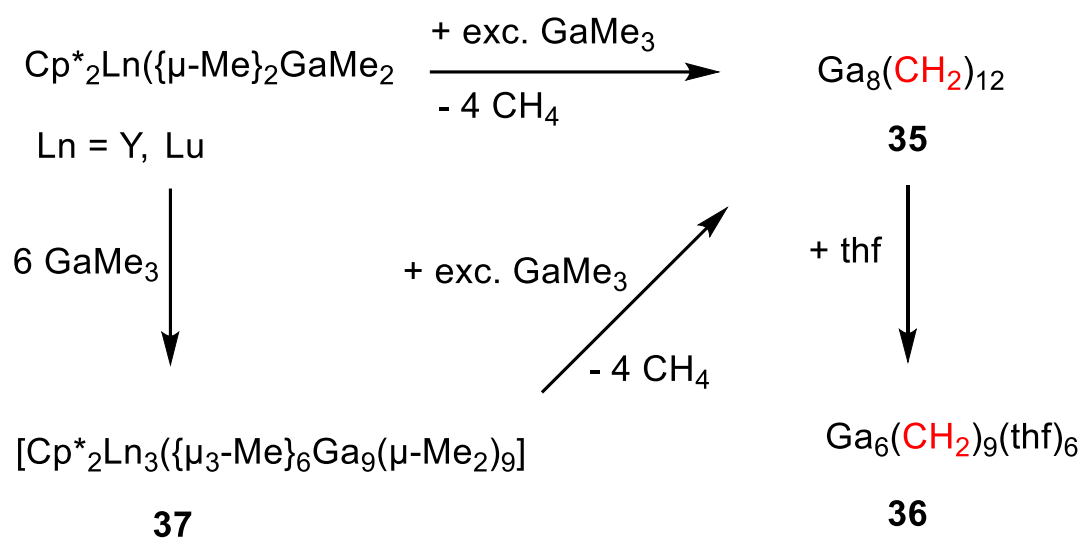
Scheme 11. Synthesis of homoleptic gallium methylene **35**.

Reactivity of Metal Alkylidenes

1.   Overview of the reactivity of metal alkylidenes

After the discovery of the first carbene complexes, the interest in applications has increased steadily. Initial studies by BANKS in 1964 demonstrated the conversion of linear olefins to lower and higher homologs on a heterogeneous molybdenum catalyst.[57] CALDERON followed shortly afterwards with a homogeneous catalytic process.[58] In the meantime, alkene metatheses are an crucial synthesis route for different natural products. These are used in organic synthesis as well as in modern organometallic chemistry. The following scheme is an overview of various reactivities of metal alkylidenes (**I** carbonyl olefination, **II** self-metathesis, **III** cross metathesis and **IV** ring opening and closing metathesis)

Scheme 12. Reactivity of metal alkylidenes in carbonyl olefination and metathesis reactions.

2. Carbonyl olefination

If we look at approach **I** of Scheme 12, a carbonyl olefination is understood as a reaction to produce C=C double bonds from a carbonyl group. As an olefin formation reaction, it has great importance in laboratory and industrial processes. This results in many well-known reactions such as the Wittig reaction,[59] Tebbe methylenation[60] and Takeda olefination.[61] However, the origin goes back to the Wittig reaction. In the latter reaction carbonyl compounds (e.g. aldehydes and ketones) can be converted via phosphorylides into olefins.[59] Georg Wittig was awarded the Nobel Prize in 1979 for his discoveries. In 1976 SCHROCK used Ta and Nb neopentylidene complexes **7** and **8** to show that various carbonyls were olefinated (including carboxylic acid derivatives).[62]

A few years later, the Tebbe reagent **11** showed its application in the methylenation of ketones and aldehydes, moreover, the formation of Tebbe's reagent has been intensively studied over the years.[13, 63] Furthermore, the active species of the Tebbe reagent (Scheme 13, [Cp$_2$Ti=CH$_2$] (**38**)) could also convert carboxylic acid derivatives into heteroatom-substituted olefins similar to the Petasis reagent [Cp$_2$Ti(CH$_3$)$_2$].[64]
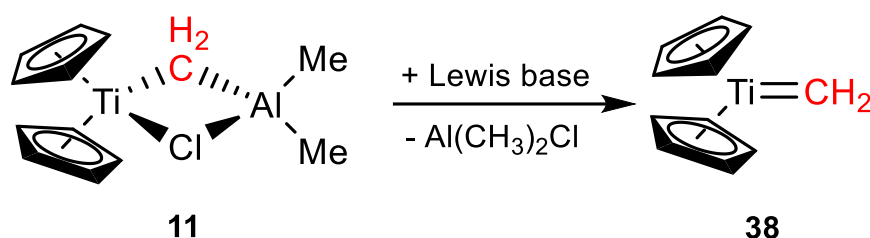
Scheme 13. Synthesis of Tebbe's reagent active species

As a LEWIS base originally pyridine (Py) or 4-dimethylaminopyridine (DMAP) have been used as a LEWIS base. Complex **38** could not be isolated and structurally characterized. The phosphine congeners [Cp$_2$TiCH$_2$·PMe$_3$], [Cp$_2$TiCH$_2$·PMe$_2$Ph], and [Cp$_2$TiCH$_2$·PEt$_3$] have been synthesized.[65] GRUBBS and co-worker showed that Tebbe's reagent **11** converts carbonyl compounds and carboxylic acid derivatives into terminal olefins (Scheme 12, approach **I**). [66-68] Table 1 compiles methylenation reactions and unsaturated organic substrates such as ketones, aldehydes, esters, lactones, amides and imides with the Tebbe reagent. The yields are significantly higher than in the Wittig reaction. The use of esters and amides also clearly demonstrates the advantage of Tebbe's reagent.

Table 1. Overview of methylenation reactions of Tebbe's reagent.

Entry	Carbonyl	Yield (Yield from Wittig reaction)	Ref.
1		96 % (80%)	[69]
2		97% (46%)	[69]
3		35% (-)	[70]
4		94% (-)	[71]
5		90% (-)	[71]
6		85% (-)	[71]
7		80% (-)	[72]
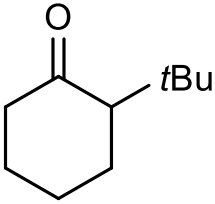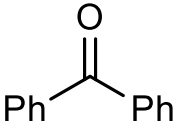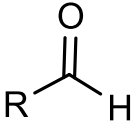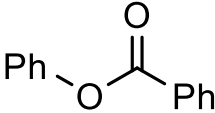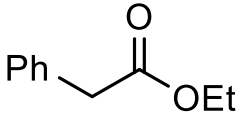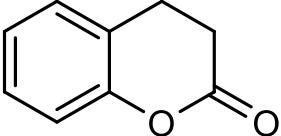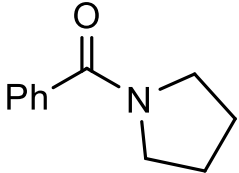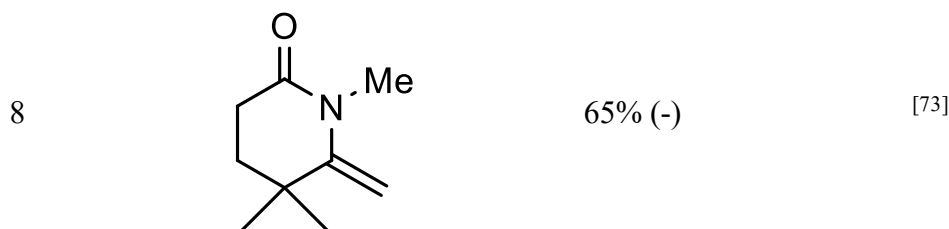
For the methylenation of ketones, the useful application or advantage of **11** over the WITTIG reaction becomes particularly noticeable. Sterically demanding ketones can be used here (Table 1, entries 1 and 2). Please note that Table 1 compiles selected examples. For further reading the article by TAKEDA is recommended.[74] In comparison, there are only a few reports of methylenation of aldehydes (Table 1, entry 3).[70] During the methylenation of carboxylic derivatives (for example esters and lactones, Table1, entries 4-6), the phosphorous ylides fail, whereby reagent **11** can be used successfully. Similar reaction behavior can also be observed with amides and imides (Table 1, entries 7 and 8). Despite the great importance of TEBBE's reagent, several analogues are known that are quite similar. Zinc and magnesium analogues have been investigated for olefination reactions of carbonyl compounds. [Cp$_2$TiCH$_2$ * ZnX$_2$] (**39**, X = halides) readily olefinate ketones[75] and the organotitanium species [Cp$_2$Ti(X)CH$_2$MgX * MgX$_2$] (**40**, X = halides) convert benzophenone into 1,1-diphenylethylene.[76] Over the years, other reagents have emerged, including well-known ones such as the Petasis reagent Cp$_2$Ti(CH$_3$)$_2$ (**41**)[77] or the Takeda olefination reagent [Cp$_2$Ti{P(OEt)$_3$}$_2$] (**42**) in the area of titanium-based compounds.[61, 78] Many other transition metal alkylidenes have been shown to be useful in carbonyl olefination. In addition to titanium compounds, complexes containing zirconium,[79-87] tantalum[14], niobium[14], molybdenum[88-99] and tungsten[100-103] are known to be active in carbonyl olefination. The tantalum and niobium neopentylidene complexes **7** and **8** have also been shown to be very valuable in carbonyl olefination reactions. Furthermore, these complexes are among the first SCHROCK type alkylidenes.[62] In the following overview (Scheme 14), all reactions have been carried out at 25 °C in diethyl ether, pentane or hexane. It should be noted that these reagents are also suitable for obtaining *tert*-butyl substituted olefins, which is generally difficult to achieve due to the increased steric demand.[14] The reactions shown in Scheme 14 are also amenable for niobium complex **8**. Due to the relatively small number of main group metal alkylidenes, reports of carbonyl olefination are also scarce. Reaction of homoleptic gallium methylidene **35** with 9-fluorene shows a conversion to 9-methylene-fluorene.

90 %

cis : trans = 1 : 1

35 %

65 %

7

77 %

> 95%, one isomer

80 %
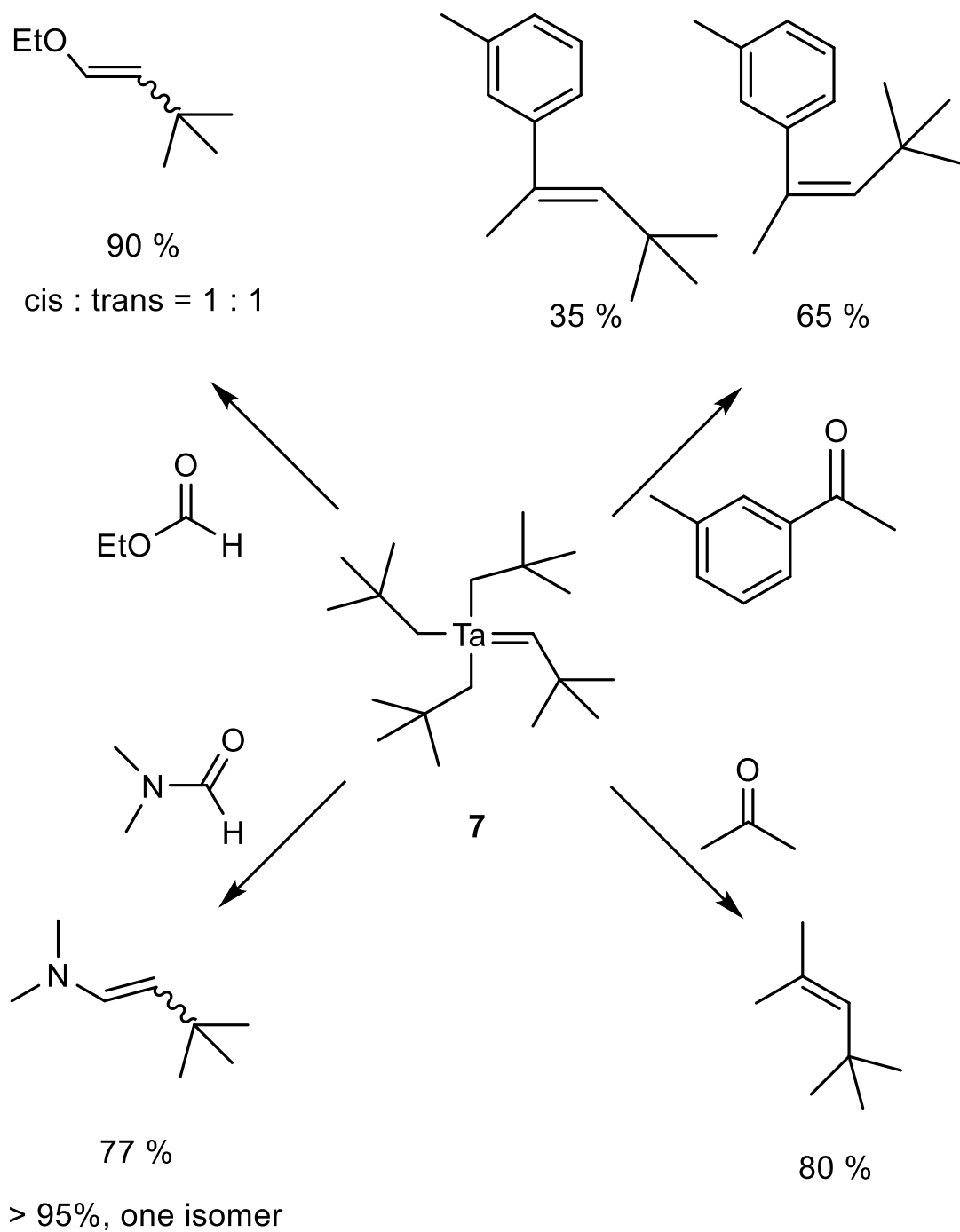
Scheme 14. Different carbonyl olefination compounds using tantalum neopentylidene complex **7**.

3.   Olefin Metathesis

Previously mentioned possibilities of heterogeneous and homogeneous metathesis reactions led in the long-term to a great industrial use as well as to a wide application in the laboratory. The reaction pathways are governed by the metal alkylidene and the olefin. A distinction is made between different metathesis reactions (Scheme 12, path **II-IV**). It is also clear that metatheses are relatively thermoneutral equilibrium reactions.[104] Furthermore, various calculations were made on this subject by nobel laureate Robert Grubbs[105-107] and Yves Chauvin[108] to clarify the possible reaction mechanism. Nerverthless, CHAUVIN was the first who predicted the mechanism correctly by postulating a metal alkylidene and metallacyclobutane intermediate. Here, the alkylidene unit [M=CH$_2$] acts as the "active center". Over the years, W, Mo, Re and Ru compounds have emerged as particularly excellent metathesis catalysts (Scheme 15).
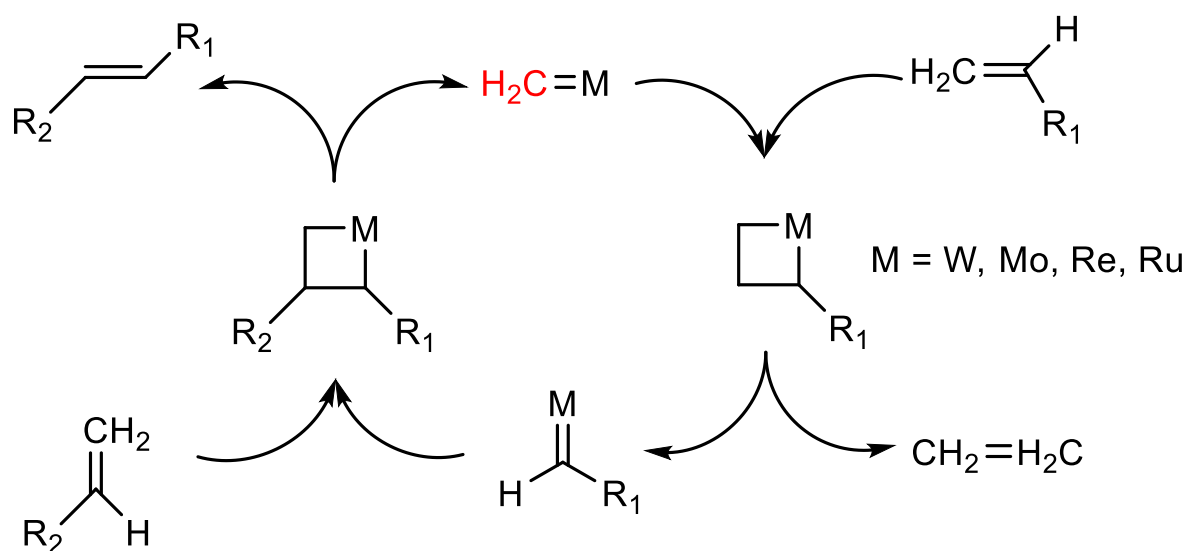
Scheme 15. Simplified reaction mechanism according to Yves Chauvin.[109]

SCHROCK successfully synthesized and characterized the metallacyclobutane W[CH(*t*-Bu)CH$_2$CH(CO$_2$Me)](NAr)[OCMe$_2$(CF$_3$)]$_2$ W   (**43),**   and   Mo[CH(*t*-Bu)CH$_2$CH(CO$_2$Me)](NAr)[OCMe$_2$(CF$_3$)]$_2$ (**44**) intermediates in 1989, confirming the validity of the mechanism (Figure 1).[110-111] Further optimization of the catalysts were carried out by GRUBBS and SCHROCK. The most famous catalysts are Mo complex **45** (Schrock-cat.)[112] and Ru complex **46** (Grubbs-cat.)[113] with distinct reactivity (Figure 1).
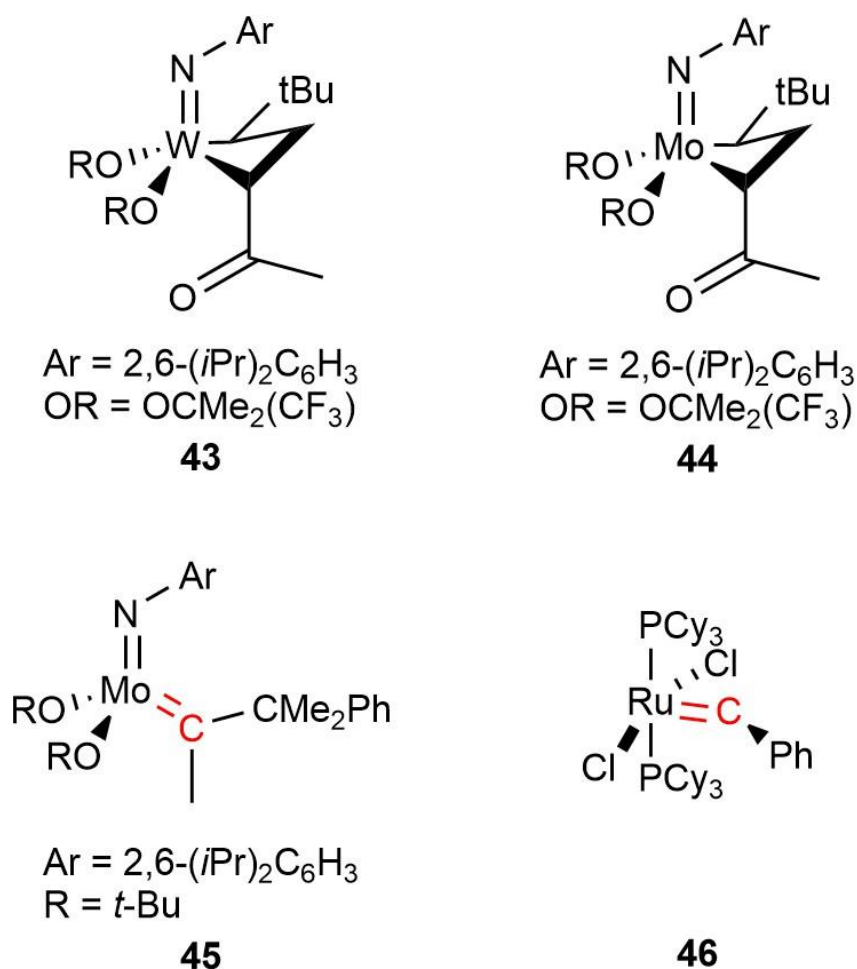
Figure 1. Schrock metallacyclobutanes (**43** and **44**), Schrock (**45**) and Grubbs metal alkylidene catalysts (**46**).

It turned out that the more electron withdrawing group on the alkoxide (e.g. $CMe(CF_3)_2$), the more reactive is the catalyst in the metathesis of olefins. The disadvantage of compound **45** is that the tolerance of certain functional groups is decreased.[104, 114] Direct comparison with the Grubbs catalyst **46** revealed a higher tolerance of functional groups (-CO, -OH, -NH$_2$). However, component **46** is selective for sterically non-demanding olefins.[104] Metathesis reactions often occur on heterogeneous catalyst for the application in industry.[115-116] Unfortunately, there are no reports of main-group metal alkylidenes showing activity in metathesis reactions.

4.   Cross Metathesis

Cross metathesis covers also the well-known Shell Higher Olefin Process (SHOP) that is used on a large industrial scale to obtain olefins of different chain lengths from C_4 to C_{30} by catalytic oligomerization, isomerization and metathesis steps.[117] Derivatization of the cross metathesis products by hydroformylation and hydrogenation affords fatty alcohols with chain lengths of C_8 - C_{22}. Various transition metal complexes are used as catalysts. Representative cross metathesis catalysts are Mo- and Ni-based compounds. In the process transition metal alkylidenes are formed which then act as a catalyst (Scheme 16).[104, 118-119] It is important to emphasize that this process is a heterogeneous catalysis. Ethylene is introduced here as a gas onto the solid catalyst.
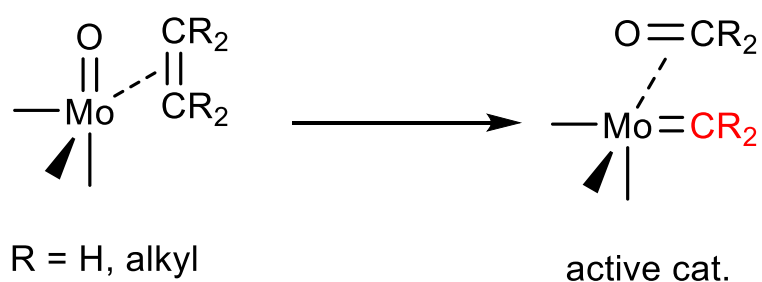
Scheme 16. Possible formation of molybdenum alkylidene as active catalyst for cross metathesis reactions.

5.   Ring opening- and ring closing metathesis (ROM / RCM)

A now indispensable tool in organic chemistry for the synthesis of many different natural products is RCM and the back reaction ROM. Hence, GRUBBS and FU investigated the molybdenum catalyst **45** (with minor change of the alkoxy to a fluorinated alkoxy group [Mo(NAr)(CHCMe$_2$Ph)(OCMe-(CF$_3$)$_2$)] (**47**) to be a versatile reagent to produce cyclic olefins bearing additional functional groups and yielding volatile gases such as ethylene, propylene or butenes as by-products (Scheme 17).[120-121] Despite the high sensitivity of W and Mo catalysts, they proved to be useful in organic synthesis to perform metathesis reactions. HOVEYDA'S group was even able to successfully apply a complex for the synthesis of natural product fluvirucin-B$_1$ via ring closing metathesis (by using the molybdenum catalyst **47**) (see Scheme 17).[122] GRUBBS examined Ru catalysts, which are more stable toward air and moisture than Mo- and W-based systems, and assessed applications in organic synthesis.[123] Furthermore, the mechanism of metatheses reactions goes back to Yves Chauvin. The [2+2] cycloaddition forming the metallacyclobutane is a key step (see Scheme 15).[109]
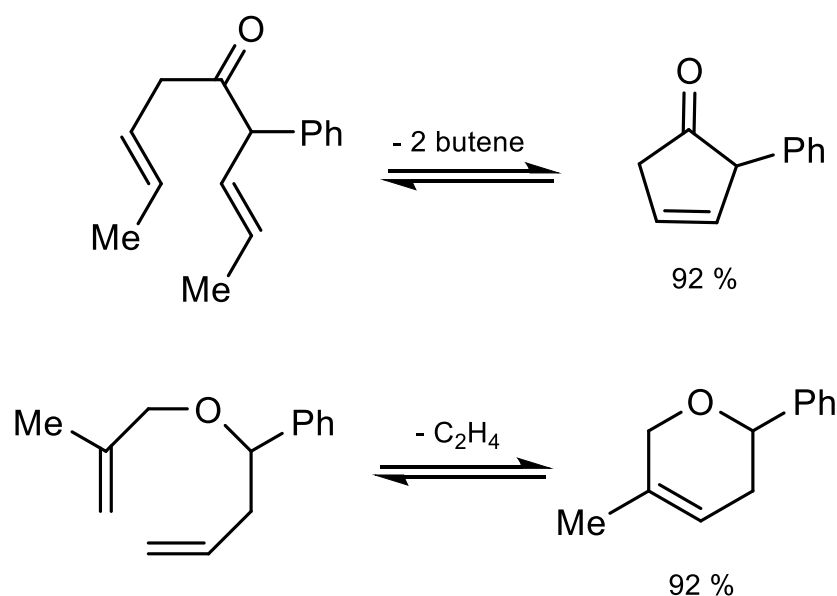
Scheme 17. RCM reactions of catalyst **47**.

Unfortunately, there are no reports of main group metal elements showing activity in RCM or ROM reactions.

B

Summary of the Main Results

Methylaluminomethylene

Earlier experiments by ZIEGLER have already shown that alkali-metal alkylidenes are likely to form.[124] It took another 35 years to determine the solid-state structure of homoleptic $[Li_2CD_2]_n$ by STUCKY.[8] Further successes came from UHL for the element aluminum generating compound $[(Me_3Si)_2CH]_2Al-CH_2-Al[CH(SiMe_3)_2]$ (**17**) with a bridging methylene unit (for a detailed overview see chapter A).[44] Nevertheless, the reports of SINN[12] and BONATH[54] gave further evidence of group 13 methylene species. By reacting sandwich complex $[Cp*_2Lu(AlMe_4)]$ (**A1**) with trimethylaluminum (TMA), the lutetium compound $[Cp*_4Lu_2Al_{10}(CH_2)_{12}(CH_3)_8]$ (**A2**) can be obtained after reacting at 130 °C for 500 h, featuring a mixed methylaluminomethylene $[Al_{12}(CH_2)_{12}(CH_3)_{12}]$ (**A4**) core (Scheme 19, upper reaction path). Unfortunately, the scale up reaction for **A2** did not lead to extrusion of **A4**. Amazingly, the reaction of gallium methylene with TMA afforded a similar structure. The difference between the structures is that the bis(cyclopentadienyl) lutetium group $[Cp*_2Lu]^+$ is replaced by an $[AlMe_2]^+$ group to afford $[Al_{12}(CH_2)_{12}(CH_3)_{12}]$ (**A4**) (Scheme 19, bottom). For an alternative approach the previously established reaction by SINN was reinvestigated, more precisely, the reaction of $[Cp_2TiCl_2]$ with excess TMA gave compound **A4** as well. Here, the Tebbe reagent is assumed to feature intermediate species. For this reason, the reaction of $[Cp_2Ti(\mu-CH_2)(\mu-Cl)Al(CH_3)_2]$ with TMA was also carried out and yielded the same product (Scheme 19, middle part).
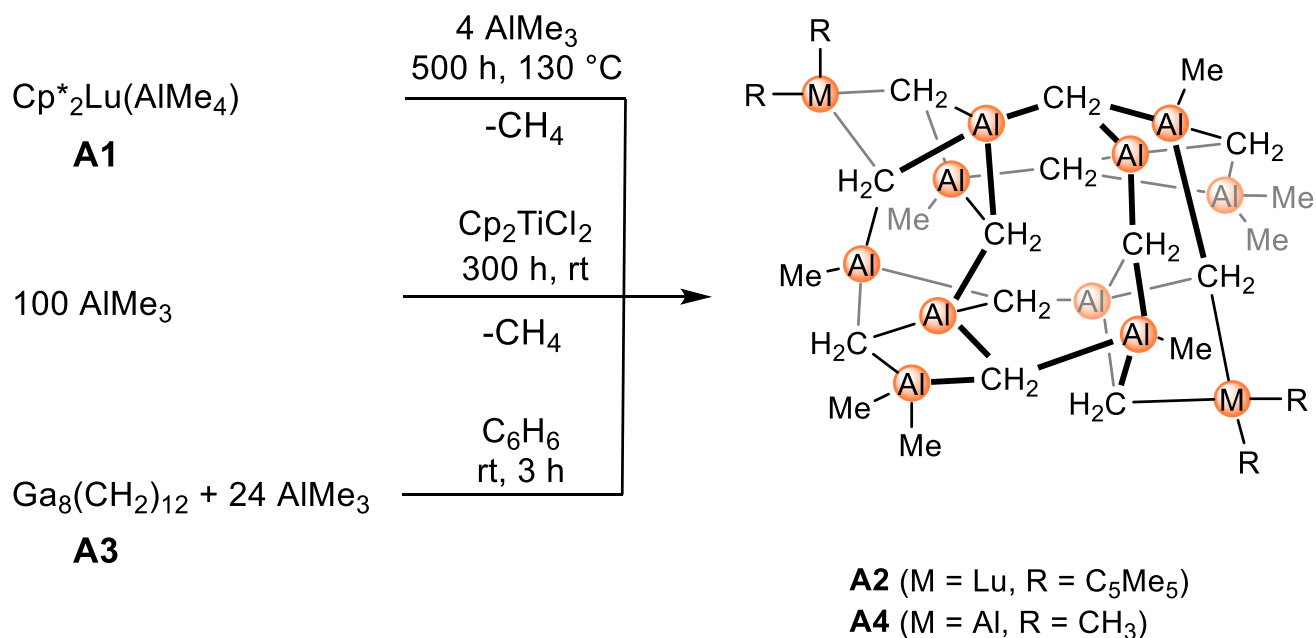
Scheme 19. Synthesis pathways toward aluminum-methyl-methylene **A4**.
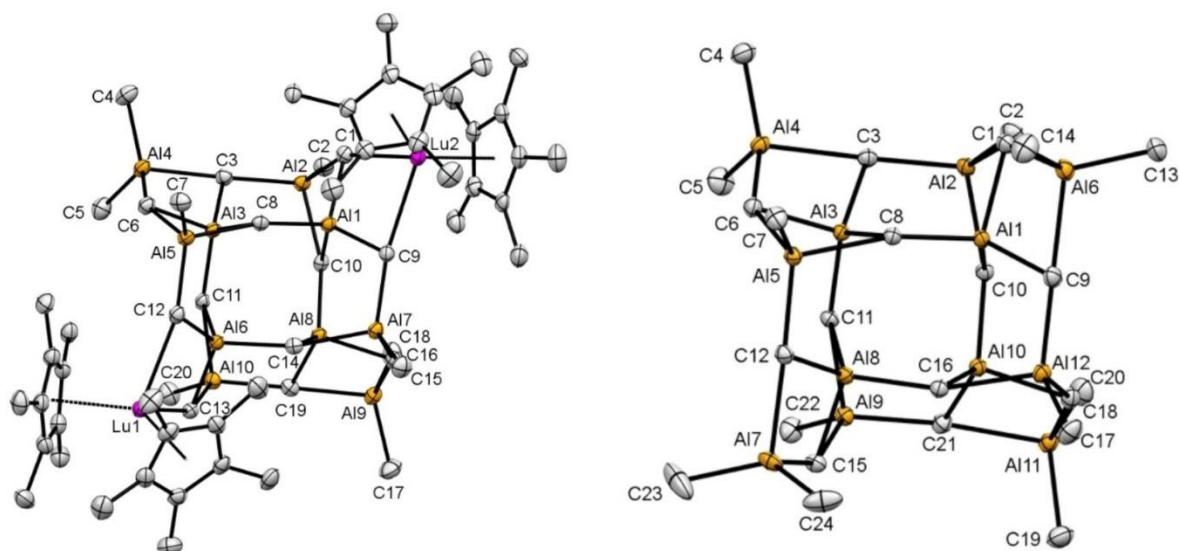
Figure 2. Crystal structures of compounds **A2** (left) and **A4** (right).

In accord with the differences in the ionic radii of aluminum and gallium the metal–C distances in compound **A2** are considerably shorter than those of the gallium congener [Cp*$_6$Lu$_3$(μ_3-CH$_2$)$_6$Ga$_9$(CH$_2$)$_9$], which was isolated as intermediate in the synthesis of [Ga$_8$(CH$_2$)$_{12}$] (**A3**). The solid-state structures of **A2** and **A4** revealed a bonding situation where the Al atoms are either coordinated by four μ_3-methylene, two methylene and two methyl groups or one methyl group and three methylene units (Figure 2). The Al–C(Me) distances of both compounds **A2** and **A4** are comparable to the starting material TMA. To demonstrate the reaction behavior of as a nucleophilic alkylidene, **A4** was treated with various carbonyls like 9-fluorenone, benzophenone and acetone at ambient temperature to result in the complete conversion to 9-methylene-fluorene, 1,1-diphenylethylene and isobutene, respectively. It is noteworthy that the alkylated product was not detected in the ^{1}H NMR spectra leaving putative methylaluminoxane (MAO) as a coproduct (Scheme 20).
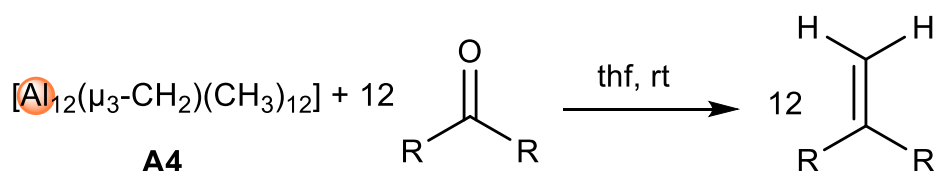
Scheme 20. Reaction of **A4** with 9-fluorenone, benzophenone and acetone.

In summary, the structure of Methylaluminomethylene **A4** has been elucidated after the seminal discovery by SINN more than 50 years ago. This provides a deeper insight into main group metal alkylidene chemistry and might contribute to a better understanding of mechanistic details in catalysis.

Reactivity of Gallium Methylene

Transition-metal complexes are widely used in carbonyl olefination.[74, 125-126] However, studies on the synthesis and reactivity of main group metal alkylidenes are scarce. BONATH et al. reported on the seminal discovery of hexa- and octanuclear gallium methylidene complexes by a σ-bond metathesis and alkane elimination protocol of lanthanocene alkyl complexes with excess trimethylgallium.[54] The quasi-catalytic synthesis afforded $[Ga_8(CH_2)_{12}]$ (**A3**) in high yields. In this section the focus is on the reactivity of **A3** towards differently substituted phenols as well as the corresponding anilines

Initially, stoichiometric reactions of **A3** were carried out with 8 equivalents of 2,4,6-trimethylphenol and 2,6-dimethylphenol, 2,4,6-trimethylthiophenol, 2,4,6-trimethylaniline and 2,6-dimethylaniline in thf-d_8 at ambient temperature to yield complexes **A5-A9** of the general composition $[Ga_4(\mu_2\text{-}CH_2)_2(CH_3)_4(\mu_2\text{-}XAr)_4]$ (X = O, S, HN) (Scheme 21).
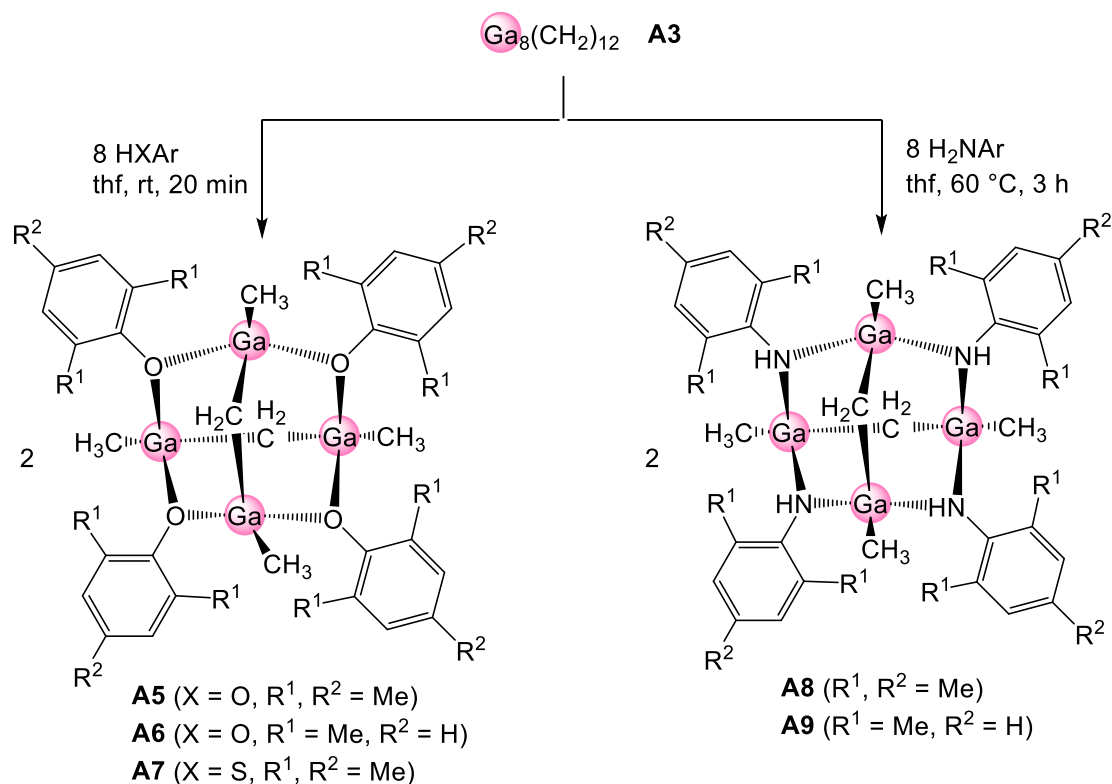
Scheme 21. Synthesis of complexes **A5-A9** bearing bridging aryloxy, arylamido and thiophenolato ligands (Paper **II**).
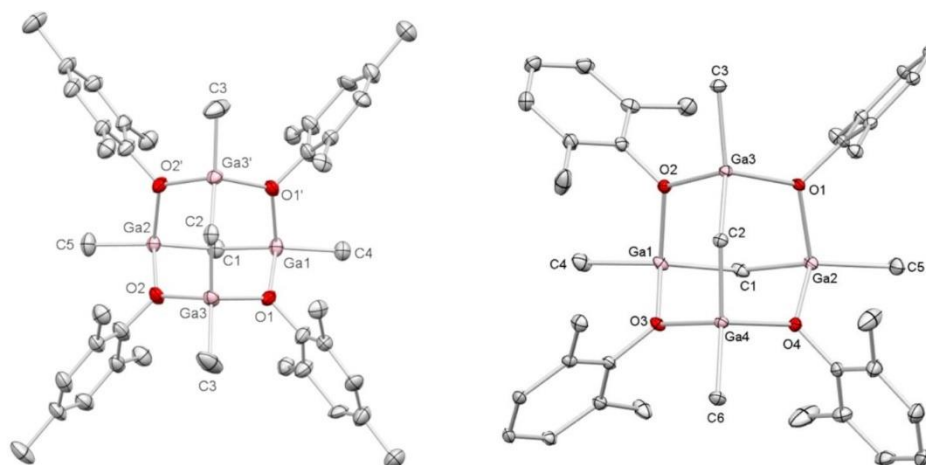
Figure 3. Crystal structure of **A5** (left) and **A6** (right, Paper **II**).

Interestingly the reaction with different molar ratios, for instance 1:2, 1:4 and 1:6 led to the same product in lower yields. Applying 8 equivalents the products could be obtained in a very high yield of approximately 90 and 70 %. Reacting gallium methylene with the sterically more demanding phenol $HOC_6H_3tBu_2$-2,6 yielded a pentagallium complex $[Ga_5(\mu_2$-$CH_2)_6(OC_6H_3tBu_2$-2,6$)_3(thf)_2]$ **A10** with bridging methylene units (Figure 4).
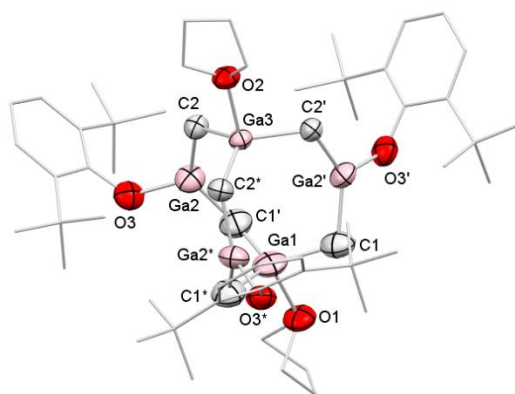
Figure 4. Crystal structure of **A7** (Paper **II**).
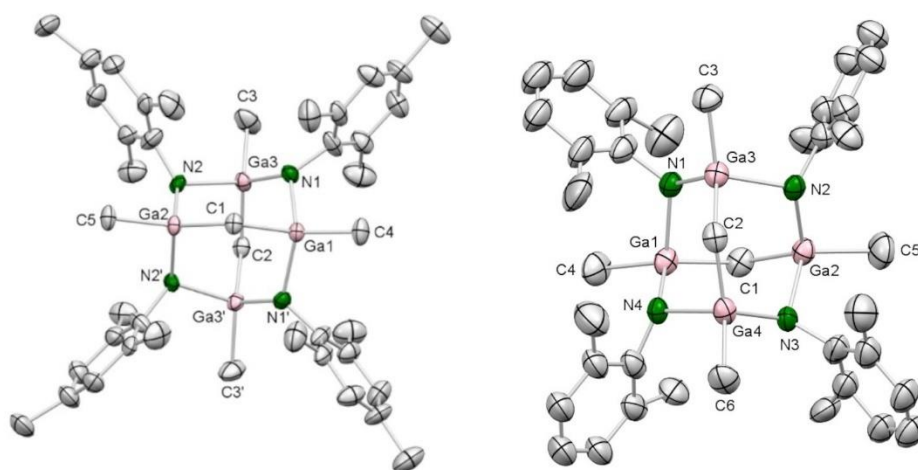
Figure 5. Crystal structure of **A8** (left) and **A9** (right, Paper **II**).

In a similar fashion, the protonolysis of **A3** with differently substituted anilines also led to tetranuclear gallium amide complexes (Scheme 21). The reaction times of the protonolysis with anilines are significantly increased compared to the (thio)phenols due to the lower Brønsted acidity (see Bordwell pK$_a$ tables).[127] Moreover, the yields are 52% for **A8** and 44% for **A9**, respectively, and are also lower compared to the gallium aryloxide compounds. Despite the isostructural motifs, differences are evident in the ^{1}H NMR spectra. There is clearly a rotational barrier present for the C–NH bond in compound **A8** and **A9**, which is indicated by the splitting of the *o*–CH$_3$ signals (see Figure 6). It should be noted that the signals for the terminal Ga–Me groups are very similar to similar gallium compounds. [128-133]
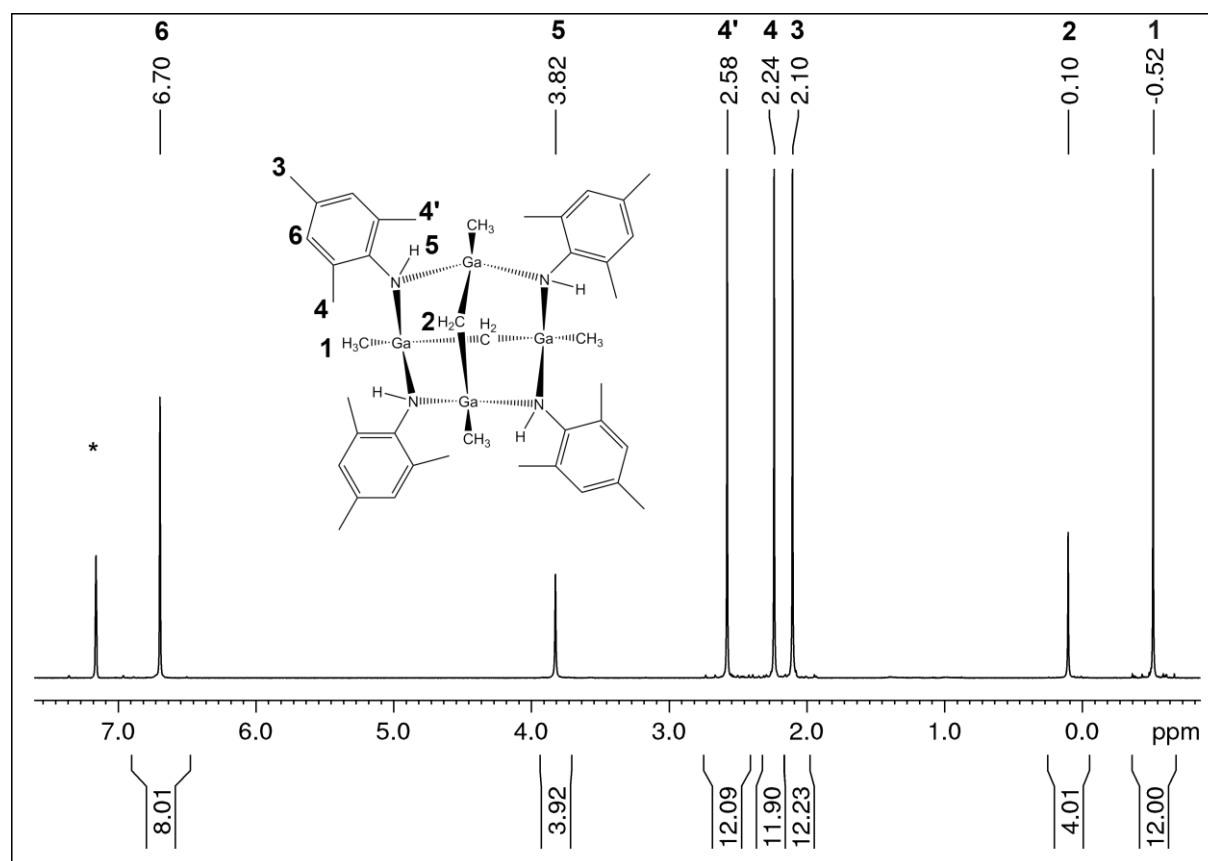
Figure 6. ^{1}H NMR spectrum of compound **A8** (Paper **II**).

In summary, Paper **II** covers the study on the protonation of homoleptic compound [Ga$_8$(CH$_2$)$_{12}$] using different phenols and anilines, which gave insight into the structural chemistry of new tetranuclear gallium aryloxide- and arylamide compounds with bridging methylidene units.

However, main group-metal alkylidene complexes are rare and not yet well studied. In order to extend the reactivity of homoleptic $[Ga_8(CH_2)_{12}]$ (**A3),** we were interested in the surface organometallic chemistry of this compound on large-pore mesoporous silica SBA-15$_{500}$ and "small-pore" mesoporous silica MCM-41$_{500}$ (see Scheme 23). Therefore, the silica materials MCM-41$_{500}$ and SBA-15$_{500}$ were treated with excess of the organometallic precursor gallium methylene **A3** and trimethylgallium **A10** in thf to generate the hybrid materials **A^{H1}-A^{H4}**. Additionally, **A10** was also grafted onto SBA-15$_{500}$ in non-coordinating solvent (*n*-hexane) instead of thf as a standard. Noteworthy, the supernatant of the reaction mixture contained only a small amount of the precursors. At the same time, the reaction of **A3** with the parent material was monitored by NMR spectroscopy, indicating that methane was not produced.
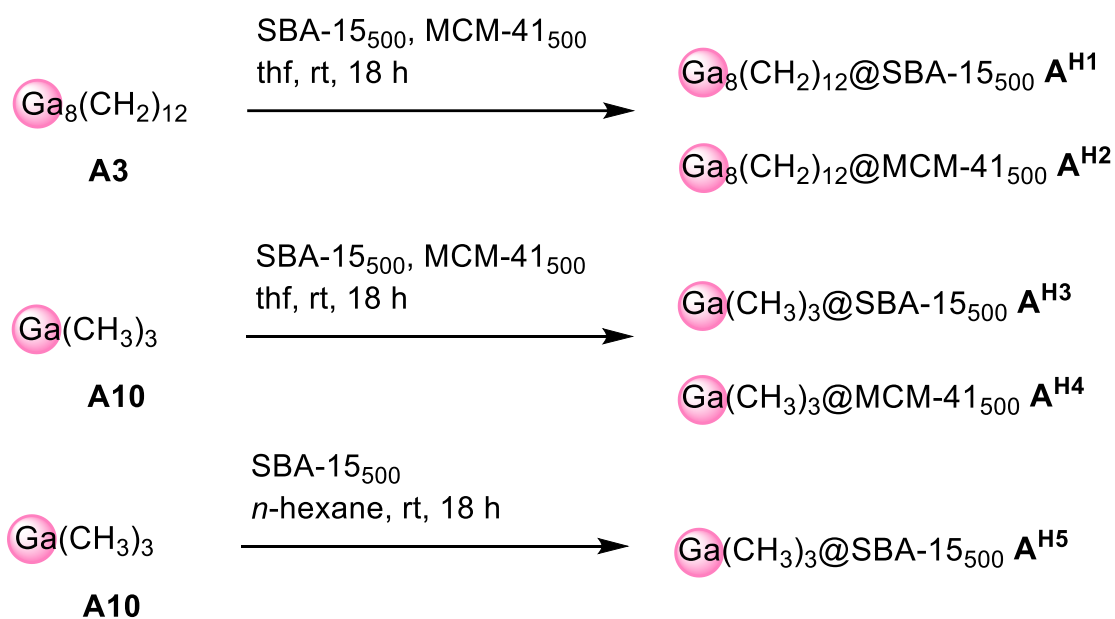
Scheme 23. Grafting experiments of precursor **A3** and **A10** on SBA-15$_{500}$ and MCM-41$_{500}$.

The study indicated that there might be intact gallium-methylene units on the material after grafting (due to performed methylenation reactions). The DRIFT analysis of the hybrid materials revealed a complete consumption of the Si–OH groups. The sharp band from the parent materials at 3743 cm^{-1} disappeared almost completely (Figure 7). ICP-OES measurements and elemental analysis revealed a high metal content which is also indicative of grafting dimetallic surface species. The nitrogen physisorption measurements showed a drastic decrease of the pore diameters and volume (6.9 to 5 nm for SBA-15$_{500}$ hybrid materials and 2.5 to 1.9 nm for MCM-41$_{500}$).
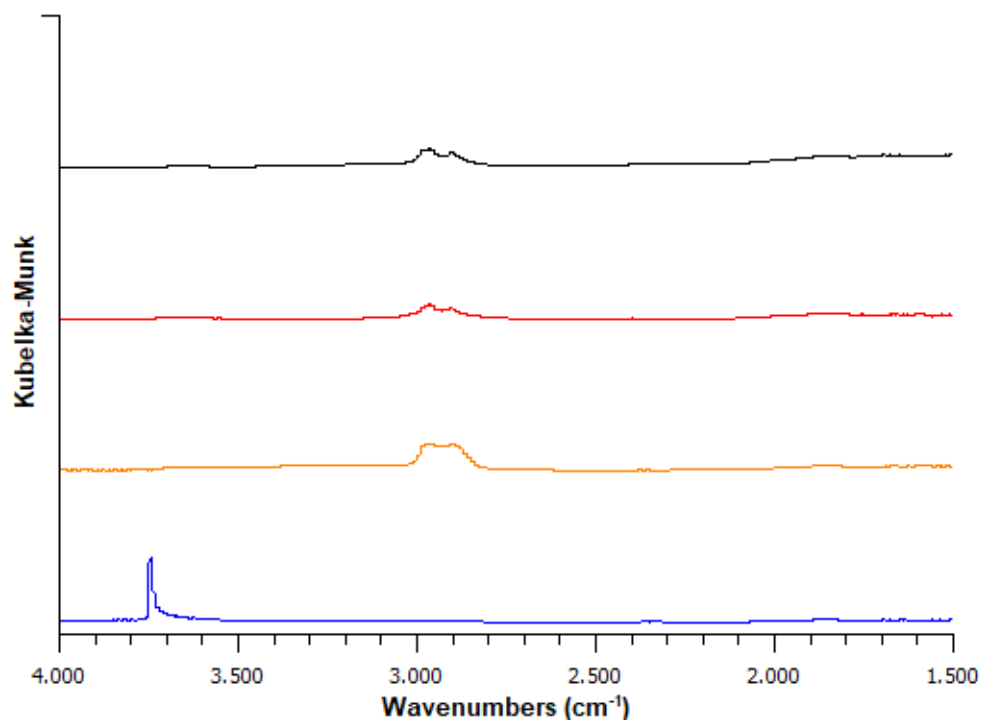
Figure 7. DRIFT spectra of parent material SBA-15 (blue), and hybrid materials A^{H1} (orange), A^{H3} (red), and A^{H5} (black) (**Manuscript**).

To demonstrate the existence of a dimetallic species, a molecular complex was synthesized by using the tris(*tert*-butoxy)siloxy ligand. The reaction of $[Ga_8(CH_2)_{12}]$ **A3** with $[HOSi(OtBu)_3]$ afforded bimetallic gallium compound $[GaMe_2\{OSi(OtBu)_3\}]_2$ which was previously isolated from the reaction of $[GaMe_3]$ and $[HOSi(OtBu)_3]$. [129, 134] This Ga_2O_2 four-membered ring is a common structural motif.

The last question was whether methylidene units are still present. For this purpose, the hybrid materials A^{H1}-A^{H2} were used and reacted with benzophenone in order to generate the corresponding 1,1-diphenylethylene *via* group transfer reaction. It is noteworthy that the conversion became visible by heating to 80 °C (tracked by ^1H NMR spectroscopy). In comparison, the molecular gallium complex **A3** needed 16 h for the conversion at ambient temperature and up to 2 h at 60 °C. 1,1-Diphenylethylene was clearly recognizable, proving that the hybrid materials A^{H1} and A^{H2} have intact methylidene units on the surface (Scheme 24).

$Ga_8(CH_2)_{12}@SBA\text{-}15_{500}$ $\mathbf{A^{H1}}$

$Ga_8(CH_2)_{12}@MCM\text{-}41_{500}$ $\mathbf{A^{H2}}$

benzophenone
thf, 80 °C, 16 h

$\xrightarrow{\hspace{3cm}}$

1,1-diphenylethylene
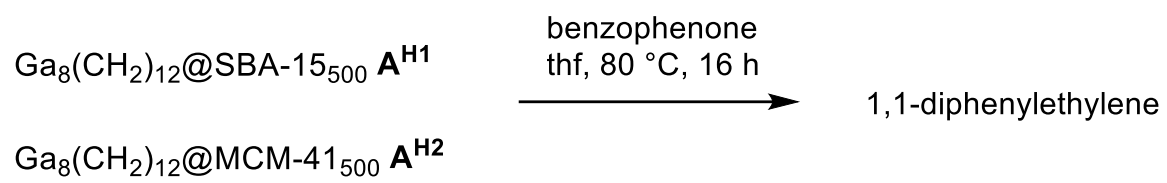
Scheme 24. Reactivity of hybrid material $\mathbf{A^{H1}}$ and $\mathbf{A^{H2}}$ toward benzophenone.

C

Unpublished Results

Reaction of Gallium Methylene toward CO_2

1.2 Introduction

As shown before, protonolysis of gallium methylidene $[Ga_8(CH_2)_{12}]$ **(A3)** with different phenols and anilines yielded tetrametallic and pentametallic gallium complexes with bridging and intact methylidene units. Therefore, it was of interest to elucidate the reactivity of $[Ga_8(CH_2)_{12}]$ **(A3)** toward CO_2.

1.3 Results and Discussion

The reaction of gallium methylene with CO_2 was performed in a J. Young NMR valve tube where the argon atmosphere was replaced by CO_2 (1 atm). A colorless precipitate formed immediately (Scheme 25). In the ^1H NMR spectrum, a signal occurred at 5.35 ppm, which can be assigned to C_2H_4. The colorless precipitate is stable in air and does not dissolve in water. The reaction of the precipitate with $KHSO_4$ gave acetic acid. Crystallization and structural elucidation of the CO_2 inserted product was not successful. Further reactions with various donors (tetrahydropyran, 2,2-bipyridin and 18-crown-6) and primary alcohols (iPrOH), silanols (($Et)_3SiOH$, (iPr)$_3SiOH$ and (Ph)$_3SiOH$) and different anilines (3,5-bis-trifluoromethylanilin) were carried out. Unfortunately, no specific structures could be obtained.
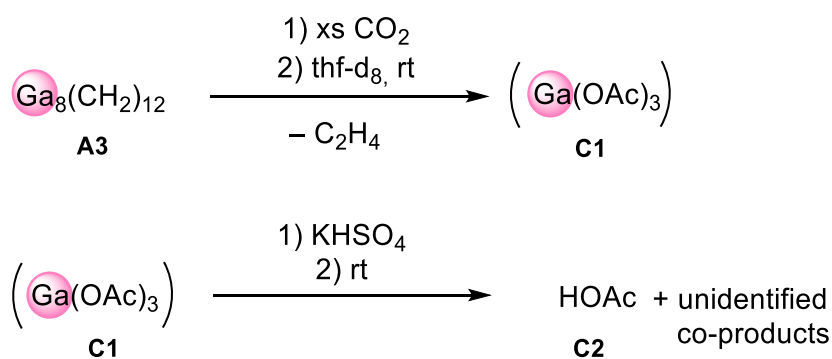
Scheme 25. Conversion of gallium methylene **A3** with CO_2.

1.3 Experimental Section

General Procedures. All manipulations were performed under an inert atmosphere (Ar) using a glovebox (*MBraun* 200B; <0.1 ppm O_2, <0.1 ppm H_2O), or according to standard Schlenk techniques in oven-dried glassware. The solvents were purified with Grubbs type columns (MBraun SPS, solvent purification system) and stored in a glovebox. $Ga_8(CH_2)_{12}$ was synthesized according to literature procedures.[54] THF-d_8 was purchased from *Euriso-top* and pre-dried over NaK alloy and filtered prior to use. Additionally, THF-d_8 was recondensed. NMR spectra were recorded at 26 °C with a Bruker AVII+400 (^{1}H: 400.13 MHz, ^{13}C, 100.61 MHz) using J. Young valve NMR tubes. ^{1}H NMR resonances are referenced to solvent residual signals and reported in parts per million (ppm) relative to tetramethylsilane. Analyses of NMR spectra were performed with Bruker TopSpin 3.6.0. CO_2 reactions were performed at a Schlenk line with a CO_2 lecture bottle (Westfalen). The pressure was set to 1 bar by a regulator.

Reaction of $Ga_8(CH_2)_{12}$ with CO_2 : In a J. Young NMR valve tube, a solution of $Ga_8(CH_2)_{12}$ (23 mg, 0.032 mmol) in thf-d_8 was treated with CO_2 (1 atm) at room temperature (J. Young NMR valve tube was evacuated before). After 5 min a colorless precipitate is forming. ^{1}H NMR (thf-d_6, 400.13 MHz, 26 °C): δ = 5.35 (s, 4 H, C_2H_4), 0.19 (s, 24 H, Ga–CH_2), 0.12 (d, $^2J_{HH}$ = 9.1 Hz, 6 H, Ga–CH_2), –0.10 (s, 6 H, Ga–CH_2), –0.49 (d, $^2J_{HH}$ = 8.8 Hz, 6 H, Ga–CH_2). The yield and subsequent analytics could not be determined more precisely
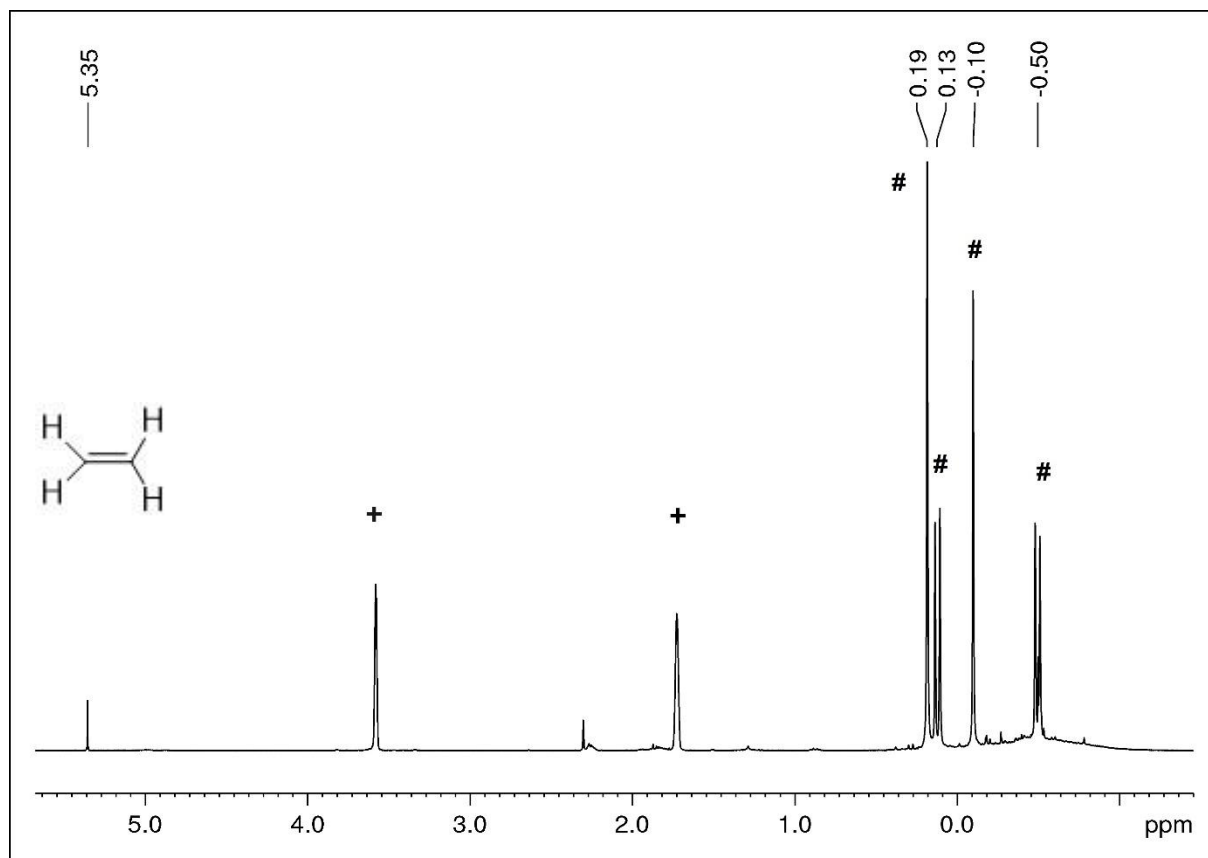
Figure 8. In situ ^{1}H NMR spectrum of the conversion of $Ga_8(CH_2)_{12}$ (#) with CO_2 in thf-d_8 (+) at 26 °C.

Alternative approach to Gallium Methylene

2.1 Introduction

While the chemistry and especially the synthesis of $[Ga_8(CH_2)_{12}]$ (**A3**) has been well investigated with the precursor $[Cp*_2Lu(GaMe_4)]$, we wondered whether there is another possibility to synthesize the homoleptic gallium methylene. Therefore, the *ansa*-Cp precursor $[Me_2Si(Cp^{Me4}H)_2]$[135-136] was synthesized to attempt a similar route as for $[Cp*_2Lu(GaMe_4)]$, aiming at $[Me_2Si(Cp^{Me4})_2Lu(GaMe_4)]$ and its reaction with an excess of $GaMe_3$ (**A10**).

2.2 Results and Discussion

For the synthesis of gallium methylene, the precursor $[Cp*_2Lu(GaMe_4)]$ is reacted with an excess of trimethylgallium to generate $[Ga_8(CH_2)_{12}]$ (**A3**) as a pale yellow precipitate.[54] While studying the reactivity of gallium methylene, we also wondered if the rare-earth-metal precursor could be modified in order to generate $[Ga_8(CH_2)_{12}]$ (**A3**). We decided to use an *ansa*-Cp^{Me4} ligand $[Me_2Si(Cp^{Me4}H)_2]$ that is already established in d- and f-element chemistry for some time.[136-137] The synthesis route is depicted in Scheme 26.

Following the synthesis route toward **C4**, colorless crystals could be obtained after heating the mixture for 2 h at 130 °C (see Figure 9). The ^{1}H NMR spectrum of **C4** shows two singlets at 1.85 and 1.84 ppm that are assigned to the Cp-Me groups with an integral of 24 H. Furthermore, the Al–CH_3 groups resonate as two doublets at –0.35 and –0.41 ppm with an integral of 12 H. The Si–CH_3 groups provide a singlet at 0.85 ppm with an integral of 6 H, which confirms that the structure in solution is in accord with the solid-state structure. X-ray crystallographic structure determination was performed for complex **C6**. Due to the coordination of *ansa*-Cp ligand, the Ct-Si-Ct angle of 97.2° is relatively acute. For comparison, the bite angles of the $Cp*_2Lu$ unit in $[Cp*_2Lu(AlMe_4)]$ and $[Cp*_2Lu(GaMe_4)]$ are 138.29° and 139.59°, respectively.[54] Particularly remarkable is that in **C6**, the bridging methyl groups between aluminum and lutetium form an almost perfect plane (interplanar angle 4.9°). The Lu–C(Me) distances are 2.499(3) - 2.513(4) Å which are slightly shorter than in metallocene $[Cp*_2Lu(AlMe_4)]$.[54] The Al–C(Me) distances are 2.080(4) – 2.082(4) Å for the bridging methyl groups and 1.976 – 1.960(4) Å for the terminal methyl groups are in the same range of other Al–Me compounds like $Al(CH_3)_3$.[138]

$$Me_2SiCl_2 + 2\ LiCp^{Me4} \xrightarrow[-\ 2\ LiCl]{thf,\ 5\ d,\ rt} Me_2Si(Cp^{Me4}H)_2$$

C3

1) Lu(AlMe$_4$)$_3$
2) 2h, 130 °C
n-hexane

- CH$_4$
- AlMe$_3$

$$Me_2Si(Cp^{Me4})_2LuMe(THF) \xleftarrow{thf,\ 18\ h,\ rt} Me_2Si(Cp^{Me4})_2Lu(AlMe_4)$$

C5   **C4**

1) 2 GaMe$_3$
2) 2 h, rt
toluene

$$Me_2Si(Cp^{Me4})_2Lu(GaMe_4)$$

C6
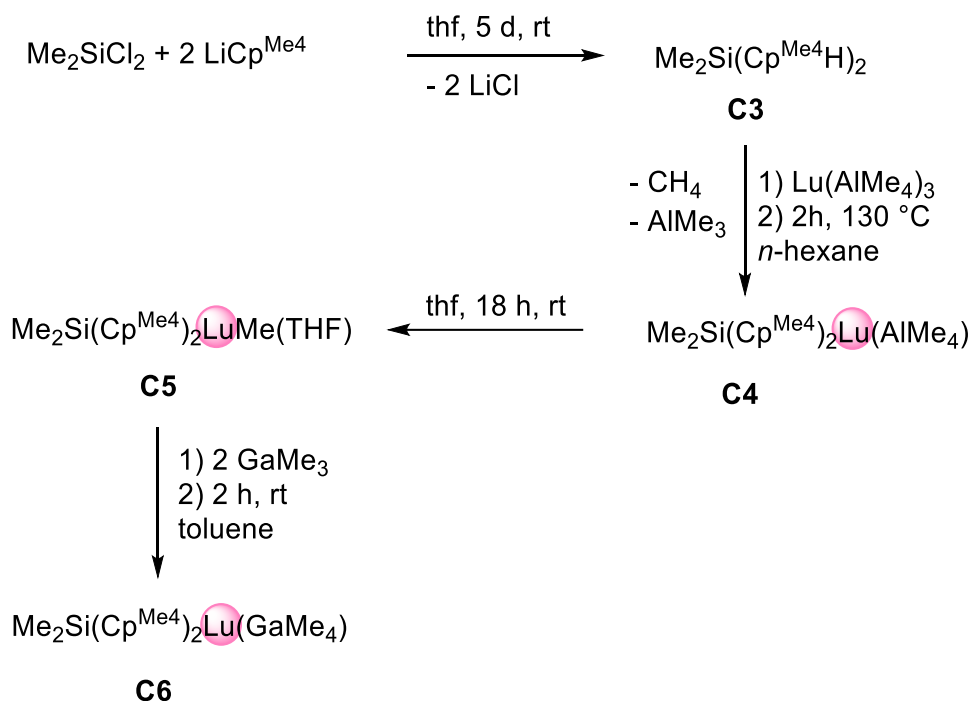
Scheme 26. Synthesis of Me$_2$Si(Cp^{Me4})$_2$Ln(MMe$_4$) (M = Al, Ga).
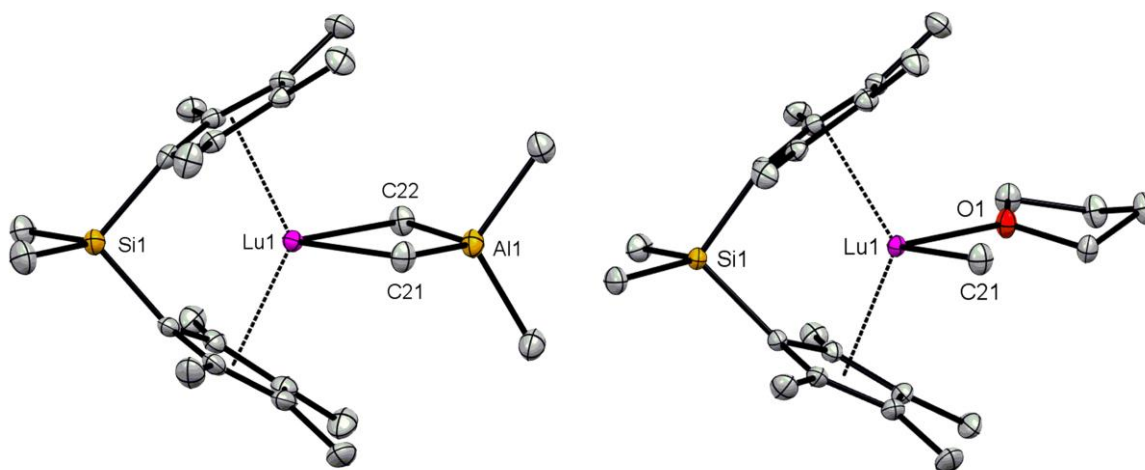
Figure 9. Crystal structures of compounds **C4** (left) and **C5** (right).

The next target was to synthesize the lutetocene methyl complex by donor-assisted cleavage of the MMe$_4$ unit. For this purpose, complex **C4** was mixed with THF and layered with *n*-hexane. This resulted in a slight color change from colorless to yellow. Single crystals of **C5** were obtained overnight (see Figure 9). The ^{1}H NMR spectrum of **C5** in C$_6$D$_6$ in shows one set of signals. The signals of the coordinated THF signals are at 3.13 and 1.02 ppm with an integral ratio of 4 H each, the Si-Me$_2$ group resonates at two singlets at 1.07 and 0.97 ppm and the Lu–

Me moiety resonates at –0.76 ppm. A more precise assignment of the splitted Cp-Me signals proved to be difficult. Furthermore, the Lu–C(Me) distances is 2.361(2) Å and is significantly shorter than the distance of the bridging methyls in compound **C4** but in the same range like in the [Cp*$_2$LuMe(thf)] congener.[54] The Ct-Si-Ct bite angle of 100° is more obtuse compared to **C4**. Nevertheless, the synthesis of the *ansa*-metallocene is quite straightforward.

The addition of three equivalents of trimethylgallium to **C5** afforded the *ansa*-metallocene complex [Me$_2$Si(Cp^{Me4})$_2$Lu(GaMe$_4$)] (**C6**) (see Scheme 26). After removing the solvent, the colorless precipitate was redissolved in toluene, filtered, and crystallized at –40 °C to give the desired structure **C6**.
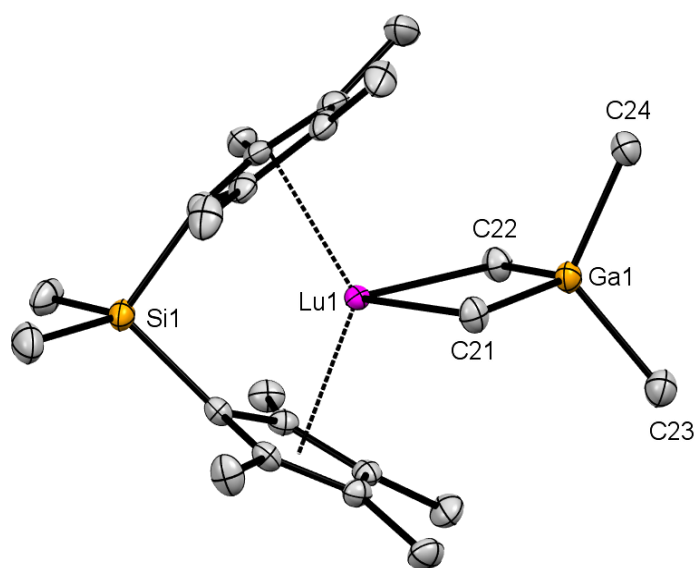
Figure 10. Crystal structure of compound **C6**.

The ^{1}H NMR spectrum of **C6** revealed a similar signal pattern as that of compound **C4** with two singlets for the Cp-CH$_3$ protons at 1.89 and 1.84 ppm with an integral of 12:12. The Si–CH$_3$ group resonates as singlet at 0.86 ppm with an integral of 6 H. Furthermore, two singlets at –0.10 ppm and –0.34 ppm are assigned to the bridging and terminal methyl groups of the GaMe$_4$ moiety with integrals of 6:6, which is in accord with the structure in the solid state. The Ct-Si-Ct angle of 96° is slightly more acute compared to **C4** and **C5**. Nevertheless, the Lu–C(Me) distances of 2.505(4) – 2.517(4) Å are comparable to the distances in compound **C6** and lutetocene [Cp*$_2$Lu(AlMe$_4$)].[54] The Ga–C(Me) distances of 1.977(4) - 1.989(4) Å and 2.102(4)

– 2.118(4) Å for the terminal and bridging methyl groups are in the expected range. Interestingly, the distances to the terminal methyls are in line with [Cp*$_2$Lu(GaMe$_4$)], while the Ga–C(μ-CH$_3$) distances are significantly shorter in **C6** than in **C4**.

$$\text{Me}_2\text{Si}(\text{Cp}^{\text{Me4}})_2\text{LuGaMe}_4 \quad \xrightarrow[\text{2) 130 °C, 3d}]{\text{1) 8 GaMe}_3} \quad\!\!/\!/\!\!\longrightarrow \quad \text{Ga}_8(\text{CH}_2)_{12}$$

C6   **A3**
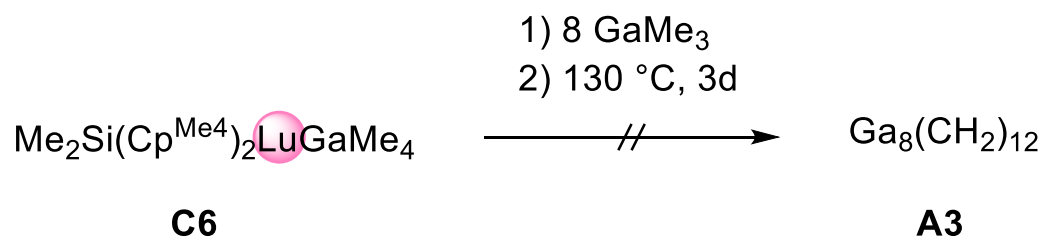
Scheme 27. Synthesis attempt toward homoleptic gallium methylene **A3**.

Next, the envisioned synthesis of gallium methylene by metal-assisted C–H bond activation of GaMe$_3$ with *ansa*-metallocene **C6** was investigated (see Scheme 27), but unfortunately, precipitation of gallium methylene was not observed.

Due to the good accessibility of the *ansa*-Cp complexes **C4** and **C6**, we also examined the reactions to the corresponding lutetium bis(indenyl) complex. For this purpose, complex [(Ind)$_2$Lu(AlMe$_4$)] was synthesized according to literature procedures.[139] Upon reaction with THF, the corresponding product [(Ind)$_2$LuMe(thf)] (**C7**) was obtained (see Figure 11). Further derivatization of **C7** of putative complex [(Ind)$_2$Lu(GaMe$_4$)] failed.
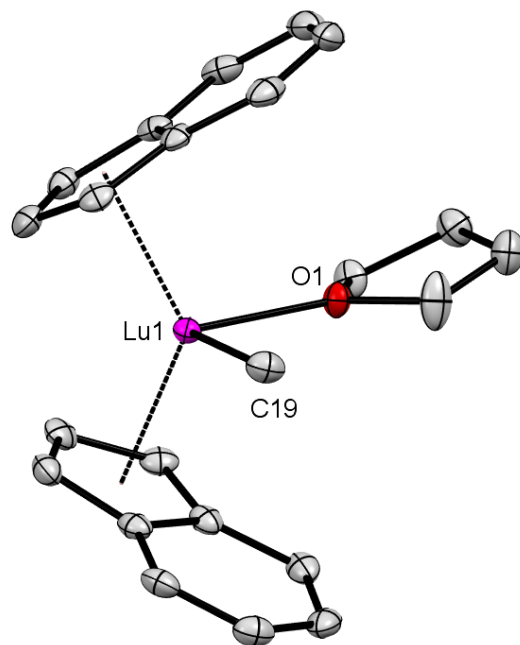
Figure 11. Crystal structure of **C7**.

Experimental Section

General Procedures. All manipulations were performed under an inert atmosphere (Ar) using a glovebox (*MBraun* 200B; <0.1 ppm O_2, <0.1 ppm H_2O), or according to standard Schlenk techniques in oven-dried glassware. The solvents were purified with Grubbs type columns (MBraun SPS, solvent purification system) and stored in a glovebox. $Me_2Si(Cp^{Me4}H)_2$,[136] $Lu(AlMe_4)_3$[140] and $(Ind)_2LuAlMe_4$[139] were synthesized according to literature procedures. C_6D_6 were purchased from *Euriso-top* and pre-dried over NaK alloy and filtered prior use. NMR spectra were recorded at 26 °C with a Bruker AVII+400 (^{1}H, 400.13 MHz; ^{13}C, 100.61 MHz) and Bruker AVII+500 (^{1}H, 500.13 MHz; ^{13}C, 125.76 MHz) using J. Young valve NMR tubes. ^{1}H NMR resonances are referenced to the solvent residual signal and reported in parts per million (ppm) relative to tetramethylsilane. Analyses of NMR spectra were performed with Bruker TopSpin 3.6.0. Infrared spectra were measured with a Bruker Vertex 70 using as Nujol mull sample with CsI plates. The IR data were converted using the Kubelka-Munk refinement ($\tilde{v}$= 4000 – 400 cm^{-1}). Elemental analyses (C, H) were performed on an *Elementar vario MICRO cube.*

$Me_2Si(Cp^{Me4})_2LuAlMe_4$ (C4). In a pressure tube, a mixture of 0.5 equivalents $Lu(AlMe_4)_3$ (145 mg, 0.33 mmol) and 1 equivalent of $Me_2Si(Cp^{Me4}H)_2$ (200 mg, 0.66 mmol) in toluene were heated to 130 °C. After stirring for 16 h all volatile parts were removed under reduced pressure and the resulting colorless solid was redissolved in 2 mL toluene to yield colorless crystals of $Me_2Si(Cp^{Me4})_2LuAlMe_4$ (**C6**) (135 mg, 0.229 mmol, 73 %). ^{1}H NMR (C_6D_6, 400.13 MHz, 26 °C): δ = 1.83 (s, 12 H, *o*–C(CH_3)), 1.82 (s, 12 H, *m*-C(CH_3)), 0.83 (s, 6 H, Si–CH_3), –0.38 (s, 6 H, Al−CH_3), –0.43 (s, 6 H, Al–CH_3) ppm. ^{13}C{^{1}H} NMR (100.6 MHz, C_6D_6, 26 °C): δ = 127.2 (Cp–*C*), 120.4 (Cp–*C*), 102.1(Cp–*C*), 14.4 (Cp–*C*(Me)), 11.7 (Cp–*C*(Me)), 11.4 (Al–*C*(Me)), 4.1 (Al–*C*(Me)) ppm; elemental analysis (%) calcd. for $C_{26}H_{48}LuAlSi$ (590.27): C 52.87, H 8.19; found: C 52.55, H 8.91. Due to the insufficient resolution, the carbon atoms cannot be assigned.

$Me_2Si(Cp^{Me4})_2LuMe(THF)$ (C5). In a glovebox, $Me_2Si(Cp^{Me4})_2Lu(AlMe_4)$ (61 mg, 0.11 mmol) was dissolved in 1.5 mL of THF and layered with 4 mL *n*-hexane. The mixture was stored at –40 °C for 2 d to afford colorless needles of $Me_2Si(Cp^{Me4})_2LuMe(THF)$ (**C5**) (40 mg, 0.071 mmol, 66 %). ^{1}H NMR (C_6D_6, 400.13 MHz, 26 °C): δ = 3.13 (m, 4 H, O–CH_2CH$_2$), 2.23 (s, 6 H, Cp–CH_3), 2.20 (s, 6 H, Cp−CH_3), 2.18 (s, 6 H, Cp–CH_3), 1.63 (s, 6 H, Cp–CH$_3$), 1.07 (s, 3 H, Si–CH$_3$), 1.02 (m, 4 H, OCH$_2$CH_2), 0.96 (s, 3 H, Si–CH$_3$), 0.76 (s, 3 H, Lu–CH$_3$) ppm. ^{13}C{^{1}H} NMR (100.6 MHz, C_6D_6, 26 °C): δ = 124.3 (Cp–C), 122.8 (Cp–C), 117.6 (Cp–C), 102.1 (Cp–C), 70.5 (OCH$_2$CH$_2$), 25.2 (OCH$_2$$CH_2$), 21.8, 14.9, 14.8, 12.3, 11.1, 4.8, 4.5 ppm; elemental analysis (%) calcd. for $C_{25}H_{41}LuO$ (560.23): C 53.56, H 7.37; found: C 53.94, H 8.18. Due to the insufficient resolution, the carbon atoms cannot be assigned.

$Me_2Si(Cp^{Me4})_2LuGaMe_4$ (C6). In a glovebox, a solution of $Me_2Si(Cp^{Me4})_2LuMe(THF)$ (**C7**) (81 mg, 0.14 mmol) was dissolved in 4 mL of toluene, treated with $GaMe_3$ (49.8 mg, 0.43 mmol) and stirred for 2 h at ambient temperature. After stirring for 2 h all volatiles were removed under reduced pressure and the resulting colorless solid was redissolved in 2 mL toluene and stored 16 h at –40 °C to yield colorless crystals of $Me_2Si(Cp^{Me4})_2Lu(GaMe_4)$ (**C8**) (79 mg, 0,131 mmol, 94 %). ^{1}H NMR (C_6D_6, 400.13 MHz, 26 °C): δ = 1.88 (s, 12 H, *o*-C(CH_3), 1.84 (s, 12 H, *m*-C(CH_3)), 0.85 (s, 6 H, Si–(CH_3)), –0.14 (s, 6 H, Ga–(μ$_2$–CH$_3$)), –0.33 (s, 6 H, Ga–(CH$_3$)) ppm. ^{13}C{^{1}H} NMR (100.6 MHz, C_6D_6, 26 °C): δ = 126.6 (Cp–

C), 119.8 (Cp–*C*), 14.1 (Cp–*C*(Me)), 11.3 (Cp–*C*(Me)), 3.7 (Al–*C*(Me)) ppm ; elemental analysis (%) calcd. for $C_{24}H_{42}LuGa$ (602.17): C 47.78, H 7.02; found: C 47.89, H 7.33.

(Ind)₂LuMe(THF) (C7). In a glovebox a solution of $Lu(AlMe_4)_3$ (100 mg, 0.23 mmol) in toluene (2 mL) was added to a suspension of lithium indenyl (56 mg, 0.46 mmol) in toluene (2 mL). After 16 h at ambient temperature, the mixture was centrifuged, washed with toluene (3 x 3 mL) and reduced under vacuo. Storage of this solution at –40 °C gave **C7** as colorless crystals. Due to impurities in the crude product, no yield was determined. ^{1}H NMR (C_6D_6, 400,13 MHz, 26 °C): = 7.53-7.35 (m, 4H, 5/8 IndH), 6.92 (s, 4H, 6/7 IndH), 6.29 (m, 2 H, 2 IndH), 6.06-5.97 (m, 4 H, 1/3 IndH), 2.73 (s, 4 H, OC*H₂*CH₂), 0.91 (s, 4 H, OCH₂C*H₂*), –0.90 (s, 3 H, Lu–(C*H₃*) ppm.
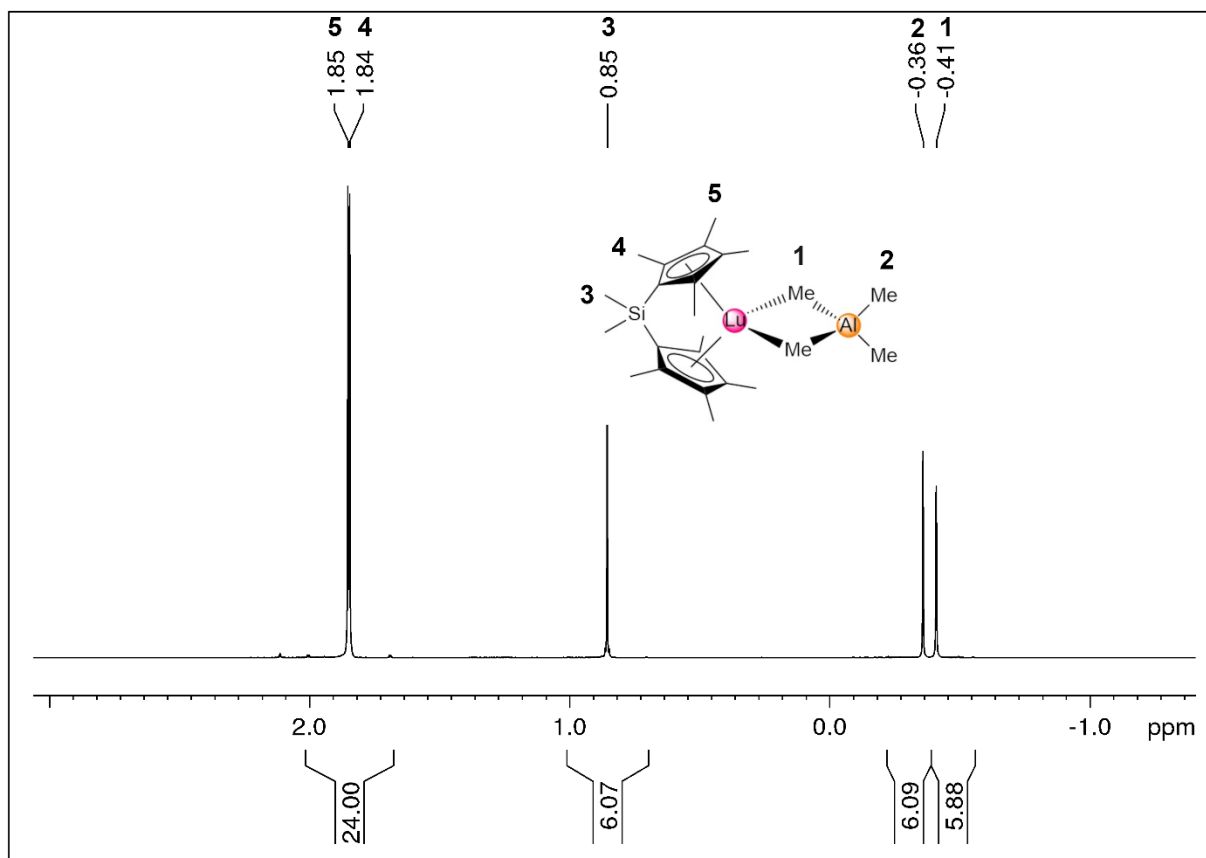
Figure 12. ^{1}H NMR spectrum of compound **C4** in C$_6$D$_6$ at 26 °C.
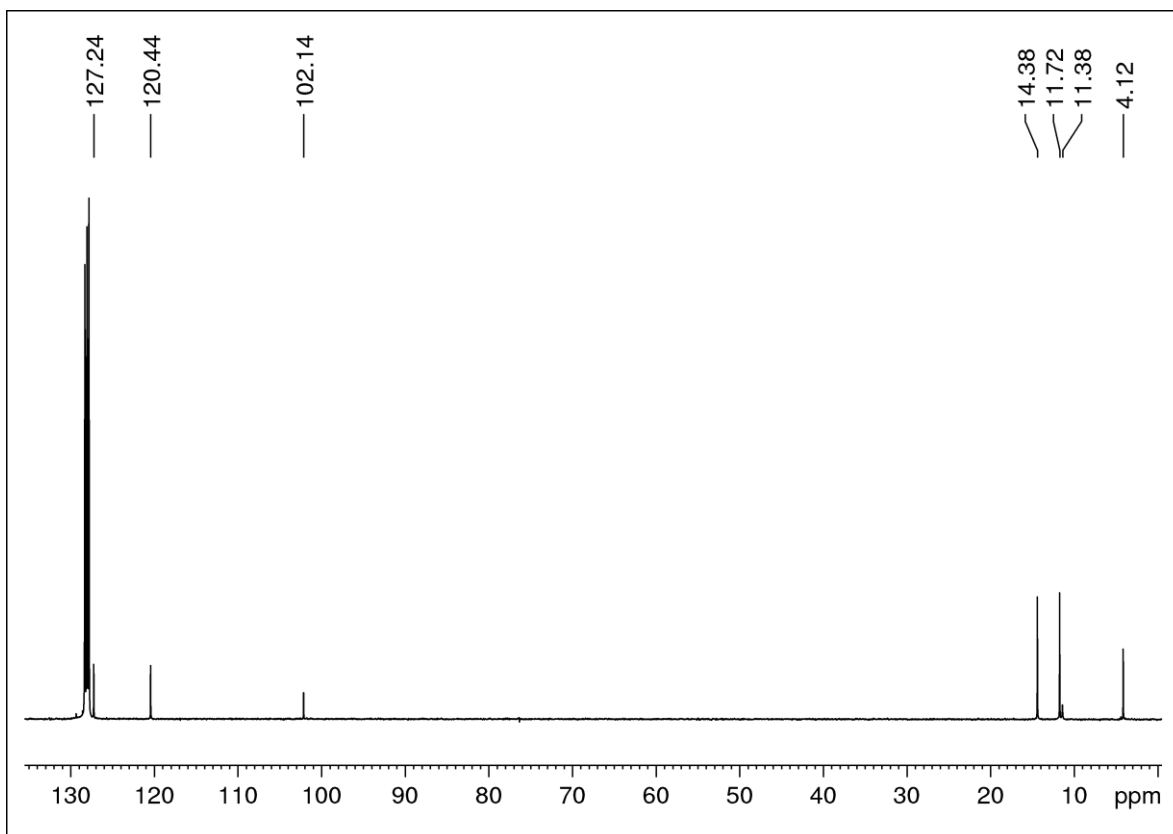
Figure 13. ^{13}C NMR spectrum of compound **C4** in C$_6$D$_6$ at 26 °C.
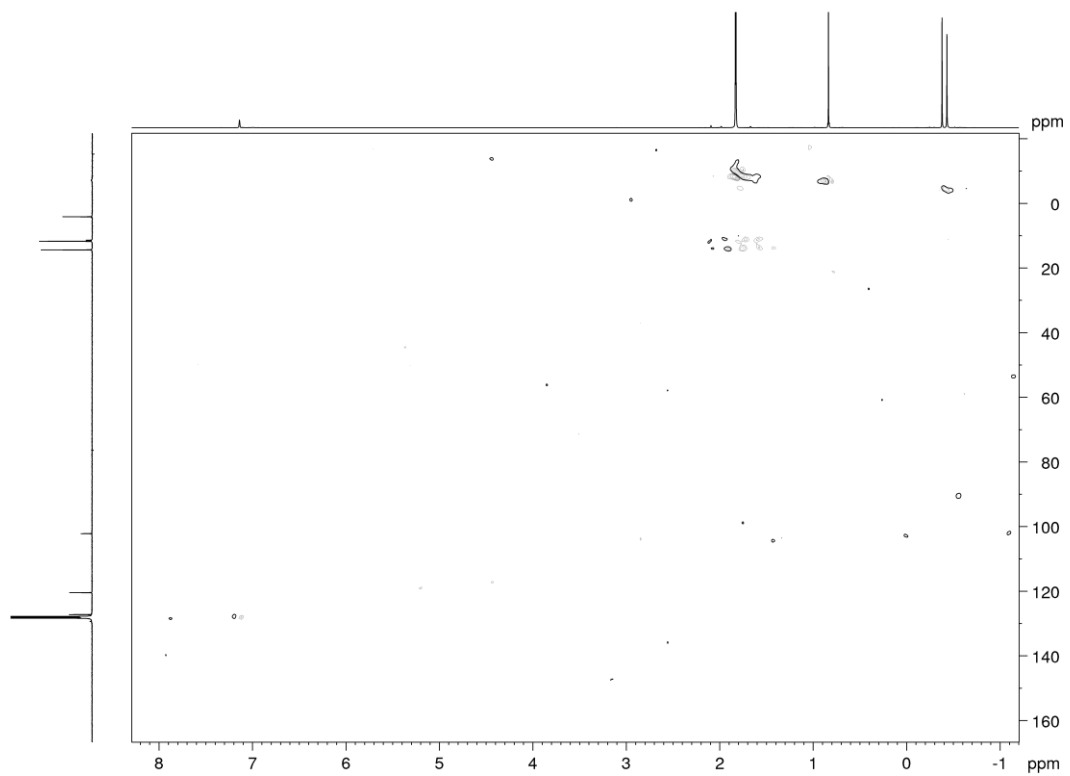
Figure 14. ^{1}H-^{13}C HSQC NMR spectrum of compound **C4** in C_6D_6 at 26 °C.
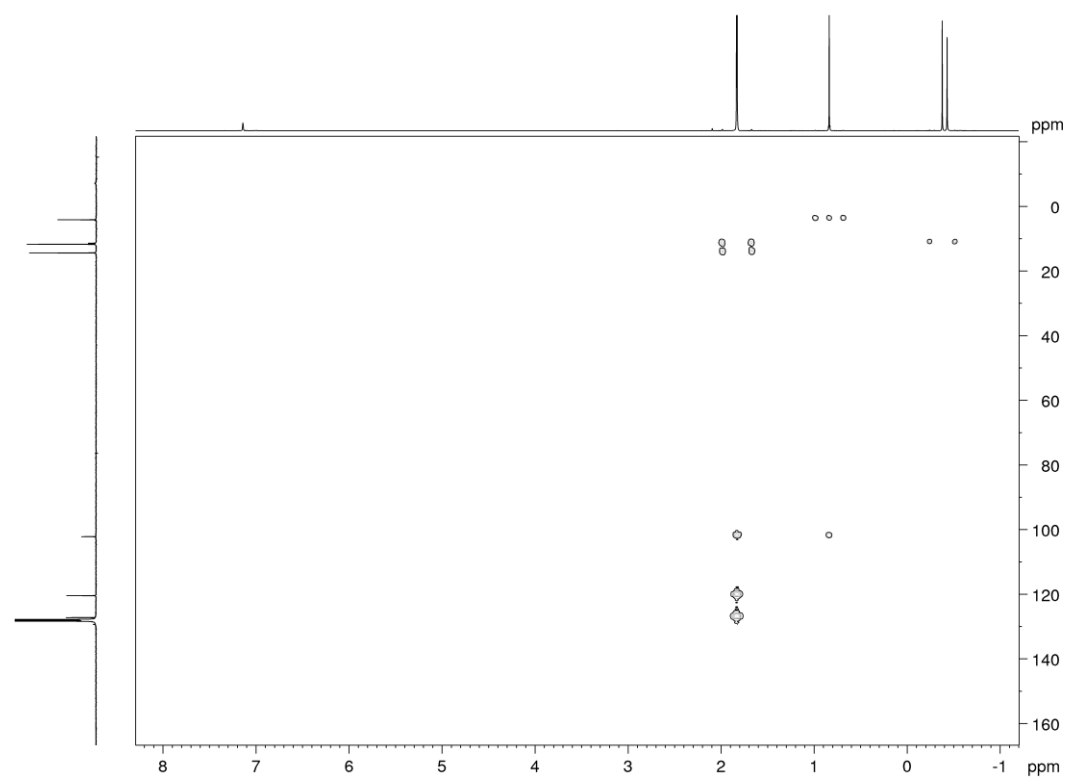
Figure 15. ^{1}H-^{13}C HMBC NMR spectrum of compound **C4** in C_6D_6 at 26 °C.
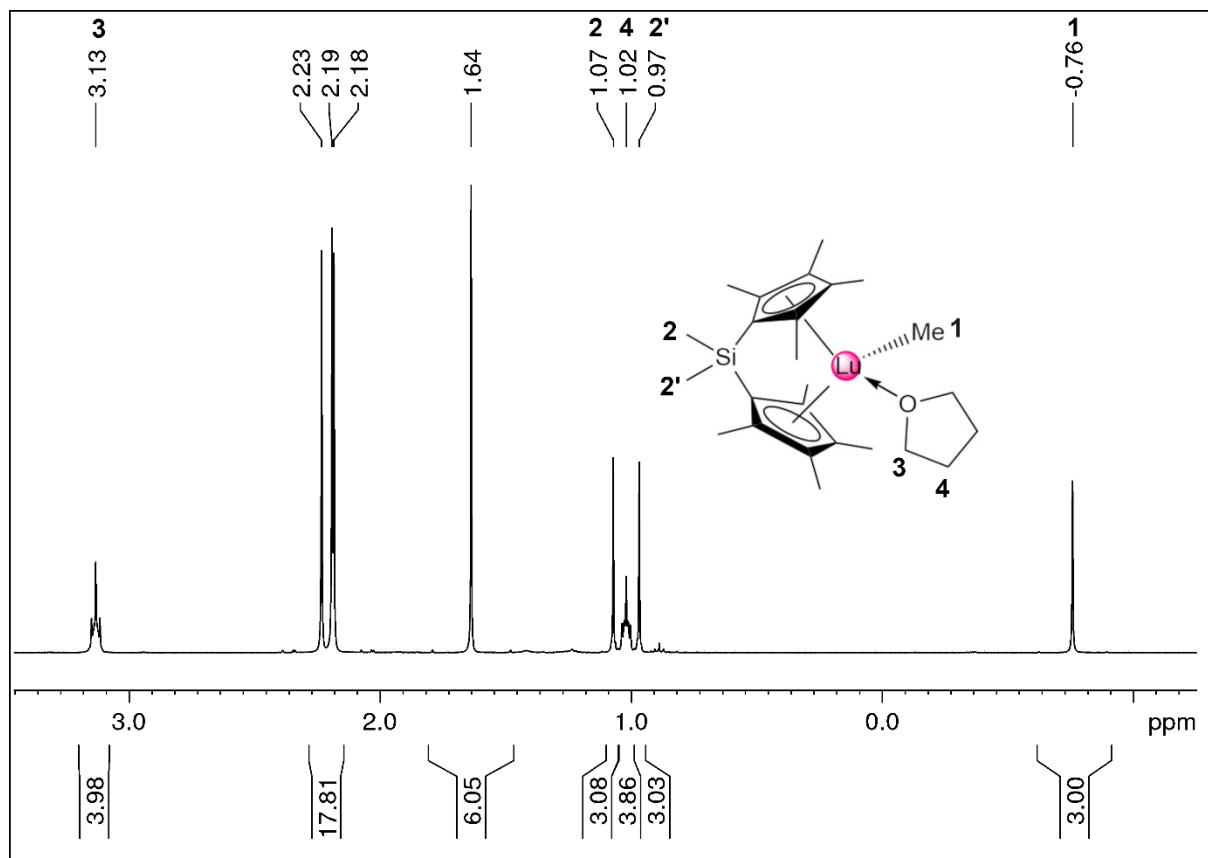
Figure 16. ^{1}H NMR spectrum of compound **C5** in C_6D_6 at 26 °C.
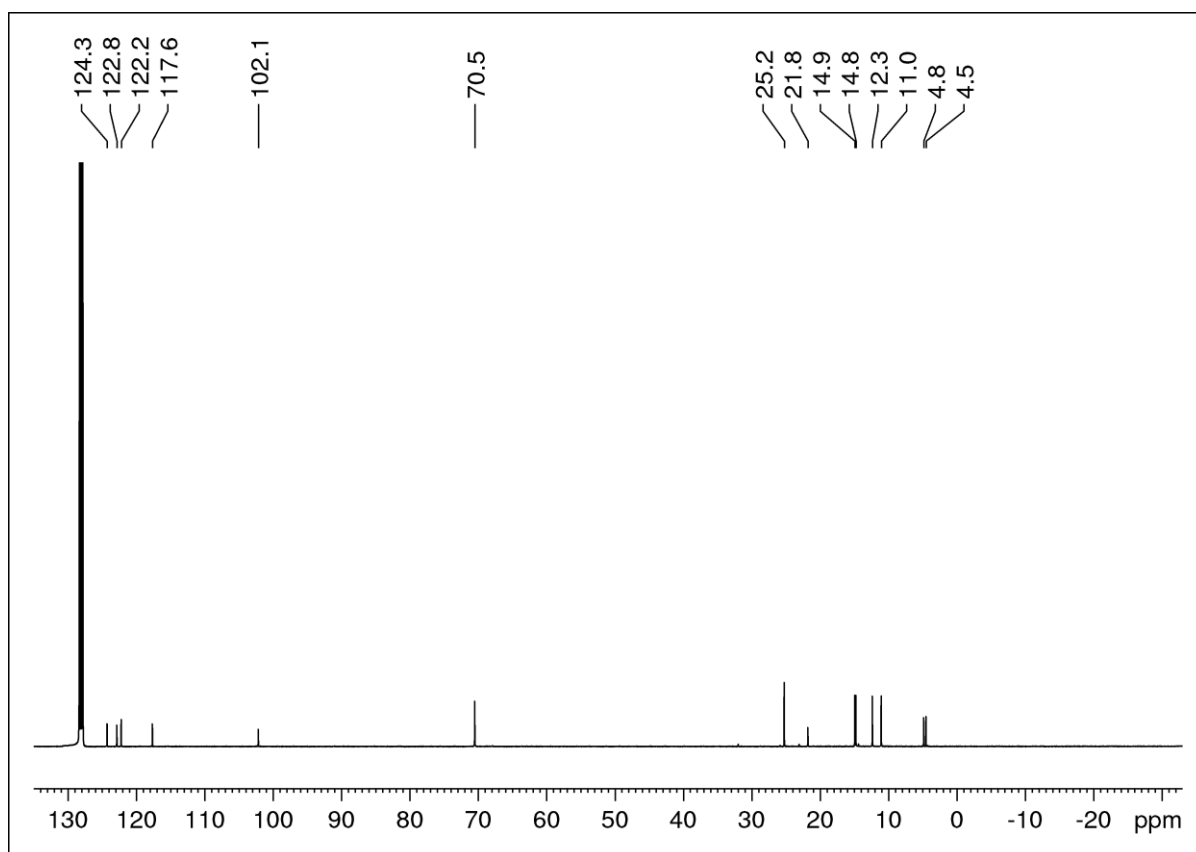
Figure 17. ^{13}C NMR spectrum of compound **C5** in C_6D_6 at 26 °C.
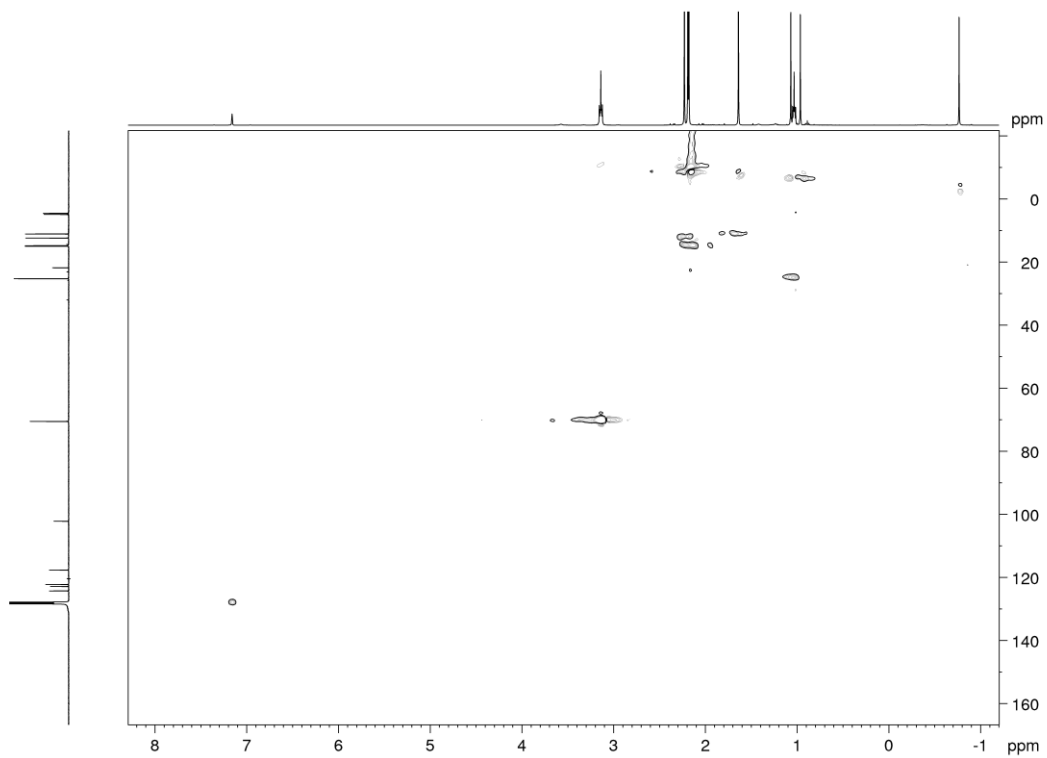
Figure 18. ^{1}H-^{13}C HSQC NMR spectrum of compound **C5** in C$_6$D$_6$ at 26 °C.
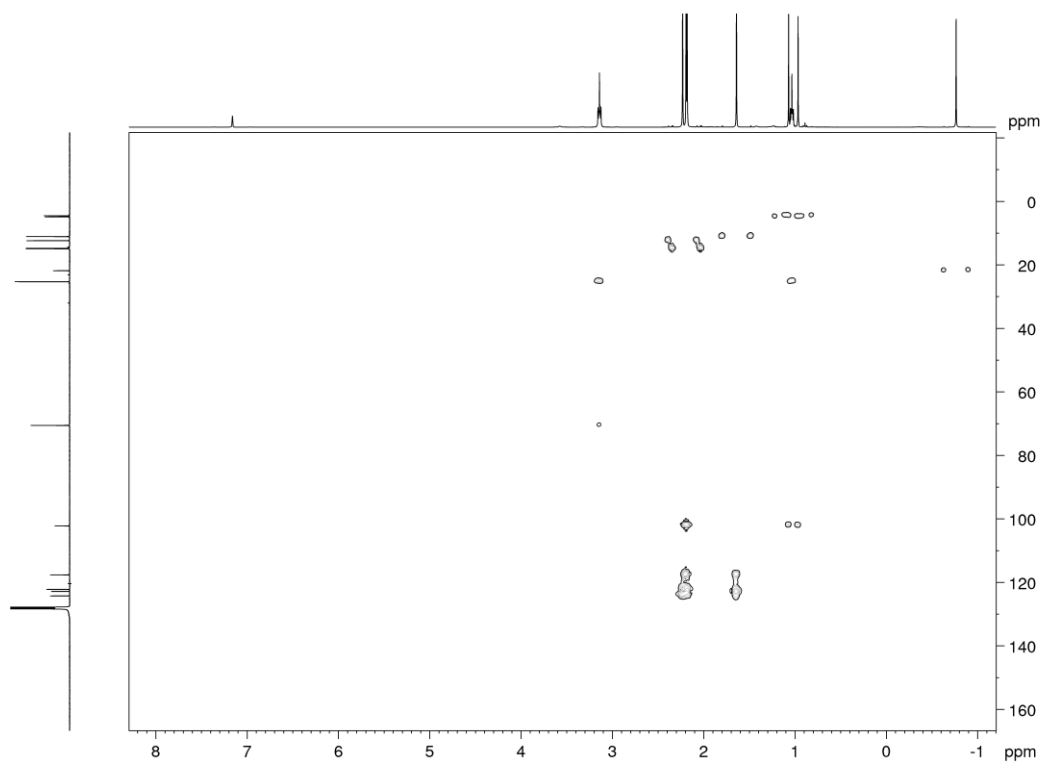
Figure 19. ^{1}H-^{13}C HMBC NMR spectrum of compound **C5** in C$_6$D$_6$ at 26 °C.
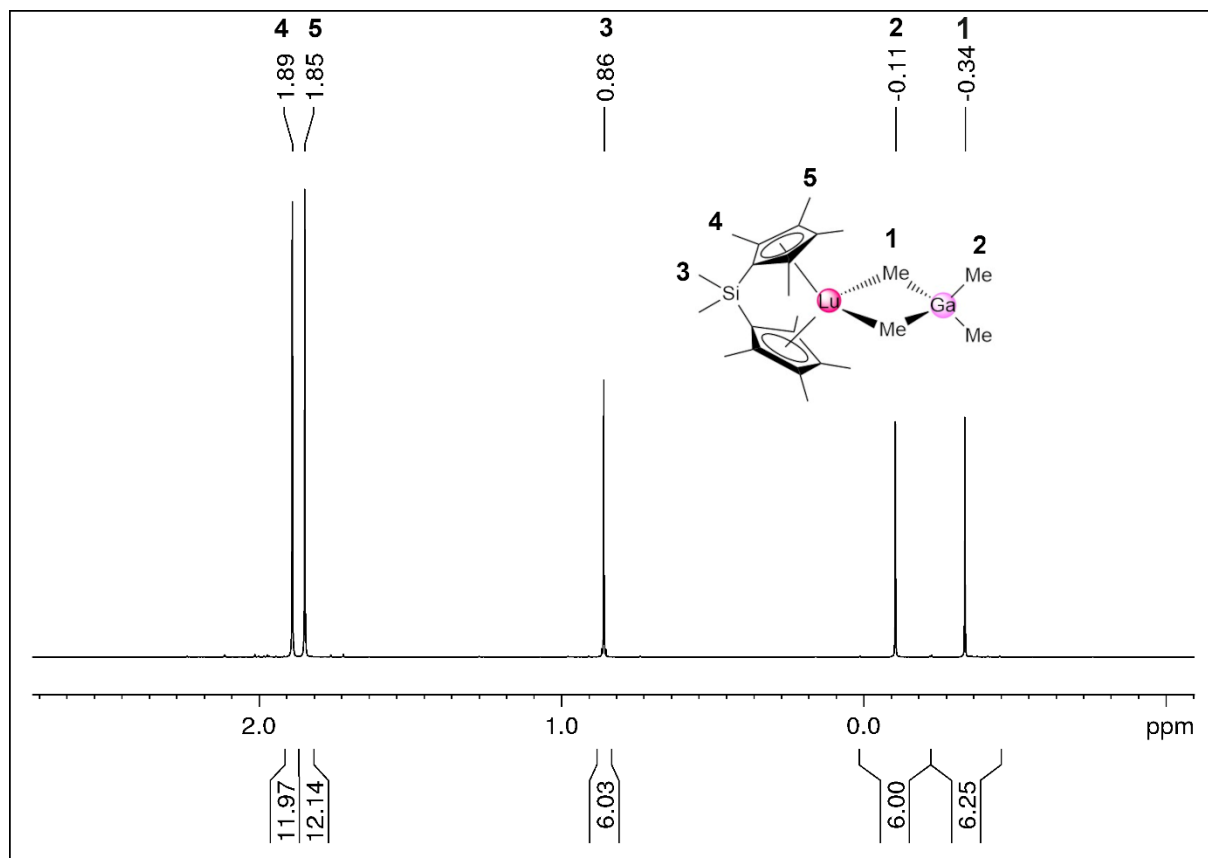
Figure 20. ^{1}H NMR spectrum of compound **C6** in C_6D_6 at 26 °C.
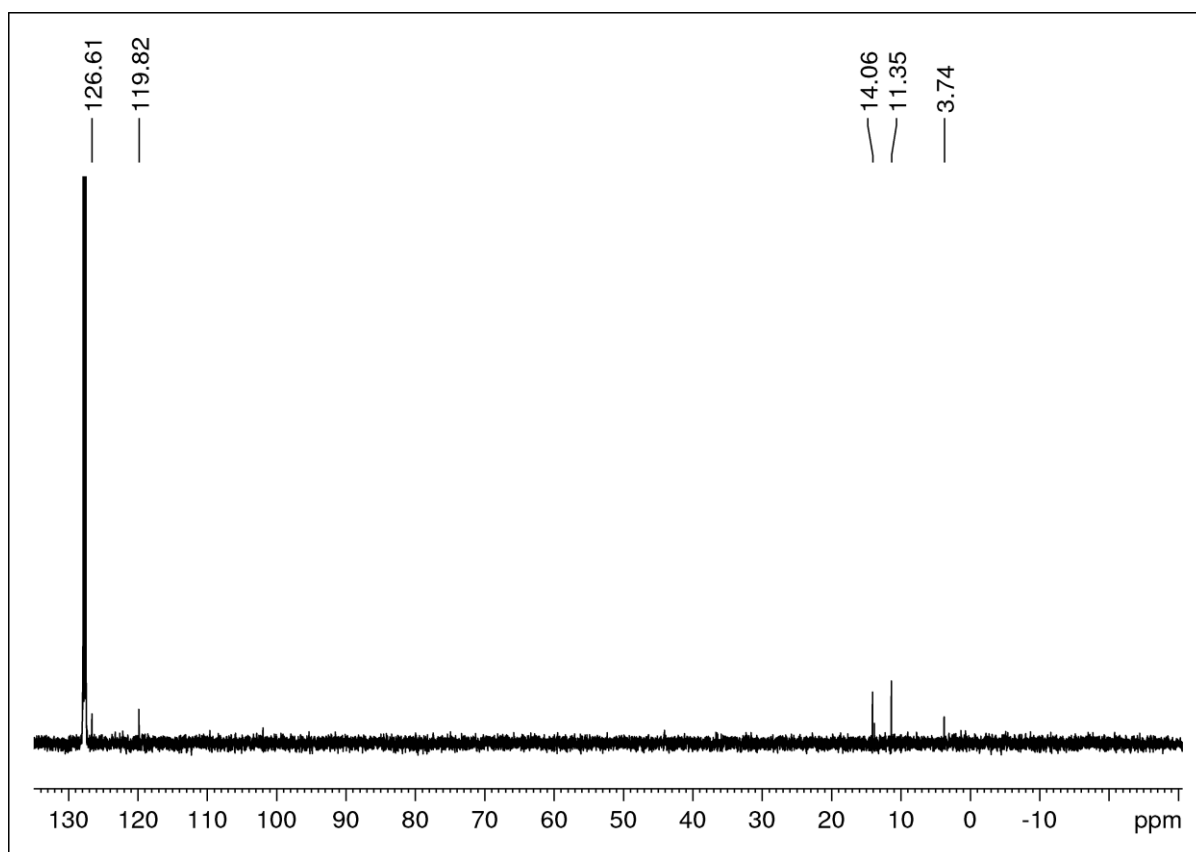
Figure 21. ^{13}C NMR spectrum of compound **C6** in C_6D_6 at 26 °C.
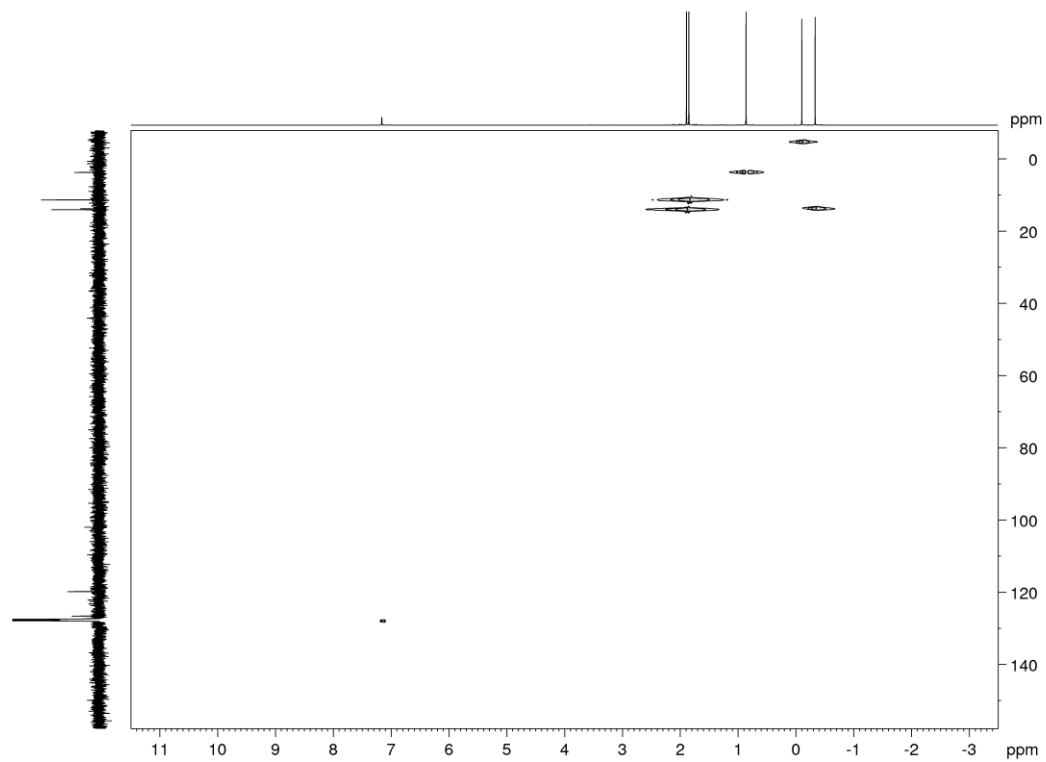
Figure 22. ^1H-^{13}C HSQC NMR spectrum of compound **C6** in C_6D_6 at 26 °C.
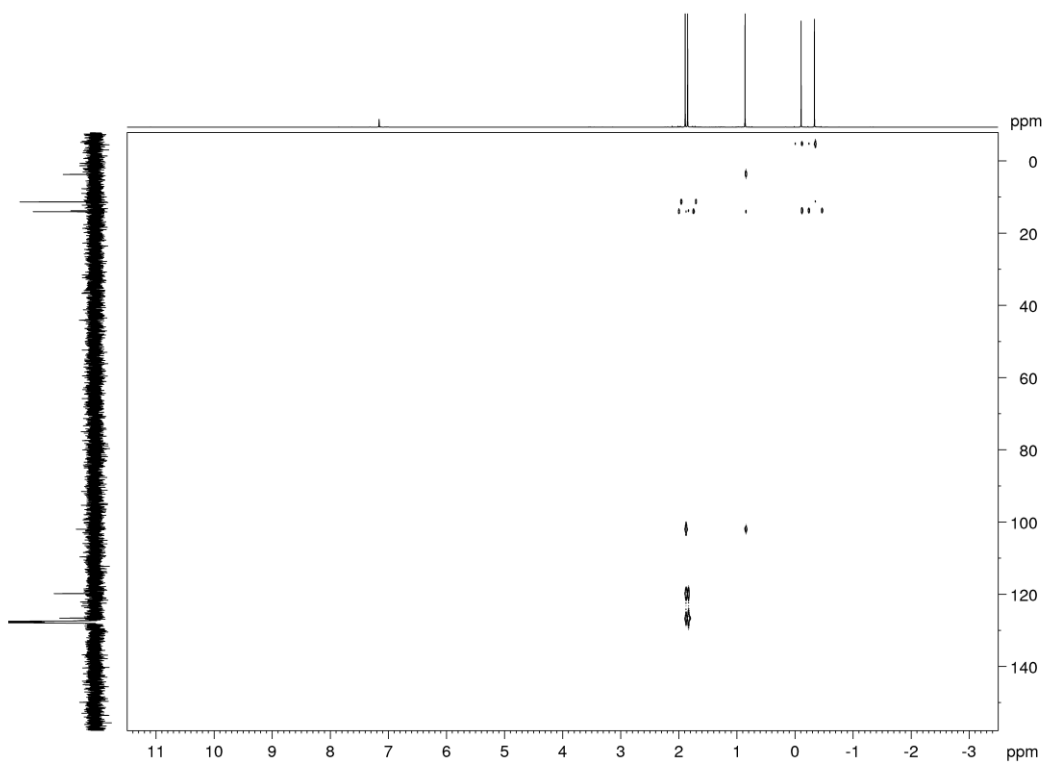
Figure 23. ^1H-^{13}C HMBC NMR spectrum of compound **C6** in C_6D_6 at 26 °C.
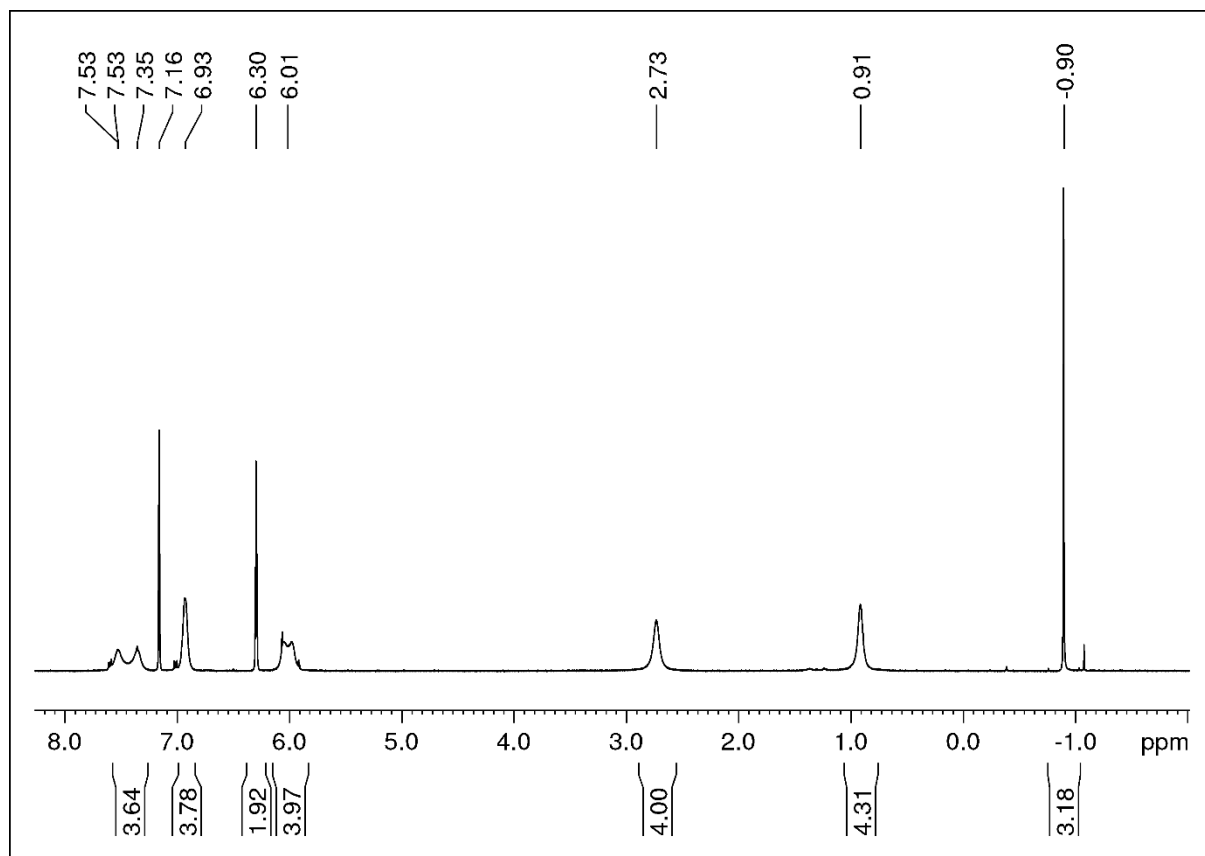
Figure 24. ^{1}H NMR spectrum of compound **C7** in C_6D_6 at 26 °C.

Table 2. Comprehensive crystallographic data for compounds **C4 – C7**

	C4	**C5**	**C6**	**C7**
formula	$C_{24}H_{42}AlLuSi$	$C_{25}H_{41}LuOSi$	$C_{24}H_{42}GaLuSi$	$C_{23}H_{25}LuO$
M [g·mol^{-1}]	560.61	560.64	603.35	492.40
λ [Å]	0.71073	0.71073	0.71073	0.71073
color	colorless	colorless	colorless	colorless
crystal dimensions [mm]	0.259 x 0.198 x 0.163	0.203 x 0.154 x 0.149	0.203 x 0.154 x 0.149	0.189 x 0.151 x 0.109
crystal system	orthorombic	Triclinic	orthorombic	orthorombic
space group	$P2\bar{1}2\bar{1}2\bar{1}$	$P\bar{1}$	$P2\bar{1}2\bar{1}2\bar{1}$	$P2\bar{1}2\bar{1}2\bar{1}$
a [Å]	10.0792(8)	10.0487(3)	10.0873(7)	8.509(2)
b [Å]	15.3891(12)	10.1377(3)	15.3714(11)	12.521(3)
c [Å]	15.7638(2)	13.7149(4)	15.7460(11)	17.759(4)
α [°]	90	70.3	90	90
β [°]	90	71.6	90	90
γ [°]	90	65.9	90	90
V [Å^3]	2445.1(3)	1174.96(6)	2441.5(3)	1892.0(8)
Z	4	2	4	4
F(000)	1136	568	1208	968
T [K]	100(2)	173(2)	100(2)	100(2)
ρ_{calcd} [g·cm^{-3}]	1.523	1.585	1.641	1.729
μ[mm^{-1}]	4.129	4.265	5.179	5.225
Data / restraints / parameters	7462 / 0 / 280	7190 / 0 / 264	7448 / 0 / 280	5765 / 0 / 231
Goodness of fit	1.003	1.108	0.999	1.036
R_1 (I > 2σ (I))[a]	0.0190	0.0157	0.0191	0.0230
$_\omega R_2$ (all data)[b]	0.0413	0.0397	0.0422	0.0460

D

Bibliography

[1]   L. Chugaev, M. Grigorizeva, *J. Russ. Chem. Soc.* **1915**, *47*, 776-782.

[2]   A. Burke, A. L. Balch, J. H. Enemark, *J. Am. Chem. Soc.* **1970**, *92*, 2555-2557.

[3]   K. Ziegler, K. Nagel, M. Patheiger, *Z. Anorg. Allg. Chem.* **1955**, *282*, 345-351.

[4]   M. P. K. Ziegler, K.Nagel, *United States Patent Office* **1960**.

[5]   H. Kawa, B. C. Manley, R. J. Lagow, *Polyhedron* **1988**, *7*, 2023-2025.

[6]   J. A. Gurak, J. W. Chinn Jr, R. J. Lagow, H. Steinfink, C. S. Yannoni, *Inorg. Chem.* **1984**, *23*, 3717-3720.

[7]   J. A. Gurak, J. W. Chinn Jr, R. J. Lagow, *J. Am. Chem. Soc.* **1982**, *104*, 2637-2639.

[8]   G. Stucky, M. Eddy, W. Harrison, R. Lagow, H. Kawa, D. Cox, *J. Am. Chem. Soc.* **1990**, *112*, 2425-2427.

[9]   E. O. Fischer, A. Maasböl, *Angew. Chem. Int. Ed. Engl.* **1964**, *3*, 580-581.

[10]   H. Lehmkuhl, R. Schäfer, *Tetrahedron Lett.* **1966**, *7*, 2315-2320.

[11]   M. R. Ort, E. H. Mottus, *J. Organomet. Chem.* **1973**, *50*, 47-52.

[12]   H. Sinn, H. Hinck, F. Bandermann, H. Grützmacher, *Angew. Chem.* **1968**, *80*, 190-190.

[13]   F. N. Tebbe, G. W. Parshall, G. S. Reddy, *J. Am. Chem. Soc.* **1978**, *100*, 3611-3613.

[14]   R. R. Schrock, *J. Am. Chem. Soc.* **1974**, *96*, 6796-6797.

[15]   C. Wood, *J. Am. Chem. Soc.* **1979**, *101*.

[16]   R. R. Schrock, L. W. Messerle, C. D. Wood, L. J. Guggenberger, *J. Am. Chem. Soc.* **1978**, *100*, 3793-3800.

[17]   S. McLain, C. Wood, L. Messerle, R. Schrock, F. J. Hollander, W. J. Youngs, M. R. Churchill, *J. Am. Chem. Soc.* **1978**, *100*, 5962-5964.

[18]   S. McLain, C. Wood, R. Schrock, *J. Am. Chem. Soc.* **1977**, *99*, 3519-3520.

[19]   R. R. Schrock, *J. Am. Chem. Soc.* **1975**, *97*, 6577-6578.

[20]   W. A. Herrmann, B. Reiter, H. Biersack, *J. Organomet. Chem.* **1975**, *97*, 245-251.

[21]   R. R. Schrock, *Chem. Rev.* **2002**, *102*, 145-180.

[22]   L. C. H. Gerber, L. A. Watson, S. Parkin, W. Weng, B. M. Foxman, O. V. Ozerov, *Organometallics* **2007**, *26*, 4866-4868.

[23]   L. Li, M. Hung, Z. Xue, *J. Am. Chem. Soc.* **1995**, *117*, 12746-12750.

[24] A. Van Asselt, B. J. Burger, V. C. Gibson, J. E. Bercaw, *J. Am. Chem. Soc.* **1986**, *108*, 5347-5349.

[25] R. Schrock, *Acc. Chem. Res.* **1990**, *23*, 158-165.

[26] D. J. Mindiola, *Acc. Chem. Res.* **2006**, *39*, 813-821.

[27] D. S. Breslow, N. R. Newburg, *J. Am. Chem. Soc.* **1959**, *81*, 81-86.

[28] G. Natta, *Angew. Chem.* **1956**, *68*, 393-403.

[29] A. Andresen, H. G. Cordes, J. Herwig, W. Kaminsky, A. Merck, R. Mottweiler, J. Pein, H. Sinn, H. J. Vollmer, *Angew. Chem. Int. Ed. Engl.* **1976**, *15*, 630-632.

[30] W. D. Bare, A. Citra, C. Trindle, L. Andrews, *Inorg. Chem.* **2000**, *39*, 1204-1215.

[31] S. C. Tyerman, G. K. Corlett, A. M. Ellis, T. A. Claxton, *J. Mol. Struct.* **1996**, *364*, 107-119.

[32] J. Kratsch, P. W. Roesky, *Angew. Chem. Int. Ed.* **2014**, *53*, 376-383.

[33] J. Scott, D. J. Mindiola, *Dalton Trans.* **2009**, 8463-8472.

[34] G. R. Giesbrecht, J. C. Gordon, *Dalton Trans.* **2004**, 2387-2393.

[35] H. Schumann, J. Müller, *J. Organomet. Chem.* **1979**, *169*, C1-C4.

[36] K. Aparna, M. Ferguson, R. G. Cavell, *J. Am. Chem. Soc.* **2000**, *122*, 726-727.

[37] T. Cantat, F. Jaroschik, L. Ricard, P. Le Floch, F. Nief, N. Mézailles, *Organometallics* **2006**, *25*, 1329-1332.

[38] T. Cantat, F. Jaroschik, F. Nief, L. Ricard, N. Mézailles, P. Le Floch, *Chem. Commun.* **2005**, 5178-5180.

[39] H. M. Dietrich, K. W. Törnroos, R. Anwander, *J. Am. Chem. Soc.* **2006**, *128*, 9298-9299.

[40] M. A. Khan, C. Peppe, D. G. Tuck, *Organometallics* **1986**, *5*, 525-530.

[41] H. E. Simmons, R. D. Smith, *J. Am. Chem. Soc.* **1958**, *80*, 5323-5324.

[42] W. v. E. Doering, P. LaFlamme, *Tetrahedron* **1958**, *2*, 75-79.

[43] E. C. Ashby, R. Scott Smith, *J. Organomet. Chem.* **1982**, *225*, 71-85.

[44] M. Layh, W. Uhl, *Polyhedron* **1990**, *9*, 277-282.

[45] K. Knabel, H. Nöth, T. Seifert, *Z. Naturforsch., B: Chem. Sci.* **2002**, *57*, 830-834.

[46] W. Uhl, M. Layh, *J. Organomet. Chem.* **1991**, *415*, 181-190.

[47]   W. Uhl, F. Hannemann, W. Saak, R. Wartchow, *Eur. J. Inorg. Chem.* **1998**, *1998*, 921-926.

[48]   W. Uhl, F. Hannemann, *J. Organomet. Chem.* **1999**, *579*, 18-23.

[49]   W. Uhl, M. Koch, M. Heckel, W. Hiller, H. H. Karsch, *Z. Anorg. Allg. Chem.* **1994**, *620*, 1427-1433.

[50]   W. Uhl, M. Layh, *Z. Anorg. Allg. Chem.* **1994**, *620*, 856-862.

[51]   W. Uhl, M. Koch, A. Vester, *Z. Anorg. Allg. Chem.* **1993**, *619*, 359-366.

[52]   W. Uhl, C. Rösener, M. Layh, A. Hepp, *Z. Anorg. Allg. Chem.* **2012**, *638*, 1746-1754.

[53]   W. Uhl, C. Rösener, C. Stefaniak, T. Choy, B. Jasper-Peter, J. Kösters, M. Layh, A. Hepp, *Z. Naturforsch., B: Chem. Sci* **2012**, *67*, 1081-1090.

[54]   M. Bonath, C. Maichle-Mössmer, P. Sirsch, R. Anwander, *Angew. Chem. Int. Ed.* **2019**, *58*, 8206-8210.

[55]   M. E. Thompson, S. M. Baxter, A. R. Bulls, B. J. Burger, M. C. Nolan, B. D. Santarsiero, W. P. Schaefer, J. E. Bercaw, *J. Am. Chem. Soc.* **1987**, *109*, 203-219.

[56]   P. L. Watson, *J. Am. Chem. Soc.* **1983**, *105*, 6491-6493.

[57]   R. Banks, G. C. Bailey, *Industrial & Engineering Chemistry Product Research and Development* **1964**, *3*, 170-173.

[58]   N. Calderon, H. Y. Chen, K. W. Scott, *Tetrahedron Lett.* **1967**, *8*, 3327-3329.

[59]   G. Wittig, U. Schöllkopf, *Chem. Ber.* **1954**, *87*, 1318-1330.

[60]   F. N. Tebbe, G. W. Parshall, D. W. Ovenall, *J. Am. Chem. Soc.* **1979**, *101*, 5074-5075.

[61]   Y. Horikawa, M. Watanabe, T. Fujiwara, T. Takeda, *J. Am. Chem. Soc.* **1997**, *119*, 1127-1128.

[62]   R. R. Schrock, *J. Am. Chem. Soc.* **1976**, *98*, 5399-5400.

[63]   K. C. Ott, E. De Boer, R. H. Grubbs, *Organometallics* **1984**, *3*, 223-230.

[64]   N. A. Petasis, E. I. Bzowej, *J. Am. Chem. Soc.* **1990**, *112*, 6392-6394.

[65]   J. D. Meinhart, E. V. Anslyn, R. H. Grubbs, *Organometallics* **1989**, *8*, 583-589.

[66]   S. H. Pine, *Org React.* **2004**, *43*, 1-91.

[67]   C. Bolm, M. Beller, *Transition metals for organic synthesis, Vol. 1*, Wiley-VCH: Weinheim, **2004**.

[68]   K. Brown-Wensley, S. Buchwald, L. Cannizzo, L. Clawson, S. Ho, D. Meinhardt, J. Stille, D. Straus, R. H. Grubbs, *Pure Appl. Chem.* **1983**, *55*, 1733-1744.

[69]   S. H. Pine, G. S. Shen, H. Hoang, *Synthesis* **1991**, *1991*, 165-167.

[70]   M. H. Ali, P. M. Collins, W. George Overend, *Carbohydr. Res.* **1990**, *205*, 428-434.

[71]   S. H. Pine, R. Zahler, D. A. Evans, R. H. Grubbs, *J. Am. Chem. Soc.* **1980**, *102*, 3270-3272.

[72]   S. H. Pine, R. J. Pettit, G. D. Geib, S. G. Cruz, C. H. Gallego, T. Tijerina, R. D. Pine, *J. Org. Chem.* **1985**, *50*, 1212-1216.

[73]   L. F. Cannizzo, R. H. Grubbs, *J. Org. Chem.* **1985**, *50*, 2316-2323.

[74]   T. Takeda, *Modern Carbonyl Olefination: Methods and Applications*, *John Wiley & Sons*, **2006**.

[75]   J. J. Eisch, A. Piotrowski, *Tetrahedron Lett.* **1983**, *24*, 2043-2046.

[76]   B. Van de Heisteeg, G. Schat, O. Akkerman, F. Bickelhaupt, *Tetrahedron Lett.* **1987**, *28*, 6493-6496.

[77]   T. Schirmeister, C. Schmuck, P. R. Wich, D. N. Bamberger, Hirzel Verlag, **2016**, pp. 700-701.

[78]   T. Takeda, *Bull. Chem. Soc. Jpn.* **2005**, *78*, 195-217.

[79]   C. E. Tucker, P. Knochel, *J. Am. Chem. Soc.* **1991**, *113*, 9888-9890.

[80]   F. M. Hartner, S. M. Clift, J. Schwartz, T. H. Tulip, *Organometallics* **1987**, *6*, 1346-1350.

[81]   S. M. Clift, J. Schwartz, *J. Am. Chem. Soc.* **1984**, *106*, 8300-8301.

[82]   F. W. Hartner Jr, J. Schwartz, S. M. Clift, *J. Am. Chem. Soc.* **1983**, *105*, 640-641.

[83]   F. W. Hartner Jr, J. Schwartz, *J. Am. Chem. Soc.* **1981**, *103*, 4979-4981.

[84]   J. Schwartz, J. A. Labinger, *Angew. Chem. Int. Ed. Engl.* **1976**, *15*, 333-340.

[85]   C. A. Bertelo, J. Schwartz, *J. Am. Chem. Soc.* **1976**, *98*, 262-264.

[86]   D. W. Hart, T. F. Blackburn, J. Schwartz, *J. Am. Chem. Soc.* **1975**, *97*, 679-680.

[87]   D. W. Hart, J. Schwartz, *J. Am. Chem. Soc.* **1974**, *96*, 8115-8116.

[88]   T. Kauffmann, M. Enk, P. Fiegenbaum, U. Hansmersmann, W. Kaschube, *Chem. Ber.* **1994**, *127*, 127-135.

[89]   T. Kauffmann, P. Fiegenbaum, M. Papenberg, R. Wieschollek, D. Wingbermühle, *Chem. Ber.* **1993**, *126*, 79-87.

[90]   T. Kauffmann, J. Baune, P. Fiegenbaum, U. Hansmersmann, C. Neiteler, M. Papenberg, R. Wieschollek, *Chem. Ber.* **1993**, *126*, 89-96.

[91]   G. C. Fu, R. H. Grubbs, *J. Am. Chem. Soc.* **1993**, *115*, 3800-3801.

[92]   T. KAUFFAMNN, P. Fiegenbaum, M. Papenberg, R. Wieschollek, J. Sander, *Chem. Ber.* **1992**, *125*, 143-148.

[93]   G. C. Bazan, J. H. Oskam, H. N. Cho, L. Y. Park, R. R. Schrock, *J. Am. Chem. Soc.* **1991**, *113*, 6899-6907.

[94]   G. Bazan, R. Schrock, H.-N. Cho, V. Gibson, *Macromolecules* **1991**, *24*, 4495-4502.

[95]   R. R. Schrock, J. S. Murdzek, G. C. Bazan, J. Robbins, M. DiMare, M. O'Regan, *J. Am. Chem. Soc.* **1990**, *112*, 3875-3886.

[96]   T. Kauffmann, M. Enk, W. Kaschube, E. Toliopoulos, D. Wingbermühle, *Angew. Chem. Int. Ed. Engl.* **1986**, *25*, 910-911.

[97]   T. Kauffmann, G. Kieper, *Angew. Chem. Int. Ed. Engl.* **1984**, *23*, 532-533.

[98]   T. Kauffmann, P. Fiegenbaum, R. Wieschollek, *Angew. Chem. Int. Ed. Engl.* **1984**, *23*, 531-532.

[99]   T. Kauffmann, B. Ennen, J. Sander, R. Wieschollek, *Angew. Chem. Int. Ed. Engl.* **1983**, *22*, 244-245.

[100]   T. Kauffmann, R. Abeln, S. Welke, D. Wingbermühle, *Angew. Chem. Int. Ed. Engl.* **1986**, *25*, 909-910.

[101]   J. H. Freudenberger, R. R. Schrock, *Organometallics* **1986**, *5*, 398-400.

[102]   A. Aguero, J. Kress, J. Osborn, *J. Chem. Soc., Chem. Commun.* **1986**, 531-533.

[103]   M. R. Churchill, J. W. Ziller, J. H. Freudenberger, R. R. Schrock, *Organometallics* **1984**, *3*, 1554-1562.

[104]   C. Elschenbroich, *Organometallchemie*, Springer-Verlag, **2009**.

[105]   R. H. Grubbs, C. R. Hoppin, *J. Chem. Soc., Chem. Commun.* **1977**, *1977*, 634-635.

[106]   R. H. Grubbs, D. D. Carr, C. Hoppin, P. Burk, *J. Am. Chem. Soc.* **1976**, *98*, 3478-3483.

[107]   R. H. Grubbs, P. L. Burk, D. D. Carr, *J. Am. Chem. Soc.* **1975**, *97*, 3265-3267.

[108]   J.-L. Hérisson, Y. Chauvin, *Makromol. Chem.* **1971**, *141*, 161-&.

[109]   J.-L. Hemsson, Y. Chauvin, *Makromol. Chem.* **1970**, *141*, 161-176.

[110] J. Feldman, J. S. Murdzek, W. M. Davis, R. R. Schrock, *Organometallics* **1989**, *8*, 2260-2265.

[111] J. Feldman, R. R. Schrock, *Prog. Inorg. Chem.* **1991**, *39*, 1-74.

[112] D. S. Williams, M. H. Schofield, J. T. Anhaus, R. R. Schrock, *J. Am. Chem. Soc.* **1990**, *112*, 6728-6729.

[113] R. H. Grubbs, S. J. Miller, G. C. Fu, *Acc. Chem. Res.* **1995**, *28*, 446-452.

[114] R. R. Schrock, *Angew. Chem. Int. Ed.* **2006**, *45*, 3748-3759.

[115] J. Van de Loosdrecht, F. Botes, I. Ciobica, A. Ferreira, P. Gibson, D. Moodley, A. Saib, J. Visagie, C. Weststrate, J. Niemantsverdriet, *Ch. 7.20.(Reedijk J. and Poeppelmeier K., Editors). Elsevier, 2013.* **2013**, 525.

[116] W. A. Herrmann, *Angew. Chem. Int. Ed. Engl.* **1982**, *21*, 117-130.

[117] B. Cornils, W. A. Herrmann, *Aqueous-phase organometallic catalysis: concepts and applications*, John Wiley & Sons, **2004**.

[118] P. C. Kamer, P. W. van Leeuwen, *Phosphorus (III) ligands in homogeneous catalysis: design and synthesis*, John Wiley & Sons, **2012**.

[119] G. Rothenberg, *Catalysis: concepts and green applications*, John Wiley & Sons, **2017**.

[120] G. C. Fu, R. H. Grubbs, *J. Am. Chem. Soc.* **1992**, *114*, 7324-7325.

[121] G. C. Fu, R. H. Grubbs, *J. Am. Chem. Soc.* **1992**, *114*, 5426-5427.

[122] A. F. Houri, Z. Xu, D. A. Cogan, A. H. Hoveyda, *J. Am. Chem. Soc.* **1995**, *117*, 2943-2944.

[123] R. H. Grubbs, *Handbook of metathesis. 1. Catalyst development*, Wiley-VCH, **2003**.

[124] K. Ziegler, K. Nagel, M. Patheiger, *Z. Anorg. Allg. Chem.* **1955**, *282*, 345-351.

[125] R. R. Schrock, *Acc. Chem. Res.* **1979**, *12*, 98-104.

[126] N. Calderon, *Acc. Chem. Res.* **1972**, *5*, 127-132.

[127] F. G. Bordwell, *Acc. Chem. Res.* **1988**, *21*, 456-463.

[128] W. Uhl, M. Willeke, A. Hepp, D. Pleschka, M. Layh, *Z. Anorg. Allg. Chem.* **2017**, *643*, 387-397.

[129] N. Dettenrieder, H. M. Dietrich, C. Maichle-Mössmer, R. Anwander, *Chem. Eur. J.* **2016**, *22*, 13189-13200.

[130] C. Stanciu, A. F. Richards, M. Stender, M. M. Olmstead, P. P. Power, *Polyhedron* **2006**, *25*, 477-483.

[131] J. Lewiński, J. Zachara, K. B. Starowieyski, *J. Chem. Soc., Dalton Trans.* **1997**, 4217-4222.

[132] H. Schumann, M. Frick, B. Heymer, F. Girgsdies, *J. Organomet. Chem.* **1996**, *512*, 117-126.

[133] H. D. Hodes, A. D. Berry, *J. Organomet. Chem.* **1987**, *336*, 299-305.

[134] K. Samedov, Y. Aksu, M. Driess, *ChemPlusChem* **2012**, *77*, 663-674.

[135] J. Eppinger, M. Spiegler, W. Hieringer, W. A. Herrmann, R. Anwander, *J. Am. Chem. Soc.* **2000**, *122*, 3080-3096.

[136] P. Jutzi, R. Dickbreder, *Chem. Ber.* **1986**, *119*, 1750-1754.

[137] C. M. Fendrick, L. D. Schertz, V. W. Day, T. J. Marks, *Organometallics* **1988**, *7*, 1828-1838.

[138] R. G. Vranka, E. L. Amma, *J. Am. Chem. Soc.* **1967**, *89*, 3121-3126.

[139] D. Diether, C. Maichle-Mössmer, R. Anwander, *Organometallics* **2019**, *38*, 3007-3017.

[140] M. Zimmermann, N. Å. Frøystein, A. Fischbach, P. Sirsch, H. M. Dietrich, K. W. Törnroos, E. Herdtweck, R. Anwander, *Chem. Eur. J.* **2007**, *13*, 8784-8800.

E

Publications

Aluminomethylene (MAM-12)

[(CH$_3$)Al(CH$_2$)]$_{12}$: Methylaluminomethylene (MAM-12)

Georgios Spiridopoulos,[a] Markus Kramer,[b] Felix Kracht,[a] Cäcilia Maichle-Mössmer,[a] and Reiner Anwander*[a]

Abstract: The molecular structure of enigmatic "poly(aluminium-methyl-methylene)" (first reported in 1968) has been unraveled in a transmetalation reaction with gallium methylene [Ga$_8$(CH$_2$)$_{12}$] and AlMe$_3$. The existence of cage-like methylaluminomethylene moieties was initially suggested by the reaction of rare-earth-metallocene complex [Cp*$_2$Lu{(μ-Me)$_2$AlMe$_2$}] with excess AlMe$_3$ affording the deca-aluminium cluster [Cp*$_4$Lu$_2$(μ_3-CH$_2$)$_{12}$Al$_{10}$(CH$_3$)$_8$] in low yield (Cp*=C$_5$Me$_5$). Treatment of [Ga$_8$(CH$_2$)$_{12}$] with excess AlMe$_3$ reproducibly gave the crystalline dodeca-aluminium complex [(CH$_3$)$_{12}$Al$_{12}$(μ_3-CH$_2$)$_{12}$] (MAM-12). Revisiting a previous approach to "poly(aluminium-methyl-methylene)" by using a (C$_5$H$_5$)$_2$TiCl$_2$/AlMe$_3$ (1:100) mixture led to amorphous solids displaying solubility behavior and spectroscopic features similar to those of crystalline MAM-12. The gallium methylene-derived MAM-12 was used as an efficient methylene transfer reagent for ketones.

Introduction

The interplay of early d-transition organometallics and organo-aluminium compounds has branched out into two major fields of organometallic research, Ziegler–Natta polymerization catalysis[1] and, subsequently, metal alkylidene chemistry.[2] In particular, the binary system (C$_5$H$_5$)$_2$TiCl$_2$/AlMe$_3$, initially probed as a model to elucidate reaction pathways and active species in Ziegler's Mischkatalysatoren,[3] strongly influenced the development of discrete metal alkylidene derivatives[2,4,5] and their use in olefination reactions[6] and catalytic olefin metathesis.[7] Initial investigations of the (C$_5$H$_5$)$_2$TiCl$_2$ reaction by Sinn and Kaminsky (1970) proved the formation of [Ti-CH$_2$-Al] moieties (proposed structure **I**, Figure 1) and concomitant methane by α-H abstraction.[8] Solvent-free mixtures of (C$_5$H$_5$)$_2$TiCl$_2$/AlMe$_3$ (1:100) slowly (100–350 h) afforded a grayish solid analyzed as "poly(aluminium-methyl-methylene)" (**II**, Figure 1), which was soluble in THF.[9] Apparently, the synthesis of **II** features the Tebbe reagent [(C$_5$H$_5$)$_2$Ti(μ-Cl)(μ-CH$_2$)AlMe$_2$] (**III**, Figure 1) as an intermediate species. Tebbe could selectively synthesize his compound in 1974 using (C$_5$H$_5$)$_2$TiCl$_2$/AlMe$_3$ in a 1:2 ratio (toluene, RT, 60 h).[5,2f] More recently, the solid-state structure of the Tebbe reagent could be elucidated by X-ray diffraction
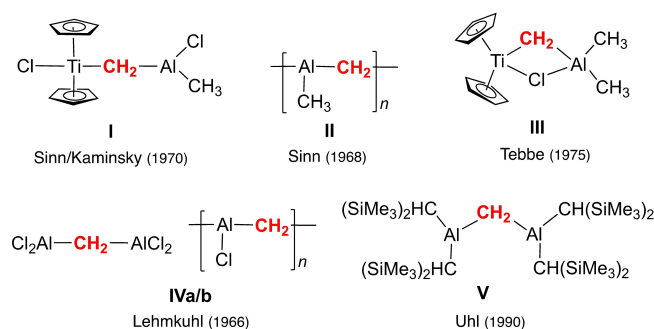
Figure 1. Milestones in aluminium methylene chemistry.

(XRD) analyses.[10,11] Interestingly, a more detailed mechanistic investigation of the system (C$_5$H$_5$)$_2$TiCl$_2$/AlMe$_3$ by Grubbs and co-workers from 1984 also pointed to the formation of red toluene-insoluble species ("poly-TiCH$_2$Al") when **III** was allowed to stand with excess AlMe$_3$ or in neat AlMe$_3$ for long reaction times.[12] Discrete [Cl$_2$Al-CH$_2$-AlCl$_2$] (**IVa**) and polymeric chloridoaluminomethylene species **IVb** (Figure 1), reminiscent of polymeric **II** were obtained in 1966 by Lehmkuhl and Schäfer from Al/CH$_2$Cl$_2$ mixtures.[13,14] Years later in 1990, Layl and Uhl converted [Cl$_2$Al-CH$_2$-AlCl$_2$] into the first alkyl aluminomethylene [R$_2$Al-CH$_2$-AlR$_2$] (**V**, R=CH(SiMe$_3$)$_2$; Figure 1) by salt metathesis with lithium bis(trimethylsilyl)methyl.[15] It is also noteworthy that partial pyrolysis of a concentrated solution of 14.8 g AlMe$_3$ in hexane at 175–180 °C in autoclaves produced 2.5 g of a white solid which was analyzed through reaction with heavy water as mixed aluminium [methyl-methylene-methine-carbide].[16]

Our research in this field was triggered by the "Lanthanide Model in Ziegler–Natta Polymerization" proposed by P. Watson in 1982[17] and the topic "Rare-Earth Metals and Aluminum Getting Close in Ziegler-type Organometallics" is the strategy we have embarked on during the past 25 years.[18] Accordingly, the interplay of rare-earth metals and group 13 compounds not

[a] G. Spiridopoulos, F. Kracht, Dr. C. Maichle-Mössmer, Prof. Dr. R. Anwander
Institut für Anorganische Chemie
Eberhard Karls Universität Tübingen
Auf der Morgenstelle 18, 72076 Tübingen (Germany)
E-mail: reiner.anwander@uni-tuebingen.de

[b] Dr. M. Kramer
Institut für Organische Chemie, Universität Tübingen
Auf der Morgenstelle 18, 72076 Tübingen (Germany)

Chemistry–A European Journal | Research Article
doi.org/10.1002/chem.202200823

Chemistry
Europe
European Chemical
Societies Publishing

only emerged in thermodynamically very stable hetero-bimetallics like homoleptic [Ln(AlMe$_4$)$_3$][19] but also in the targeted formation of isolable [Ln-CH$_2$-Al][20] and [Ln-CH–Al] moieties.[21] More recently, the Ln/group 13 approach paved the way to unprecedented group 13 organometallics: the pseudo-catalytic reaction of [Cp*$_2$Ln{(μ-Me)$_2$GaMe$_2$}] (Ln=Y, Lu; Cp*=C$_5$Me$_5$) with excess GaMe$_3$ at elevated temperatures afforded homoleptic gallium methylene [Ga$_8$(CH$_2$)$_{12}$].[22] Noteworthy, the isolation of dodecametallic intermediate [(Cp*$_2$Lu)$_3$(μ_3-CH$_2$)$_6$Ga$_9$(μ-CH$_2$)$_9$] gave insight into the mechanism of such methylidene formation. Aiming at a wider applicability of this methyl degradation (α-H abstraction) approach, the present study targets the activation of trimethylaluminium.

Results and Discussion

Treatment of [Cp*$_2$Lu{(μ-Me)$_2$AlMe$_2$}][23] with 4 equiv. AlMe$_3$ at 130 °C in [D$_8$]toluene generated methane (Figure S1 in the Supporting Information) and produced a few colorless crystals of [Cp*$_4$Lu$_2$(μ_3-CH$_2$)$_{12}$Al$_{10}$(CH$_3$)$_8$] (**1**, Scheme 1). The XRD analysis of compound **1** revealed an asymmetric cage-like structural motif (Figure 2). Two opposite corners of the molecule are occupied by [Cp*$_2$Lu] metallocene units which are bridged by two μ_3-methylidene groups to the {Al$_{10}$} entity. The Lu–C$_{methylene}$ distances range from 2.499(4) to 2.630(4) Å (avg. 2.568 Å), being significantly shorter than those in the gallium congener [Cp*$_6$Lu$_3$(μ_3-CH$_2$)$_6$Ga$_9$(CH$_2$)$_9$] (avg. 2.614 Å).[22]

The distinct coordination environments of the aluminium atoms featuring two Al(μ_3-CH$_2$)$_2$(CH$_3$)$_2$, four Al(μ_3-CH$_2$)$_3$(CH$_3$), and four Al(μ_3-CH$_2$)$_4$ tetrahedra are striking. The Al–C(Me) distances average 1.958 Å, similar to the terminal aluminium methyls in Al$_2$Me$_6$ (avg. 1.9556 Å).[24] As expected, the Al–C(μ_3-CH$_2$) distances are longer for the Al(μ_3-CH$_2$)$_4$ moieties (avg. 2.011 Å) compared to the Al atoms that carry two and three methylene groups (avg 1.952 Å). For comparison, the Al–C(μ_2-CH$_2$) distances in Uhl's trigonal planar [(AlR$_2$)$_2$(μ-CH$_2$)] (R=CH(SiMe$_3$)$_2$,[14] and tetranuclear heteroadamantane [Al$_4$(μ-CH$_2$)$_2$Cl$_4$R$_4$][25] amount to 1.938(1) and 1.959(2) Å, respectively. The ^{1}H NMR spectrum of **1** in [D$_8$]THF shows a signal at 1.87 ppm for the C$_5$Me$_5$ ancillary ligands. Separate resonances at −0.96, −0.99, −1.16, and −1.81 ppm are assigned to [AlCH$_3$], [LuCH$_2$Al], and [AlCH$_2$Al] moieties (Figure S2), respectively, thus suggesting the absence of CH$_2$/CH$_3$ exchange processes. Such a rigid arrangement is in agreement with the observations made for [Tp^{tBu,Me}La(μ_3-CH$_2$)-{(μ_2-Me)AlMe$_2$}$_2$][20a] and [(PNP)Sc(μ_3-CH$_2$){(μ_2-Me)AlMe$_2$}$_2$] having revealed separate signals for CH$_2$/CH$_3$ at ambient temperature.[20b] Unfortunately, a scale-up reaction using [Cp*$_2$Lu(AlMe$_4$)] and excess trimethylaluminium did not lead to the extrusion of a methylaluminomethylene (MAM) species [(CH$_3$)$_x$Al$_y$(μ_3-CH$_2$)$_2$] or homoleptic aluminium methylene, as observed in the gallium methylene study.[22]

In the quest for alternative approaches to putative MAM species, we sought to reinvestigate the synthesis reported by Sinn et al.[8] As originally described, the reaction of dichlorido titanocene (C$_5$H$_5$)$_2$TiCl$_2$ or Tebbe's [(C$_5$H$_5$)$_2$Ti(μ-CH$_2$)(μ-Cl)Al(CH$_3$)$_2$] and neat AlMe$_3$ (100 equiv.) afforded aluminium-methyl-meth-

Cp*$_2$Lu(AlMe$_4$) + 4 AlMe$_3$

toluene-d$_8$
130 °C, 500 h
− CH$_4$ → 0.5

1
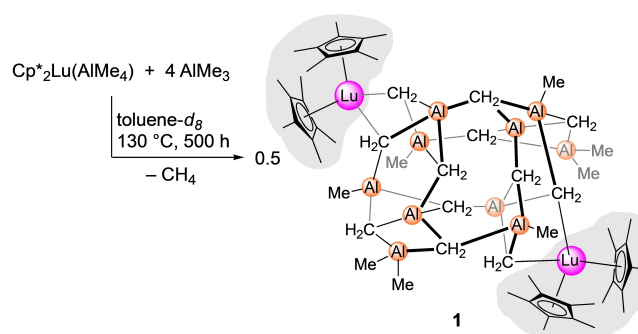
Scheme 1. Synthesis of complex [Cp*$_4$Lu$_2$(μ_3-CH$_2$)$_{12}$Al$_{10}$(CH$_3$)$_8$] (**1**), which was obtained in very low crystalline yield; a larger quantity of single-crystalline **1** could not be obtained, thus impeding a more comprehensive characterization.
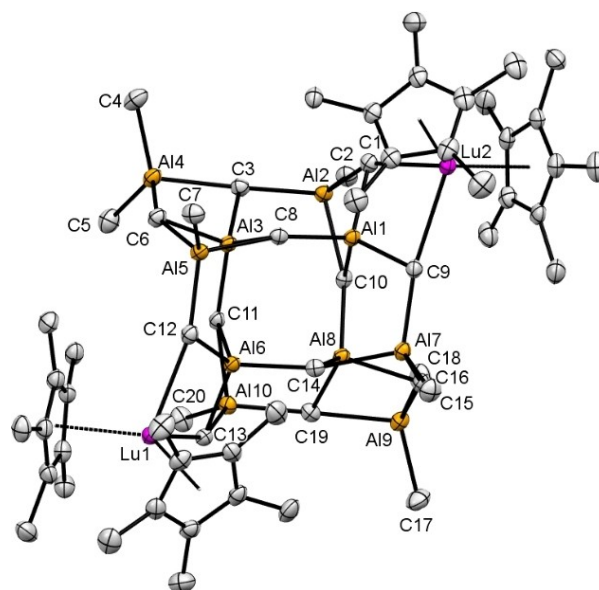
Figure 2. Crystal structure of complex **1**. Atomic displacement parameters are set at 50% probability, and hydrogen atoms are omitted for clarity. For selected interatomic distances and angles, see the Supporting Information.

ylene (**2**^{Tebbe}; Scheme 2, left). Purification of **2**^{Tebbe} by the Soxhlet method (benzene, 3 d) left a reddish powder (not gray as described by Sinn for **II**,[9] but red as mentioned by Grubbs for "poly-TiCH$_2$Al").[12] The color indicated minor contamination with a titanium(III) species which was confirmed by EPR and ICP-OES analysis (Ti 0.33%; see the Supporting Information Figure S5). Compound **2**^{Tebbe} is insoluble in aliphatic and aromatic solvents but dissolves slightly in THF. The ^{1}H NMR spectrum of **2**^{Tebbe} in [D$_8$]THF shows a signal pattern similar to compound **1** with resonances of the Al-CH$_2$/CH$_3$ moieties detectable at −0.96, −0.99, −1.03 and −1.81 ppm (Figure S3).

With the homoleptic gallium methylene [Ga$_8$(CH$_2$)$_{12}$] in hands, we next examined the feasibility of a Ga/Al transmetalation.[26] Treatment of pale yellow suspensions of [Ga$_8$(CH$_2$)$_{12}$] in non-coordinating solvents (benzene or n-hexane) with excess AlMe$_3$ (12 or 24 equiv.) led to a steady decoloriza-

Chemistry–A European Journal

Research Article
doi.org/10.1002/chem.202200823

Chemistry Europe
European Chemical
Societies Publishing
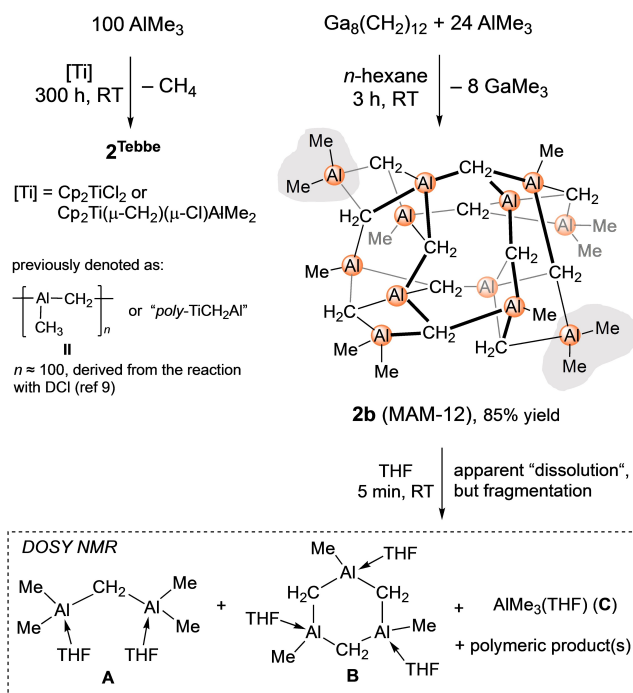
Scheme 2. Synthesis of 2^{Tebbe} and dodecametallic [(CH$_3$)$_{12}$Al$_{12}$(μ$_3$-CH$_2$)$_{12}$] (2b), along with fragmentation of 2b in THF.

Figure 3. Crystal structure of [(CH$_3$)$_{12}$Al$_{12}$(μ$_3$-CH$_2$)$_{12}$] (2b, MAM-12). The atomic displacement parameters are set at 50% probability. All hydrogen atoms except those for C19 were located in the difference Fourier maps, but are omitted for clarity. For a representation of all atoms, selected interatomic distances and angles, see the Supporting Information.

tion of the mixture and the temporary generation of a clear solution. After stirring the mixtures for 2–3 h at ambient temperature colorless precipitates had formed (Scheme 2, right). The obtained powders 2a (12 equiv. AlMe$_3$) and 2b (24 equiv. AlMe$_3$) feature limited solubility and the ^{1}H NMR spectra in [D$_8$]THF revealed signal patterns similar to treddish 2^{Tebbe} and compound 1. Consequently, this encourages the assumption that the two protocols depicted in Scheme 2 generated similar compounds/materials. Fortunately, single crystals of 2a/2b were obtained from microscale reactions and crystallization at 70 °C. The XRD analysis of [(CH$_3$)$_{12}$Al$_{12}$(μ$_3$-CH$_2$)] (2b, MAM-12) revealed again a cage-like structural motif similar to compound 1 (Figure 2). In 2b the two peripheral [Cp*$_2$Lu]$^+$ units in 1 are displaced by [AlMe$_2$]$^+$ moieties (see the gray areas depicted in Figures 2 and 3).

The aluminium coordination environments in fully Ga/Al-exchanged compound 2b now each comprise four Al(μ$_3$-CH$_2$)$_2$(CH$_3$)$_2$, Al(μ$_3$-CH$_2$)$_2$(CH$_3$)$_2$, and Al(μ$_3$-CH$_2$)$_4$ tetrahedra. Incompletely Ga/Al-exchanged compound 2a displays a partial occupancy for the four M(CH$_3$)$_2$ positions as a special case of substitutional disorder. Accordingly, the group 13 metal M was refined on the same position in a ratio Al/Ga = 0.66:0.34 (Figure S27). The Al–C(Me) distances in 2b average 1.952 Å, and are thus similar to those in compound 1. The average Al–C(μ-methylene) distances of 2.011 Å also match those in compound 1 and other clusters containing Al–CH$_2$ moieties (e.g., [La$_4$Al$_8$(C)(CH)$_2$(CH$_2$)$_2$(CH$_3$)$_{22}$(toluene)]).[27] Other cage-like organo-{Al$_{12}$} clusters include low-valent icosahedral K$_2$[Al$_{12}$iBu$_{12}$][28] and ellipsoidal Li[Al$_{12}${N(SiMe$_3$)$_2$}$_8$].[29] It is also interesting to note that (CH$_3$)$_{18}$Al$_{12}$O$_9$ cage clusters have been suggested (from exper-

imental studies and DFT calculations) as a model for methylaluminoxane (MAO) cocatalyst solutions, employed in olefin polymerization.[30]
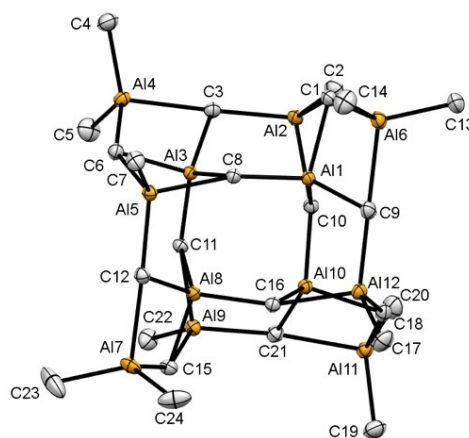
Compound 2b decomposes at 380 °C, is insoluble in aliphatic and aromatic solvents but apparently "dissolves" in THF, in accordance with the solution behavior of II.[8] The ^{1}H NMR spectrum of 2b in [D$_8$]THF shows four resonances at −0.97, −1.00, −1.04 and −1.82 ppm. The slightly broadened high-field signal at −1.82 ppm can be assigned to Al–CH$_2$ moieties and the remaining signals represent terminal aluminium methyl groups. The proton signal of trimethylaluminium in [D$_8$]THF is detected at −1.02 ppm. For further comparison, the methylene signal of 3-coordinate [{(Me$_3$Si)$_2$HC}$_2$Al-CH$_2$-Al{CH(SiMe$_3$)$_2$}$_2$] (V) was reported as −0.50 ppm (in C$_6$D$_6$) while the CH$_2$ signals of alkynyl ate complexes of V involving 4-coordinate aluminium centers were found significantly shifted upfield in the range −1.03 to −1.76 ppm ([D$_8$]THF).[31] The ^{13}C NMR spectrum of 2b in [D$_8$]THF shows also four signals for aluminium-bonded carbon atoms at −4.79, −6.58, −7.63, and −9.20 ppm, while the ^{27}Al NMR spectrum in [D$_8$]THF gave three signals in the range 160–127 ppm. ^{13}C-DEPT135, ^{1}H,^{13}C HSQC, and ^{1}H,^{13}C HMBC NMR spectra were recorded as well as a VT ^{1}H NMR study in the range −80 °C to +80 °C (ruling out any dynamic behavior or exchange processes) carried out to further elucidate the behavior of 2b in solution. Particularly enlightening proved the ^{1}H,^{13}C HMBC NMR spectrum (Figure S15) combined with a ^{1}H DOSY NMR experiment (Figures S20–S22). Clearly, the experimental data obtained suggest fragmentation of the dodecametallic cluster 2b into at least three species with molecular masses matching those of putative {[(THF)Me$_2$Al-CH$_2$-AlMe$_2$(THF)]} (A), {[MeAl(CH$_2$)(THF)]$_3$} (B), and {AlMe$_3$(THF)} (C) (Scheme 2, Figure S20). Species A is reminiscent of [{(Me$_3$Si)$_2$HC}$_2$Al-CH$_2$-Al{CH(SiMe$_3$)$_2$}$_2$] (V). V-type complexes have been previously also reported for the smaller terminal alkyl ligands methyl and ethyl, but have remained elusive. Compounds [Me$_2$Al-CH$_2$-AlMe$_2$] and [Et$_2$Al-CH$_2$-AlEt$_2$] were described

Chem. Eur. J. 2022, 28, e202200823 (3 of 5)

© 2022 The Authors. Chemistry - A European Journal published by Wiley-VCH GmbH

Chemistry–A European Journal

Research Article
doi.org/10.1002/chem.202200823

Chemistry Europe
European Chemical
Societies Publishing
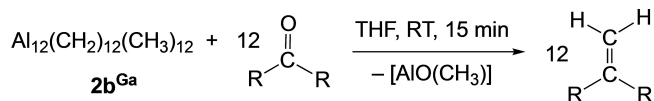
Scheme 3. Methylidene-transfer reactivity of $[(CH_3)_{12}Al_{12}(\mu_3\text{-}CH_2)_{12}]$ (**2b**) with 9-fluorenone, benzophenone or acetone.

as thermally labile and unstable in hydrocarbons decomposing to AlR_3 and (polymeric) methylene-bridged aluminium species (δCH_2: -1.88 to -2.11 ppm), but could be stabilized in the presence of diethyl ether.[15,32] Desolvated trimetallic species **B** ($\{[MeAl(CH_2)]_3\}$) and decomposition products thereof could be detected by EI mass spectrometry. Monometallic $AlMe_3(THF)$ (**C**) could originate from the excessive $AlMe_3$ used for the synthesis of **2b** (Figures S7–S9) or dismutation of **2b** when fragmentation occurred in THF. The latter dismutation reaction would also involve the formation of a methyl-depleted (methylene-rich) organoaluminium polymer which could not be identified. The likely occurrence of a respective dismutation reaction seems supported by the following experiment: dissolving compound **2b** in THF, and subsequent removal of the solvent under vacuum, and treatment of the residue at 110 °C under high vacuum for 6 h gave a material whose elemental analysis indicated the reformation of **2b**; however, the ^1H NMR spectrum of such reformed material revealed a considerably changed **A/B/C** integral ratio, when redissolved in $[D_8]THF$ (Figures S10 and S11). For further comparison, homoleptic gallium methylene undergoes a reversible $[Ga_8(\mu\text{-}CH_2)_{12}]/[Ga_6(\mu\text{-}CH_2)_9](Do)_x$ oligomer switch in donor (Do) solvents including THF.[22]

Compound **2b** promotes carbonyl methylenation as efficiently as the Tebbe reagent or related rare-earth-metal variants.[11] Treatment of compound **2b** with 12 equiv. 9-fluorenone, benzophenone or acetone at ambient temperatures in $[D_8]THF$ resulted in the complete consumption of the $AlCH_2$ moieties and conversion to 9-methylene-fluorene, 1,1-diphenyl-ethylene and isobutene, respectively, within 15 minutes (Scheme 3, Figures S23–S25). Unsurprisingly, aluminium methylene **2b** converts the carbonylic substrates considerably faster than gallium methylene $[Ga_8(CH_2)_{12}]$ (RT, 5 d), featuring an increasingly covalent Ga–C bond.[22] It should be noted that, as indicated by ^1H NMR spectroscopy, no carbonyl alkylation was observed, leaving putative methylaluminoxane (MAO) as a coproduct.

Conclusion

After more than 50 years since its first appearance, the structure of methylaluminomethylene could be elucidated. Crucially, a transmetalation reaction involving gallium methylene $[Ga_8(CH_2)_{12}]$ and $AlMe_3$ has proven expedient. The crystal structure of $[(CH_3)_{12}Al_{12}(\mu_3\text{-}CH_2)_{12}]$ exhibits $\{Al(CH_2)_4\}$ tetrahedra as an organometallic variant of the ubiquitous $\{AlO_4\}$ tetrahedra. The aluminium-methylene moieties efficiently engage in carbonyl olefination reactions.

The synthesis procedures are described in the Supporting Information.

Conflict of Interest

The authors declare no conflict of interests.

Data Availability Statement

The data that support the findings of this study are available in the supplementary material of this article.

[1] a) H. Sinn, W. Kaminsky, *Adv. Organomet. Chem.* **1980**, *18*, 99–149; b) H. H. Brintzinger, D. Fischer, R. Mülhaupt, B. Rieger, R. M. Waymouth, *Angew. Chem. Int. Ed. Engl.* **1995**, *34*, 1143–1170; *Angew. Chem.* **1995**, *107*, 1255–1283.

[2] a) R. R. Schrock, *J. Am. Chem. Soc.* **1974**, *96*, 6796–6797; b) R. R. Schrock, *J. Am. Chem. Soc.* **1975**, *97*, 6577–6578; c) L. J. Guggenberger, R. R. Schrock, *J. Am. Chem. Soc.* **1975**, *97*, 6578–6579; d) W. A. Herrmann, B. Reiter, H. Biersack, *J. Organomet. Chem.* **1975**, *97*, 245–251; e) D. A. Clemente, B. Rees, G. Bandoli, M. C. Biagini, B. Reiter, W. A. Herrmann, *Angew. Chem. Int. Ed. Engl.* **1981**, *20*, 887–888; *Angew. Chem.* **1981**, *93*, 920–921; f) F. N. Tebbe, G. W. Parshall, G. D. Reddy, *J. Am. Chem. Soc.* **1978**, *100*, 3611–3613; g) F. N. Tebbe, G. W. Parshall, D. W. Ovenall, *J. Am. Chem. Soc.* **1979**, *101*, 5074–5075; h) R. Thompson, E. Nakamaru-Ogiso, C.-H. Chen, M. Pink, D. J. Mindiola, *Organometallics* **2014**, *33*, 429–432; i) M. Kamitani, B. Pinter, C. H. Chen, M. Pink, D. J. Mindiola, *Angew. Chem. Int. Ed.* **2014**, *53*, 10913–10915; *Angew. Chem.* **2014**, *126*, 11093–11095; j) L. N. Grant, S. Ahn, B. C. Manor, M.-H. Baik, D. J. Mindiola, *Chem. Commun.* **2017**, *53*, 3415–3417.

[3] a) G. Natta, P. Pino, G. Mazzanti, U. Giannini, *J. Am. Chem. Soc.* **1957**, *79*, 2975–2976; b) D. S. Breslow, N. R. Newburg, *J. Am. Chem. Soc.* **1957**, *79*, 5072–5073.

[4] a) R. R. Schrock, *Acc. Chem. Res.* **1979**, *12*, 98–104; b) R. R. Schrock, *Chem. Rev.* **2002**, *102*, 145–180; c) R. R. Schrock, *Chem. Rev.* **2009**, *109*, 3211–3226.

[5] J. Scott, D. J. Mindiola, *Dalton Trans.* **2009**, 8463–8472.

[6] *Modern Carbonyl Olefination: Methods and Applications* (Ed.: T. Takeda), Wiley, **2006**.

[7] a) N. Calderon, *Acc. Chem. Res.* **1972**, *5*, 127–132; b) R. Schrock, *Acc. Chem. Res* **1990**, *23*, 158–165; c) Y. Chauvin, *Angew. Chem. Int. Ed.* **2006**, *45*, 3740–3747; *Angew. Chem.* **2006**, *118*, 3824–3831; d) *Handbook of Metathesis* (Ed.: R. H. Grubbs), Wiley-VCH, Weinheim, **2003**; e) R. R.

Chemistry–A European Journal

Research Article
doi.org/10.1002/chem.202200823

Chemistry Europe
European Chemical
Societies Publishing

Schrock, *Angew. Chem. Int. Ed.* **2006**, *45*, 3748–3759; *Angew. Chem.* **2006**, *118*, 3832–3844.

[8] E. Heins, H. Hinck, W. Kaminsky, G. Oppermann, P. Paulinat, H. Sinn, *Makromol. Chem.* **1970**, *134*, 1–22.

[9] H. Sinn, H. Hinck, F. Bandermann, H. Grützmacher, *Angew. Chem. Int. Ed. Engl.* **1968**, *3*, 217; *Angew. Chem.* **1968**, *80*, 190.

[10] R. Thompson, E. Nakamaru-Ogiso, C.-H. Chen, M. Pink, D. J. Mindiola, *Organometallics* **2014**, *33*, 429–432.

[11] V. M. Birkelbach, F. Kracht, H. M. Dietrich, C. Stuhl, C. Maichle-Mössmer, R. Anwander, *Organometallics* **2020**, *39*, 3490–3504.

[12] K. C. Ott, E. J. M. DeBoer, R. H. Grubbs, *Organometallics* **1984**, *3*, 223–230.

[13] H. Lehmkuhl, R. Schäfer, *Tetrahedron Lett.* **1966**, *7*, 2315–2320.

[14] a) M. R. Ort, E. H. Mottus, *J. Organomet. Chem.* **1973**, *50*, 47–52; b) K. Domen, T. J. Chuang, *J. Am. Chem. Soc.* **1987**, *109*, 5288–5289.

[15] M. Layh, W. Uhl, *Polyhedron* **1990**, *9*, 277–282.

[16] K. Ziegler, K. Nagel, W. Pfohl, *Liebigs Ann.* **1960**, *629*, 210–221.

[17] P. L. Watson, *J. Am. Chem. Soc.* **1982**, *104*, 337–339.

[18] A. Fischbach, R. Anwander, *Adv. Polym. Sci.* **2006**, *204*, 155–281.

[19] a) W. J. Evans, R. Anwander, R. Doedens, J. W. Ziller, *Angew. Chem. Int. Ed. Engl.* **1994**, *33*, 1641–1644; *Angew. Chem.* **1994**, *106*, 1725–1728; b) M. Zimmermann, N. Å. Frøystein, A. Fischbach, P. Sirsch, H. M. Dietrich, K. W. Törnroos, E. Herdtweck, R. Anwander, *Chem. Eur. J.* **2007**, *13*, 8784–8800; c) G. Occhipinti, C. Meermann, H. M. Dietrich, R. Litlabø, F. Auras, K. W. Törnroos, C. Maichle-Mössmer, V. R. Jensen, R. Anwander, *J. Am. Chem. Soc.* **2011**, *133*, 6323–6337; d) D. Barisic, D. Diether, C. Maichle-Mössmer, R. Anwander, *J. Am. Chem. Soc.* **2019**, *141*, 13931–13940.

[20] a) R. Litlabø, M. Zimmermann, K. Saliu, J. Takats, K. W. Törnroos, R. Anwander, *Angew. Chem. Int. Ed.* **2008**, *47*, 9560–9564; *Angew. Chem.* **2008**, *120*, 9702–9706; b) J. Scott, H. Fan, B. F. Wicker, A. R. Fout, M.-H. Baik, D. J. Mindiola, *J. Am. Chem. Soc.* **2008**, *130*, 14438–14439; c) P.

[21] H. M. Dietrich, H. Grove, K. W. Törnroos, R. Anwander, *J. Am. Chem. Soc.* **2006**, *128*, 1458–1459.

[22] M. Bonath, C. Maichle-Mössmer, P. Sirsch, R. Anwander, *Angew. Chem. Int. Ed.* **2019**, *58*, 8206–8210; *Angew. Chem.* **2019**, *131*, 8290–8294.

[23] a) M. A. Busch, R. Harlow, P. L. Watson, *Inorg. Chim. Acta* **1987**, *140*, 15–20; b) H. M. Dietrich, K. W. Törnroos, E. Herdtweck, R. Anwander, *Organometallics* **2009**, *28*, 6739–6749.

[24] H.-G. Stammler, S. Blomeyer, R. J. F. Berger, N. W. Mitzel, *Angew. Chem. Int. Ed.* **2015**, *54*, 13816–13820; *Angew. Chem.* **2015**, *127*, 14021–14026.

[25] W. Uhl, M. Layh, *J. Organomet. Chem.* **1991**, *415*, 181–190.

[26] a) H. M. Dietrich, C. Maichle-Mössmer, R. Anwander, *Dalton Trans.* **2010**, *39*, 5783–5785; b) Q. Lai, N. Bhuvanesh, O. V. Ozerov, *J. Am. Chem. Soc.* **2020**, *142*, 20920–20923.

[27] L. C. H. Gerber, E. Le Roux, K. W. Törnroos, R. Anwander, *Chem. Eur. J.* **2008**, *15*, 9555–9564.

[28] W. Hiller, K.-W. Klinkhammer, W. Uhl, J. Wagner, *Angew. Chem. Int. Ed. Engl.* **1991**, *30*, 179–180; *Angew. Chem.* **1991**, *103*, 182–183.

[29] A. Purath, R. Köppe, H. Schnöckel, *Chem. Commun.* **1999**, 1933–1934.

[30] a) M. Ystenes, J. L. Eilertsen, J. Liu, M. Ott, E. Rytter, J. A. Støvneng, *J. Polym. Sci. Part A: Polym. Chem.* **2000**, *38*, 3106–3128; b) E. Y.-X. Chen, T. J. Marks, *Chem. Rev.* **2000**, *100*, 1391–1434; c) H. S. Zijlstra, S. Harder, *Eur. J. Inorg. Chem.* **2015**, 19–43.

[31] W. Uhl, C. Rösener, M. Layh, A. Hepp, *Z. Anorg. Allg. Chem.* **2012**, *638*, 1746–1754.

[32] E. C. Ashby, R. S. Smith, *J. Organomet. Chem.* **1982**, *225*, 71–85.

Zatsepin, E. Lee, J. Gu, M. R. Gau, P. J. Carroll, M. H. Baik, D. J. Mindiola, *J. Am. Chem. Soc.* **2020**, *142*, 10143–10152.

Chemistry–A European Journal

[(CH$_3$)Al(CH$_2$)]$_{12}$: Methylaluminomethylene (MAM-12)

Georgios Spiridopoulos, Markus Kramer, Felix Kracht, Cäcilia Maichle-Mössmer, and Reiner Anwander*

S2

Table of Contents

Experimental Section

General Considerations. All operations were performed under rigorous exclusion of air and water by using standard Schlenk, high-vacuum, and glovebox techniques (MBraun 200B; <0.1ppm O_2, <0.1 ppm H_2O). Solvents were purified by using Grubbs-type columns (MBraun SPS, solvent purification system) and stored inside a glovebox. [D_8]THF was obtained from Sigma-Aldrich, stirred over NaK and distilled. [D_6]benzene was obtained from Sigma-Aldrich stirred over NaK and filtered at ambient temperature. $Cp_2Ti(\mu\text{-}CH_2)(\mu\text{-}Cl)AlMe_2$,[1] $Ga_8(CH_2)_{12}$,[2] and $Cp*_2Lu(AlMe_4)$[2] were synthesized according to literature procedures. $AlMe_3$, 9-fluorenone, and benzophenone were purchased from Sigma-Aldrich and used as received. Acetone was purchased from Honeywell and a small amount was stored in the glovebox over molecular sieve. If not otherwise stated, the NMR spectra were recorded by using J.Young-valved NMR tubes on a Bruker AVII+400 spectrometer (^1H, 400.13 MHz; ^{13}C, 100.61 MHz) and a Bruker AVII+500 spectrometer (^1H, 500.13 MHz; ^{13}C, 125.76 MHz) at 26 °C. NMR chemical shifts are referenced to internal solvent resonances and reported in parts per million relative to tetramethylsilane (TMS). All pulse gradient spin echo-NMR measurements were performed on an Avance III HD spectrometer (Bruker) operating at 700.29 MHz for ^1H, using a TCI prodigy cryoprobe head equipped with a z-gradient unit. The gradient was calibrated using "doped water" (1% H_2O in D_2O with traces of $CuSO_4$) assuming a diffusion coefficient of $1.91 \cdot 10\text{-}5$ cm^2 s^{-1} for HDO. The diffusion measurements used a modified bipolar gradient pulse pair-stimulated echo sequence incorporating a longitudinal eddy current delay (BPP-LED). The gradient pulse length (δ) and the diffusion time (Δ) were kept at fixed values while gradually increasing the gradient strength. Typical values for δ and Δ were 1,6 and 75 ms, respectively. A longitudinal eddy cur-rent delay (Te) of 5 ms was used. Sine-shaped gradient pulses were linearly varied between 1 and 52 G cm^{-1} (2 to 98%) in 32 steps and at each step 16 scans were acquired. Four measurements per sample were performed at a constant sample temperature of 298 ± 0.1 K (Bruker Variable Temperature Unit BCU II). The data were analyzed with the T_1/T_2 relaxation module of Topspin 4.1.3. The signal areas were plotted against the gradient strength and the best fit was calculated using the Stejskal-Tanner equation

$I_g = I_0 \cdot \exp[-4\pi^2\gamma^2\delta^2G^2(\Delta\text{-} \delta/3)]$

(with D being the diffusion coefficient in cm^2 s^{-1}, γ the gyromagnetic ratio in Hz/G, G the gradient strength in G cm^{-1}, δ the gradient length in ms, Δ the interval between gradient pulses (diffusion time) in ms, I_g the signal area, and I_0 the signal intensity at G = 0%). Mean values for each sample are reported. EPR spectra were measured on a continuous wave X-band Bruker ESP 300E using 5 mm O.D. Wilmad quartz (CFQ) EPR tubes. Spectra are referenced to the Bruker strong pitched standard g_{iso} = 2.0088. Elemental analyses were performed on an Elementar Vario Micro Cube. IR spectra were recorded on a Thermo Fisher Scientific NICOLET 6700 FTIR spectrometer using a DRIFT chamber with dry KBr/sample mixture and KBr windows. The DRIFT data were converted using the Kubelka-Munk refinement. Additionally, IR spectra were measured on a Bruker Vertex 70 using CsI plates with Nujol.

[$Cp*_4Lu_2Al_{10}(CH_2)_{12}(CH_3)_8$] (1): A solution of $Cp*_2LuAlMe_4$ (21 mg, 0.039 mmol) in toluene-d_8 (0.5 mL) was added to a stirred solution of $AlMe_3$ (11.3 mg, 0.157 mmol) in toluene-d_8 (0.2 mL). The reaction mixture was allowed to stir for 15 min at ambient temperature. Afterwards the reaction mixture was transferred to a J.Young-valved NMR tube and heated at 130 °C for 500 h. Colorless single crystals were obtained at 130 °C from the reaction mixture. ^1H NMR (400.11 MHz, THF-d_8, 26 °C): δ 1.87 (s, 60 H, Cp*Me), –0.96 (s, Al–CH_2 / Al–CH_3), –0.99 (s, Al–CH_2 / Al–CH_3), –1.16 (s, Al–CH_2 / Al–CH_3) ppm. Due to the small available amount of compound **1**, any further analysis could not be performed. Repeated attempts to obtain additional crystalline compound **1**, both under identical and similar reaction conditions, were unsuccessful. The similar reaction conditions included heating of $Cp*_2LuAlMe_4$/$AlMe_3$ mixtures (ratios: 1:4, 1:6, 1:8) in toluene-d_8 (0.5 mL) at 130 °C for 500±20 h.

2^{Tebbe} (Tebbe route): a) In a glovebox, $Cp_2Ti(\mu\text{-}Cl)(\mu\text{-}CH_2)(AlMe_2)$ (26 mg, 0.092 mmol) was stirred in neat $AlMe_3$ (659.7 mg, 9.15 mmol) at ambient temperature. While stirring for 170 h methane evolution occurred and a red solid precipitated. The precipitate was subjected to Soxhlet extraction (benzene, 3 d), washed with benzene (3 x 5 mL), and evaporated to dryness in vacuo to yield **2^{Tebbe}** as a red solid (350 mg, 0.520 mmol, 68%). ^1H NMR (400.11 MHz, THF-d_8, 26 °C, cluster fragmentation):): δ –0.96 (s, 24H, Al–CH_3), –0.99 (s, 22H, Al–CH_3), –1.03 (s, 18H, Al–CH_3), –1.81 (s, 24H, Al–CH_2) ppm. $^{13}C\{^1H\}$ NMR (100.6 MHz, THF-d_8, 26 °C): δ –5.1 (Al–CH_2), –6.9 (Al–CH_3), –7.9 (Al–CH_3), –9.4 (Al–CH_3) ppm. Elemental analysis [%]: Calcd. C 42.86, H 8.99; found C 41.54, H 7.66. ICP-OES : Ti 0.33%. IR (Nujol) [cm^{-1}]: v = 2952, 2923, 2854, 1456, 1377, 1199 (w), 687 (w), 611 (w), 525 (w).

b) In a glovebox, Cp_2TiCl_2 (20 mg, 0.08 mmol) was stirred in neat $AlMe_3$ (579 mg, 8.03 mmol) at ambient temperature. While stirring for 7 d methane evolution occurred and a red solid precipitated. The precipitate was washed with benzene (3 x 5 mL) and evaporated to dryness in vacuo to yield **2^{Tebbe}** as a reddish solid (329 mg, 0.489 mmol, 73%) with characterization data comparing to the material isolated via procedure a).

[(CH$_3$)$_{12}$Al$_{12}$(CH$_2$)$_{12}$] (2a/b) (gallium-methylene route): a) A J.Young-valved NMR tube was charged with (51 mg, 0.07 mmol) of Ga$_8$(CH$_2$)$_{12}$. Then, a solution of AlMe$_3$ (60.7 mg, 0.84 mmol, 12 equivalents) in 0.5 mL C$_6$D$_6$ was added. The J. Young NMR tube was removed from the glovebox and heated in an oil bath at 70 °C overnight. Colorless single crystals of **2a** were obtained at 70 °C from the reaction mixture. Due to the contamination with gallium, no further analysis was performed.

(b) In a glovebox, a pale yellow suspension of Ga$_8$(CH$_2$)$_{12}$ (100 mg, 0.14 mmol) in *n*-hexane (3 mL) and excess AlMe$_3$ (238.3 mg, 3.31 mmol, 24 equivalents) in *n*-hexane (2 mL) were stirred together at ambient temperature. After stirring for 16 h a colorless solid precipitated. The precipitate was washed with benzene (3 x 5 mL) and dried in vacuo to yield **2b** as white solid (80 mg, 0.12 mmol, 85%). ^{1}H NMR (400.11 MHz, THF-d_8, 26 °C): δ −0.97 (s, 22H, Al–CH_3), −0.99 (s, 18H, Al–CH_3), −1.04 (s, 24H, Al–CH_3), −1.81 (s, 24H, Al–CH_2) ppm. Cluster fragmentation was revealed by DOSY measurements (see Figure S16). ^{13}C{^{1}H NMR (100.6 MHz, THF-d_8, 26 °C): δ −4.8 (Al–CH_2), −6.6 (Al–CH_3), −7.6 (Al–CH_3), −9.2 (Al–CH_3) ppm. ^{27}Al NMR (130.32 MHz, THF-d_8, 26 °C): δ −180.7 (very broad) ppm. Elemental analysis [%] Al$_{12}$(CH$_2$)$_{12}$(CH$_3$)$_{12}$ (672.52 g mol$^{−1}$): Calcd. C 42.86, H 8.99; found C 43.37, H 8.51. ICP-OES: Ga 0.66%, Al 34.21%. DRIFT (KBr): v 2926 (w), 2887 (w), 1324 (vw), 1249 (vw), 1198 (s), 824 (s), 696 (s), 662 (s), 663 (s), 649 (s), 613 (s), 547 (s) cm^{-1}. IR (Nujol) [cm^{-1}]: v = 2953 (Nujol), 2924 (Nujol), 2854 (Nujol), 1461 (Nujol), 1377 (Nujol), 1199 (w), 817 (w), 721 (w), 688 (w), 611 (w), 521 (w). Compound **2b** (10 mg) was dissolved in 0.5 mL THF and stirred for 5 min. After removing the solvent under vacuum, the residue was heated to 110 °C at a high vacuum unit for 6 h, without any color change. Elemental analysis of the residue indicated the reformation of **2b**: calcd. C 42.86, H 8.99; found C 43.48, H 8.44 (see also Figure S11). Single crystals of **2b** were obtained by heating a suspension of Ga$_8$(CH$_2$)$_{12}$ (50.4 mg, 0.07 mmol) and AlMe$_3$ (117.6 mg, 1.66 mmol, 24 equivalents) in benzene (1 mL) in a J.-Young-valved NMR tube to 70 °C overnight (16 h). The crystals of **2b** formed at 70 °C, attaching to the glass wall at the liquid/gas interface.

5 min   10 min   15 min   30 min
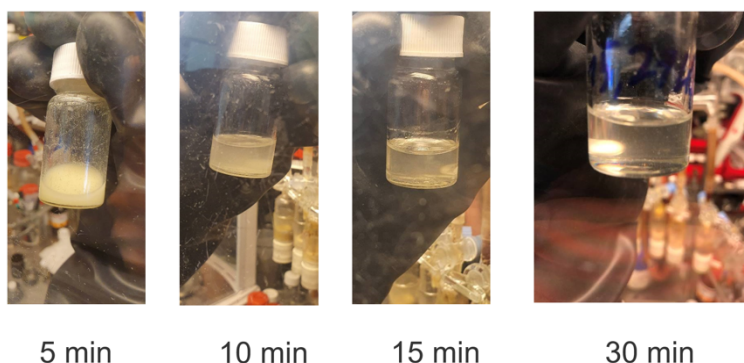
Figure S1. Gradual dissolution of gallium methylene Ga$_8$(CH$_2$)$_{12}$ (suspension in *n*-hexane) upon addition of excess of AlMe$_3$ (solution in *n*-hexane). The reaction progress, involving the formation of methylaluminomethylene MAM as a white precipitate, is not shown.

General procedure for carbonyl olefination experiments. A J.-Young-valved NMR tube was charged with 10 mg of [(CH$_3$)$_{12}$Al$_{12}$(CH$_2$)$_{12}$] (**2b**). Subsequently, 12 equivalents of the respective carbonylic compound dissolved in 0.4 mL THF-d_8 was added and after 15 min a ^{1}H NMR spectrum was recorded (see Figures S24-S26).

NMR and EPR Spectra
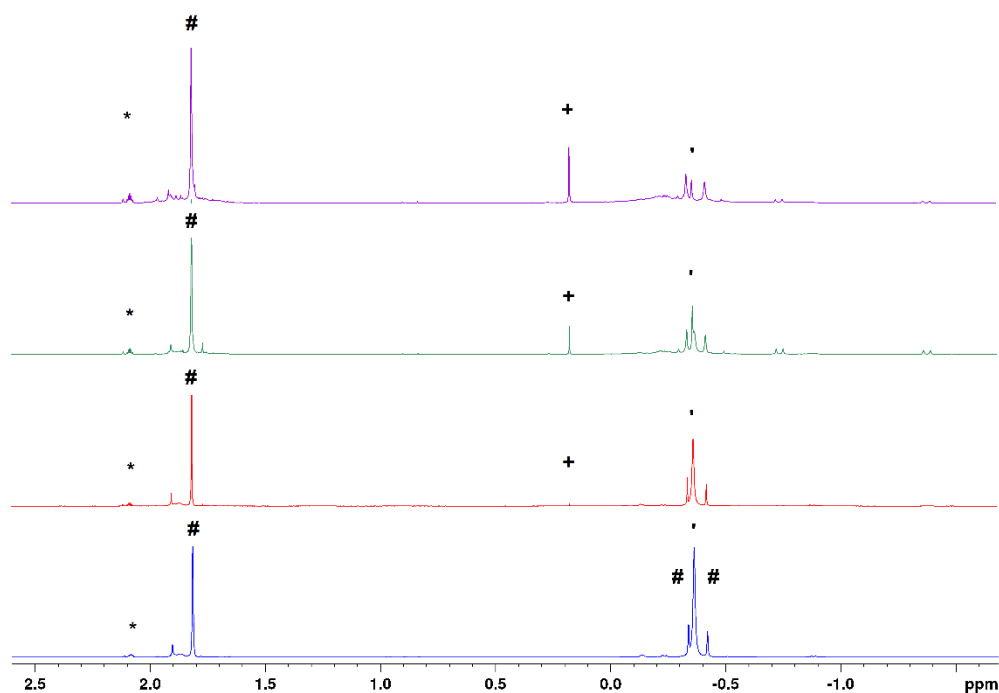
Figure S2. ^{1}H NMR spectra (400.11 MHz) of the reaction of [Cp*$_2$Lu(AlMe$_4$)] (#) with AlMe$_3$ (') toward complex **1** in toluene-d_8 (*). From bottom to top : 20 min, RT (blue), 40 h, 130 °C (red), 240 h, 130 °C (green) and 500 h at 130 °C (purple). Decrease of the AlMe$_3$ signal (') and simultaneous appearance of the signal of methane (+) and signals in the (high field) range assignable to [Al–CH$_2$] moieties are observed.
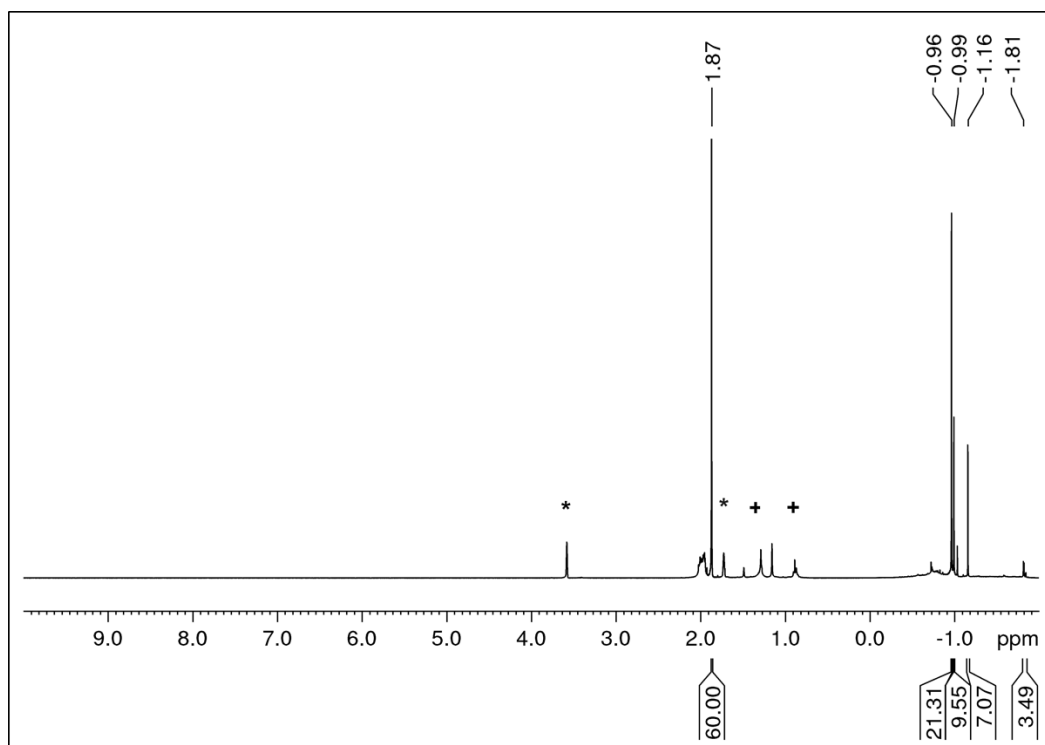
Figure S3a. ^{1}H NMR spectrum (400.11 MHz) of [Cp*$_4$Lu$_2$Al$_{10}$(CH$_2$)$_{12}$(CH$_3$)$_8$] (**1**) in THF-d_8 (*). Assumed fragmentation of **1** is indicated by the appearance of a high-field AlCH$_3$/AlCH$_2$ signal pattern similar to that of a solution of **2b** in THF. The signal at 1.87 ppm is assigned to the remaining [Cp*$_2$Lu] fragment. (+) n-hexane, from washings of compound **1**.
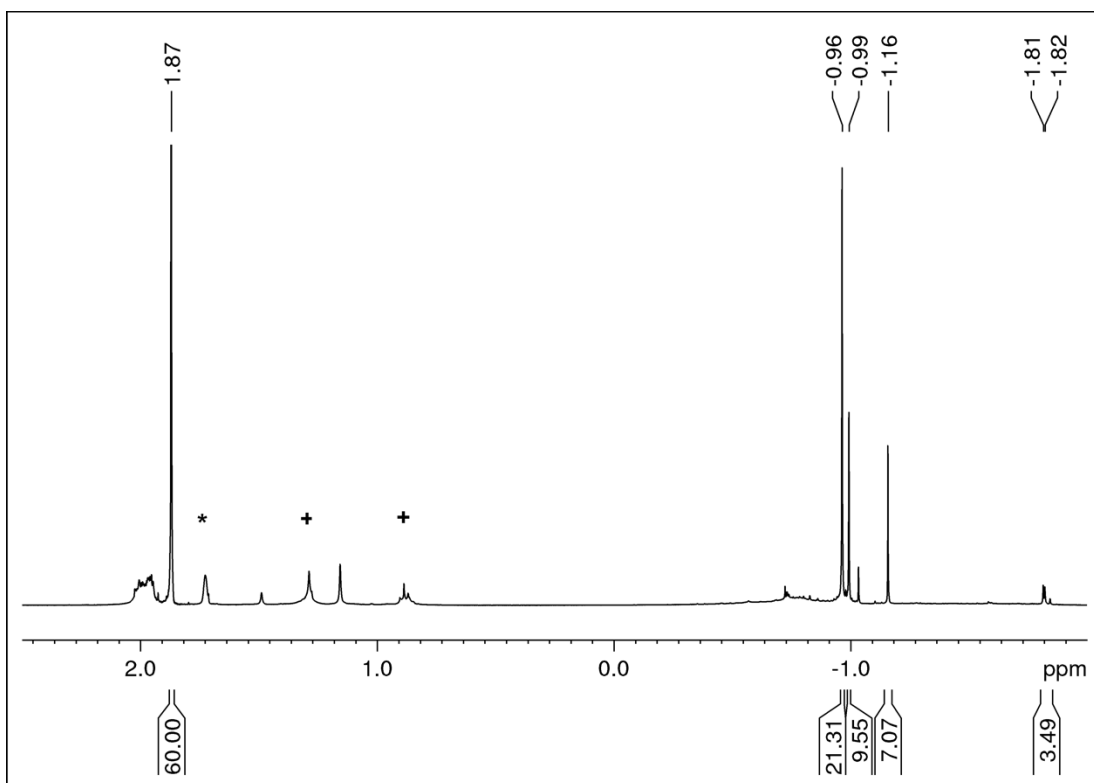
Figure S3b. Section of the ^{1}H NMR spectrum (400.11 MHz) of [Cp*$_4$Lu$_2$Al$_{10}$(CH$_2$)$_{12}$(CH$_3$)$_8$] (**1**) in THF-d_8 (*). Assumed fragmentation of **1** is indicated by the appearance of a high-field AlCH$_3$/AlCH$_2$ signal pattern similar to a solution of **2b** in THF. The signal at 1.87 ppm is assigned to the remaining [Cp*$_2$Lu] fragment.
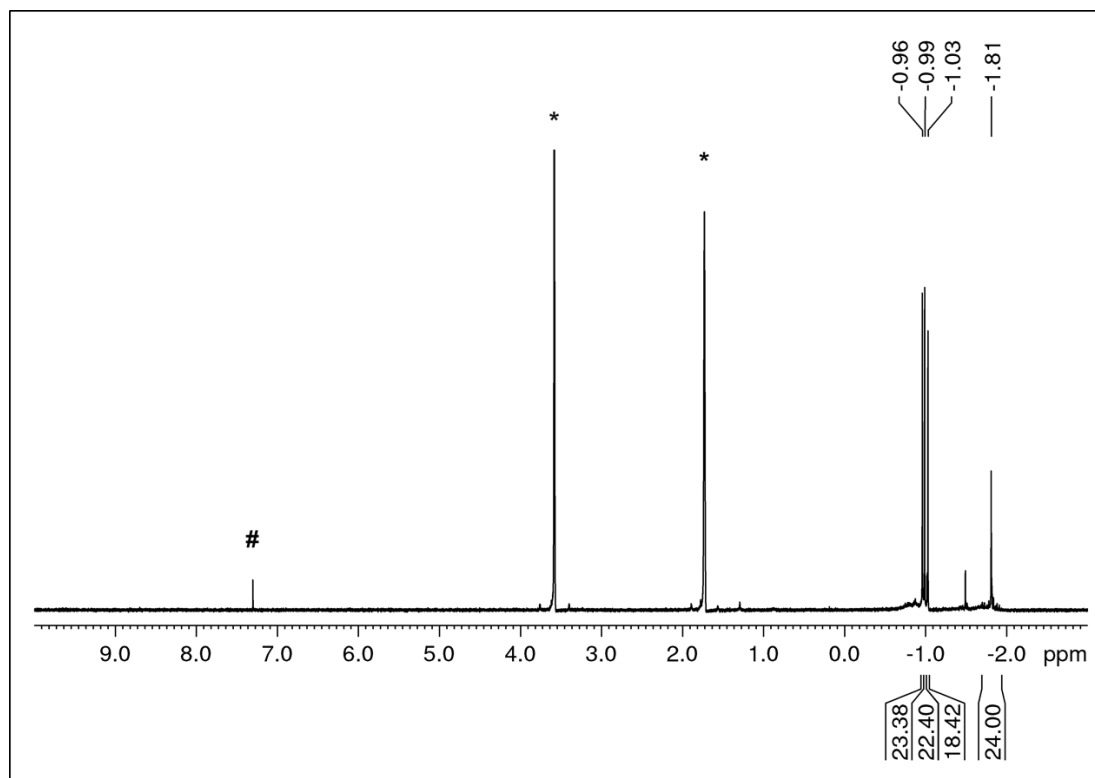
Figure S4. ^{1}H NMR spectrum (400.11 MHz) of **2**$^{\text{Tebbe}}$ obtained via the Tebbe route in THF-d_8 (*).
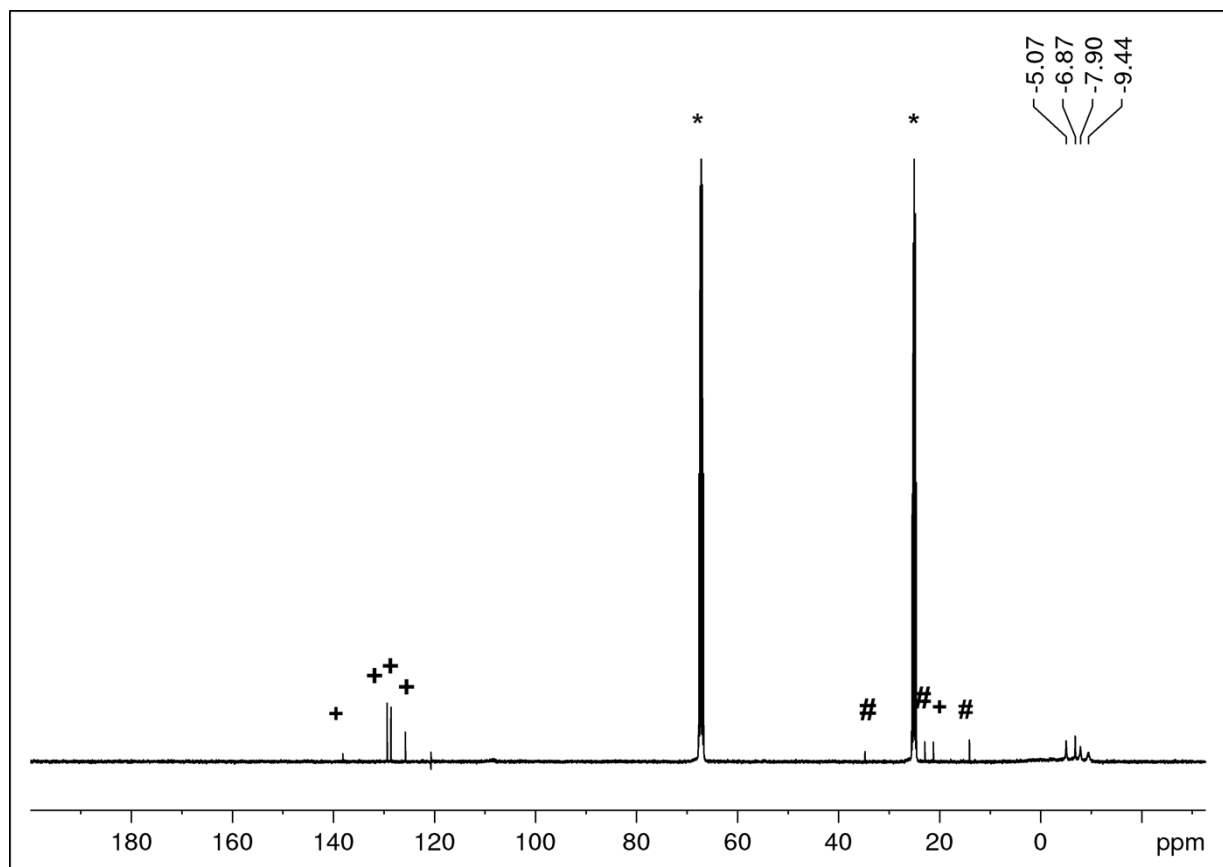
Figure S5. ^{13}C NMR spectrum (100.6 MHz) of **2^{Tebbe}** in THF-d_8 (*); n-pentane (#) and toluene (+) from washings.
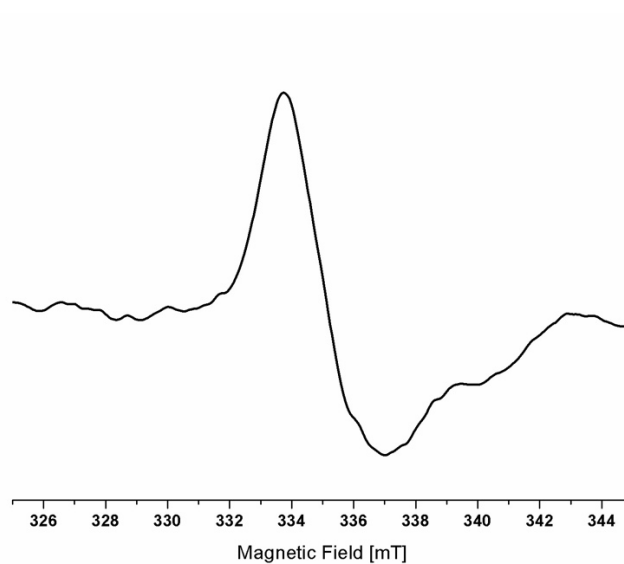
Figure S6. X-band cw-EPR spectrum of **2^{Tebbe}** (neat).
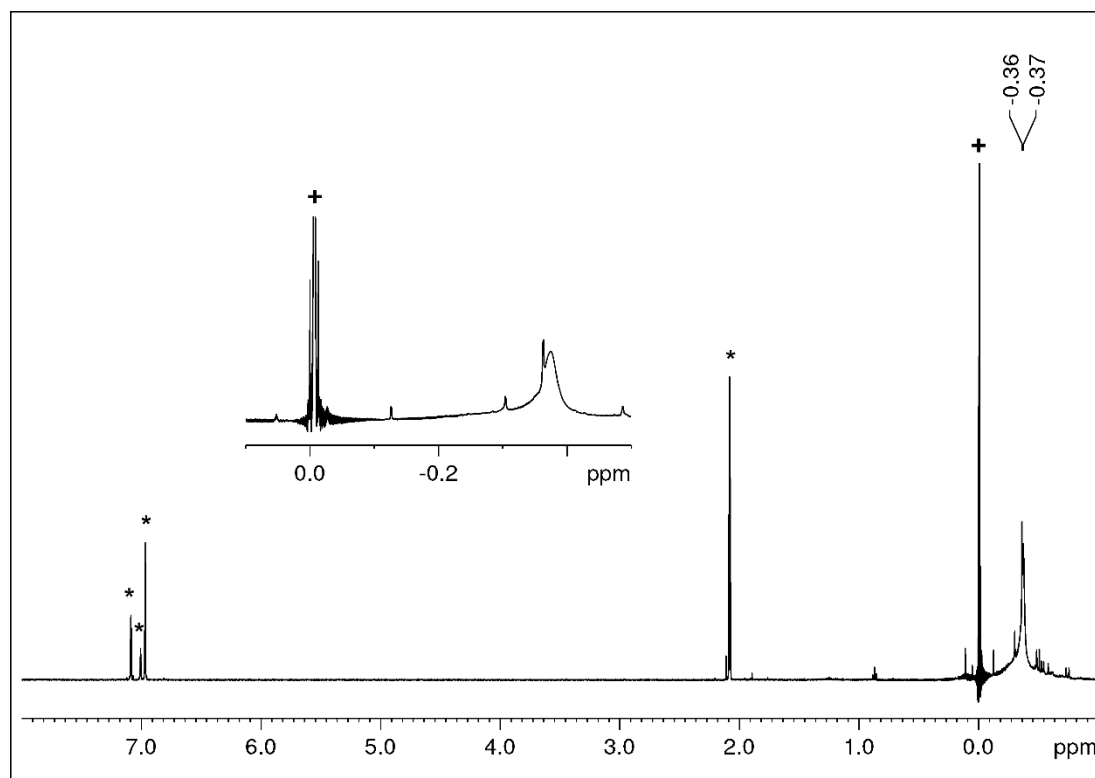
Figure S7. ^{1}H NMR spectrum (500.13 MHz) of "[(CH$_3$)$_{12}$Al$_{12}$(CH$_2$)$_{12}$] (**2b**)" in toluene-d_8 (*) at 26 °C. Signal from TMS is marked with +.
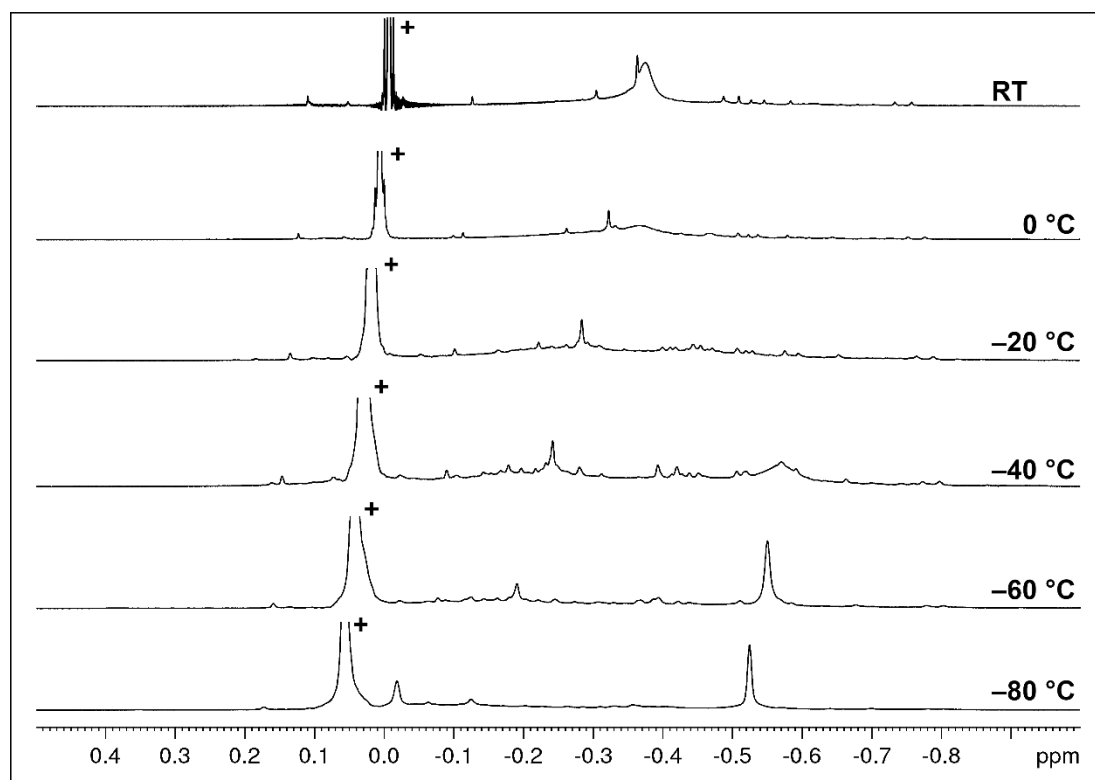
Figure S8. Variable temperature ^{1}H NMR spectra (500.13 MHz) of "[(CH$_3$)$_{12}$Al$_{12}$(CH$_2$)$_{12}$] (**2b**)" in toluene-d_8. Signal from TMS is marked with +.
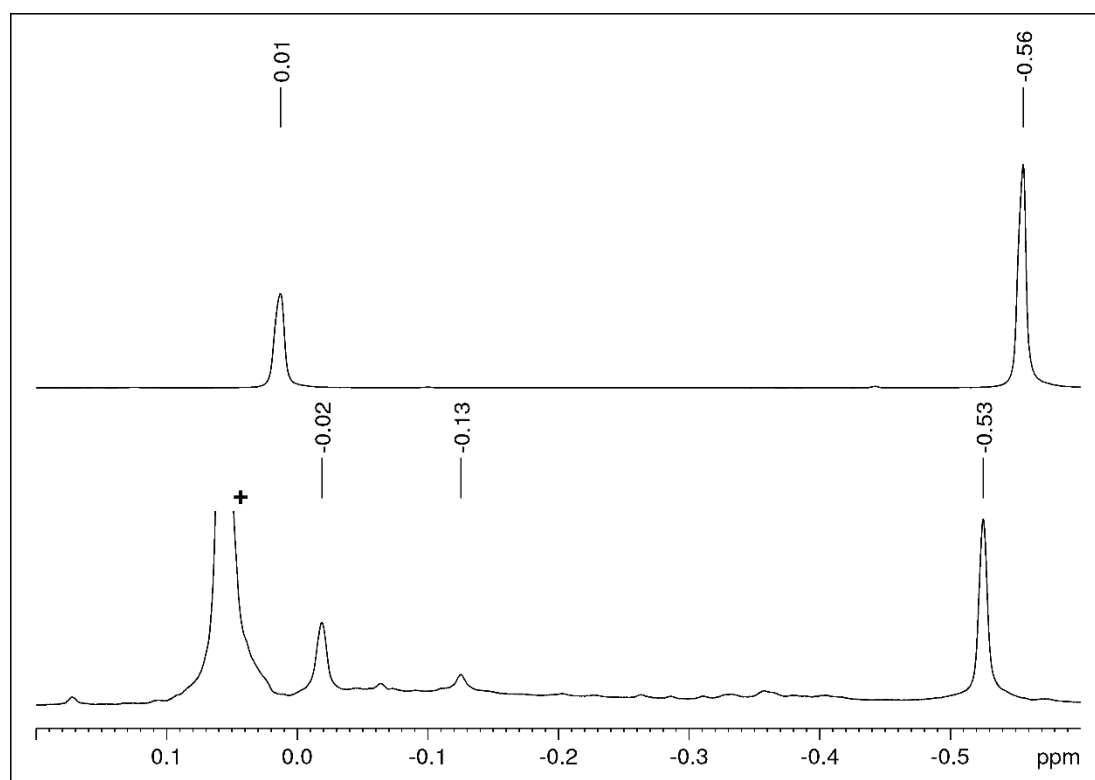
Figure S9. Comparison of the ^{1}H NMR spectra (500.13 MHz) of AlMe$_3$ (top) and "[(CH$_3$)$_{12}$Al$_{12}$(CH$_2$)$_{12}$] (**2b**)" (bottom) in toluene-d_8 at –80 °C. Signal from TMS is marked with +.
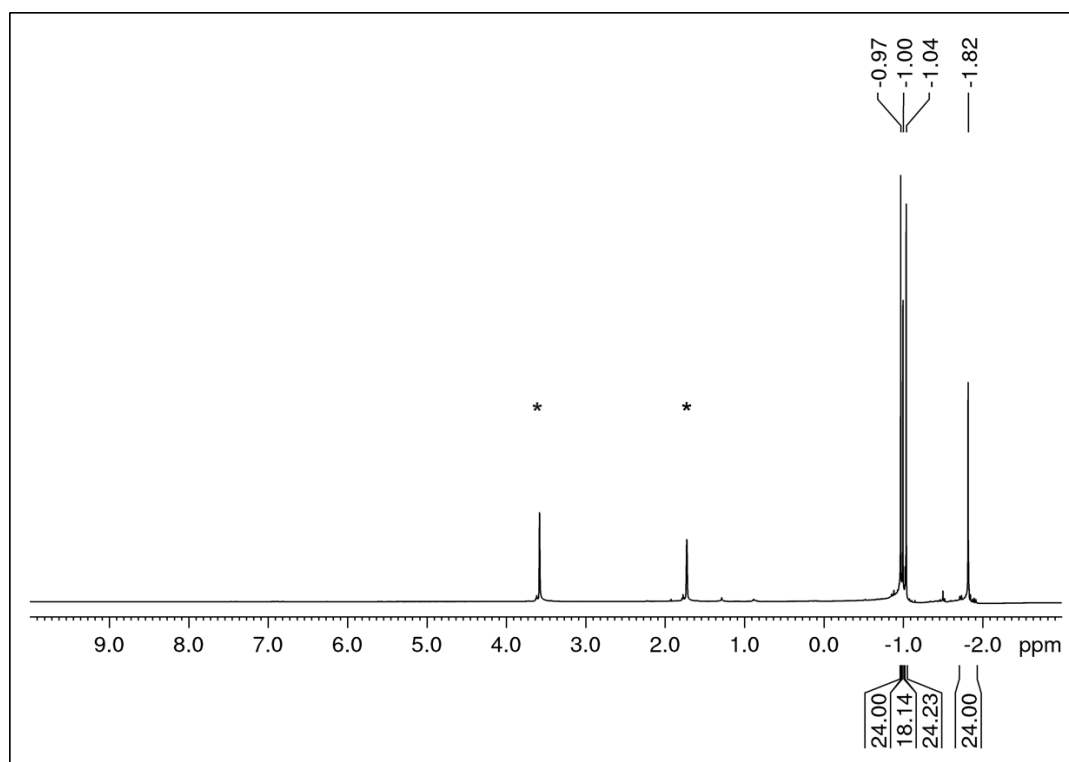
Figure S10. ^{1}H NMR spectrum of (400.11 MHz) [(CH$_3$)$_{12}$Al$_{12}$(CH$_2$)$_{12}$] (**2b**) obtained via the gallium methylene route (24 equiv.) in THF-d_8 (*).
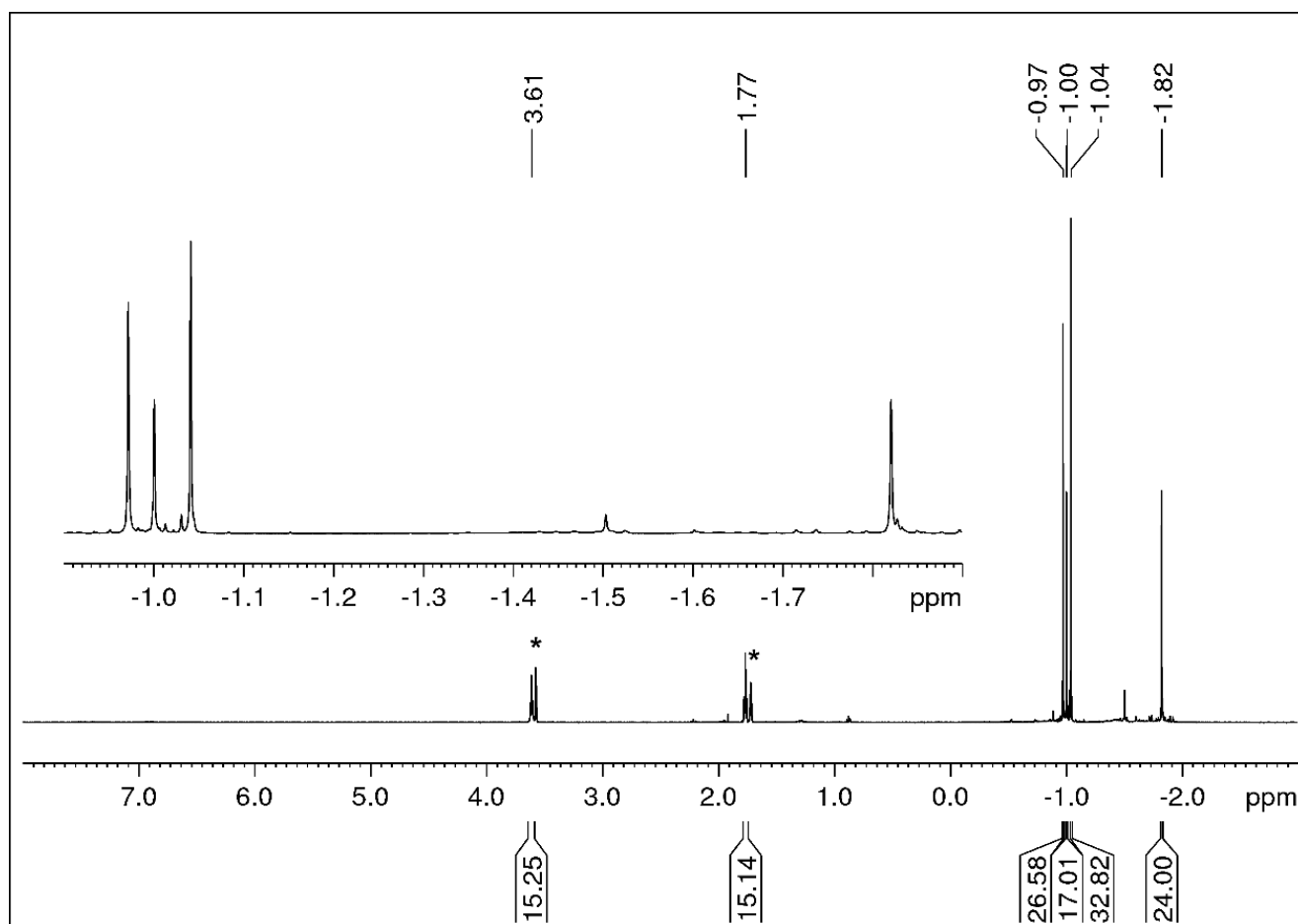
Figure S11. ^{1}H NMR spectrum (500.13 MHz) of a sample of [(CH$_3$)$_{12}$Al$_{12}$(CH$_2$)$_{12}$] (**2b**, obtained via the gallium methylene route (24 equiv.)), after dissolving in THF for 5 min, removing the solvent under vacuum, heating the residue to 110 °C under high vacuum for 6 h, and redissolving it in THF-d_8 (*).
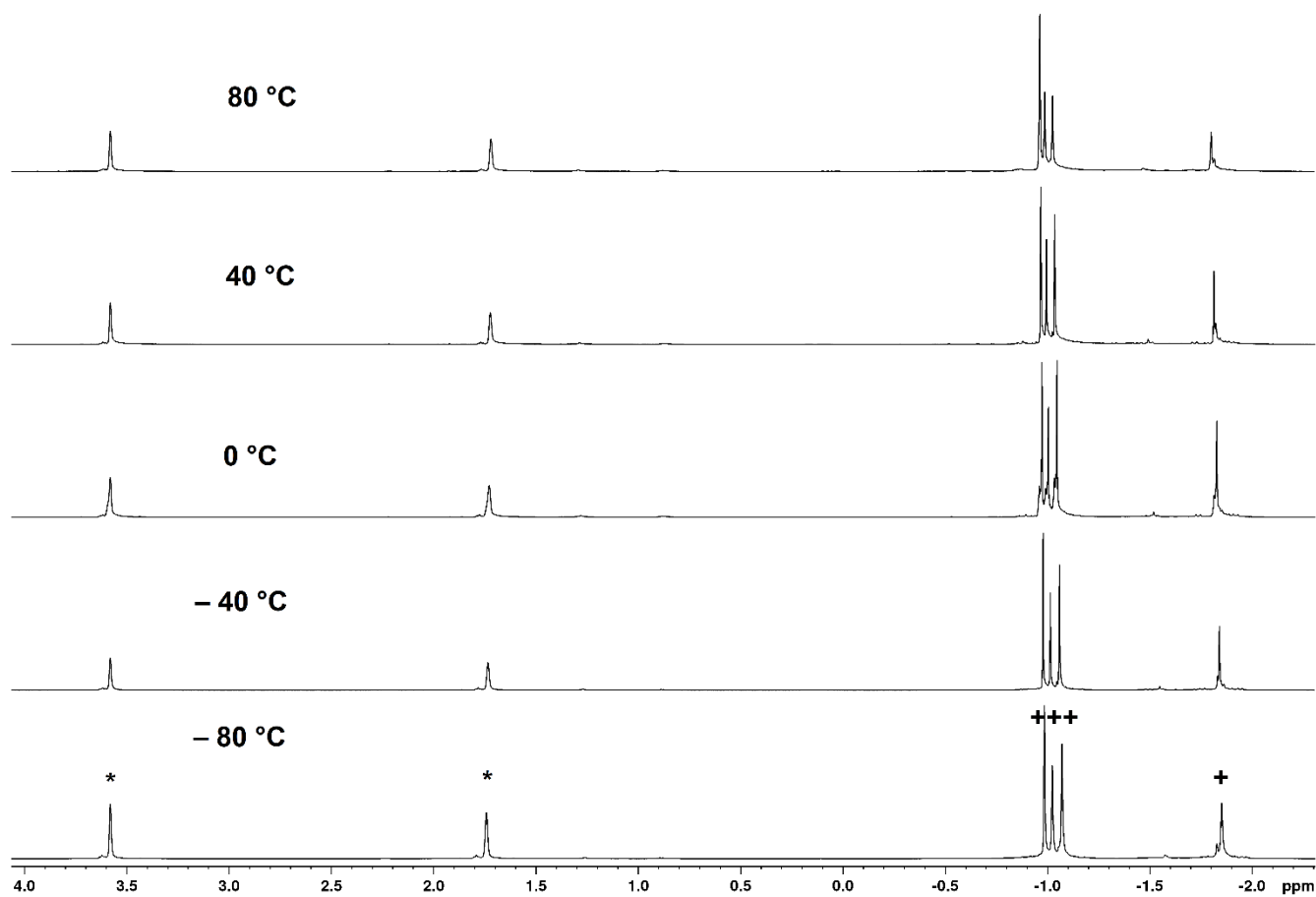
Figure S12. Variable-temperature ^1H NMR spectra (500.13 MHz) of complex $[(CH_3)_{12}Al_{12}(CH_2)_{12}]$ (**2b**) obtained via the gallium methylene route (24 equiv.) in THF-d_8 (*)..
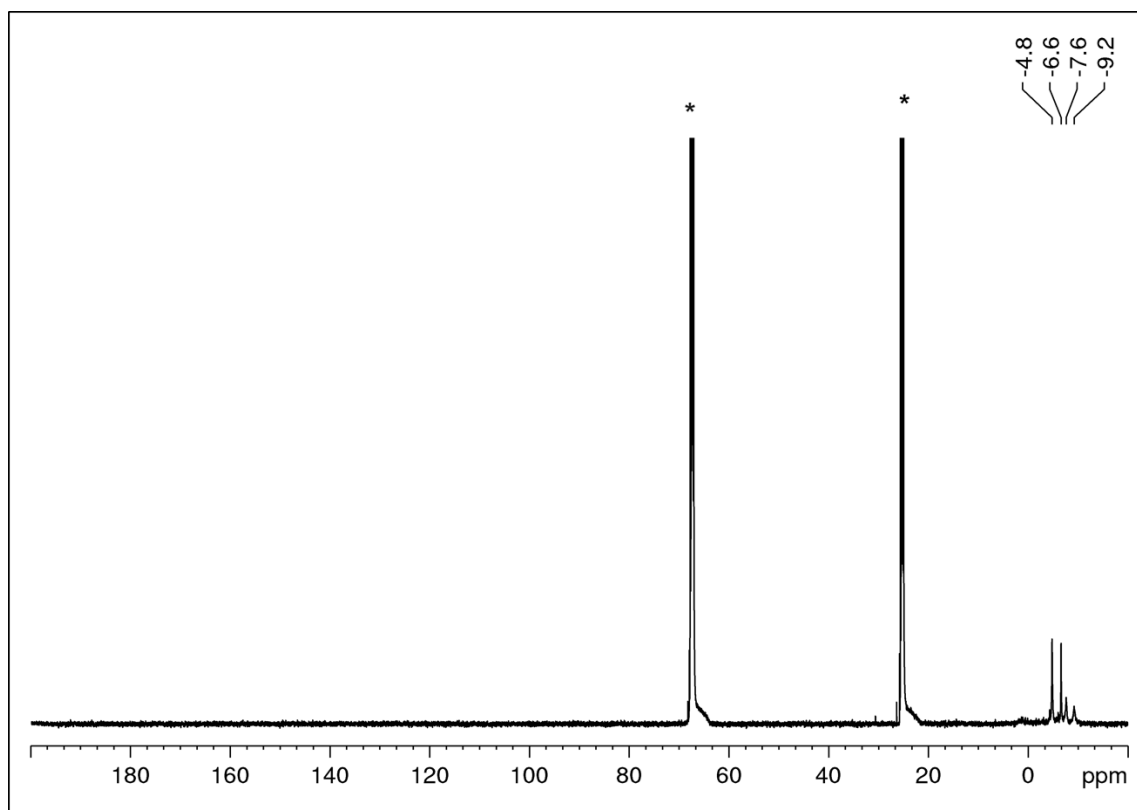
Figure S13. ^{13}C NMR spectrum (100.6 MHz) of $[(CH_3)_{12}Al_{12}(CH_2)_{12}]$ (**2b**) obtained via the gallium methylene route (24 equiv.) in THF-d_8 (*).
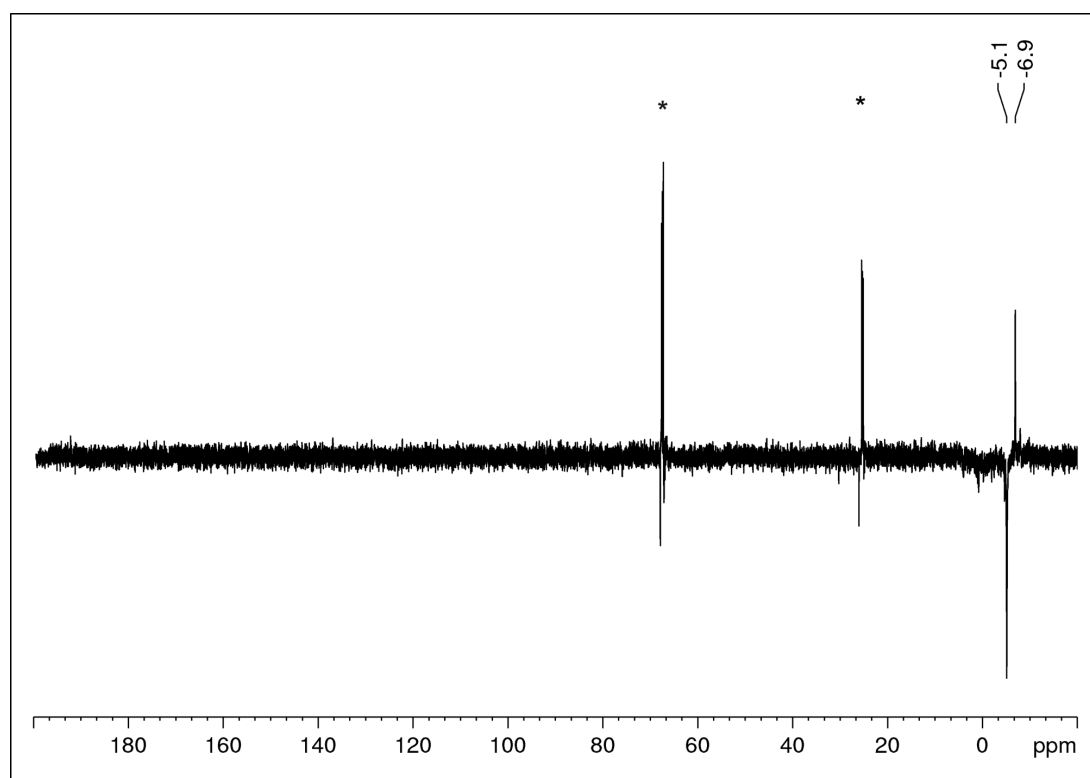
Figure S14. ^{13}C-DEPT135 NMR spectrum of $[(CH_3)_{12}Al_{12}(CH_2)_{12}]$ (**2b**) obtained via the gallium methylene route (24 equiv.) in THF-d_8 (*).
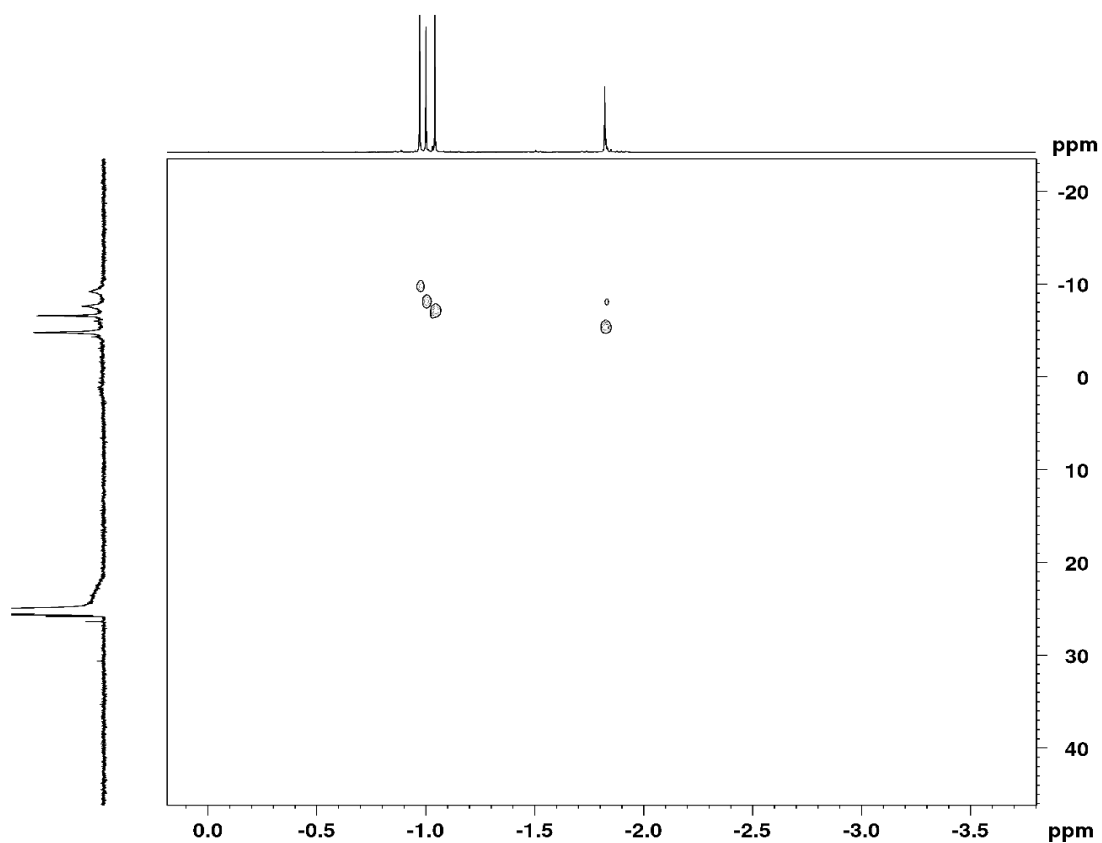
Figure S15. $^1H–^{13}C$ HSQC NMR spectrum of $[(CH_3)_{12}Al_{12}(CH_2)_{12}]$ (**2b**) obtained via the gallium methylene route (24 equiv.) in THF-d_8 (*).
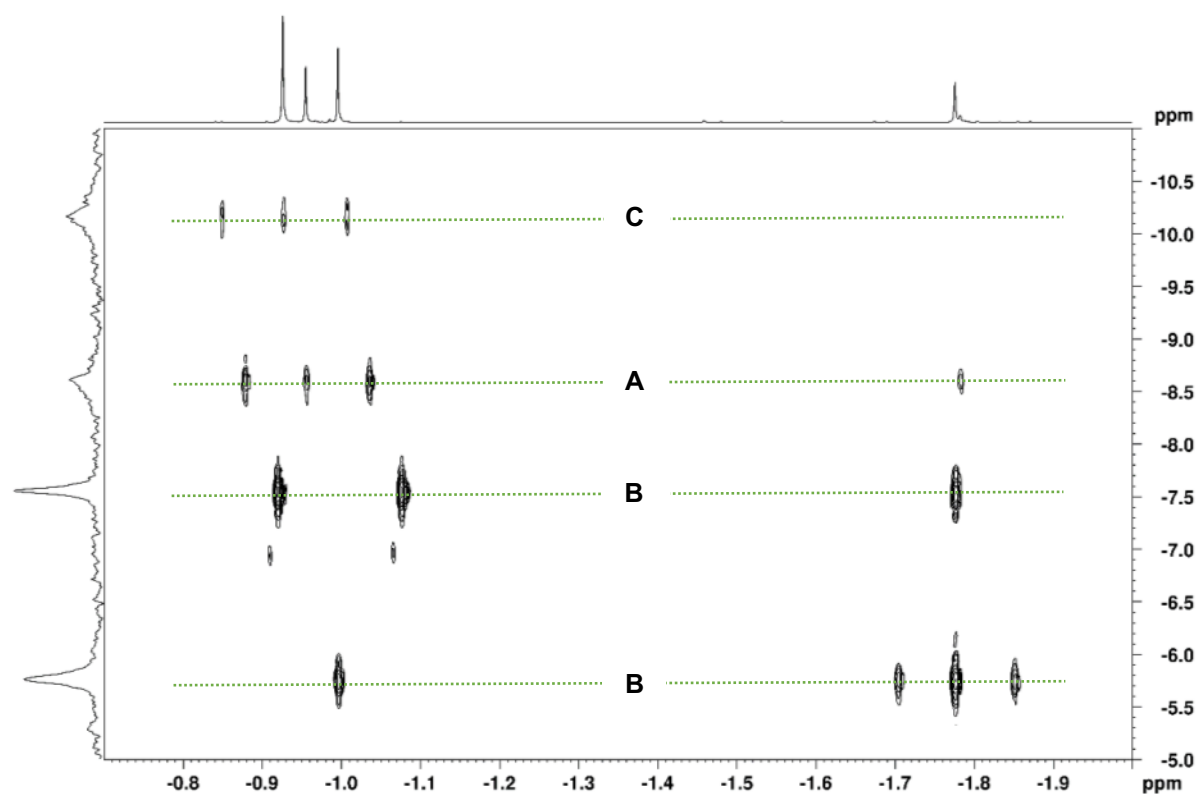
Figure S16. ^1H–^{13}C HMBC NMR spectrum of of $[(CH_3)_{12}Al_{12}(CH_2)_{12}]$ (**2b**) obtained via the gallium methylene route (24 equiv.) in THF-d_8 (*). The denomination of the cross peaks corresponds to the structure denomination shown in Figure S20.
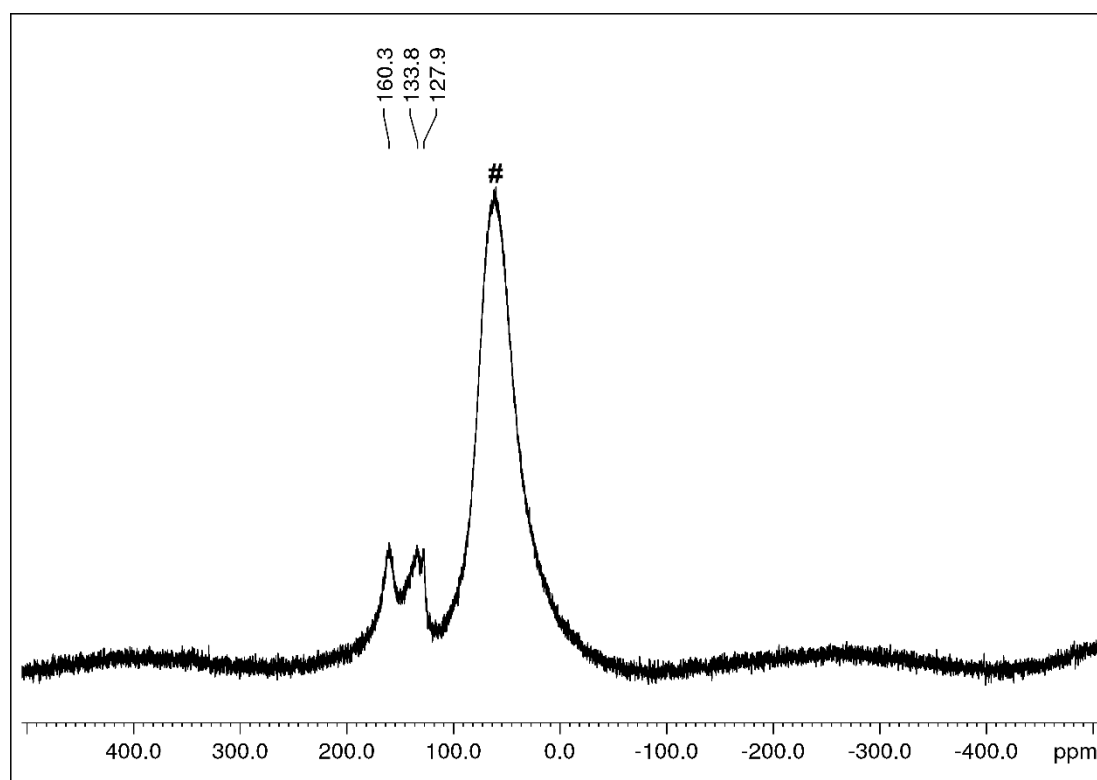
Figure S17. ^{27}Al NMR spectrum (130.32 MHz) of [(CH$_3$)$_{12}$Al$_{12}$(CH$_2$)$_{12}$] (**2b**) in toluene-d_8. Signal from probe head is marked with #.
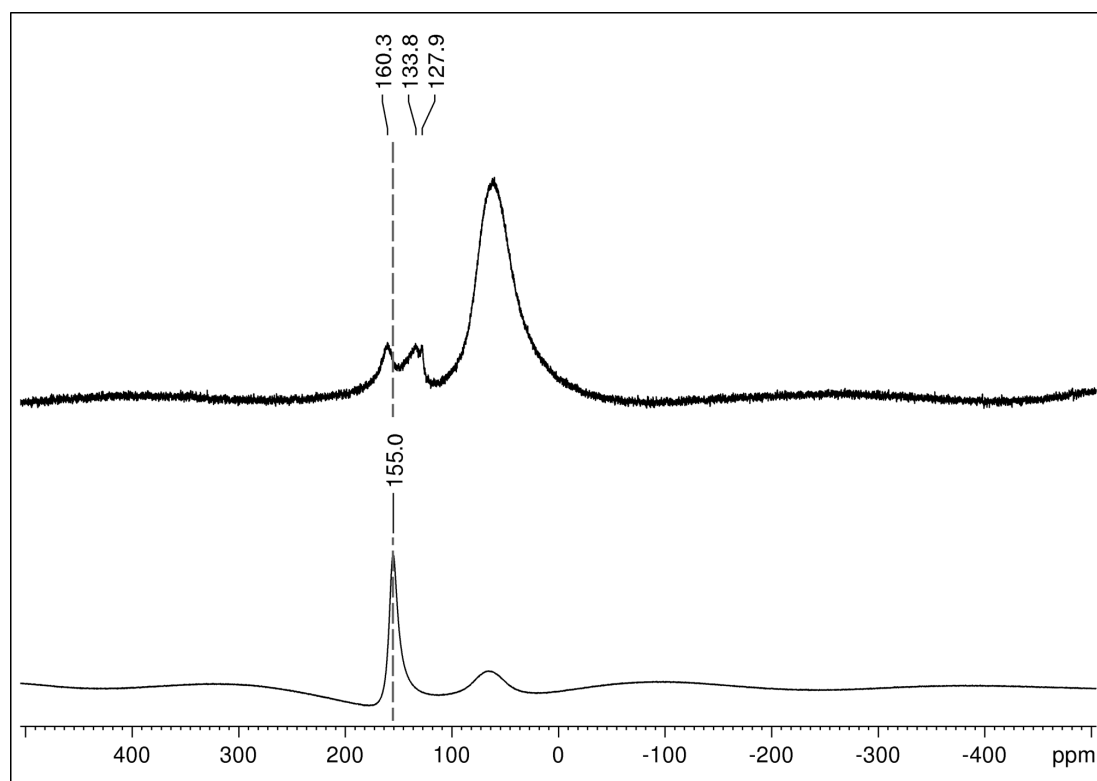
Figure S18. Comparison of the ^{27}Al NMR spectra (130.32 MHz) of [(CH$_3$)$_{12}$Al$_{12}$(CH$_2$)$_{12}$] (**2b**, top) and AlMe$_3$ (bottom) both in toluene-d_8.
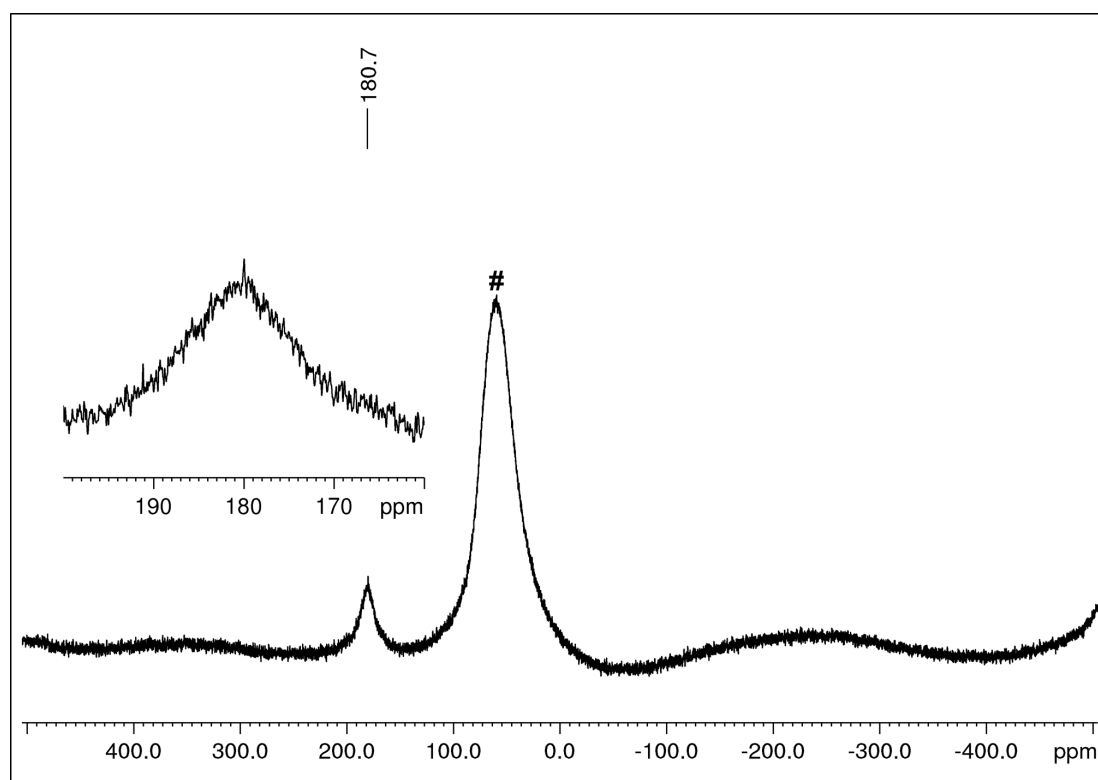
Figure S19. ^{27}Al NMR spectrum (130.32 MHz) of [(CH$_3$)$_{12}$Al$_{12}$(CH$_2$)$_{12}$] (**2b**) in THF-d_8. Signal from probe head is marked with #.
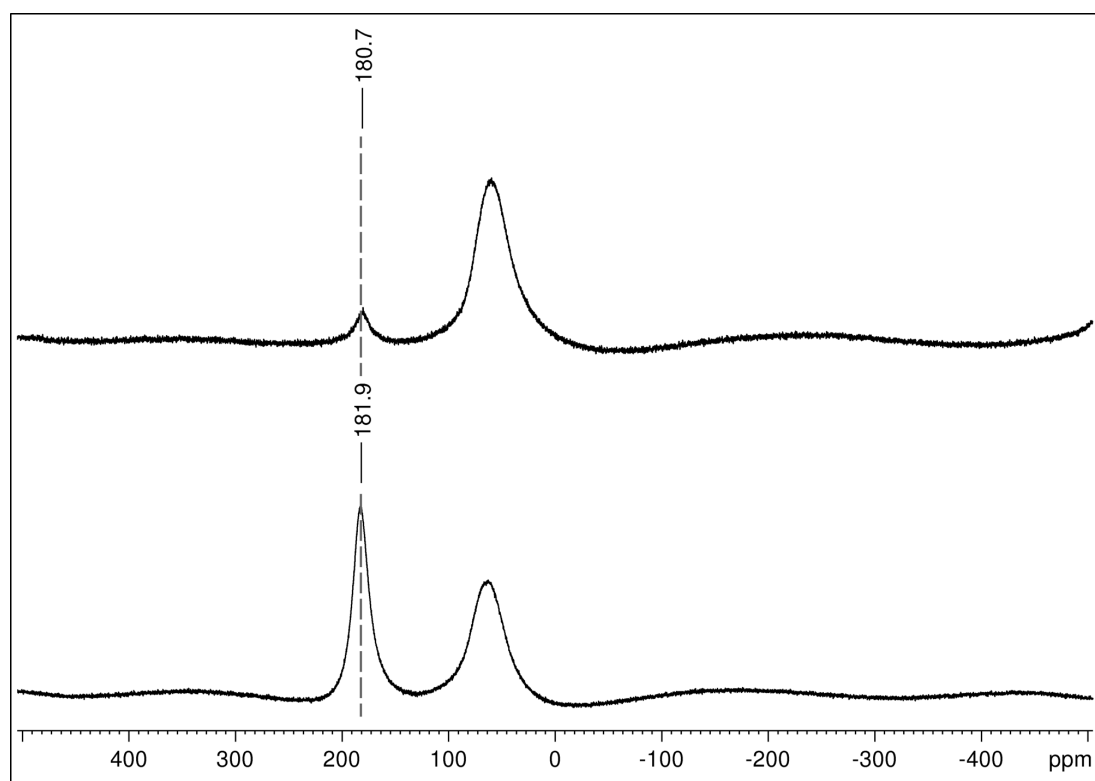
Figure S20. Comparison of the ^{27}Al NMR spectra (130.32 MHz) of [(CH$_3$)$_{12}$Al$_{12}$(CH$_2$)$_{12}$] (**2b**, top) in THF-d$_8$ and AlMe$_3$(THF) (bottom) in toluene-d_8.

PGSE/DOSY Experiment Data

The "solubility" of $[Al_{12}(CH_2)_{12}(CH_3)_{12}]$ (**2b**) is limited to THF, where the cluster disaggregates into several species. Three species $[(THF)Me_2Al–CH_2–AlMe_2(THF)]$ (**A**), $[MeAl(CH_2)(THF)]_3$ (**B**), and $Me_3Al(THF)$ (**C**) are suggested. The evaluation of the DOSY experiment confirmed three species. Furthermore, the presumed structures with molecular weights match well with those calculated (see Table S1b).[3]

Table S1a. Diffusion coefficients in THF-d_8 determined via PGSE NMR experiments

Signal	Diffusion coefficient	Hydrodynamic radii (measured)	Hydrodynamic radii (calculated)	Species
0 ppm	$2.458 \cdot 10^{-9}$ m^2/s	--	3.15 Å	TMS (internal reference)
-0.966 ppm (C**H**$_3$)	$2.121 \cdot 10^{-9}$ m^2/s	3.65 Å	3.73 Å	**C**
-0.995 ppm (C**H**$_3$)	$1.552 \cdot 10^{-9}$ m^2/s	5.12 Å	4.66 Å	**A**
-1.823 ppm (C**H**$_2$)	$1.473 \cdot 10^{-9}$ m^2/s			
-1.036 ppm (C**H**$_3$)	$1.317 \cdot 10^{-9}$ m^2/s	5.89 Å	5.26 Å	**B**
-1.816 ppm (C**H**$_2$)	$1.311 \cdot 10^{-9}$ m^2/s			

The measured hydrodynamic radii were calculated from the PGSE experiments using the T1/T2 module of Topspin, a sample viscosity of η = 0,282 mPa·s which was derived from the diffusion coefficient of TMS in the sample and its calculated hydrodynamic radius at 298 K using the Stokes-Einstein equation $\eta = \frac{k_B \cdot T}{6 \cdot \pi \cdot r_H \cdot D}$.
The calculated hydrodynamic radii were obtained from the energy optimized geometries of the molecules and the calculated solvent accessible volumes with a probe radius of 1.4 Å.

Table S1b. Molecular weight determination *via* PGSE experiment and the method described in [3]

	Species **C** [g/mol]	Species **A** [g/mol]	Species **B** [g/mol]
Highly compacted spheres	125	248	330
Ellipsoids	137	244	311
Expanded discs	161	252	304
Merged	143	249	313
Calculated	*144*	*272*	*384*

These results together with the NMR experiments performed on the THF sample lead to the following three structures present after dissolving $[(CH_3)_{12} Al_{12}(CH_2)_{12}]$ in THF-d_8.

A   **B**   **C**
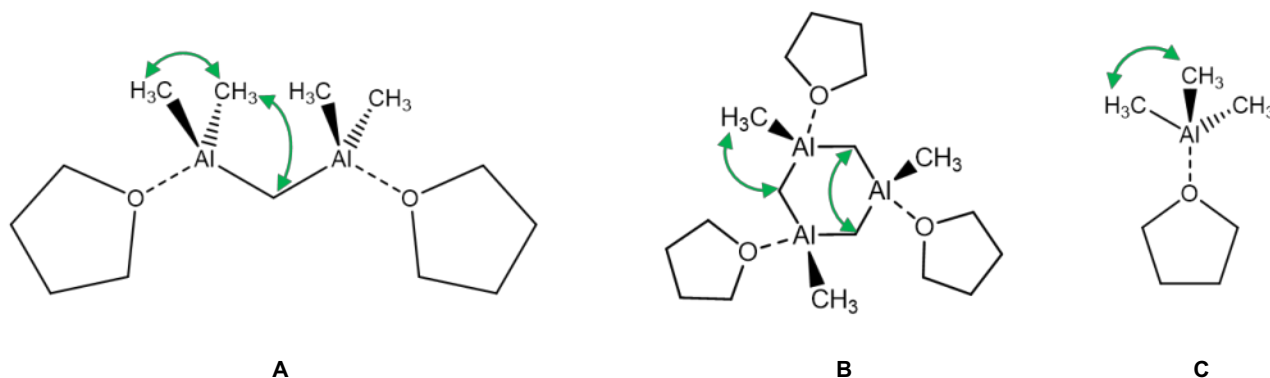
Figure S21. Structures in THF-d_8 derived by PGSE experiments (the green arrows indicate the correlations which can be seen in the HMBC spectrum (Figure S14).
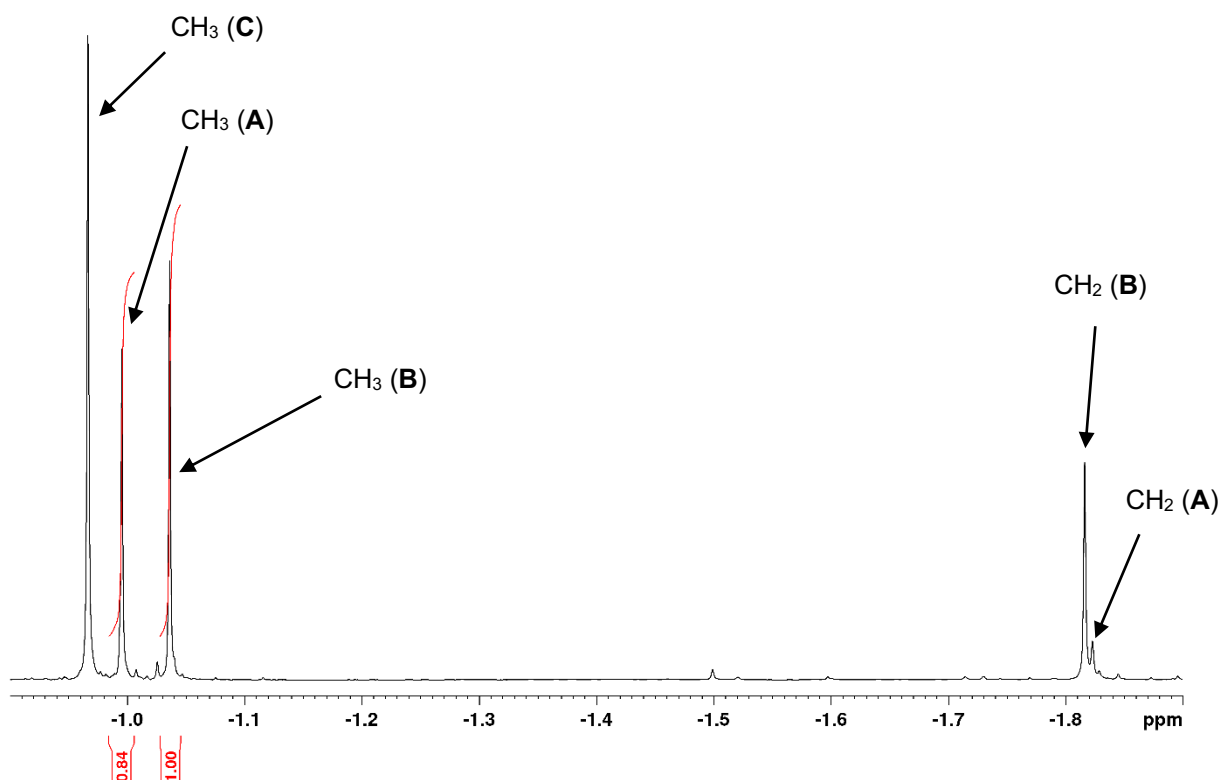
Figure S22. ^{1}H NMR spectrum of $[(CH_3)_{12}Al_{12}(CH_2)_{12}]$ (**2b**) in THF-d_8 with signal assignment and integrals.

From the methyl signals at -0.99 and -1.03 ppm for **A** and **B**, respectively, the ratio of the three species formed in THF can be calculated:

Table S2a. Ratios of the two methylene species in THF derived from the integrals of the NMR methyl signals

Signal	Species (number of CH$_3$ groups)	Integral	Normalized Integral	Percentage	Molar ratio (**A:B**)
-0.99 ppm	**A** (4)	0.84	0.63	38.7%	7:11
-1.03 ppm	**B** (3)	1	1	61.3%	

Taking into account species **C**, a percentage and molar ratio (**A:B:C**) of 19%:30%:50% and 7:11:19, respectively, is obtained.

This result correlates well with the ratio obtained by evaluating the integrals of the CH_2 groups. Due to signal overlap this can only be derived from a deconvolution of the two signals at app. -1.82 ppm:
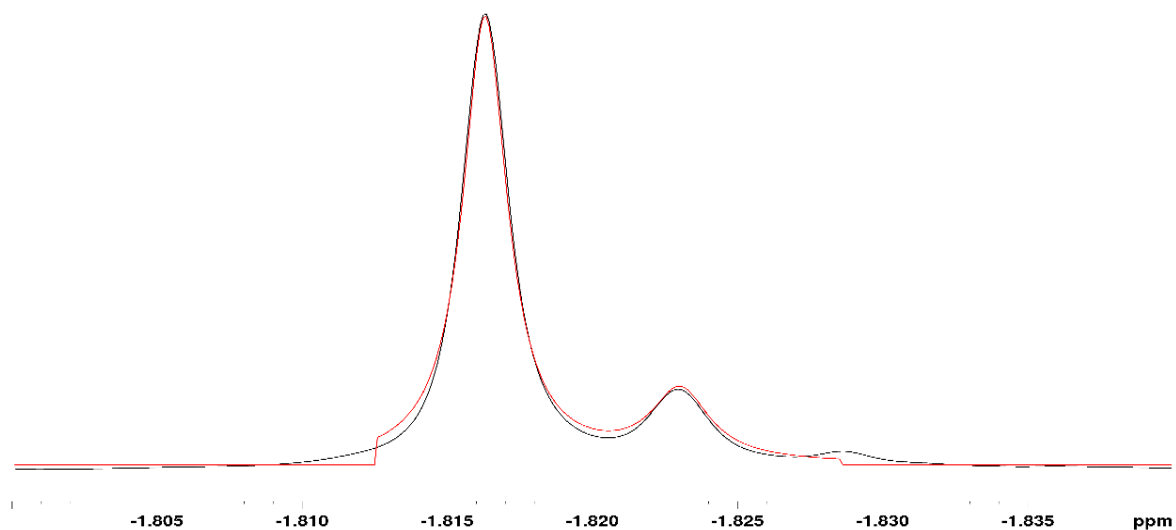
Figure S23. ^{1}H NMR signals of the CH_2 groups and the corresponding deconvolution result (red curve).

Table S2b. Ratios of the two species in THF derived from the integrals of the NMR methylene signals

Signal	Species (number of CH_2 groups)	Integral	Normalized integral	Percentage	Molar ratio (**A**:**B**)
-1.816 ppm	**B** (3)	4.83	1.61	38.3 %	5:8
-1.823 ppm	**A** (1)	1	1	61.7 %	
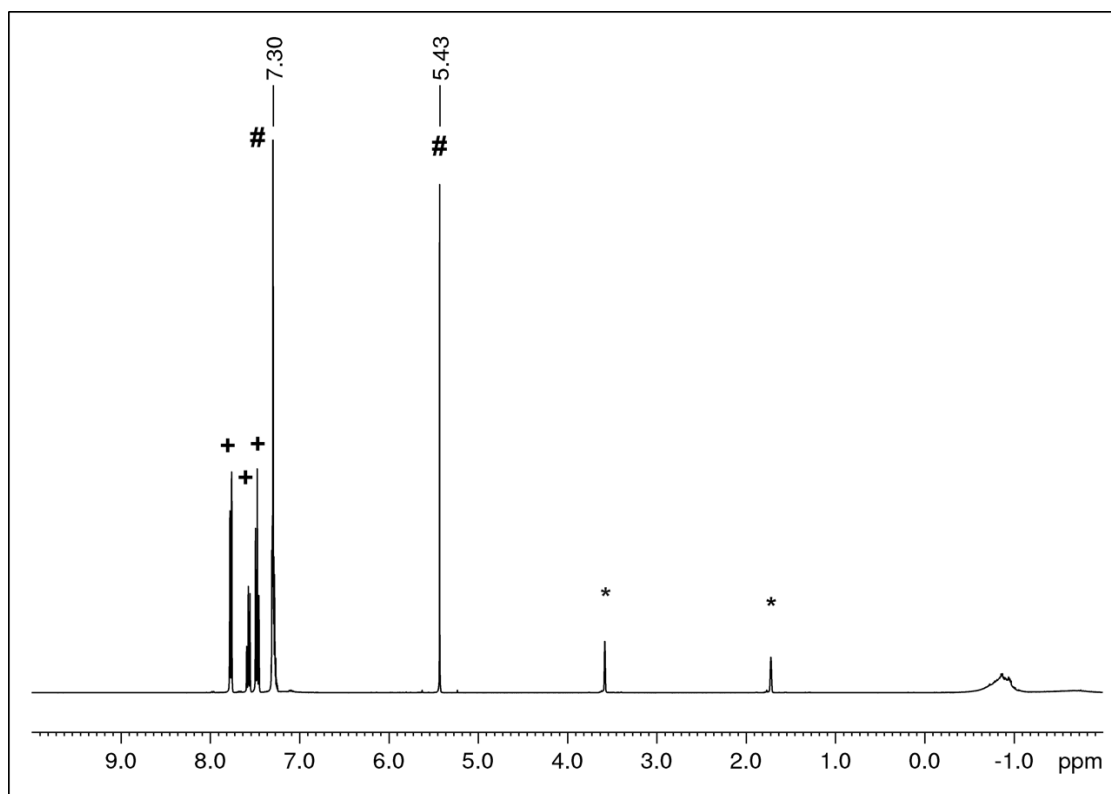
Figure S24. ^1H NMR spectrum (400.11 MHz) of the reaction of $[(CH_3)_{12}Al_{12}(CH_2)_{12}]$ (**2b**) with 12 equiv. benzophenone (+) in THF-d_8 (*). Product 1,1-diphenylethylene (#).
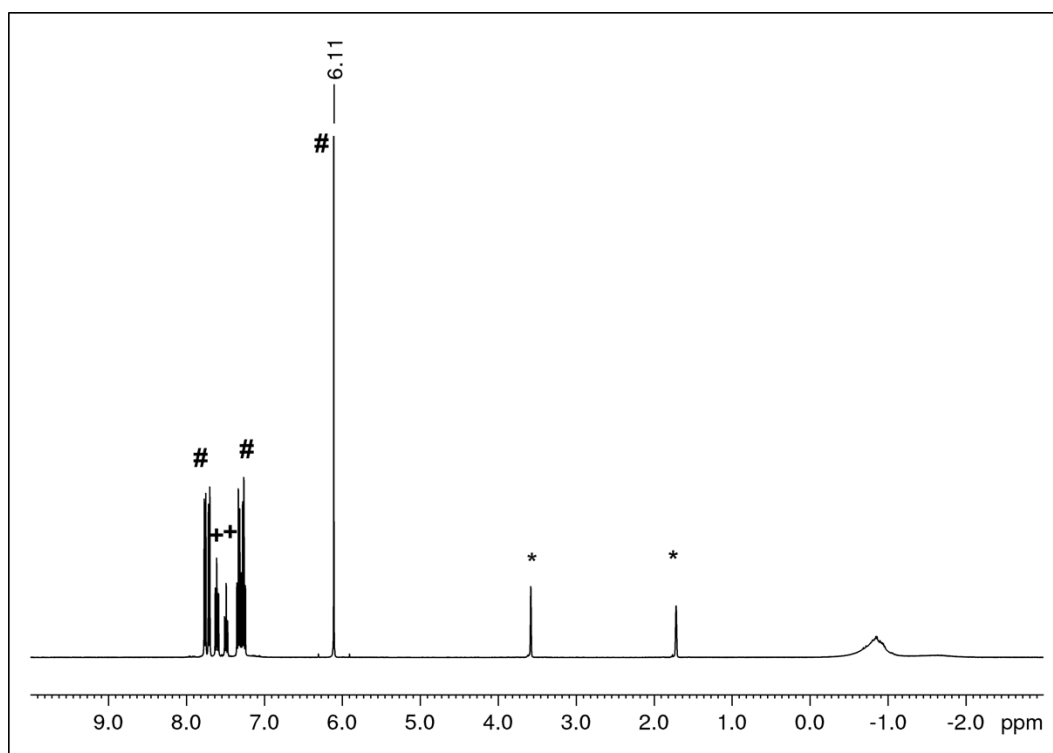
Figure S25. ^1H NMR spectrum (400.11 MHz) of the reaction of $[(CH_3)_{12}Al_{12}(CH_2)_{12}]$ (**2b'**) with 12 equiv. 9-fluorenone (+) in THF-d_8 (*). Product 9-methylene-fluorenone (#).
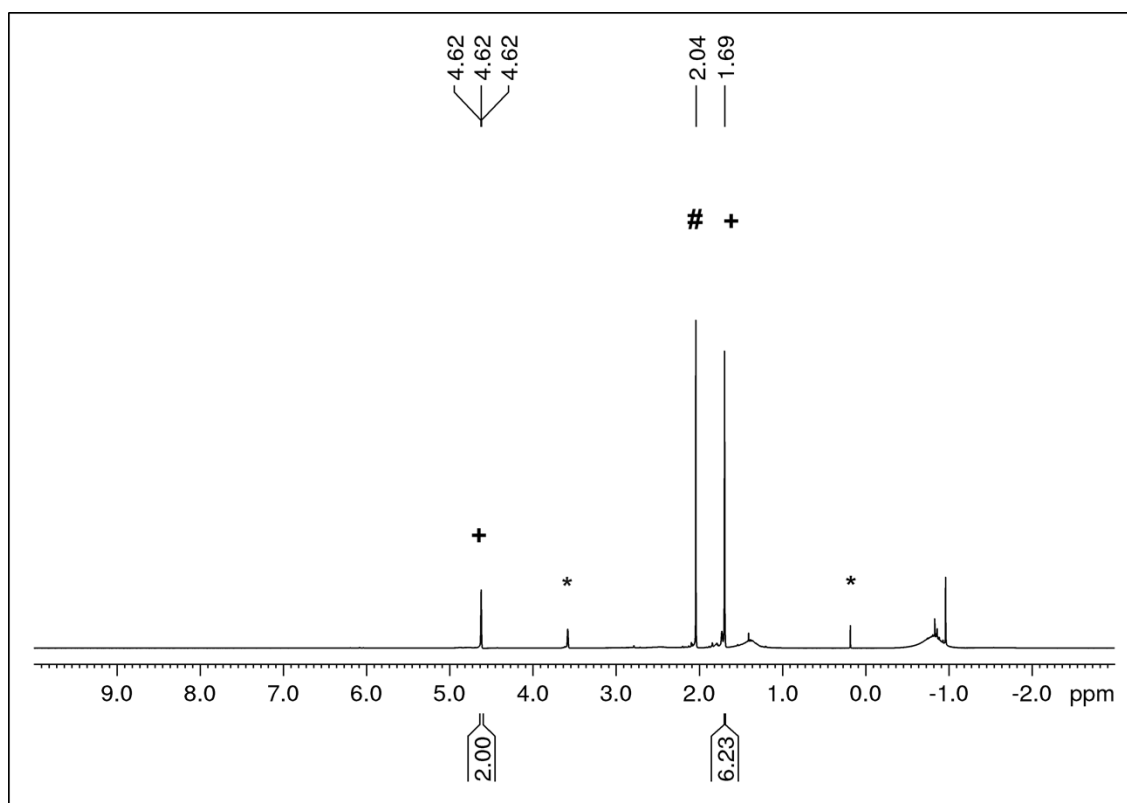
Figure S26. ^{1}H NMR spectrum (400.11 MHz) of the reaction of compound $[(CH_3)_{12}Al_{12}(\mu_3\text{-}CH_2)_{12}]$ (**2b**) with 12 equiv. acetone (#) in THF-d_8 (*). Product isobutene (+).

X-Ray Crystallography

Compound **1** was crystallized from a reaction mixture of $Cp^*_2LuAlMe_4$ and $AlMe_3$ in toluene-d_8 heated to 130 °C. Single crystals of **2a/b** were obtained by heating a suspension of $Ga_8(CH_2)_{12}$ and $AlMe_3$ in benzene to 70 °C. Single crystals were selected and coated with Paratone N (known as Parabar 10312) on a microloop. The crystals were mounted under an argon stream to prevent possible decomposition. Single crystal X-ray diffraction studies were performed on a Bruker APEX DUO instrument with an IµS microfocus sealed tube and QUAZAR optic for MoK$_\alpha$ radiation (λ = 0.71073 Å). The data collection strategy was determined using COSMO[4] employing ω-scans. Raw data were processed with APEX[5] and SAINT,[6] corrections for absorption were performed using SADABS.[7] The solid-state structures were solved and refined against all data by full-matrix least-squares methods on F^2 with SHELXTL[8] and Shelxle.[9] All graphics were produced by using Mercury.[10] Data of complexes **1**, **2a**, and **2b** are given in Table S3.

Table S3. Crystallographic data for compounds **1** and **2a**, and **2b**

	1	**2a**	**2b**
CCDC	2157627	2157626	2157628
formula	$C_{60}H_{108}Al_{10}Lu_2$ $\cdot\ C_7H_8$	$C_{24}H_{60}Al_{10.64}Ga_{1.36}$	$C_{24}H_{60}Al_{12}$
M_r [g/mol^{-1}]	1541.33	730.44	672.48
colour/shape	colourless needles	colourless needles	colourless needles
crystal dimensions [mm]	0.252 x 0.135 x 0.126	0.237 x 0.100 x 0.086	0.169 x 0.166 x 0.164
crystal system	triclinic	monoclinic	monoclinic
space group	P-1	C2/c	C2/c
a [Å]	11.7305(6)	31.188(3)	31.268(2)
b [Å]	16.3987(8)	17.1757(16)	17.1633(12)
c [Å]	20.3079(10)	21.3486(19)	21.384(3)
α [°]	73.782(2)	90	90
β [°]	85.711(2)	131.4490(10)	131.5820(10)
γ [°]	78.890(2)	90	90
V [Å^3]	3679.9(3)	8571.7(14)	8584.2(13)
Z	2	8	8
T [K]	100(2)	100(2)	100(2)
λ [Å]	0.71073	0.71073	0.71073
ρ_{calcd} [g cm^{-3}]	1.391	1.132	1.041
μ [mm^{-1}]	2.823	1.077	0.285
F (000)	1580	3072	2880
θ range [°]	1.315/28.700	1.471/28.760	2.293/30.525
unique reflections	18987	11132	13103
observed reflections (I > 2σ)	14048	8769	10187
R1/wR2 (I > 2σ)[a]	0.0392/0.0853	0.0315/0.0785	0.0350/0.0905
R1/wR2 (all data)[a]	0.0628/0.0968	0.0458/0.0853	0.0905/0.0994
GOF	1.032	1.043	1.032

[a] $R1 = \Sigma(||F_0|-|F_c||)/\Sigma|F_0|$, $F_0 > 4\sigma(F_0)$. $wR2 = \{\Sigma[w(F_0^2-F_c^2)^2/\Sigma[w(F_0^2)^2]\}^{1/2}$.
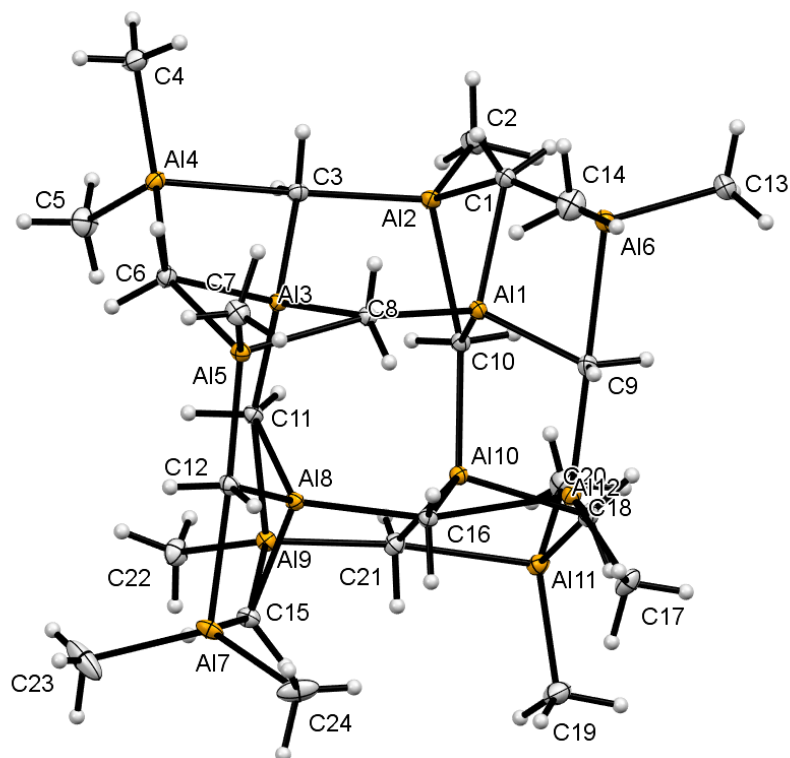
Figure S27. Crystal structure of $[(CH_3)_{12}Al_{12}(\mu_3\text{-}CH_2)_{12}]$ (**2b**). Atomic displacement parameters set at 50% probability. All hydrogen atoms except C19 were located from difference Fourier maps and refined isotropic or in some cases a constant temperature-independent multiplier of 1.5 was given.
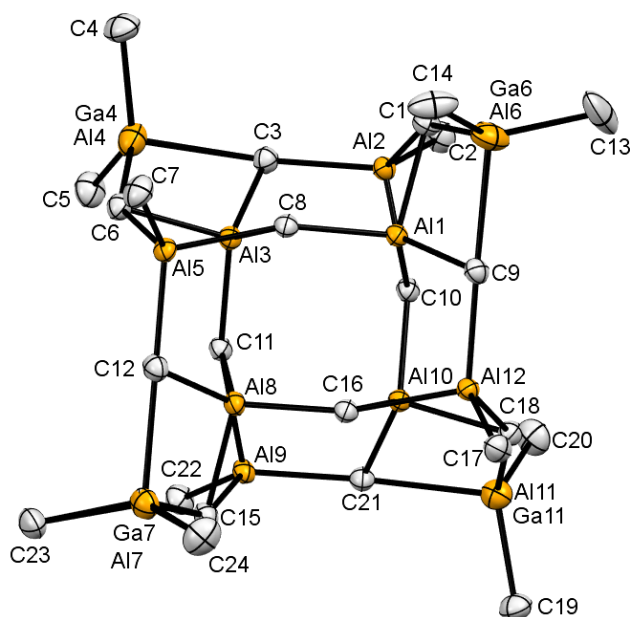
Figure S28. Crystal structure of $[(CH_3)_{12}Al_{12}(\mu_3\text{-}CH_2)_{12}]$ (**2a**). Atomic displacement parameters set at 50% probability. Hydrogen atoms are omitted for clarity.

IR Spectra
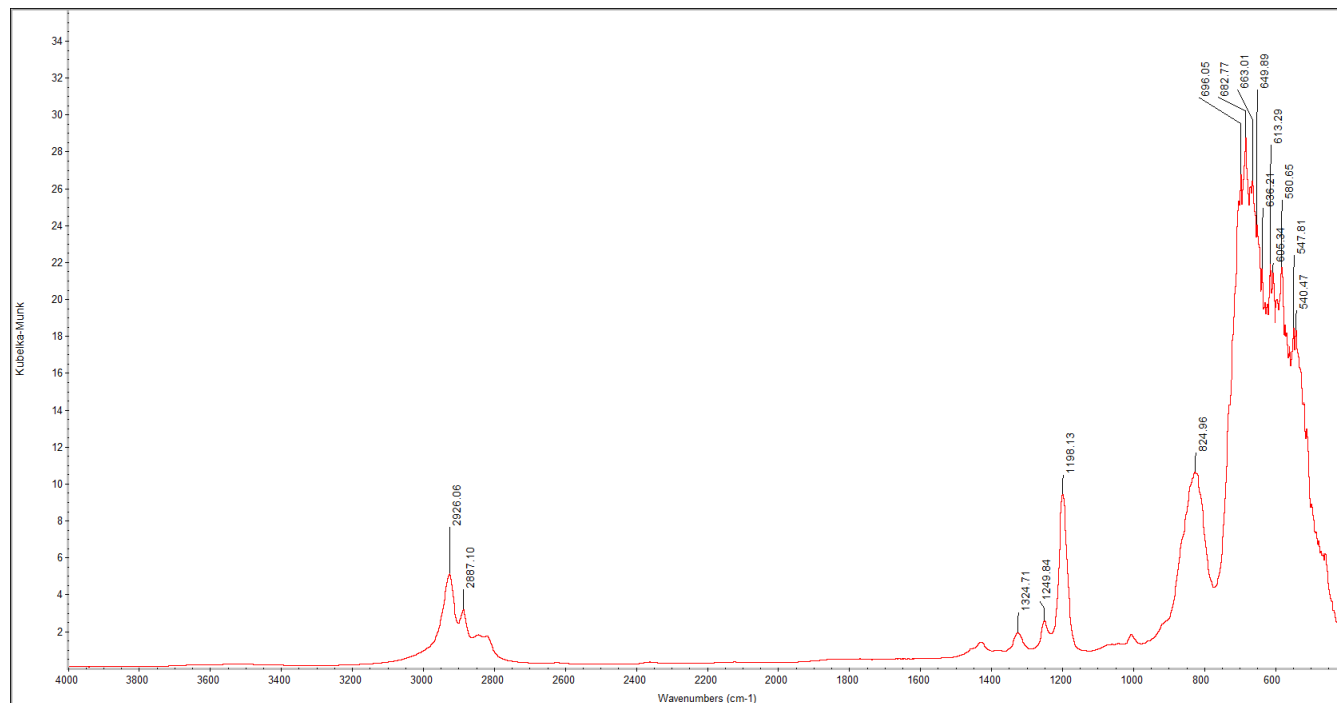
Figure S29. DRIFT spectrum of compound **2b**.

References

[1] V. M. Birkelbach, F. Kracht, H. M. Dietrich, C. Stuhl, C. Maichle-Mössmer, R. Anwander, *Organometallics* **2020**, *39*, 3490-3504.

[2] M. Bonath, C. Maichle-Mössmer, P. Sirsch, R. Anwander, *Angew. Chem. Int. Ed.* **2019**, *58*, 8206-8210; *Angew. Chem.* **2019**, *131*, 8290-8294.

[3] R. Neufeld, D. Stalke, *Chem. Sci.* **2015**, *6*, 3354-3364.

[4] *COSMO v. 1.61*, Bruker AXS Inc., Madison, WI, 2012.

[5] APEX3 v2019.11-0, Bruker AXS Inc., Madison, WI, 2019.

[6] *SAINT V8.40B, Bruker Nano, Inc., 2019*.

[7] *SADABS*: L. Krause, R. Herbst-Irmer, G. M. Sheldrick, D. Stalke, *J. Appl. Cryst.* **2015**, *48***,** 3-10.

[8] *SHELXT*: G. M. Sheldrick, *Acta Cryst.* **2015**, *A71*, 3-8.

[9] SHELXLE: C. B. Huebschle, G. M. Sheldrick, B. Dittrich, *J. Appl. Crystallogr.* **2011**, *44*, 1281-1284.

[10] Mercury CSD 2.0: C. F. Macrae, I. J. Bruno, J. A. Chisholm, P. R. Edgington, P. McCabe, E. Pidcock, L. Rodriguez-Monge, R. Taylor, J. van de Streek, P. A. Wood, *J. Appl. Cryst.* **2008**, *41*, 466-470.

Gallium Methylene in the Pocket

ORGANOMETALLICS

Gallium Methylene in the Pocket

Georgios Spiridopoulos, Martin Bonath, Cäcilia Maichle-Mössmer, and Reiner Anwander*

Read Online

ACCESS | Metrics & More | Article Recommendations | Supporting Information

ABSTRACT: Adduct complexes $Ga_6(\mu\text{-}CH_2)_9(DMAP)_3(THF)$ and $Ga_8(\mu\text{-}CH_2)_{12}(PEt_3)_x$ (x = 4 and 6) could be obtained upon crystallization of $Ga_8(CH_2)_{12}$ from THF/DMAP (hard Lewis bases) and PEt_3 (soft Lewis base), respectively. Mixed methyl/methylene $\{Ga_4\}$ species with either bridging aryloxy, thiophenolato, or arylamido ligands were accessible via the treatment of $Ga_8(CH_2)_{12}$ with phenols ($HOC_6H_2Me_3$-2,4,6 and $HOC_6H_3Me_2$-2,6), thiophenol $HSC_6H_2Me_3$-2,4,6, and anilines ($H_2NC_6H_2Me_3$-2,4,6 and $H_2NC_6H_3Me_2$-2,6). Such tetrametallic complexes $Ga_4(\mu_2\text{-}CH_2)_2(CH_3)_4(\mu_2\text{-}XAr)_4$ (X = O, S, NH) are isostructural, displaying an adamantane-like core structure. The sterically more demanding phenol $HOC_6H_3tBu_2$-2,6 afforded the $\{Ga_5\}$ cluster $Ga_5(\mu_2\text{-}CH_2)_6(OC_6H_3tBu_2$-2,6$)_3(THF)_2$ with the gallium centers exclusively bridged by methylene groups. Treatment of $Ga_8(CH_2)_{12}$ with other protic substrates HOR/H_2NR', including $HOCH_2tBu$, $HOSi(OtBu)_3$, $H_2NC_6H_3iPr_2$-2,6, and H_2NSiPh_3 point to a pronounced stereoelectronic dependency and intricacy of such transformations but provided helpful information about potential side products such as $[(CH_3)_2Ga(\mu\text{-}X)]_2$ (X = OR, HNR') and reaction intermediates. Efficient methylene → imido transformations using $Ga_8(CH_2)_{12}$/aniline mixtures could not be implemented.
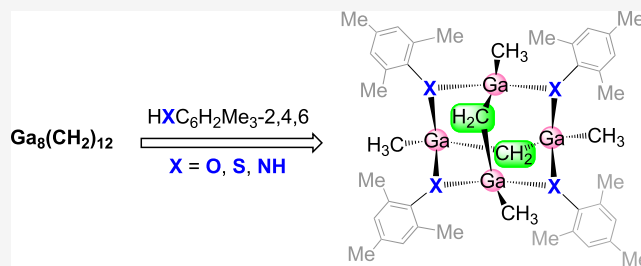
INTRODUCTION

Gallium methylene, $Ga_8(CH_2)_{12}$ (**1**), was recently shown to emerge from a cascade C−H-bond activation of trimethylgallium, promoted by rare-earth-metallocene complexes $(C_5Me_5)_2Ln[(\mu\text{-}Me)_2GaMe_2]$ (Ln = Lu, Y), in a pseudo-catalytic manner.[1] Octametallic **1** displays the first molecular homoleptic metal methylene complex. For comparison, dilithium methylene Li_2CH_2, which was first described by Ziegler et al. in 1955,[2] exhibits a highly distorted antifluorite structure (cf., Li_2O) in the solid state.[3] Initial reactivity studies on **1** revealed an unprecedented reversible $Ga_8(\mu\text{-}CH_2)_{12}$/ $Ga_6(\mu\text{-}CH_2)_9$ oligomer switch in THF solutions.[1]

Moreover, **1** engages in Ga/Al transmetalation, when treated with trimethylaluminum, giving access to the enigmatic methylaluminumomethylene $Al_{12}(CH_2)_{12}(CH_3)_8$ (MAM-12) (Scheme 1).[4] Besides, compound **1** was shown to act as a Schrock-type methylene transfer reagent toward ketones.[1] The present study expands on the coordination behavior of $Ga_8(CH_2)_{12}$ (**1**) with different donor molecules and presents the first protonolysis reactions of **1** with differently substituted phenols and anilines as well as a thiophenol.

RESULTS AND DISCUSSION

Reactivity of $Ga_8(CH_2)_{12}$ (1) Toward Donor Molecules. We have previously shown that compound **1** crystallizes from THF-d_8 solutions as the smaller oligomer $Ga_6(\mu\text{-}CH_2)_9(THF)_6$.[1] However, crystallization of **1** from THF solutions by overlaying with n-pentane revealed the rearrangement of the $Ga_8(\mu\text{-}CH_2)_{12}$ cage as confirmed by the solid-state

structures of $Ga_8(\mu\text{-}CH_2)_{12}(THF)_4$ and $Ga_8(\mu\text{-}CH_2)_{12}(THF)_5$.[1] Partial THF coordination seemed to be indicative of a rather weak Ga−THF interaction. The $\{Ga_6\}$ cage persisted as the preferred species upon THF/pyridine donor exchange, as confirmed by the solid-state structure $Ga_6(\mu\text{-}CH_2)_9(pyr)_6$.[1] Because the ease of donor-mediated disruption and formation of Ga−C(methylene) bonds seemed remarkable, herein, we performed some additional crystallization experiments with compound **1**. Addition of substoichiometric amounts (3 equivalents) of DMAP as another hard donor to a THF solution of **1** led to the crystallization of $Ga_6(\mu\text{-}CH_2)_9(DMAP)_3(THF)$ (**2**) (Figure 1). Clearly, the formation of this mixed donor adduct is indicative of a stepwise exchange of THF by the stronger donor DMAP. The Ga−C distances (av. 1.982 Å) in adduct **2** match those in $Ga_6(\mu\text{-}CH_2)_9(pyr)_6$ ranging from 1.970(4) to 1.989(4) Å (Ga−C), while the Ga−N distances (av. 2.128 Å) in **2** appear shorter than those in $Ga_6(\mu\text{-}CH_2)_9(pyr)_6$ (2.209(3)−2.232(4) Å).[1] For further comparison, the Ga−C distances in precursor **1** amount to 1.972(2) and 1.960(2) Å.[1] Compound **1** also dissolves in neat triethyl phosphine, accomplishing the cocrystallization of adducts $[Ga_8(\mu\text{-}CH_2)_{12}(PEt_3)_4]$ (**3a**) and
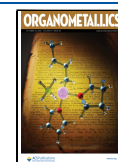
Scheme 1. Distinct Reactivity Pathways Shown Previously for Homoleptic Gallium Methylene (1): $Ga_8(\mu\text{-}CH_2)_{12}$/ $Ga_6(\mu\text{-}CH_2)_9$ Oligomer Switch[1] and Ga/Al Transmetalation[4]
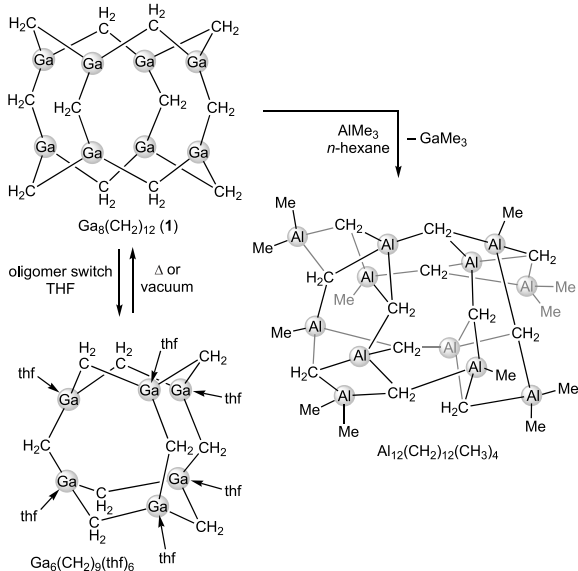
$[Ga_8(\mu\text{-}CH_2)_{12}(PEt_3)_6]$ (**3b**) (Figure 1). Compound **3** was not further characterized, but the solid-state structures suggest that the coordination of the soft donor triethyl phosphine does not promote any oligomer switch.

Protonolyses of $Ga_8(CH_2)_{12}$ (1) with (Thio)Phenols and Anilines. Initial microscale test runs on **1** were performed with 2,4,6-trimethylphenol in THF-d_8 at ambient temperatures, in molar ratios of 1:8. Full consumption of phenol, and hence a complete reaction, was indicated by ^{1}H NMR spectroscopy and a color change from yellow to colorless. Subsequently, the reactions of **1** with phenols $HOC_6H_2Me_3$-2,4,6 and $HOC_6H_3Me_2$-2,6 in a 1:8 ratio were examined more closely and shown to be complete after a minimum time of 20 min (Scheme 2). X-ray diffraction (XRD) analyses revealed a cagelike structural motif with the formula $Ga_4(\mu_2\text{-}CH_2)_2(CH_3)_4(\mu_2\text{-}OAr^R)_4$ ($Ar^R = C_6H_2Me_3$-2,4,6 (**4a**), $C_6H_3Me_2$-2,6 (**4b**); vide infra). Similarly, the reaction of **1** with thiophenol $HSC_6H_2Me_3$-2,4,6 was complete after 20 min,

affording the isostructural complex $[Ga_4(\mu_2\text{-}CH_2)_2(CH_3)_4(\mu_2\text{-}SC_6H_2Me_3$-2,4,6$)_4]$ (**5**, Scheme 2). In contrast, treatment of **1** with the respective methyl-substituted anilines $H_2NC_6H_2Me_3$-2,4,6 and $H_2NC_6H_3Me_2$-2,6 took a maximum time of 7 days for completion under optimized conditions (1:8 ratio) (Scheme 2). The respective XRD analyses of complexes $Ga_4(\mu_2\text{-}CH_2)_2(CH_3)_4(\mu_2\text{-}HNAr^R)_4]$ ($Ar^R = C_6H_2Me_3$-2,4,6 (**6a**), $C_6H_3Me_2$-2,6 (**6b**); vide infra) revealed the same cagelike structural motif as for complexes **4** and **5** (vide infra). Applying less equivalents of the methyl-substituted phenols, for instance, performing the reactions in 1:2, 1:4, or 1:6 ratios, led to incomplete conversion, but nevertheless to the isolation of complexes **4** in lower yields of approximately 20−40%. The markedly slower formation of the anilide complexes **6** can be rationalized primarily on the basis of the decreased Brønsted acidity of the proligands (compared to (thio)phenols).[5] Complexes **6** do form more rapidly at elevated temperatures, however, to the expense of undesired co-products, which were not identified. Clearly, the formation of the $\{Ga_4\}$ complexes **4−6** involves the disruption of the $\{Ga_6\}$ cages (formed via initial $\{Ga_8\} \rightarrow \{Ga_6\}$ oligomer switch in THF) and the addition of the $OH/SH/NH_2$ protic moieties across the Ga−CH_2 bond. The formation of methane was not observed in the reactions depicted in Scheme 2.

The phenolysis reaction outcome is tremendously affected by the steric bulk of the Brønsted-acidic substrate molecules. Treatment of **1** with the sterically more demanding phenol $HOC_6H_3tBu_2$-2,6 gave access to the pentanuclear gallium complex $Ga_5(\mu_2\text{-}CH_2)_6(OC_6tBu_2$-2,6$)_3(THF)_2$ (**7**), featuring a $\{Ga_5\}$ cage structure (Scheme 3 and vide infra). Noteworthy, the 1:6 or 1:4 reactions of **1** with 2,6-di-*tert*-butylphenol afforded complex **7** reproducibly. Unfortunately, we could only identify the formation of a small amount of methane, but likely coproducts resulting from the restructuring via ligand redistribution might include $GaMe_3$ or $Me_2Ga(OC_6tBu_2$-2,6). Formation of the latter heteroleptic gallium alkyl was suggested from the reaction of **1** with silanol $HOSi(OtBu)_3$ (1:8 ratio) which resulted in the crystallization of a small amount of known $[Me_2Ga\{\mu_2\text{-}OSi(OtBu)_3\}]_2$.[6,7] The intricacy of such alcoholysis reactions and cluster degradation products was further revealed by the reaction of **1** with neopentanol (1:8 ratio). Although this reaction provided only a structural snapshot, the XRD analysis of $Me_2Ga(\mu_2\text{-}OCH_2tBu)_2Ga(\mu_2\text{-}CH_2)_2\{GaMe(\mu_2\text{-}OCH_2tBu)\}_2$ (**8**) (Figure S9) proved the
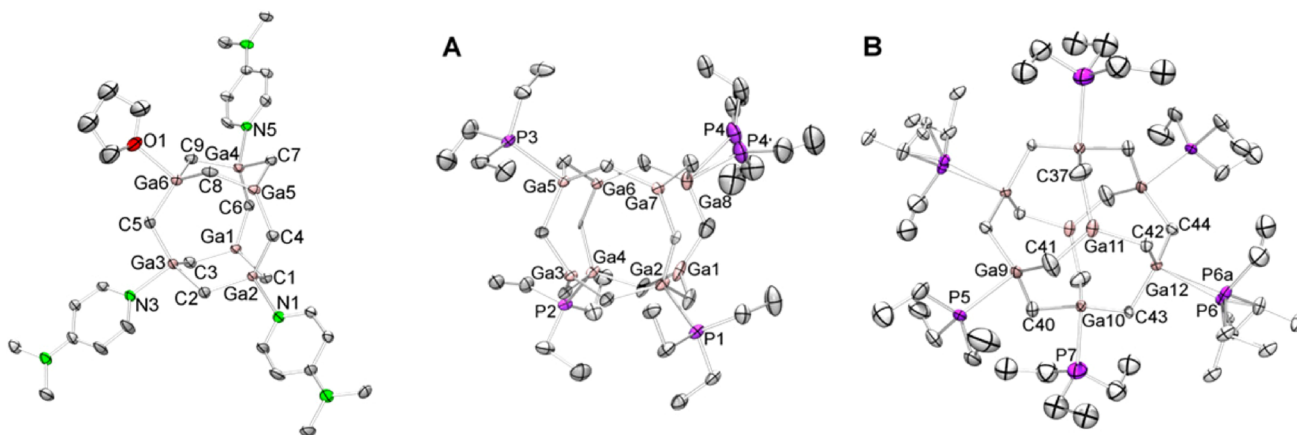
Figure 1. Crystal structures **2** and **3** (**A** and **B**). Atomic displacement parameters set at 50% probability. Hydrogen atoms and the disorder in the coordinated THF molecule have been omitted for clarity. For selected interatomic distances and angles, see the Supporting Information.

Scheme 2. Synthesis of Heteroleptic Gallium Methylene-Methyl Complexes Bearing Bridging Aryloxy, Thiophenolato, and Arylamido Ligands
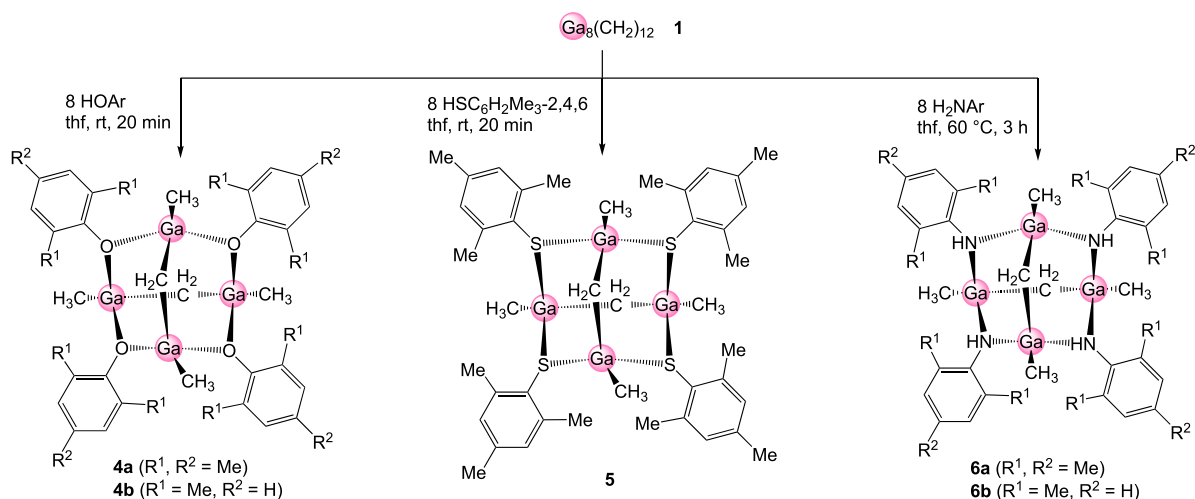
Scheme 3. Synthesis of Complex 7 Bearing the Sterically Demanding 2,6-Di-*tert*-butylphenolato Ligand
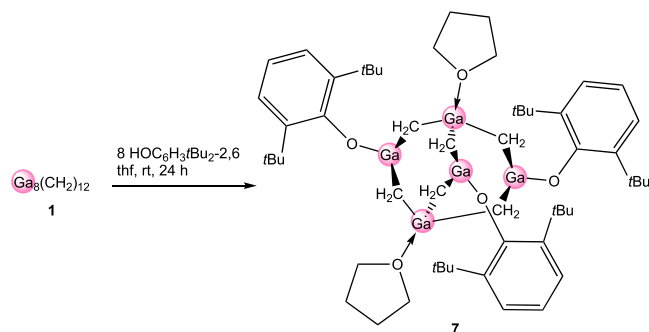
simultaneous occurrence of alcohol addition across the Ga–CH_2 bond and ligand redistribution (methyl-group migration).

Steric factors also applied for the reaction of **1** with anilines. Sterically demanding $H_2NC_6H_3iPr_2$-2,6 engaged in a very sluggish reaction (1:8 ratio), providing inconclusive NMR spectra but again little single-crystalline material. The crystals were analyzed by XRD as incompletely converted compound $[Ga_4(\mu_2\text{-}CH_2)_3(CH_3)_3(\mu_2\text{-}HNC_6H_3iPr_2\text{-}2,6)_3(H_2NC_6H_3iPr_2\text{-}2,6)]$ (**9**) (vide infra). Compound **9** can be considered as the final intermediate en route to putative $[Ga_4(\mu_2\text{-}CH_2)_2(CH_3)_4(\mu_2\text{-}HNC_6H_3iPr_2\text{-}2,6)_4]$. Apparently, the last step of the four-time aniline addition across the Ga–CH_2 bond is sterically strongly hindered.

The originally envisaged gallium methylene → imide transformation from treating **1** with anilines was affected by decomposition reactions at elevated temperatures (vide supra). However, imide formation could be observed in the reaction of **1** with primary silylamine H_2NSiPh_3. At ambient temperature, all starting materials were consumed to produce $[Me_2Ga(\mu_2\text{-}HNSiPh_3)]_2$ (**10**) (Figure S11) and other amido proton containing products according to ^{1}H NMR spectral data. However, heating the clear colorless solution at 130 °C for 2 h and subsequent condensing of *n*-pentane into the concentrated reaction mixture at ambient temperatures resulted in the concomitant formation of morphologically distinct crystals of $[Me_2Ga(\mu_2\text{-}HNSiPh_3)]_2$ (**10**, colorless square crystals) and $[Ga_4Me_3(CH_2)(NSiPh_3)(NSiPh_2\{C_6H_4\})_2][Li(THF)_4]$ (**11**,
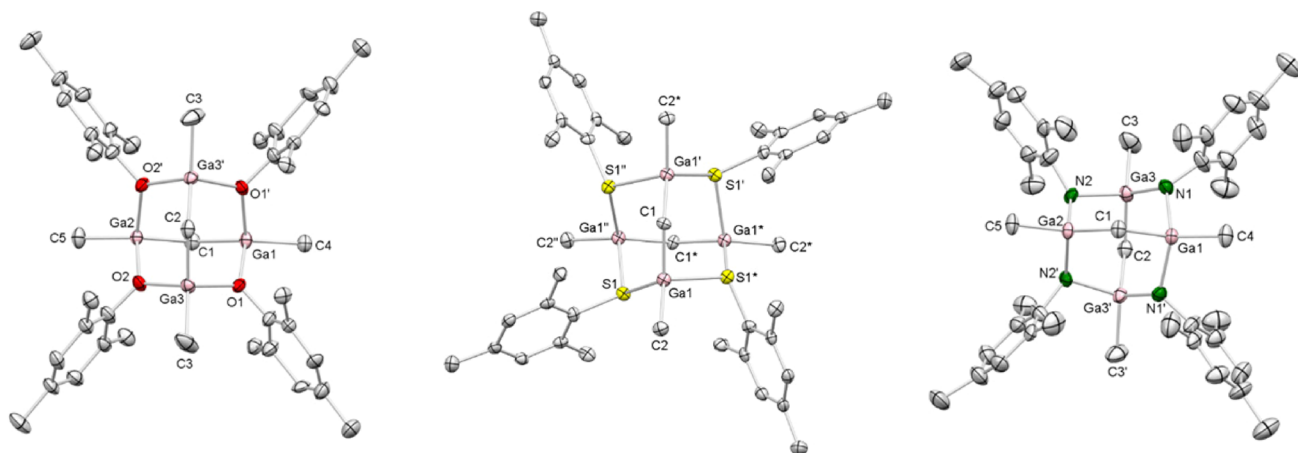
Figure 2. Crystal structures **4a**, **5**, and **6a** (from the left to right), hydrogen atoms are omitted for clarity. Atomic displacement parameters set at 50% probability. For **4a**, two lattice solvent molecules (THF) and the disorder in all aryloxy rings are omitted for clarity. For **6a**, one lattice solvent molecule (THF) and the disorder in all arylamido rings are omitted for clarity. For selected interatomic distances and angles, see Table 1 and the Supporting Information.

Table 1. Selected Interatomic Distances (Å) of Complexes 4a, 4b, 5, 6a, 6b, 7, 8, and 9

	4a	4b	5	6a	6b	7	8	9
Ga–X (X = O/S/N)	1.975(3)–1.989(3)	1.986(2)–2.001(2)	2.380(1)–2.403(1)	2.023(10)–2.089(10)	2.000(5)–2.112(5)	1.830(8)–2.097(17)	1.947(5)–1.965(5)	2.034(3)–2.126(3)/2.174(3)*
Ga–C$_{methyl}$	1.946(6)–1.958(6)	1.944(3)–1.965(3)	1.967(4)	1.967(8)–1.997(8)	1.971(3)–1.974(3)		1.951(6)–1.957(7)	1.974(3)–1.992(3)
Ga–C$_{methylene}$	1.949(6)–1.953(6)	1.957(3)–1.963(3)	1.951(2)	1.970(4)–1.984(7)	1.966(2)–1.979(2)	1.932(9)–1.978(9)	1.943(6)–1.967(6)	1.958(3)–2.014(3) *terminal N

colorless needles) suitable for XRD analyses (Figures S11 and S12). Because imide formation could not be reproduced with other mixtures of **1**/H$_2$NSiPh$_3$, we hypothesized that it was triggered by the adventitious presence of LiNH$_2$ (used for the synthesis of H$_2$NSiPh$_3$ from ClSiPh$_3$). Because of this and the C–H-bond activation of one silylamine phenyl substituent, we did not follow up these transformations. It was previously shown that ortho-substituted anilides [Me$_2$Ga(μ_2-HNArR)]$_2$ suffer ortho-metalation (C–H-bond activation and cyclometallation) upon thermal treatment.[8] Furthermore, imides of the group 13 metals have a strong tendency to oligomerize (especially for the heavier elements).[9−12] Only a few monomeric gallium imides have been obtained by the reaction of low valent gallium precursors with organic azides.[13,14]

X-Ray Crystallographic Studies on Protonolysis Products. Complexes [Ga$_4$(μ_2-CH$_2$)$_2$(CH$_3$)$_4$(μ_2-OC$_6$H$_2$Me$_3$-2,4,6)$_4$] (**4a**) and [Ga$_4$(μ_2-CH$_2$)$_2$(CH$_3$)$_4$(μ_2-OC$_6$H$_3$Me$_2$-2,6)$_4$] (**4b**) are isostructural, featuring an heteroadamantane core structure with four gallium, four aryloxy oxygen, and two methylidene carbon sites (Figures 2 and S4 in the Supporting Information). The highly distorted tetrahedral coordination of each gallium atom is completed by a terminal methyl group. The C–Ga–C angle of av. 130.9° is more obtuse than the O–Ga–O angle of av. 103.1°. Selected interatomic distances are depicted in Table 1. The Ga–O distances in complexes **4** are in the range of other 4-coordinate gallium(III) alkoxides and aryloxides, which mainly display bridged Ga$_2$O$_2$ motifs.[15−17] For comparison, heteroleptic complexes derived from GatBu$_3$ form distorted trigonal planar geometries with terminal alkoxy/ aryloxy ligands.[18] Consequently, the Ga–O distances of 1.821(3)−1.831(3) Å detected in monomeric tBu$_2$Ga(OR) (OR = OCPh$_3$, OC$_6$H$_4$-2,4-tBu$_2$-4-Me) are significantly shorter than those in bridged complexes **4**. The rich organogallium cluster chemistry reported by Uhl has also revealed the heteroadamantane entity as an integral structural motif.[19] For example, complexes [Ga$_4$[μ_2-C(SiR$_2$R′)(CH$_2$Ph)$_2$]-(CMe$_3$)$_4$(μ_2-H)$_4$] (R = Me, Ph; R′ = Me, Ph, CMe$_3$) were obtained via a salt metathesis/β-H-elimination (butene) tandem reaction from (Cl$_2$Ga)$_2$C(SiR$_2$R′)(CH$_2$Ph) and $tert$-butyllithium.[19b] The latter heteroadamantane core is arranged similarly to complexes **4**, showing four hydrido and two alkylidene carbon sites.

The thiophenolato and anilido derivatives **5** and **6a/b**, respectively, exhibit a heteroadamantane cage structure similar to complexes **4** (Figures 2 and S4). The gallium centers are coordinated by two bridging sulfur/nitrogen atoms, one terminal methyl and one bridging methylene group. The overall cage structure is more distorted because of the significantly increased Ga–heteroatom distances of the admantane core (Table 1). The molecular structures of **4−6** are isostructural but not isotype because of different solvents in the lattice. The Ga–S distances in complex **5** appear shorter than those in complex [(CH$_3$)$_2$Ga(μ_2-SC$_6$F$_5$)]$_2$ (2.436(3)−2.460(2) Å).[20] The Ga–N(anilido) and Ga–C(methyl)

distances match those in other anilido-bridged complexes such as [(CH$_3$)$_2$Ga(μ_2-HNArR)]$_2$ (ArR = C$_6$H$_5$ (av. 2.037 Å) and C$_6$H$_3$iPr$_2$-2,6 (av. 2.025 Å)).[8] Overall, the Ga–N distances of gallium arylamides are found in the range of 1.851(3)−2.082(4) Å (CN = 4).[8,21−24] Because of the highly distorted tetrahedral geometry of the gallium atoms in complexes **6**, the C–Ga–C angles of av. 126.4° are more obtuse than the N–Ga–N angles of av. 102.1°.

The main structural difference of the aryloxide and thiophenolate complexes **4** and **5** is the geometry around the bridging 3-coordinate heteroatoms. While the oxygen atoms adopt an almost trigonal planar coordination (range ∠Ga–O–Ga: **4a**, 119.97(13) and 120.17(14)°; **4b**, 118.02(9)−121.35(9)°; range ∠Ga–O–C$_{ipso}$: **4a**, 118.5(3)−121.5(3)°; **4b**, 117.54(17)−123.31(15)°), the sulfur atoms in **5** display a rather distorted trigonal pyramidal coordination (∠Ga–S1–Ga: 114.12(4)°; range ∠Ga–S1–C3: 108.24(12) and 118.24(12)°). For comparison, a similar pyramidal coordination around the sulfur atom was described for dimeric complex [(CH$_3$)$_2$Ga(μ_2-SC$_6$F$_5$)]$_2$ (∠Ga–S–Ga: 87.8°; range ∠Ga–S–C: 106.7 and 126.2°).[20]

Although complex [Ga$_4$(μ_2-CH$_2$)$_3$(CH$_3$)$_3$(μ_2-HNC$_6$H$_3$iPr$_2$-2,6)$_3$(H$_2$NC$_6$H$_3$iPr$_2$-2,6)] (**9**) was identified as a structural snapshot only, its molecular structure is briefly discussed because of its "intermediate character" (Figure 3). In comparison to anilide complexes **6**, in compound **9**, one of the [Ga(CH$_3$)(μ_2-HNArR)] fragments is displaced by a [Ga(μ_2-CH$_2$)(H$_2$NArR)] entity. The 2,6-diisopropylaniline proligand coordinates to the gallium atom Ga$_4$ in a terminal fashion with a significantly longer Ga–N distance of 2.174(3)
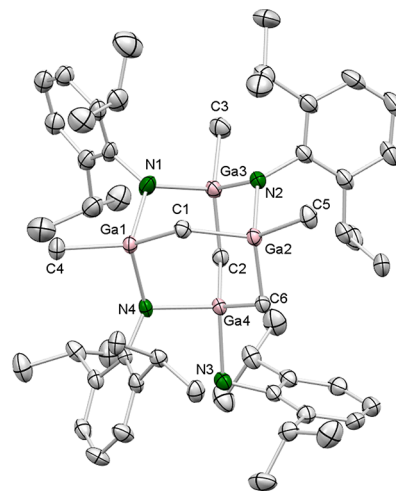
Figure 3. Crystal structure of **9**. Hydrogen atoms and the disorder in all arylamido/aniline rings are omitted for clarity. Atomic displacement ellipsoids were set at 50% probability. For selected interatomic distances and angles, see Table 1 and the Supporting Information.

Å. The Ga4 atom is further coordinated by a bridging anilido (Ga−N 2.034(3) Å) and two bridging methylene units.

Consequently, the heavily distorted heteroadamantane core is now composed of four gallium, three anilido nitrogen, and three methylidene carbon sites.

The pentanuclear complex $[Ga_5(\mu_2\text{-}CH_2)_6(OC_6tBu_2\text{-}2,6)_3(THF)_2]$ (**7**), bearing the sterically demanding aryloxy ligand, features a cage structure entirely different from complexes **4−6** and **9**. The bridging positions of the {Ga5} cage are occupied exclusively by six methylene moieties (Figure 4). The gallium atoms Ga2, Ga2*, and Ga′ bearing the
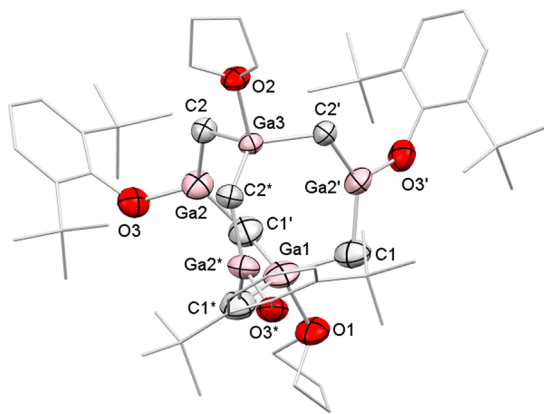
Figure 4. Crystal structure of **7**. Hydrogen atoms and the disorder in the THF molecules are omitted for clarity. The aryloxy and THF carbon atoms are represented by a wireframe model for the sake of clarity. Atomic displacement ellipsoids were set at 50% probability. For selected interatomic distances and angles, see Table 1 and the Supporting Information.

aryloxy ligands adopt a trigonal planar geometry ($\sum_{\angle}359.9°$). The O1−Ga2−C2/C1 angles of 107.7(5)° and 118.9(4)° involving two bridging methylenes are more acute than the C1−Ga2−C2 angle of 133.5(5)°. The gallium atoms Ga1 and Ga3 are coordinated tetrahedrally by three bridging methylenes and a THF molecule. The heavily distorted coordination geometry is reflected in the sum of the CH_2−Ga−CH_2 angles of 352.3°.

NMR Spectroscopy. The ^1H and $^{13}C\{^1H\}$ NMR spectra of the aryloxide complexes **4a** and **4b** in benzene-d_6 show one set of signals consistent with the solid-state structure. The proton singlets at −0.51 and −0.58 ppm are assigned to the terminal methyl groups of **4a** and **4b**, respectively (see Figures S15 and S18). Similarly, the respective methyl protons of complexes **6a/6b** (Figures S25 and S26) are detected at −0.52/−0.56 while those of the thiophenolate **5** appeared at −0.11 ppm (Figure S21). Overall, the protons of the terminal methyl groups resonate similar to GaMe3 (−0.10 ppm, benzene-d_6, 90 MHz).[25] The bridging methylene moieties of compounds **4−6** appeared as sharp singlets in the ^1H NMR spectra in the range of 0.69 to 0.32 ppm, which is significantly shifted to lower field compared to the homoleptic gallium methylene $Ga_8(CH_2)_{12}$ (**1**) and the smaller gallium methylene oligomer $Ga_6(\mu\text{-}CH_2)_9(THF)_6$ (0.19 to −0.49 ppm).[1] Noteworthy, the splitting of the ortho-CH_3 signals of the anilido phenyl backbone indicates a rotational barrier around the C−NH bond in compounds **6a** and **6b**. Accordingly, the aryl-bonded methyl groups of **6a** display an integral ratio of 12:12:12, in contrast to those of the (thio)phenolate complexes **4a** and **5** (24:12). The rotational barrier around the C−N bond in **6a/**

6b is also revealed by the ^{13}C NMR spectra (Figures S16 and S19). The methylene units in pentanuclear cluster **7** gave one sharp signal at 0.13 ppm in the ^1H NMR spectrum, indicating rapid exchange of the bridging positions.

■ CONCLUSIONS

The previously reported $Ga_8(\mu\text{-}CH_2)_{12}/Ga_6(\mu\text{-}CH_2)_9(THF)_6$ oligomer switch could be corroborated by the addition of a substoichiometric amount of DMAP to a solution of $Ga_8(\mu\text{-}CH_2)_{12}$ in THF. The obtained mixed donor adduct $Ga_6(\mu\text{-}CH_2)_9(DMAP)_3(THF)]$ suggests a stepwise exchange of THF by the stronger donor DMAP. Dissolving $Ga_8(\mu\text{-}CH_2)_{12}$ in triethyl phosphine led to the crystallization of $Ga_8(\mu\text{-}CH_2)_{12}(PEt_3)_x$ (x = 4 and 6), suggesting that the soft Lewis base cannot promote the disruption of Ga−C(methylene) bonds and hence cannot trigger an oligomer switch.

Protonolysis reactions of $Ga_8(CH_2)_{12}$ carried out with moderately bulky (thio)phenols and anilines led to a preferred {Ga8} → {Ga4} cluster transformation. Complexes $Ga_4(\mu_2\text{-}CH_2)_2(CH_3)_4(\mu_2\text{-}XAr^R)_4$ (X = O, S, NH; Ar^R = $C_6H_2Me_3$-2,4,6, $C_6H_3Me_2$-2,6), which emerged from an addition of the OH/SH/NH_2 protic moieties across the Ga−CH_2 bond, feature an adamantane-like core structure. The products obtained with other protic substrates, including HOCHtBu, HOSi(OtBu)3, and $H_2NC_6H_3iPr_2$-2,6 could not be fully characterized (due to very low yield) but provided structural snapshots of relevance for possible side products and reaction intermediates. The effect of the steric bulk of the protic proligand and hence the intricacy of such reactions was revealed by the {Ga5} complex $[Ga_5(\mu_2\text{-}CH_2)_6(OC_6tBu_2\text{-}2,6)_3(THF)_2]$, showing the bulky aryloxy ligands exclusively in the terminal position. The formation of gallium imido derivatives via the treatment of $Ga_8(CH_2)_{12}$ with anilines was mostly unsuccessful. Only on one occasion, the $Ga_8(CH_2)_{12}/H_2NSiPh_3$ reaction produced crystalline imide complex $[Ga_4Me_3(CH_2)(NSiPh_3)(NSiPh_2\{C_6H_4\})_2][Li(THF)_4]$ along with $[Me_2Ga(\mu\text{-}HNSiPh_3)]_2$, possibly triggered by the adventitious presence of $LiNH_2$. Because this reaction did not only suffer from major side-product formation but also C−H-bond activation of the imido phenyl substituents, this protocol were not further investigated.

■ EXPERIMENTAL SECTION

All operations were performed under rigorous exclusion of air and water by using standard Schlenk, high-vacuum, and glovebox techniques (MBraun 200B; <0.1 ppm O_2, <0.1 ppm H_2O). Solvents were purified by using Grubbs-type columns (MBraun SPS, solvent purification system) and stored inside a glovebox. THF-d_8 was obtained from Sigma-Aldrich, stirred over NaK, and distilled. Benzene-d_6 was obtained from Sigma-Aldrich stirred over NaK and filtered at ambient temperature. DMAP, 2,4,6-trimethylphenol, 2,6-dimethylphenol, 2,6-di-$tert$-butylphenol, 2,4,6-trimethylthiophenol, 2,4,6-trimethylaniline, 2,6-dimethylaniline, triphenylsilylamine, 2,2-dimethyl-1-propanol, and tris($tert$-butoxy)silanol were also purchased from Sigma-Aldrich. All chemicals were used as received. $Ga_8(CH_2)_{12}$ (**1**) was synthesized according to a literature procedure.[1] The NMR spectra were recorded by using J. Young-valved NMR tubes on a Bruker AVII+400 spectrometer (^1H, 400.13 MHz; ^{13}C, 100.61 MHz). NMR chemical shifts are referenced to internal solvent resonances and reported in parts per million relative to tetramethylsilane (TMS). Elemental analyses were performed on an Elementar Vario Micro Cube. IR spectra were recorded on a Thermo Fisher Scientific NICOLET 6700 FTIR spectrometer using a DRIFT chamber with a dry KBr/sample mixture and KBr windows. The IR data were converted using the Kubelka−Munk refinement.

[Ga$_6$(CH$_2$)$_9$](DMAP)$_3$(THF) (2). A solution of DMAP (13.8 mg, 0.113 mmol) in THF (1 mL) was added dropwise to a stirred solution of **1** (53.8 mg, 0.074 mmol) in THF (2 mL). Then, without stirring, the reaction mixture was carefully layered with 2 mL of THF. The clear colorless solution was stored at ambient temperatures. After several days, crystals of [Ga$_6$(CH$_2$)$_9$](DMAP)$_3$(THF) formed. ^{1}H NMR (400 MHz, THF-d_8, 26 °C): δ = 8.24 (d, $^3J_{HH}$ = 6.7 Hz, 6 H, CHNCH), 6.57 (d, $^3J_{HH}$ = 6.8 Hz, 6 H, CHCHNCHCH), 3.01 (s, 18 H, N(CH_3)$_2$), 0.17 (s, 24 H, [Ga$_6$(CH_2)$_{12}$]), 0.15 (d, $^2J_{HH}$ = 8.9 Hz, 6 H, [Ga$_6$(CH_2)$_9$]), −0.11 (s, 6 H, [Ga$_6$(CH_2)$_9$]), −0.51 (d, $^2J_{HH}$ = 8.9 Hz, 6 H, [Ga$_6$(CH_2)$_9$]) ppm.

[Ga$_8$(CH$_2$)$_{12}$](PEt$_3$)$_4$ (3a)/[Ga$_8$(CH$_2$)$_{12}$](PEt$_3$)$_6$ (3b). A sample of **1** (20 mg, 0.028 mmol) was dissolved in PEt$_3$ (1 mL). The clear colorless solution was kept at −40 °C to form colorless crystals suitable for XRD analysis within 16 h.

Synthesis of [Ga$_4$(μ_2-CH$_2$)$_2$(CH$_3$)$_4$(μ_2-OC$_6$H$_2$Me$_3$-2,4,6)$_4$] (4a). A solution of 2,4,6-trimethylphenol (75.3 mg, 0.551 mmol) in THF (1 mL) was added to a stirred solution of **1** (50.0 mg, 0.069 mmol) in THF (1 mL). The reaction mixture was allowed to stir for 20 min at ambient temperature. Afterward, the solvent was reduced in volume and the solution was stored at −40 °C overnight. The supernatant was removed, and the residual colorless crystals were washed with n-pentane (2 × 2 mL) and dried in vacuo to afford **4a** (56 mg, 0.062 mmol, 90%). ^{1}H NMR (400.11 MHz, THF-d_8, 26 °C): δ = 6.74 (s, 8 H, Ar$_m$-CH), 2.38 (s, 24 H, Ar$_o$-CH_3), 2.14 (s, 12 H, Ar$_p$-CH_3), 0.23 (s, 4 H, Ga−CH_2), −0.92 (s, 12 H, Ga−CH_3) ppm. ^{13}C{^{1}H} NMR (100.6 MHz, THF-d_8, 26 °C): δ = 152.9 (Ar-C1), 131.9 (Ar-C4), 130.2 (Ar$_m$-CH), 129.8 (Ar-C2/C6), 20.3 (Ar$_o$-C(CH$_3$)), 20.2 (Ar$_p$-C(CH$_3$)), 3.8 (Ga−CH$_2$), −8.1 (Ga−CH$_3$) ppm; IR (KBr): $\tilde{\nu}$ = 2922 (w), 1477 (s), 1434 (vw), 1195 (vs), 1138 (vs), 958 (w), 852 (w), 778 (s), 775 (s), 733 (w), 727 (w), 579 (w), 503 (vw), 493 (w), 486 (w), 479 (w), 469 (w) cm^{-1}; elemental analysis calcd (%) for C$_{42}$H$_{60}$Ga$_4$O$_4$ (907.79 g mol^{-1}): C 55.57, H 6.66; found C 55.16, H 6.54. Although these results are outside the range viewed as establishing analytical purity (H: +0.46%), they are provided to illustrate the best values obtained to date.

Synthesis of [Ga$_4$(μ_2-CH$_2$)$_2$(CH$_3$)$_4$(μ_2-OC$_6$H$_3$Me$_2$-2,6)$_4$] (4b). A solution of 2,6-dimethylphenol (67.3 mg, 0.551 mmol) in THF (1 mL) was added to a stirred solution of **1** (50.0 mg, 0.069 mmol) in THF (1 mL). The reaction mixture was allowed to stir for 20 min at ambient temperature. Afterward, the solvent was reduced in volume and the solution was stored at −40 °C overnight. The supernatant was removed, and the residual colorless crystals were washed with n-pentane (2 × 2 mL) and dried in vacuo to afford **4b** (40.0 mg, 0.047 mmol, 69%). ^{1}H NMR (400.11 MHz, THF-d_8, 26 °C): δ = 6.93 (d, $^3J_{HH}$ = 7.45 Hz, 8 H, Ar$_m$-CH), 6.77 (t, $^3J_{HH}$ = 7.68 Hz, 4 H, Ar$_p$-CH), 2.45 (s, 24 H, Ar$_o$-CH_3), 0.32 (s, 4 H, Ga−CH_2), −0.90 (s, 12 H, Ga−CH_3) ppm. ^{13}C{^{1}H} NMR (100.6 MHz, THF-d_8, 26 °C): δ = 155.2 (Ar-C1), 130.2 (Ar-C2/C6), 129.7 (Ar$_p$-CH), 123.1 (Ar$_m$-CH), 20.3 (Ar$_o$-C(CH$_3$)), 4.0 (Ga−CH$_2$), −8.0 (Ga−CH$_3$) ppm; IR (KBr): $\tilde{\nu}$ = 2955 (vw), 2925 (vw), 2899 (vw), 1591 (vw), 1469 (s), 1463 (s), 1427 (w), 1264 (w), 1208 (vw), 1176 (vs), 1097 (s), 963 (w), 833 (s), 767 (s), 762 (s), 742 (s), 733 (w), 722 (w), 715 (w), 668 (s), 603 (vw), 592 (w), 582 (w), 572 (w), 512 (w), 490 (vw), 468 (s), 449 (w), 435 (w) cm^{-1}; elemental analysis calcd (%) for C$_{38}$H$_{52}$Ga$_4$O$_4$ (851.68 g mol^{-1}): C 53.59, H 6.15; found C 53.98, H 6.61. Although these results are outside the range viewed as establishing analytical purity (H: +0.46%), they are provided to illustrate the best values obtained to date.

Synthesis of [Ga$_4$(μ_2-CH$_2$)$_2$(CH$_3$)$_4$(μ_2-SC$_6$H$_2$Me$_3$-2,4,6)$_4$] (5). A solution of 2,4,6-trimethylthiophenol (117.4 mg, 0.771 mmol) in benzene (1 mL) was added to a stirred suspension of **1** (71.2 mg, 0.098 mmol) in benzene (1 mL). The reaction mixture was allowed to stir for 20 min at ambient temperature, and afterward, the solvent was reduced in volume. Diffusion of n-pentane into the solution afforded colorless crystals, which were washed with n-pentane (2 × 2 mL) and dried in vacuo to afford **5** (22.4 mg, 0.062 mmol, 24%). ^{1}H NMR (400.11 MHz, benzene-d_6, 26 °C): δ = 6.78 (s, 8 H, Ar$_m$-CH), 2.73 (s, 24 H, Ar$_o$-CH_3), 2.05 (s, 12 H, Ar_p-CH_3), 0.69 (s, 4 H, Ga−CH_2), −0.11 (s, 12 H, Ga−CH_3) ppm. ^{13}C{^{1}H} NMR (100.6 MHz,

benzene-d_6, 26 °C): δ = 141.3 (Ar-C1), 136.6 (Ar-ortho-C(CH$_3$), 129.8 (Ar$_m$-CH), 24.5 (Ar$_p$-C(CH$_3$)), 20.8 (Ar$_o$-C(CH$_3$)), 9.2 (Ga−CH$_2$), −2.8 (Ga−CH$_3$) ppm; elemental analysis calcd (%) for C$_{42}$H$_{60}$Ga$_4$S$_4$ (972.06 g mol^{-1}): C 51.90, H 6.22, S 13.19; found C 52.20, H 6.84, S 13.39. Although these results are outside the range viewed as establishing analytical purity (H: +0.62%), they are provided to illustrate the best values obtained to date.

Synthesis of [Ga$_4$(μ_2-CH$_2$)$_2$(CH$_3$)$_4$(μ_2-HNC$_6$H$_2$Me$_3$-2,4,6)$_4$] (6a). A solution of 2,4,6-trimethylaniline (74.5 mg, 0.551 mmol) in THF (1 mL) was added to a solution of **1** (50.0 mg, 0.069 mmol) in THF (1 mL) and stirred for 3 h at 60 °C. The solution was filtered, reduced in volume, and stored at −40 °C overnight. The supernatant was removed, and the residual colorless crystals were washed with n-pentane (2 × 2 mL) and dried in vacuo to afford **6a** (32.0 mg, 0.035 mmol, 52%). ^{1}H NMR (400.11 MHz, benzene-d_6, 26 °C): δ = 6.70 (s, 8 H, Ar$_m$-CH), 3.82 (s, 4 H, NH), 2.58 (s, 12 H, Ar$_o$-CH_3), 2.24 (s, 12 H, Ar$_o$-CH_3), 2.10 (s, 12 H, Ar$_p$-CH_3), 0.10 (s, 4 H, Ga−CH_2), −0.52 (s, 12 H, Ga−CH_3) ppm. ^{13}C{^{1}H} NMR (100.6 MHz, benzene-d_6, 26 °C): δ = 142.9 (Ar-C1), 131.2 (Ar-C2/C6), 130.8 (Ar$_m$-CH), 130.4 (Ar$_m$-CH), 129.5 (Ar-C2/C6), 127.1 (Ar-C4), 23.3 (Ar$_o$-C(CH$_3$)), 20.5 (Ar$_p$-C(CH$_3$)), 20.4 (Ar$_o$-C(CH$_3$)), 4.6 (Ga−CH$_2$), −7.7 (Ga−CH$_3$) ppm; IR (KBr): $\tilde{\nu}$ = 3286 (w), 3007 (w), 2916 (w), 1479 (s), 1378 (vw), 1329 (vw), 1295 (vw), 1226 (w), 1199 (vs), 1141 (s), 1009 (vw), 939 (w), 852 (w), 769 (w), 719 (w), 678 (vw), 640 (w), 616 (vw), 566 (vw), 552 (vw), 521 (vw), 485 (s) cm^{-1}; elemental analysis calcd (%) for C$_{42}$H$_{64}$Ga$_4$N$_4$ (903.85 g mol^{-1}): C 55.81, H 7.14, N 6.20; found C 55.74, H 7.16, N 6.24.

Synthesis of [Ga$_4$(μ_2-CH$_2$)$_2$(CH$_3$)$_4$(μ_2-HNC$_6$H$_3$Me$_2$-2,6)$_4$] (6b). A solution of 2,6-dimethylaniline (66.8 mg, 0.551 mmol) in THF (1 mL) was added to a solution of **1** (50.0 mg, 0.069 mmol) in THF (1 mL) and stirred for 3 h at 60 °C. The solution was filtered, reduced in volume, and stored at −40 °C overnight. The supernatant was removed, and the residual colorless crystals (26 mg, 0.031 mmol, 44%) were washed with n-pentane (2 × 2 mL). ^{1}H NMR (400.11 MHz, benzene-d_6, 26 °C): δ = 6.87 (d, $^3J_{HH}$ = 7.49 Hz, 8 H Ar$_m$-CH), 6.78 (t, $^3J_{HH}$ = 7.49 Hz, 4 H, Ar$_p$-CH), 3.84 (s, 4 H, NH), 2.52 (s, 12 H, Ar$_o$-CH_3), 2.18 (s, 12 H, Ar$_o$-CH_3), 0.04 (s, 4 H, Ga−CH_2), −0.58 (s, 12 H, Ga−CH_3) ppm. ^{13}C{^{1}H} NMR (100.6 MHz, benzene-d_6, 26 °C): δ = 145.5 (Ar-C1), 130.2 (Ar$_m$-CH), 129.7 (Ar-C2/C6), 129.6 (Ar$_m$-CH), 127.4 (Ar-C2/C6), 122.5 (Ar$_p$-CH), 23.4 (Ar$_o$-CH$_3$), 20.4 (Ar$_o$-CH$_3$), 4.7 (Ga−CH$_2$), −7.8 (Ga−CH$_3$) ppm; IR (KBr): $\tilde{\nu}$ = 3286 (vw), 2914 (vw), 1594 (vw), 1467 (s), 1330 (vw), 1253 (vw), 1227 (vw), 1180 (vs), 1099 (s), 943 (w), 922 (w), 873 (vw), 825 (s), 763 (s), 721 (s), 640 (vs), 598 (vw), 548 (vw), 514 (vw), 467 (vw) cm^{-1}; elemental analysis calcd (%) for C$_{38}$H$_{56}$Ga$_4$N$_4$ (847.75 g mol^{-1}): C 53.84, H 6.66, N 6.61; found C 53.42, H 6.65, N 6.35. Although these results are outside the range viewed as establishing analytical purity (C: −0.42%), they are provided to illustrate the best values obtained to date.

Synthesis of [Ga$_5$(μ_2-CH$_2$)$_6$(OC$_6$H$_3$tBu$_2$-2,6)$_3$(Thf)$_2$] (7). A solution of 2,6-di-tert-butylphenol (159 mg, 0.771 mmol) in THF (1 mL) was added to a stirred solution of **1** (70.0 mg, 0.096 mmol) in THF (1 mL). The reaction mixture was stirred overnight at ambient temperature. Afterward, the solvent was removed in vacuo and the sticky yellowish oil was triturated with n-pentane (2 mL) and stirred for 2 h. A white precipitate formed. The precipitate was washed with n-pentane (2 × 2 mL). The solvent was removed in vacuo, and compound **7** was redissolved in benzene (1 mL). Diffusion of n-pentane into the solution afforded colorless crystals (45.0 mg, 0.033 mmol, 39%). ^{1}H NMR (400.11 MHz, benzene-d_6, 26 °C): δ = 7.38 (d, 6 H, $^3J_{HH}$ = 7.85 Hz, Ar$_m$-CH), 6.90 (t, 3 H, $^3J_{HH}$ = 7.85 Hz, Ar$_p$-CH), 2.99 (m, 8 H, THF, OCH_2), 1.77 (s, 54 H, Ar$_o$-C(CH_3)$_3$), 0.84 (m, 8 H, THF, CH_2), 0.13 (s, 12 H, Ga−CH_2) ppm. ^{13}C{^{1}H} NMR (100.6 MHz, benzene-d_6, 26 °C): δ = 162.1 (Ar-C2/C6), 139.8 (Ar-C1), 125.4 (Ar$_p$-CH), 118.3 (Ar$_m$-CH), 68.5 (THF, OCH$_2$), 35.5 (Ar$_o$-(C(CH$_3$)), 32.7 (Ar$_o$-C(CH$_3$)$_3$), 24.8 (THF, CH$_2$), 6.8 (Ga−CH$_2$) ppm; IR (KBr): $\tilde{\nu}$ = 2950 (w), 1412 (s), 1384 (vw), 1241 (s), 897 (w), 858 (s), 754 (w), 667 (w), 618 (vs), 509 (vw) cm^{-1}; elemental analysis calcd (%) for C$_{56}$H$_{91}$Ga$_5$O$_5$ (1192.9 g mol^{-1}): C 56.38, H 7.69; found C 57.14, H 7.40. Although these results are

outside the range viewed as establishing analytical purity (C: +0.76%), they are provided to illustrate the best values obtained to date.

Me₂Ga(μ₂-OCH₂tBu)₂Ga(μ₂-CH₂)₂{GaMe(μ₂-OCH₂tBu)}₂ (8). A solution of **1** (50 mg, 0.068 mmol) and 8 equivalents of 2,2-dimethyl-1-propanol (12 mg, 0.145 mmol) in 2 mL of THF were stirred at ambient temperature. After stirring for 16 h, the volatile parts were removed under reduced pressure, and the resulting colorless oil was redissolved in 0.5 mL of THF to afford a small amount of colorless crystals of **8**. The crystals were used for XRD analysis ruling out any further analytics of **8**.

Reaction of 1 with Silanol HOSi(OtBu)₃. A solution of **1** (50 mg, 0.068 mmol) and 8 equivalents of silanol (145.7 mg, 0.551 mmol) in 2 mL of THF were stirred at ambient temperature. After stirring for 16 h, the volatile parts were removed under reduced pressure, and the resulting colorless residue was redissolved in 0.5 mL of THF to afford a small amount of colorless crystals of [Me₂Ga{μ₂-OSi(OtBu)₃}]₂.[6] Analyzed and identified by unit cell check.

[Ga₄(μ₂-CH₂)₃(CH₃)₃(μ₂-HNC₆H₃iPr₂-2,6)₃(H₂NC₆H₃iPr₂-2,6)] (9). A solution of 2,6-diisopropylaniline (106.3 mg, 0.600 mmol) in THF (1 mL) was added to a solution of **1** (54.5 mg, 0.075 mmol) in THF (1 mL) and stirred at ambient temperature for 5 d. The solution was filtered, reduced in volume, and stored at −40 °C overnight. The supernatant was removed, and the residual colorless crystals (3 mg, 0.003 mmol, 4%) were washed with *n*-pentane (2 × 2 mL), and employed for XRD analysis. Repeated attempts to obtain additional crystalline compound **9**, both under identical and similar reaction conditions, were unsuccessful. Therefore, further analytics of **9** could not be performed.

Synthesis of [Me₂Ga(μ₂-HNSiPh₃)]₂ (10) and [Ga₄Me₃(CH₂)-(NSiPh₃)(NSiPh₂{C₆H₄})₂][Li(THF)₄] (11). In a J-Young-valved NMR tube, **1** (4.9 mg, 0.007 mmol) and Ph₃SiNH₂ (14.8 mg, 0.054 mmol) were dissolved in THF-*d₈* (0.5 mL). After 4.5 h at ambient temperature, all starting materials were consumed to produce **10** and other amido proton containing products according to ¹H NMR spectral data. Therefore, the clear colorless solution was heated at 130 °C for 2 h. According to ¹H NMR measurements, **10** was still present while the unknown amide products reacted to further products without methane formation. Condensing *n*-pentane at ambient temperatures into the concentrated reaction mixture resulted in concomitant formation of single crystals suitable for XRD analyses of **10** (colorless square crystals) and **11** (colorless needles). Compound **10**: ¹H NMR (400 MHz, benzene-*d₆*, 26 °C): δ = 6.59 (m, 12 H, C₆H₅), 7.19 (m, 6 H, p-C₆H₅), 7.13 (m, 12 H, C₆H₅; interfered by C₆D₆ resonances at 7.16 ppm), 1.52 (bs, 1 H, NH), 1.50 (bs, 1 H, NH), 0.08 (s, 3 H, GaCH₃), −0.27 (s, 6 H, GaCH₃), −0.58 (s, 3 H, GaCH₃) ppm. ¹H NMR (400 MHz, THF-*d₈*, 26 °C): δ = 2.07 (bs, 1 H, NH), 2.02 (bs, 1 H, NH), −0.08 (s, 3 H, GaCH₃), −0.58 (s, 6 H, GaCH₃), −0.95 (s, 3 H, GaCH₃) ppm (aromatic resonances were not assignable due to the massive signal overlap of other products). Further characterization of **10** and **11** was not performed because of the occurrence of product mixtures.

X-Ray Crystallography and Crystal Structure Determinations. Single crystals of **2**, **3**, **4a**, **4b**, **5**, **6a**, **6b**, and **7**–**11** were grown using standard techniques from saturated solutions in *n*-hexane, toluene, or THF at −35 °C, as stated in the Experimental section. Suitable crystals were collected in a glovebox and coated with Parabar 10312 (previously known as Paratone N, Hampton Research) and fixed on a nylon loop. X-ray data for all complexes were collected on a Bruker APEX II DUO instrument equipped with an IµS microfocus sealed tube and QUAZAR optics for MoK$_\alpha$ (λ = 0.71073 Å) and CuK$_\alpha$ (λ = 1.54184 Å) radiation. The data collection strategy was determined using COSMO[26] employing ω-scans. Raw data were processed using APEX[27] and SAINT,[28] and corrections for absorption effects were applied using SADABS.[29] The structures were solved using direct methods and refined against all data by full-matrix least-squares methods on F^2 using SHELXTL[30] and ShelXle.[31] Disorder models are calculated using DSR,[32] a program for refining structures in ShelXl. Solvent molecules in compounds **4a**, **6a**, **7**, **9**, and **11** were neglected using the SQUEEZE option in the program package PLATON.[33] All graphics were produced employing ORTEP-3[34] and POV-Ray.[35] Further details of the refinement and crystallographic data are listed in Table S1 (ESI) and in the CIF files.

■ ASSOCIATED CONTENT

ⓈⒾ Supporting Information

The Supporting Information is available free of charge at https://pubs.acs.org/doi/10.1021/acs.organomet.2c00391.

    Supporting figures; detailed crystallographic data and spectroscopic data (NMR, FTIR) (PDF)

Accession Codes

CCDC 2193556−2193567 contain the supplementary crystallographic data for this paper. These data can be obtained free of charge via www.ccdc.cam.ac.uk/data_request/cif, or by emailing data_request@ccdc.cam.ac.uk, or by contacting The Cambridge Crystallographic Data Centre, 12 Union Road, Cambridge CB2 1EZ, UK; fax: +44 1223 336033.

■ AUTHOR INFORMATION

Corresponding Author

    Reiner Anwander − *Institut für Anorganische Chemie, Eberhard Karls Universität Tübingen, 72076 Tübingen, Germany;* ⓞ orcid.org/0000-0002-1543-3787; Email: reiner.anwander@uni-tuebingen.de

Authors

    Georgios Spiridopoulos − *Institut für Anorganische Chemie, Eberhard Karls Universität Tübingen, 72076 Tübingen, Germany*

    Martin Bonath − *Institut für Anorganische Chemie, Eberhard Karls Universität Tübingen, 72076 Tübingen, Germany*

    Cäcilia Maichle-Mössmer − *Institut für Anorganische Chemie, Eberhard Karls Universität Tübingen, 72076 Tübingen, Germany;* ⓞ orcid.org/0000-0001-7638-1610

Complete contact information is available at:
https://pubs.acs.org/10.1021/acs.organomet.2c00391

Notes

The authors declare no competing financial interest.

■ ACKNOWLEDGMENTS

■ REFERENCES

(1) Bonath, M.; Maichle-Mössmer, C.; Sirsch, P.; Anwander, R. Gallium Methylene. *Angew. Chem., Int. Ed.* **2019**, *58*, 8206−8210.

(2) Ziegler, K.; Nagel, K.; Patheiger, M. Metallorganische Verbindungen. XX. Lithium- und Magnesium-Methylen. *Z. Anorg. Allg. Chem.* **1955**, *282*, 345−351.

(3) Stucky, G.; Eddy, M.; Harrison, W.; Lagow, R.; Kawa, H.; Cox, D. Some observations concerning the structure of dilithiomethane. *J. Am. Chem. Soc.* **1990**, *112*, 2425−2427.

(4) Spiridopoulos, G.; Kramer, M.; Kracht, F.; Maichle-Mössmer, C.; Anwander, R. (CH₃)Al(CH₂)₁₂: Methylaluminomethylene (MAM-12). *Chem. − Eur. J.* **2022**, *28*, No. e202200823.

(5) (a) Benzencon, J.; Wittwer, M. B.; Cutting, B.; Smieško, M.; Wagner, B.; Kansy, M.; Ernst, B. pKa determination by ¹H NMR spectroscopy-An old methodology revisited. *J. Pharm. Biomed. Anal.* **2014**, *93*, 147−155. (b) Pankratov, A. N.; Uchaeva, I. M.; Doronin, S. Y.; Chernova, R. K. Correlations between the basicity and proton affinity of substituted anilines. *J. Struct. Chem.* **2001**, *42*, 739−746. (c) Hall, H. K. Correlation of the Base Strengths of Amines. *J. Am. Chem. Soc.* **1957**, *79*, 5441−5444.

(6) Samedov, K.; Aksu, Y.; Driess, M. From Molecular Gallium and Indium Siloxane Precursors to Amorphous Semiconducting Transparent Oxide Layers for Applications in Thin-Film Field-Effect Transistors. *ChemPlusChem* **2012**, *77*, 663−674.

(7) Dettenrieder, N.; Dietrich, H. M.; Maichle-Mössmer, C.; Anwander, R. Yttrium Siloxide Complexes Bearing Terminal Methyl Ligands: Molecular Models for Ln-CH₃. *Chem. − Eur. J.* **2016**, *22*, 13189−13200.

(8) Waggoner, K. M.; Power, P. P. Reactions of trimethylaluminum or trimethylgallium with bulky primary amines: structural characterization of the thermolysis products. *J. Am. Chem. Soc.* **1991**, *113*, 3385−3393.

(9) Downs, A. J. *Chemistry of aluminium, gallium, indium and thallium*, Springer Science & Business Media 1993.

(10) Belgardt, T.; Roesky, H. W.; Noltemeyer, M.; Schmidt, H. G. $(C_6F_5NGaMe)_4$ and $(C_6F_5NInMe)_4$: The First Gallium-Nitrogen and Indium-Nitrogen Compounds with Cubane Structures. *Angew. Chem., Int. Ed. Engl.* **1993**, *32*, 1056−1058.

(11) Cesari, M.; Cucinella, S., *The Chemistry of Inorganic Homo-and Heterocycles*. Academic, New York, 1987; pp 167−190.

(12) Amirkhalili, S.; Hitchcock, P.; Smith, J. Complexes of organoaluminium compounds. Part 10. Crystal and molecular structures of the cage compounds bis-*μ*-methylamido-hexa-*μ* 3-methylimido-bis (dimethylaluminium)-hexakis (methylaluminium) and bis-*μ*-methylamido-hexa-*μ* 3-methylimido-bis (dimethylgallium)-hexakis-(methylgallium). *J. Chem. Soc., Dalton Trans.* **1979**, 1206−1212.

(13) (a) Wright, R. J.; Phillips, A. D.; Allen, T. L.; Fink, W. H.; Power, P. P. Synthesis and characterization of the monomeric imides Ar 'MNAr "(M = Ga or in; Ar 'or Ar "= terphenyl ligands) with two-coordinate gallium and indium. *J. Am. Chem. Soc.* **2003**, *125*, 1694−1695. (b) Wright, R. J.; Brynda, N.; Fettinger, J. C.; Betzer, A. R.; Power, P. P. Quasi-Isomeric Gallium Amides and Imides GaNR₂ and RGaNR (R= Organic Group): Reactions of the Digallene, Ar 'GaGaAr '(Ar '= C_6H_3-2, 6-$(C_6H_3$-2, 6-Pri₂)₂) with Unsaturated Nitrogen Compounds. *J. Am. Chem. Soc.* **2006**, *128*, 12498−12509.

(14) Hardman, N. J.; Cui, C.; Roesky, H. W.; Fink, W. H.; Power, P. P. Stable, Monomeric Imides of Aluminum and Gallium: Synthesis and Characterization of $[\{HC(MeCDippN)_2\}MN$-2, 6-Trip₂$C_6H_3]$-(M= Al or Ga; Dipp= 2, 6-iPr₂C_6H_3; Trip= 2, 4, 6-iPr₃C_6H_2). *Angew. Chem., Int. Ed.* **2001**, *40*, 2172−2174.

(15) (a) Carmalt, C. J. Amido compounds of gallium and indium. *Coord. Chem. Rev.* **2001**, *223*, 217−264. (b) Carmalt, C. J.; King, S. J. Gallium(III) and indium(III) alkoxides and aryloxides. *Coord. Chem. Rev.* **2006**, *250*, 682−709.

(16) Keys, A.; Barbarich, T. J.; Bott, S. G.; Barron, A. R. Tert-Butyl compounds of gallium. *J. Chem. Soc., Dalton Trans.* **2000**, 577−588.

(17) Cleaver, W. M.; Barron, A. R.; McGufey, A. R.; Bott, S. G. Alcoholysis of tri-tert-butylgallium: synthesis and structural characterization of $[(But)_2Ga(\mu$-OR)]_2$. *Polyhedron* **1994**, *13*, 2831−2846.

(18) Petrie, M. A.; Olmstead, M. M.; Power, P. P. Synthesis and characterization of the mononuclear compounds *t*-Bu₂MOAr (M = Al or Ga, Ar = bulky aryl group): are the short Al−O and Ga−O bonds a consequence of *π*-interactions? *J. Am. Chem. Soc.* **1991**, *113*, 8704−8708.

(19) For examplexes, see: (a) Uhl, W.; Cuypers, L.; Neumüller, B.; Weller, F. Hydrogallation of Alkynes: Syntheses of Carbon−Gallium Cages Possessing Heteroadamantane Structures. *Organometallics* **2002**, *21*, 2365−2368. (b) Uhl, W.; Kovert, D.; Zemke, S.; Hepp, A. Unexpected Formation of Ga₄C₂H₄ Heteroadamantane Cages by the Reaction of Carbon-Bridged Bis(dichlorogallium) Compounds with *tert*-Butyllithium. *Organometallics* **2011**, *30*, 4736−4741.

(20) Hendershot, D. G.; Kumar, R.; Barber, M.; Oliver, J. P. Phenoxides and thiophenoxides of aluminum and gallium. Evidence of a ¹H-¹⁹F coupling in $(R_2MOC_6F_5)_2$ in solution. Crystal and molecular structures of $(Me_2AlOC_6F_5)_2$ and $(Me_2GaSC_6F_5)_2$. *Organometallics* **1991**, *10*, 1917−1922.

(21) Waggoner, K. M.; Ruhlandt-Senge, K.; Wehmschulte, R. J.; He, X.; Olmstead, M. M.; Power, P. P. Synthesis and characterization of

the monomeric gallium monoamides tert-Bu₂GaN (R) SiPh₃ (R = tert-Bu, 1-adamantyl), Trip₂MN (H) Dipp (M = Al, Ga; Trip = 2, 4, 6-iso-Pr₃C_6H_2; Dipp = 2, 6-iso-Pr₂C_6H_3), and Trip₂GaNPh₂. *Inorg. Chem.* **1993**, *32*, 2557−2561.

(22) Atwood, D. A.; Atwood, V. O.; Carriker, D. F.; Cowley, A. H.; Gabbai, F. P.; Jones, R. A.; Bond, M. R.; Carrano, C. J. Short Ga⋯ H-N distances in gallium amine and amide complexes. *J. Organomet. Chem.* **1993**, *463*, 29−35.

(23) Beachley, O. T.; Noble, M. J.; Churchill, M. R.; Lake, C. H. The Dihydronaphthalene Elimination Reaction as a Route to Gallium−Nitrogen Compounds. Crystal and Molecular Structure of $[(PhMe_2CCH_2)_2GaNHPh]_2$. *Organometallics* **1998**, *17*, 3311−3315.

(24) Solis-Ibarra, D.; Gómora-Figueroa, A. P.; Zavala-Segovia, N.; Jancik, V. *β*-Diketiminate Gallium Amides: Useful Synthons in Gallium Chemistry. *Eur. J. Inorg. Chem.* **2009**, *2009*, 4564−4571.

(25) Samedov, K.; Aksu, Y.; Driess, M. The reversible adduct formation of group III trialkyls with relatively involatile phosphines; x-ray crystal structures of $(Me_3M)_2(Ph_2PCH_2)_2$ (M = Al, Ga, In) and $(Me_3Al)_3(Ph_2PCH_2CH_2)_2$PPh. *Polyhedron* **1988**, *14*, 1289−1298.

(26) *COSMO V. 1.61*, Bruker AXS Inc., Madison, WI, 2012.

(27) *APEX3 v2019.11-0*, Bruker AXS Inc., Madison, WI, 2019.

(28) *SAINT V8.40B* (Bruker Nano, Inc., 2019).

(29) SADABS Krause, L.; Herbst-Irmer, R.; Sheldrick, G. M.; Stalke, D. *J. Appl. Crystallogr.* **2015**, *48*, 3−10.

(30) Sheldrick, G. M. *Acta Cryst.* **2015**, *C71*, 3−8.

(31) Huebschle, C. B.; Sheldrick, G. M.; Dittrich, B. ShelXle: a Qt Graphical user interface for SHELXL. *J. Appl. Crystallogr.* **2011**, *44*, 1281−1284.

(32) Kratzert, D.; Holstein, J. J.; Krossing, I. DSR: enhanced modelling and refinement of disordered structures with SHELXL. *J. Appl. Crystallogr.* **2015**, *48*, 933−938.

(33) Spek, A. L. PLATON SQUEEZE: a tool for the calculation of the disordered solvent contribution to the calculated structure factors. *Acta Crystallogr., Sect. C: Struct. Chem.* **2015**, *C71*, 9−18.

(34) Farrugia, L. WinGX and ORTEP for Windows: an update. *J. Appl. Crystallogr.* **2012**, *849*. *45*, 849−854.

(35) *V. 3.6, P. o. V. P. L.*, POV-Ray William-town, Victoria, Australia, 2004, http://www.povray.org

Gallium Methylene in the Pocket

Georgios Spiridopoulos, Martin Bonath, Cäcilia Maichle-Mössmer, and Reiner Anwander*[a]

[a]   G. Spiridopoulos, Dr. M. Bonath, Dr. C. Maichle-Mössmer,
        Prof. Dr. R. Anwander
        Institut für Anorganische Chemie, Eberhard Karls Universität Tübingen
        Auf der Morgenstelle 18, 72076 Tübingen (Germany)
        E-Mail : reiner.anwander@uni-tuebingen.de
        Homepage : http://uni-tuebingen.de/syncat-anwander

Table of contents

Figure S1. Crystal structure of $Ga_6(CH_2)_9(DMAP)_3(THF)$ (**2**). All atoms are represented by atomic displacement ellipsoids set at 50% probability. Hydrogen atoms are omitted for clarity. Selected interatomic distances [Å] and angles [°]: Ga(1)–C(1) 1.967(4), Ga(1)–C(3) 1.951(5), Ga(1)–C(6) 1.962(4), Ga(2)–C(1) 2.004(5), Ga(2)–C(2) 1.974(5), Ga(2)–C(4) 2.012(5), Ga(2)–N(1) 2.142(4), Ga(3)–C(2) 1.987(4), Ga(3)–C(3) 2.013(5), Ga(3)–C(5) 1.989(5), Ga(3)–N(3) 2.125(4), Ga(4)–C(6) 2.002(5), Ga(4)–C(7) 2.004(4), Ga(4)–C(9) 1.995(5), Ga(4)–N(5) 2.118(4), Ga(5)–C(4) 1.952(4), Ga(5)–C(7) 1.957(5), Ga(5)–C(8) 1.959(5), Ga(6)–C(5) 1.954(5), Ga(6)–C(8) 2.000(5), Ga(6)–C(9) 1.967(5), Ga(6)–O(1) 2.232(4); Ga(1)–C(1)–Ga(2) 105.8(2), Ga(1)–C(3)–Ga(3) 109.1(2), Ga(1)–C(6)–Ga(4) 113.5(2).
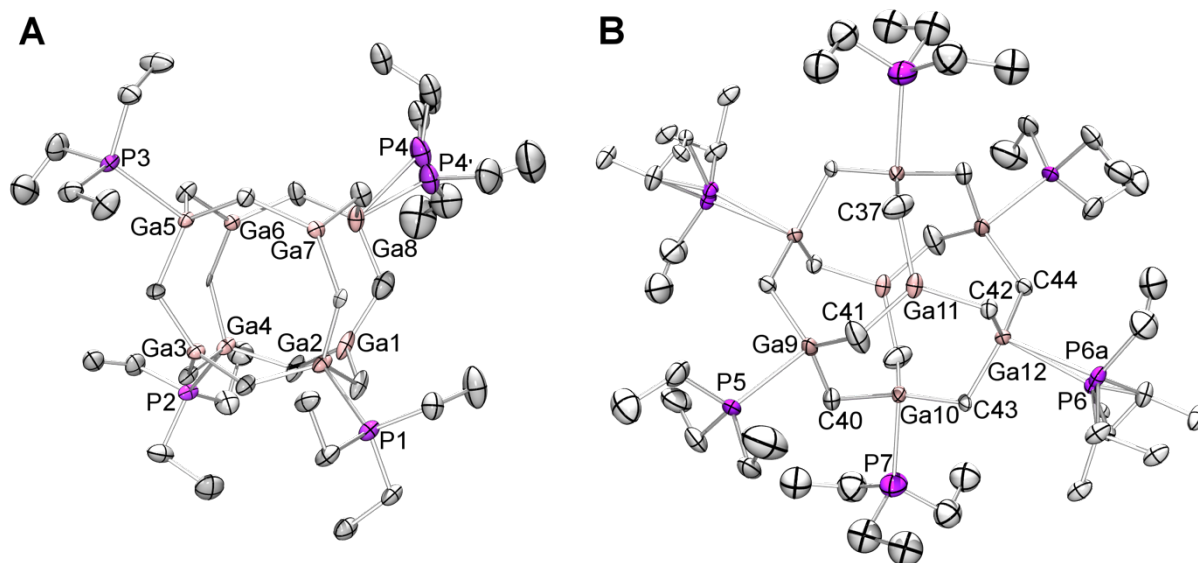
Figure S2. Crystal structure of [Ga$_8$(CH$_2$)$_{12}$](PEt$_3$)$_4$ (**3a**)/[Ga$_8$(CH$_2$)$_{12}$](PEt$_3$)$_6$ (**3b**). All atoms are represented by atomic displacement ellipsoids set at 50% probability. Hydrogen atoms are omitted for clarity. Selected interatomic distances [Å] and angles [°]: **3a:** Ga(1)–C(1) 1.94(2), Ga(2)–C(1) 2.015(19), Ga(3)–C(2) 1.949(18), Ga(2)–C(2) 1.983(19), Ga(4)–C(3) 1.93(2), Ga(3)–C(3) 1.964(17), Ga(1)–C(4) 1.963(19), Ga(4)–C(4) 1.98(2), Ga(1)–C(5) 1.94(3), Ga(8)–C(5) 1.99(2), Ga(2)–C(6) 1.919(16), Ga(7)–C(6) 2.032(17), Ga(3)–C(7) 1.933(18), Ga(5)–C(7) 1.988(18), Ga(6)–C(8) 2.006(16), Ga(4)–C(8)–2.028(18), Ga(6)–C(9) 1.950(18), Ga(5)–C(9) 1.990(19), Ga(6)–C(10) 1.93(2), Ga(8)–C(10) 2.02(2), Ga(7)–C(11) 1.94(2), Ga(8)–C(11) 2.02(2), Ga(7)–C(12) 1.960(19), Ga(5)–C(12) 1.978(17), Ga(2)–P(1) 2.563(6), Ga(4)–P(2) 2.542(6), Ga(5)–P(3) 2.548(6), Ga(8)–P(4A) 2.454(16), Ga(8)–P(4) 2.663(14); Ga(1)–C(1)–Ga(2) 118.1(10), Ga(3)–C(2)–Ga(2) 117.7(10), Ga(4)–C(3)–Ga(3) 121.8(10), Ga(1)–C(4)–Ga(4) 117.1(10), C(6)–Ga(2)–C(2) 113.3(7), C(6)–Ga(2)–C(1) 122.7(9), C(2)–Ga(2)–C(1) 117.6(8), C(6)–Ga(2)–P(1) 95.9(5), C(2)–Ga(2)–P(1) 100.8(6), C(1)–Ga(2)–P(1) 98.8(6). **3b:** Ga(9)–C(40) 1.81(2), Ga(10)–C(40) 2.12(2), Ga(11)–C(41) 1.87(2), Ga(9)–C(41) 2.04(2), Ga(11)–C(42) 1.943(18), Ga(12)–C(42) 1.987(19), Ga(10)–C(43) 1.934(18), Ga(12)–C(43) 2.019(18), Ga(9)'–C(44) 1.941(17), Ga(12)–C(44) 2.005(18), Ga(11)–C(37) 1.96(2), Ga(10)–C(37) 2.00(2), Ga(9)– P(5) 2.584(7), Ga(10)–P(7) 2.594(7), Ga(12)–P(6) 2.553(14); Ga(9)–C(40)–Ga(10) 123.8(11), Ga(11)–C(41)–Ga(9) 114.3(12), C(40)–Ga(9)–C(44)' 128.3(10), C(40)–Ga(9)–C(41) 114.0(11), C(44)–Ga(9)–C(41)' 113.7(10), C(40)–Ga(9)–P(5) 91.1(7), C(44)–Ga(9)–P(5)' 98.2(6), C(41)–Ga(9)–P(5) 101.3(7).

'-X+1,-Y+1,-Z+1
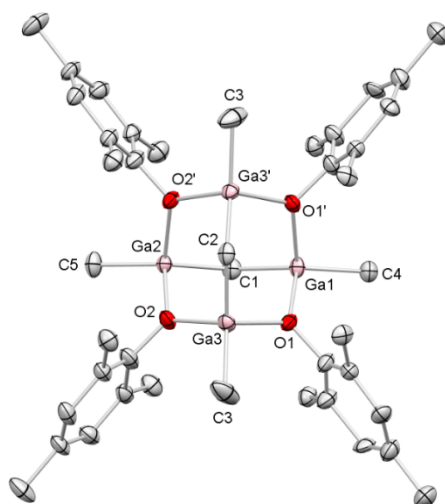
Figure S3. Crystal structure of **4a**. All atoms are represented by atomic displacement ellipsoids set at 50% probability. Hydrogen atoms and co-crystalized THF molecules are omitted for clarity. Selected interatomic distances [Å] and angles [°]: Ga(2)–C(1) 1.949(6), Ga(1)–C(1) 1.953(6), Ga(3)–C(2) 1.953(3), Ga(3)–C(3) 1.952(5), Ga(1)–C(4) 1.946(6), Ga(2)–C(5) 1.958(6), Ga(1)–O(1) 1.980(3), Ga(2)–O(2) 1.980(3); Ga(2)–C(1)–Ga(1) 122.4(3), Ga(3)–C(2) Ga(3)' 120.7(3), C(4)–Ga(1)–C(1) 130.4(3), C(4)–Ga(1)–O(1) 106.69(13),C(1)–Ga(1)–O(1) 104.03(13),C(4)–Ga(1)–O(1)' 106.69(13), C(1)–Ga(1)–O(1)' 104.03(13), O(1)–Ga(1)–O(1)' 101.62(16).

' y, x, z
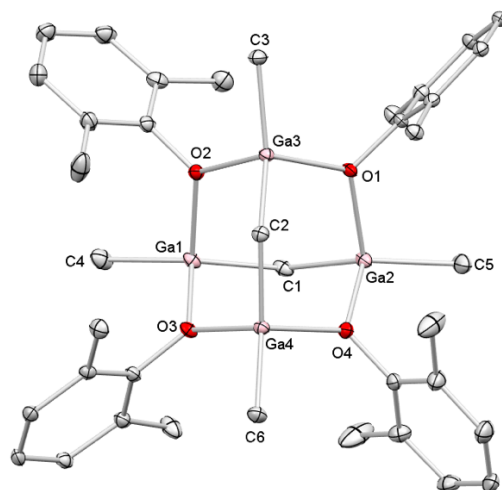
Figure S4. Crystal structure of **4b**. Hydrogen atoms are omitted for clarity. Atomic displacement ellipsoids were set at 50% probability. Selected interatomic distances [Å] and angles [°]: Ga(2)–C(1) 1.957(3), Ga(1)–C(1) 1.963(3), Ga(4)–C(2) 1.958(3), Ga(3)–C(2) 1.960(3), Ga(3)–C(3) 1.959(3), Ga(1)–C(4) 1.951(3), Ga(2)–C(5) 1.965(3), Ga(4)–C(6) 1.944(3), Ga(1)–O(3) 1.9845(18), Ga(1)–O(2) 2.0087(18), Ga(2)–O(1) 1.9815(17), Ga(2)–O(4) 1.9825(17), Ga(3)–O(1) 1.9858(18), Ga(3)–O(2) 2.0008(18), Ga(4)–O(3) 1.9985(18), Ga(4)–O(4) 2.0059(18); Ga(2)–C(1)–Ga(1) 123.27(13), Ga(4)–C(2)–Ga(3) 120.82(13), C(7)–O(1)–Ga(2) 121.08(15), C(7)–O(1)–Ga(3) 117.54(15), Ga(2)–O(1)–Ga(3) 121.35(9), C(4)–Ga(1)–C(1) 132.06(11), C(4)–Ga(1)– O(3) 105.88(10), C(1)–Ga(1)–O(3) 102.56(9), C(4)–Ga(1)–O(2) 106.20(10), C(1)–Ga(1)–O(2) 104.28(9), O(3)–Ga(1)–O(2) 102.43(7).
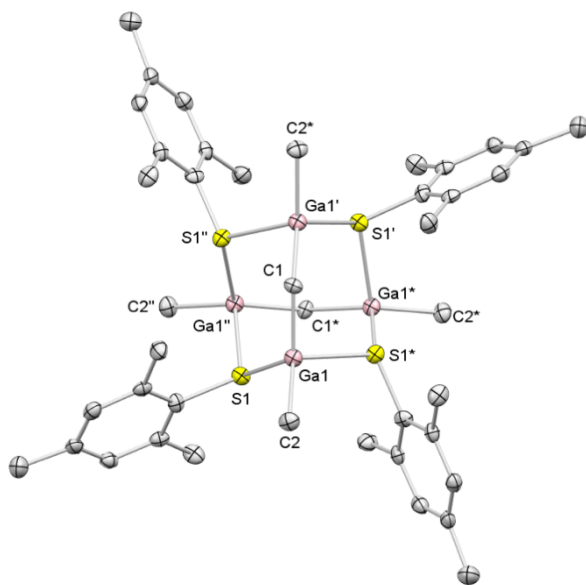
Figure S5. Crystal structure of **5**. All atoms are represented by atomic displacement ellipsoids set at 50% probability. Hydrogen atoms and co-crystalized benzene molecules are omitted for clarity. Selected interatomic distances [Å] and angles [°]:Ga(1)–C(1) 1.951(2), Ga(1)–C(2) 1.967(4), Ga(1)–S(1)* 2.3801(10), Ga(1)–S(1) 2.4029(11), Ga(1)'–C(1) 1.951(2); C(1)–Ga(1)–C(2) 124.81(18), C(1)–Ga(1)–S(1)* 97.61(8), C(2)–Ga(1)–S(1)* 111.08(12), C(1)–Ga(1)–S(1) 117.15(10), C(2)–Ga(1)–S(1) 106.26(12), S(1)*–Ga(1)–S(1) 95.28(3), Ga(1)''–S(1) –Ga(1) 114.12(4).

' -x+1/2, -y+3/2, z

'' -y+1, x+1/2, -z+1

*y-1/2, -x+1, -z+1
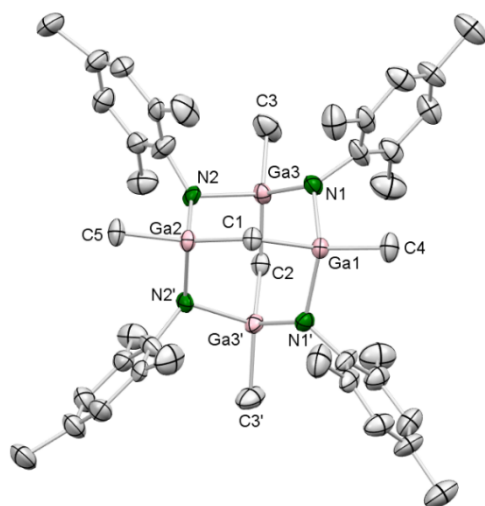
Figure S6. Crystal structure of **6a**. All atoms are represented by atomic displacement ellipsoids set at 50% probability. Hydrogen atoms, co-crystalized THF molecules and the disorder are omitted for clarity. Selected interatomic distances [Å] and angles [°]: Ga(1)–C(1) 1.974(7), Ga(2)–C(1) 1.984(7), Ga(3)–C(2) 1.970(4), Ga(3)'–C(2) 1.970(4), Ga(3)–C(3) 1.970(7), Ga(1)–C(4) 1.997(8), Ga(2)–C(5) 1.967(8), Ga(3)–N(1) 2.023(10), Ga(1)–N(1) 2.089(10), Ga(2)–N(2) 2.037(9), Ga(3)–N(2) 2.058(8); C(3)–Ga(3)–C(2) 126.8(4), C(3)–Ga(3)–N(1) 104.5(4), C(2)–Ga(3)–N(1) 113.7(4), C(3)–Ga(3)–N(2) 108.7(4), C(2)–Ga(3)–N(2) 97.6(4), N(1)–Ga(3)–N(2) 103.0(5).
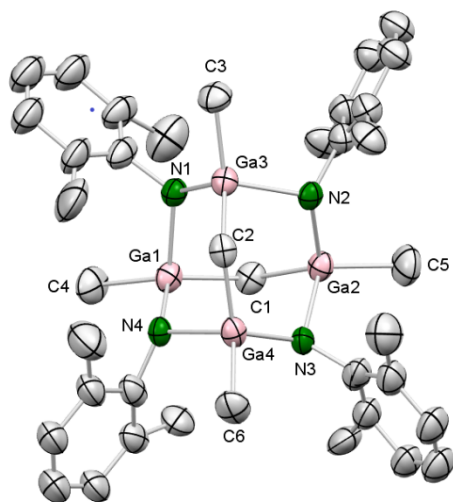
'y,x, z

Figure S7. Crystal structure of **6b**. Hydrogen atoms and the disorder in the aryl rings are omitted for clarity. Atomic displacement ellipsoids were set at 50% probability. Selected interatomic distances [Å] and angles [°]: Ga(1)–C(1) 1.978(2), Ga(2)–C(1) 1.979(2), Ga(3)–C(2) 1.966(2), Ga(4)–C(2) 1.970(3), Ga(1)–C(4) 1.974(3), Ga(2)–C(5) 1.974(3), Ga(3)–C(3) 1.971(3), Ga(4)–C(6) 1.974(3), Ga(1)–N(1) 2.043(5), Ga(1)–N(4) 2.079(4), Ga(2)–N(2) 2.023(6), Ga(2)–N(3) 2.112(5), Ga(3)–N(1) 2.053(5), Ga(3)–N(2) 2.090(5); Ga(2)–C(1)–Ga(1) 120.33(12), Ga(3)–C(2)–Ga(4) 120.12(12), C(4)–Ga(1)–C(1) 128.36(13), C(4)–Ga(1)–N(1) 108.09(16), C(1)–Ga(1)–N(1) 95.43(18), C(4)–Ga(1)–N(4) 104.76(16), C(1)–Ga(1)–N(4) 112.85(15), N(1)–Ga(1)–N(4) 104.7(2), N(1)–Ga(3)–N(2) 103.0(2), N(4)–Ga(4)–N(3) 103.67(19).
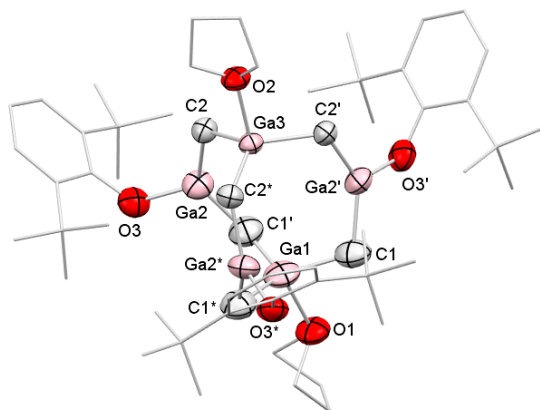
Figure S8. Crystal structure of **7**. All atoms are represented by atomic displacement ellipsoids set at 50% probability. Hydrogen atoms are omitted for clarity. Selected interatomic distances [Å] and angles [°]: Ga(2)–C(1) 1.932(9), Ga(1)–C(1) 1.978(9), Ga(2)–C(2) 1.923(13), Ga(3)–C(2) 2.014(16), Ga(2)–O(1) 1.831(9), Ga(3)–O(2) 2.097(17), Ga(1)–O(3) 2.060(11); Ga(2)–C(1)–Ga(1) 116.5(5), Ga(2)–C(2)–Ga(3) 110.8(7), C(1)–Ga(1)–C(1)' 117.48(14), C(1)–Ga(1)–C(1)* 117.48(14), C(1)'–Ga(1)–C(1)* 117.48(14), C(2)–Ga(3)–C(2)' 117.1(2).

' -z+1/2, -x+1, y-1/2

* -y+1, z+1/2, -x+1/2
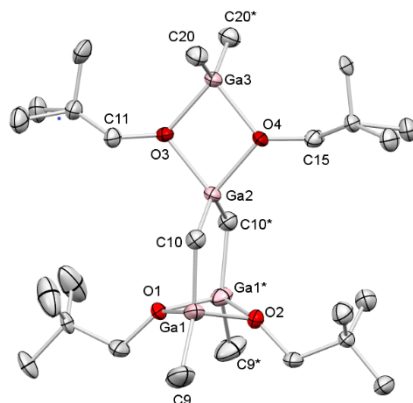
Figure S9. Crystal structure of **8**. All atoms are represented by atomic displacement ellipsoids set at 50% probability. Hydrogen atoms are omitted for clarity. Selected interatomic distances [Å] and angles [°]: Ga(1)–C(9) 1.957(7), Ga(2)–C(10) 1.967(6), Ga(3)–C(20) 1.951(6), Ga(1)'–O(1) 1.964(4), Ga(1)–O(1) 1.964(4), Ga(1)'–O(2) 1.960(4), Ga(1)–O(2) 1.960(4), O(3)–C(11)' 1.425(12), Ga(3)–O(3) 1.957(5), Ga(2)–O(3) 1.965(5), O(4)–C(15)' 1.487(12), Ga(3)–O(4) 1.947(5), Ga(2)–O(4)–1.952(5), Ga(2)'–C(10) 1.967(6); Ga(1)–C(10)–Ga(2) 110.4(3), Ga(1)'–O(1)–Ga(1) 95.9(2), Ga(1)'–O(2) Ga(1) 96.1(2), Ga(3)–O(3)–Ga 2 98.9(2), Ga(3)–O(4)–Ga 2 99.7(2), O(2)–Ga(1)–O(1) 81.67(17), O(4)–Ga(2)–O(3) 80.6(2), C(10)–Ga(2)–C(10)' 123.1(3), O(4)–Ga(3)–O(3) 80.9(2), C(20)–Ga(3)–C(20)' 128.5(4).

' x, -y+1/2, z
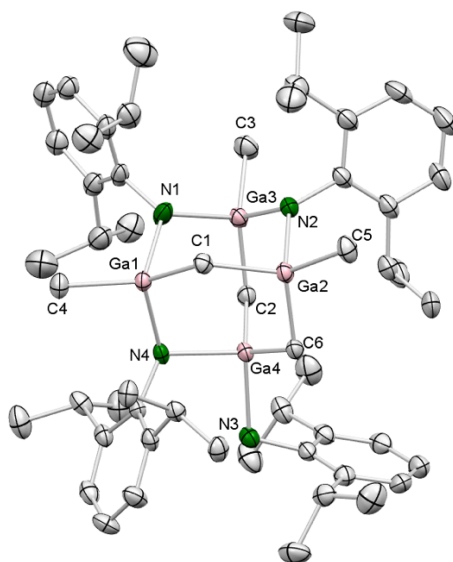
Figure S10. Crystal structure of **9**. Hydrogen atoms are omitted for clarity. Atomic displacement ellipsoids were set at 50% probability. Selected interatomic distances [Å] and angles [°]:Ga(1)–C(1) 1.966(3), Ga(1)–C(4) 1.981(3), Ga(1)–N(1) 2.093(3), Ga(1)–N(4) 2.100(3), Ga(2)–C(5) 1.932(3), Ga(2)–C(1) 2.014(3), Ga(2)–C(6) 2.007(3), Ga(2)–N(4) 2.034(3), Ga(3)–C(2) 1.983(4), Ga(3)–N(2) 2.037(3). Ga(3)–N(1) 2.083(3), Ga(4)–C(6) 1.932(3), Ga(4)–C(2) 1.958(3), Ga(4)–N(3) 2.174(3), Ga(4)–N(4) 2.034(3); Ga(1)–C(1)–Ga(2) 119.02(17), Ga(4)–C(2)–Ga(3) 111.32(17), Ga(3)–N(1)–Ga(1) 118.21(14), Ga(3)–N(2)–Ga(2) 116.03(13), Ga(2)–C(6)–Ga(4) 107.04(16).
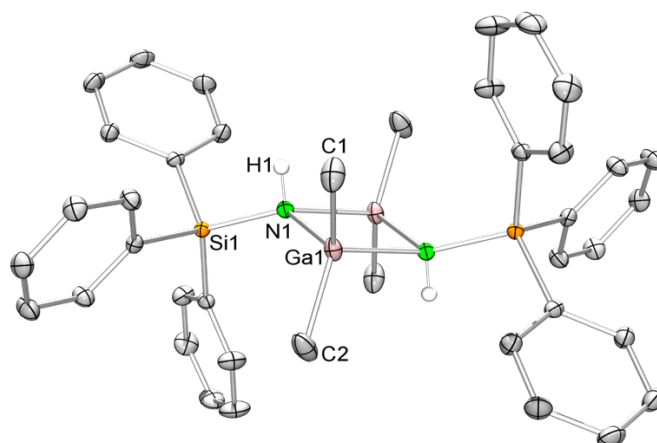
Figure S11. Crystal structure of [Me$_2$Ga(μ-HNSiPh$_3$)]$_2$ (**10**). All atoms are represented by atomic displacement ellipsoids set at 50% probability. Hydrogen atoms except for N–H are omitted for clarity. Selected interatomic distances [A] and angles [°]: Si(1)–N(1) 1.7570(10), Ga(1)–N(1) 2.0396(10), Ga(1)–N(1)' 2.0492(9), Ga(1)–C(1) 1.9654(14), Ga(1)–C(2) 1.9683(14), N(1)–H(1) 0.867(19); Si(1)–N(1)–Ga(1) 125.76(5), Si(1)–N(1)–Ga(1)' 126.03(5), Ga(1)–N(1)–Ga(1)' 92.80(4), N(1)–Ga(1)–N(1)' 87.20(4). The solid-state structure of **10** is isostructural to that reported for the aluminum congener, [Me$_2$Al(μ-HNSiPh$_3$)]$_2$ (Choquette, D. M.; Timm, M. J.; Hobbs, J. L.; Rahim, M. M.; Ahmed, K. J.; Planalp, R. P., *Organometallics* **1992**, *11*, 529-534).

' -x+1,-y+1,-z
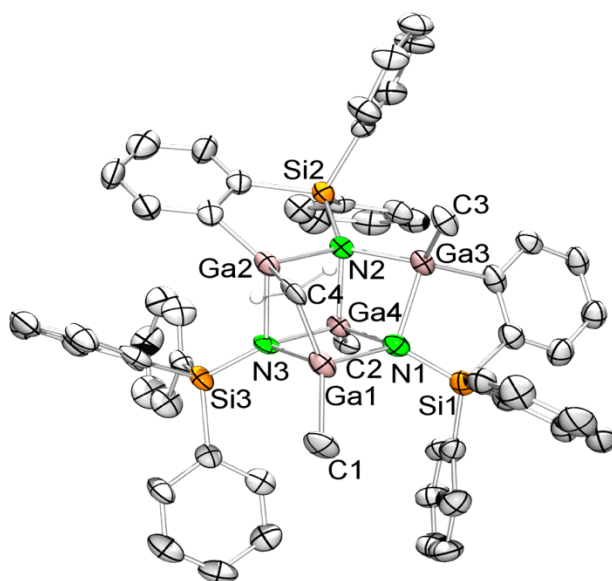
Figure S12. Crystal structure of [Ga$_4$Me$_3$(CH$_2$)(NSiPh$_3$)(NSiPh$_2${C$_6$H$_4$})$_2$][Li(THF)$_4$] (**11**). All atoms are represented by atomic displacement ellipsoids set at 50% probability. Hydrogen atoms except for methylene and [Li(THF)$_4$] are omitted for clarity. Selected interatomic distances [A] and angles [°]: Si(1)–N(1) 1.692(7), Si(2)–N(2) 1.710(7), Si(3)–N(3) 1.706(7), Ga(1)–N(1) 1.990(7), Ga(3)–N(1) 2.049(7), Ga(4)–N(1) 2.022(6), Ga(2)–N(2) 2.049(6), Ga(3)–N(2) 1.974(7), Ga(4)–N(2) 2.007(7), Ga(1)–N(3) 2.058(7), Ga(2)–N(3) 2.063(6), Ga(4)–N(3) 1.941(7), Ga(1)–C(4) 1.994(9), Ga(2)–C(4) 1.959(9), Ga(3)–C(11) 2.000(9), Ga(2)–C(36) 1.960(9); Ga(1)–N(1)–Ga(4) 90.2(3), Ga(3)–N(2)–Ga(4) 89.2(3), Ga(3)–N(2)–Ga(2) 111.6(3), Ga(1)–N(3)–Ga(4) 90.6(3), Ga(1)–N(1)–Ga(3) 115.3(3), Ga(1)–N(3)–Ga(2) 84.3(2), Ga(2)–N(2)–Ga(3) 111.6(3), Ga(2)–C(4)–Ga(1) 88.8(4).

Table S1. Crystallographic data for compounds **2**, **3**, **4a**, **4b**, **5**, **6a**, **6b**, **7**, **8**, **9**, **10**, and **11**

	2	**3a/3b**[b]	**4a**	**4b**
CCDC	2193556	2193559	2193557	2193558
formula	$C_{38}H_{64}Ga_6N_6O_2$	$C_{48}H_{114}Ga_8P_6$, $C_{36}H_{84}Ga_8P_4$	$C_{54}H_{84}Ga(4)O_7$	$C_{38}H_{52}Ga(4)O_4$
M_r [g/mol]	1055.27	1435.05/1198.74	1124.09	851.67
colour/shape	colorless plates	colorless plates	colorless needles	colorless needles
crystal dimensions [mm]	0.150 x 0.119 x 0.037	0.175 x 0.117 x 0.062	0.252 x 0.135 x 0.126	0.325 x 0.048 x 0.039
crystal system	triclinic	monoclinic	tetragonal	tetragonal
space group	P$\bar{1}$	P2$_1$/n	P4$_2$nm	I4$_1$/a
a [Å]	10.7027(12)	13.35(2)	26.7948(17)	30.538(6)
b [Å]	11.5022(13)	12.870(16)	26.7948(17)	30.538(6)
c [Å]	18.070(2)	49.63(7)	7.8536(5)	16.319(3)
α [°]	88.192(2)	90	90	90
β [°]	81.135(2)	91.24(4)	90	90
γ [°]	81.607(2)	90	90	90
V [Å³]	2174.3(4)	8525(20)	5638.6(8)	15219(7)
Z	2	2	4	16
T [K]	100(2)	100	100(2)	100(2)
λ [Å]	0.71073	0.71073	0.71073	0.71073
ρ_{calcd} [g cm^{-3}]	1.612	1.493	1.324	1.487
μ [mm^{-1}]	3.703	3.887	1.937	2.839
F (000)	1072	3912	2352	6976
θ range [°]	1.141/ 27.687	1.231/25.561	1.699/27.103	1.415/28.277
unique reflections	10088	15991	6399	9396
observed reflections (I > 2σ)	6611	10900	5911	7242
R1/wR2 (I > 2σ)[a]	0.0460/ 0.0987	0.1128/0.2846	0.0303/0.0744	0.0340/0.0765
R1/wR2 (all data)	0.0896/ 0.1183	0.1581/0.3116	0.0357/0.0772	0.0.528/0.0846
GOF	1.023	1.603	1.038	1.024

[a] $R_1 = \Sigma(||F_0|-|F_c||)/\Sigma|F_0|$, $wR_2 = \{\Sigma[w(F_0^2-F_c^2)^2/\Sigma[w(F_0^2)^2]\}^{1/2}$.

* bad crystal quality

Table S1 continued.

	5	6a	6b	7
CCDC	2193562	2193560	2193565	2193567
formula	$C_{78}H_{96}Ga_4S_4$	$C_{50}H_{80}Ga_4N_4O_2$	$C_{38}H_{56}Ga_4N_4$	$C_{56}H_{91}Ga_5O_5$
M_r [g/mol]	1440.66	1048.06	847.74	1192.88
colour/shape	colorless columns	colorless needles	colorless needles	colorless blocks
crystal dimensions [mm]	0.365 x 0.190 x 0.148	0.475 x 0.084 x 0.076	0.178 x 0.141 x 0.114	0.373 x 0.318 x 0.220
crystal system	tetragonal	tetragonal	triclinic	cubic
space group	P4/n	P4$_2$nm	P$\bar{1}$	P2$_1$3
a [Å]	20.878(3)	26.868(4)	8.0775(4)	18.7198(8)
b [Å]	20.878(3)	26.868(4)	11.3598(6)	18.7178(8)
c [Å]	8.3345(15)	8.0003(11)	23.6119(12)	18.7178(8)
α [°]	90	90	81.499(2)	90
β [°]	90	90	84.148(2)	90
γ [°]	90	90	69.5760(10)	90
V [Å^3]	3633.1(11)	5775.5(17)	2005.12(18)	6557.9(8)
Z	2	4	2	4
T [K]	100	100(2)	170(2)	160(2)
λ [Å]	0.71073	0.71073	0.71073	0.71073
ρ_{calcd} [g cm^{-3}]	1.317	1.205	1.404	1.208
μ [mm^{-1}]	1.623	1.882	2.668	2.065
F (000)	1504	2192	872	2488
θ range [°]	1.379/27.100	1.516/27.119	1.747/27.113	1.884/23.635
unique reflections	4012	6567	8848	3312
observed reflections (I > 2σ)	2348	5772	6923	2463
R1/wR2 (I > 2σ)[a]	0.0481/0.0853	0.0397/0.0932	0.0317/0.0767	0.0476/0.1196
R1/wR2 (all data)	0.1116/0.1031	0.0499/0.0995	0.0462/0.0835	0.0733/0.1431
GOF	0.962	1.028	1.037	1.010

[a] $R_1 = \Sigma(||F_0|-|F_c||)/\Sigma|F_0|$, $wR_2 = \{\Sigma[w(F_0^2-F_c^2)^2/\Sigma[w(F_0^2)^2]\}^{1/2}$.

* Connectivity only due to bad crystal quality.

Table S1 continued.

	8	9	11	10
CCDC	2193563	2193561	2193564	2193566
formula	$C_{26}H_{60}Ga_4O_4$	$C_{54}H_{88}Ga_4N_4$	$C_{74}H_{86}Ga_4LiN_3O_4 Si_3$	$C_{40}H_{44}Ga_2N_2Si_2$
M_r [g/mol]	715.62	1072.16	1451.54	748.39
colour/shape	colorless needles	colorless needles	colorless needles	colorless block
crystal dimensions [mm]	0.287 x 0.111 x 0.054	0.362 x 0.085 x 0.073	0.424 x 0.159 x 0.088	0.408 x 0.351 x 0.315
crystal system	monoclinic	monoclinic	orthorhombic	triclinic
space group	$P2_1/m$	$P2_1/c$	$Pna2_1$	$P\bar{1}$
a [Å]	11.8681(14)	13.223(4)	27.419(4)	8.6967(6)
b [Å]	11.6452(14)	17.192(6)	20.777(3)	9.3638(7)
c [Å]	12.7244(15)	26.744(9)	14.231(2)	13.2900(10)
α [°]	90	90	90	70.2100(10)
β [°]	92.258(2)	90.124(8)	90	74.0810(10)
γ [°]	90	90	90	65.9230(10)
V [Å³]	1757.2(4)	6080(3)	8107(2)	917.99(12)
Z	2	4	4	1
T [K]	100(2)	173(2)	100(2)	100(2)
λ [Å]	0.71073	0.71073	0.71073	0.71073
ρ_{calcd} [g cm⁻³]	1.352	1.171	1.189	1.354
μ [mm⁻¹]	3.058	1.787	1.402	1.563
F (000)	744	2256	3008	388
θ range [°]	2.302/26.344	1.408/28.356	1.780/23.605	2.466/ 29.603
unique reflections	3754	14871	12043	5142
observed reflections (I > 2σ)	3142	10214	10116	4738
R1/wR2 (I > 2σ)[a]	0.0569/0.1211	0.0522/0.1208	0.0490/0.1067	0.0228/0.0586
R1/wR2 (all data)	0.0704/0.1255	0.0843/0.1363	0.0629/0.1123	0.0257 /0.0599
GOF	1.253	1.005	1.029	1.049

[a] $R_1 = \Sigma(||F_0|-|F_c||)/\Sigma|F_0|$, $wR_2 = \{\Sigma[w(F_0^2-F_c^2)^2/\Sigma[w(F_0^2)^2]\}^{1/2}$.
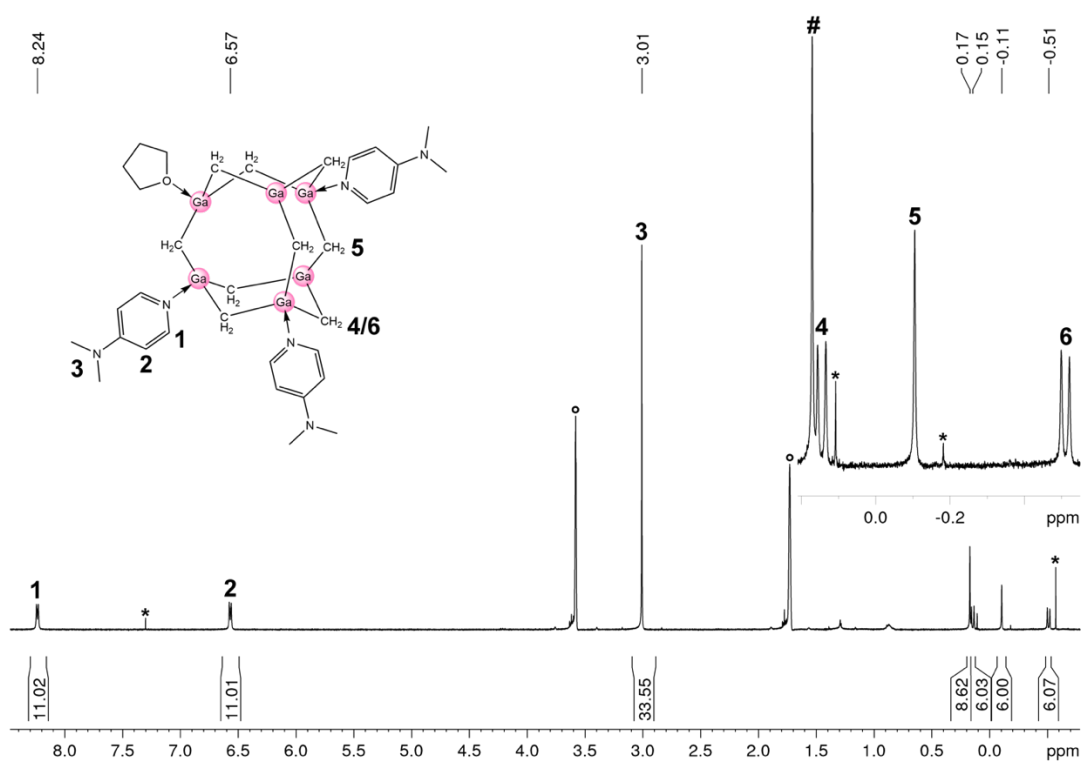
NMR Spectra

Figure S13. ^{1}H NMR spectrum (400 MHz) of $Ga_6(CH_2)_9(DMAP)_3(THF)$ (**2**) in THF-d$_8$ at 26 °C (# [$Ga_8(CH_2)_{12}$](DMAP)$_x$(THF)$_y$, * minor side-products).
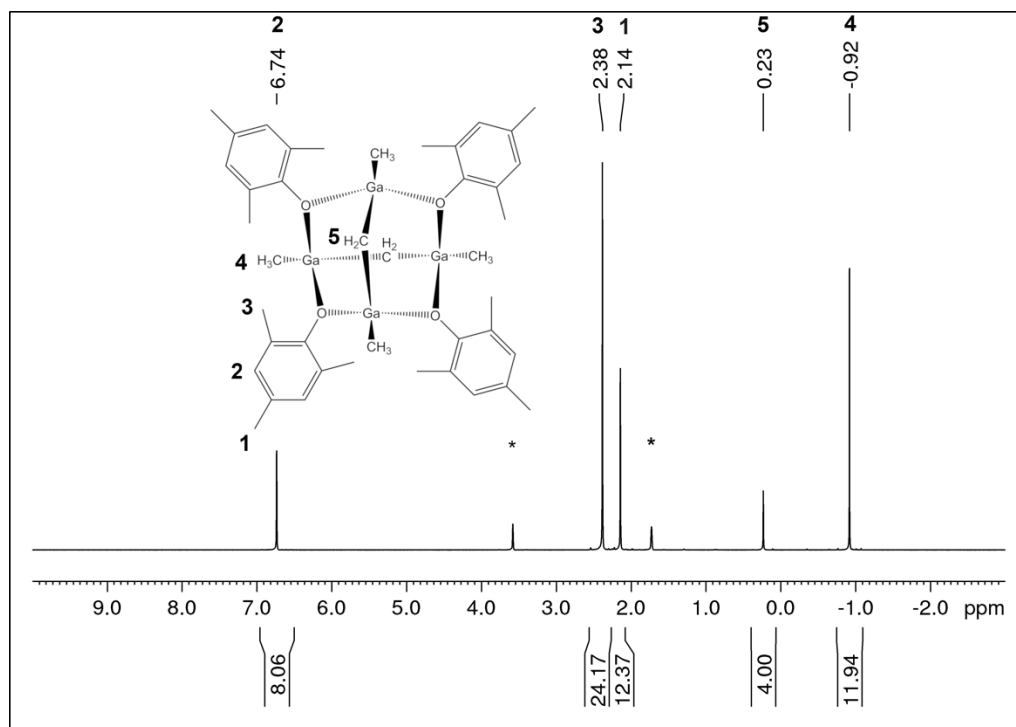
Figure S14. ^{1}H NMR spectrum (400 MHz, THF-d$_8$ of complex $Ga_4(CH_3)_4(\mu_2\text{-}CH_2)_2(\mu_2\text{-}OC_6H_2Me_3\text{-}2,4,6)_4$ (**4a**) at 26 °C.
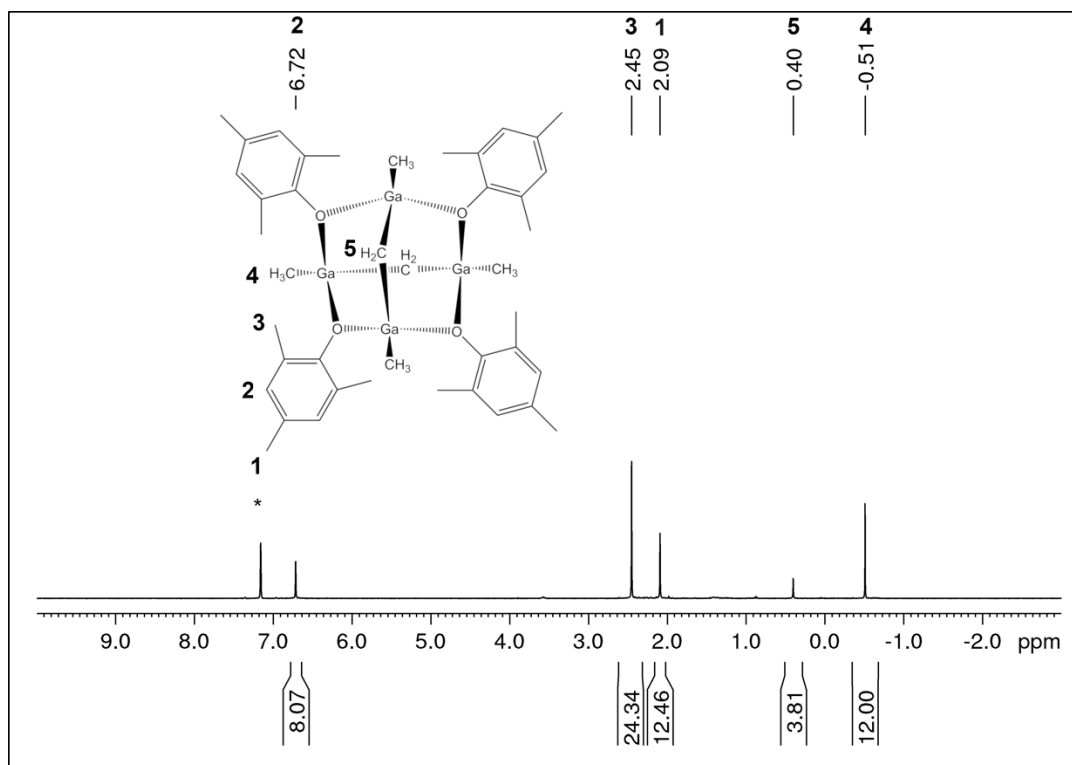
Figure S15. ^{1}H NMR spectrum (400 MHz, benzene-d_6 of complex $Ga_4(CH_3)_4(\mu_2\text{-}CH_2)_2(\mu_2\text{-}OC_6H_2Me_3\text{-}2,4,6)_4$ (**4a**) at 26 °C.
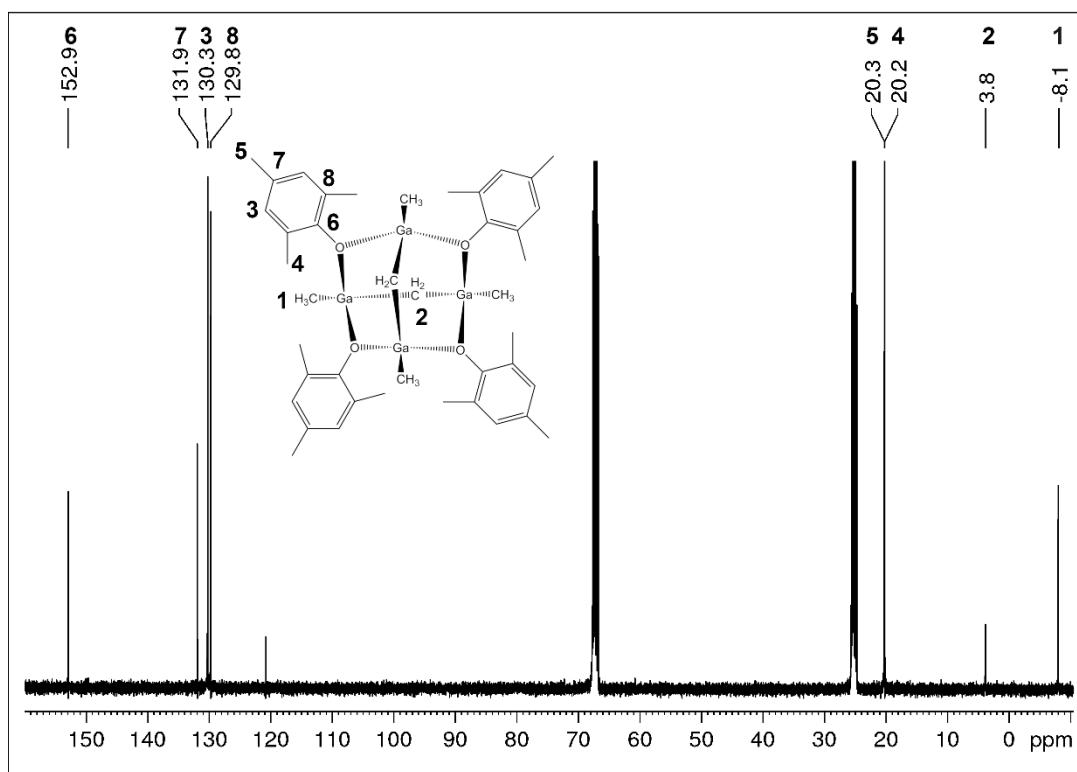
Figure S16. ^{13}C{^{1}H} NMR spectrum (100 MHz, THF-d_8 of complex $Ga_4(CH_3)_4(\mu_2\text{-}CH_2)_2(\mu_2\text{-}OC_6H_2Me_3\text{-}2,4,6)_4$ (**4a**) at 26 °C.
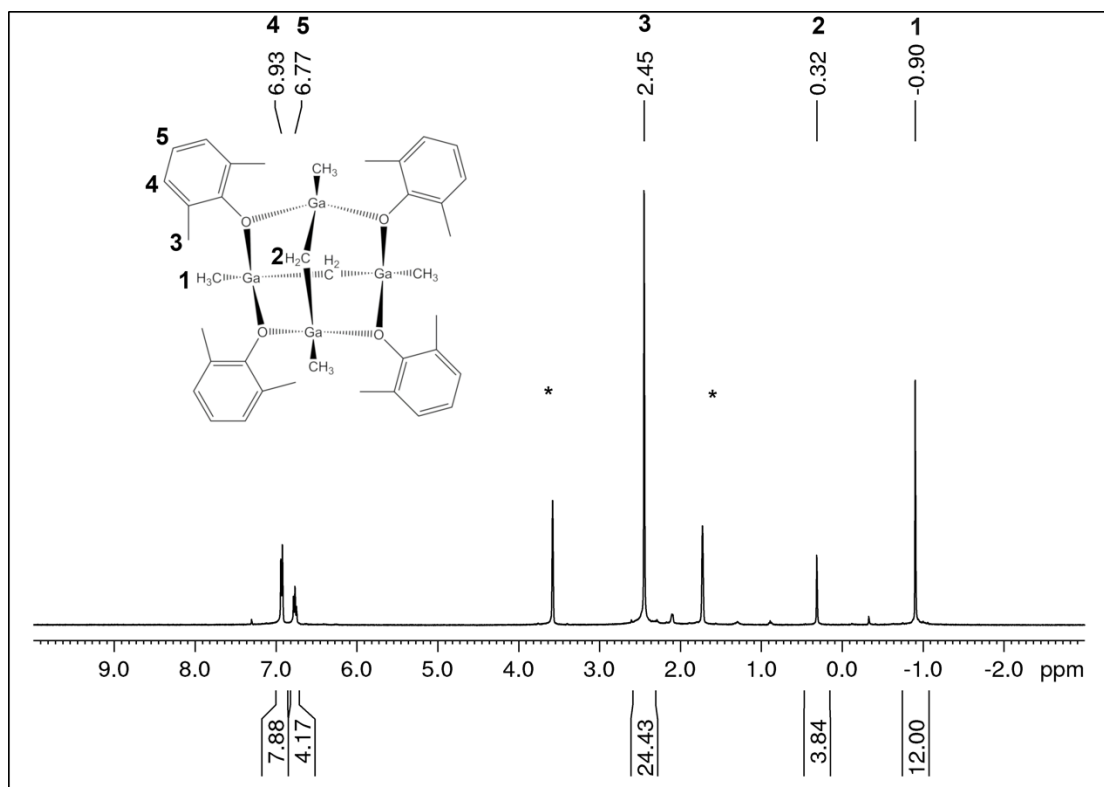
Figure S17. ^{1}H NMR spectrum (400 MHz, THF-d$_8$ of complex Ga$_4$(CH$_3$)$_4$(μ_2-CH$_2$)$_2$(μ_2-OC$_6$H$_3$Me$_2$-2,6)$_4$ (**4b**) at 26 °C.
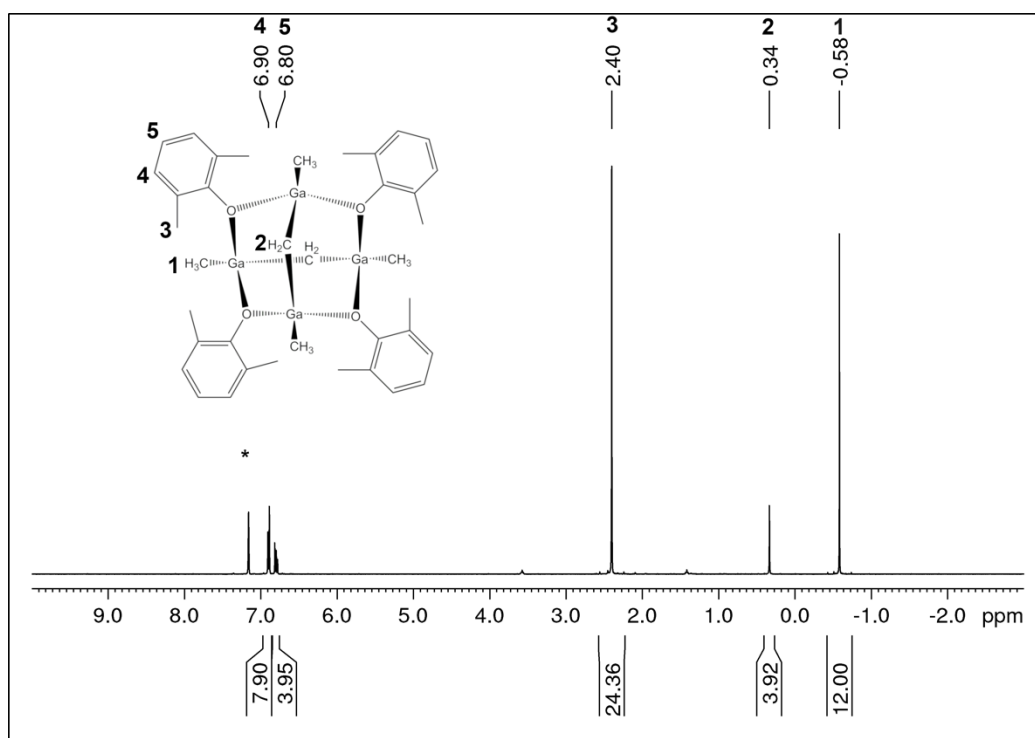
Figure S18. ^{1}H NMR spectrum (400 MHz, benzene-d$_6$ of complex Ga$_4$(CH$_3$)$_4$(μ_2-CH$_2$)$_2$(μ_2-OC$_6$H$_3$Me$_2$-2,6)$_4$ (**4b**) at 26 °C.
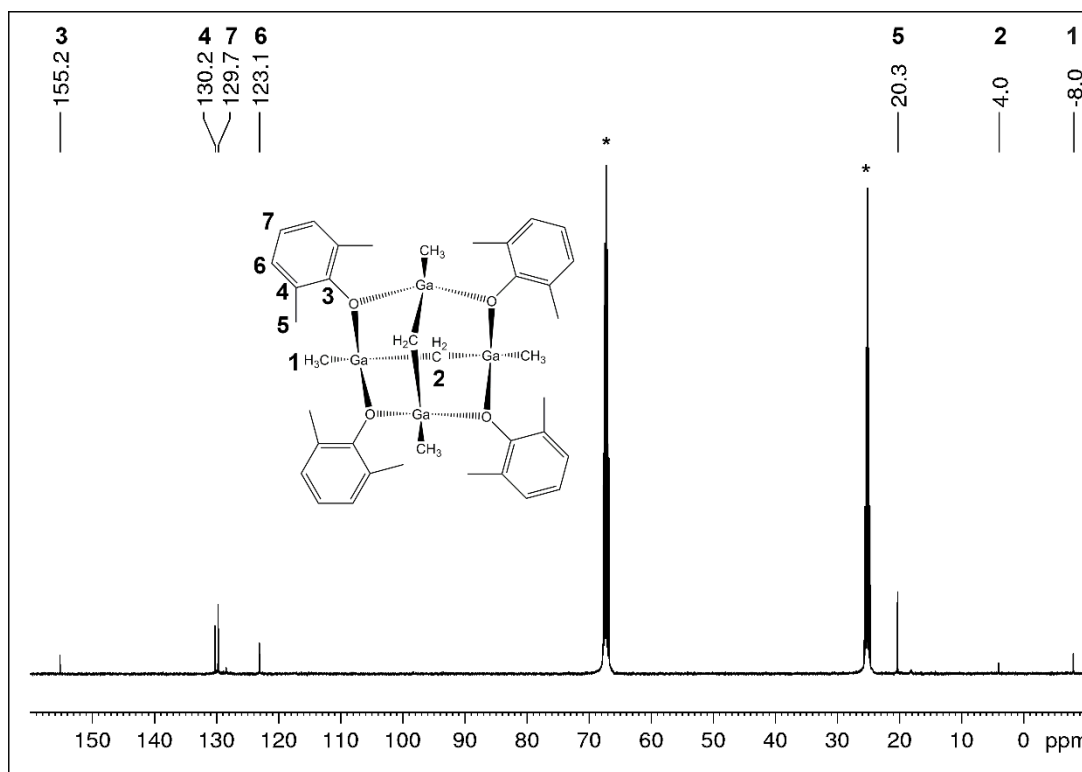
Figure S19. $^{13}C\{^1H\}$ NMR spectrum (100 MHz, THF-d_8 of complex Ga$_4$(CH$_3$)$_4$(μ_2-CH$_2$)$_2$(μ_2-OC$_6$H$_3$Me$_2$-2,6)$_4$ (**4b**) at 26 °C.
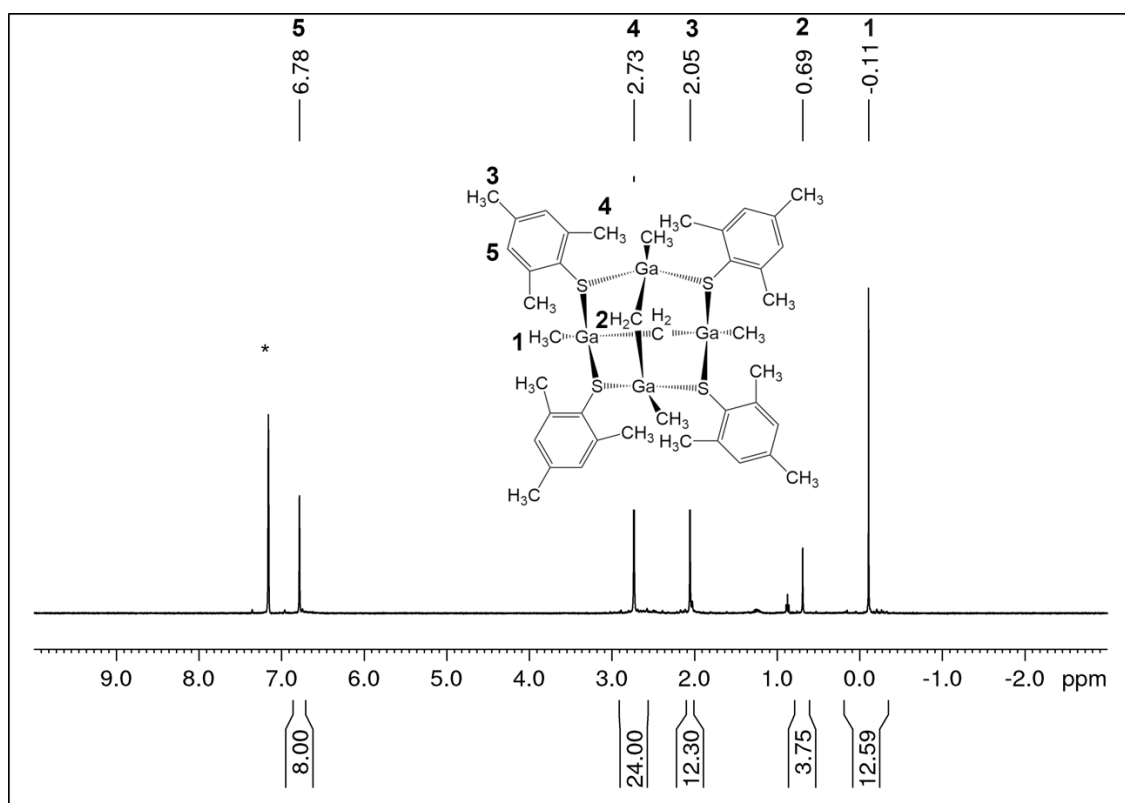
Figure S20. ^1H NMR spectrum (400 MHz, benzene-d_6 of complex Ga$_4$(CH$_3$)$_4$(μ_2-CH$_2$)$_2$(μ_2-SC$_6$H$_2$Me$_3$-2,4,6)$_4$ (**5**) at 26 °C.

Figure S21. $^{13}C\{^{1}H\}$ NMR spectrum (100 MHz, benzene-d_6 of complex $Ga_4(CH_3)_4(\mu_2\text{-}CH_2)_2(\mu_2\text{-}SC_6H_2Me_3\text{-}2,4,6)_4$ (**5**) at 26 °C.
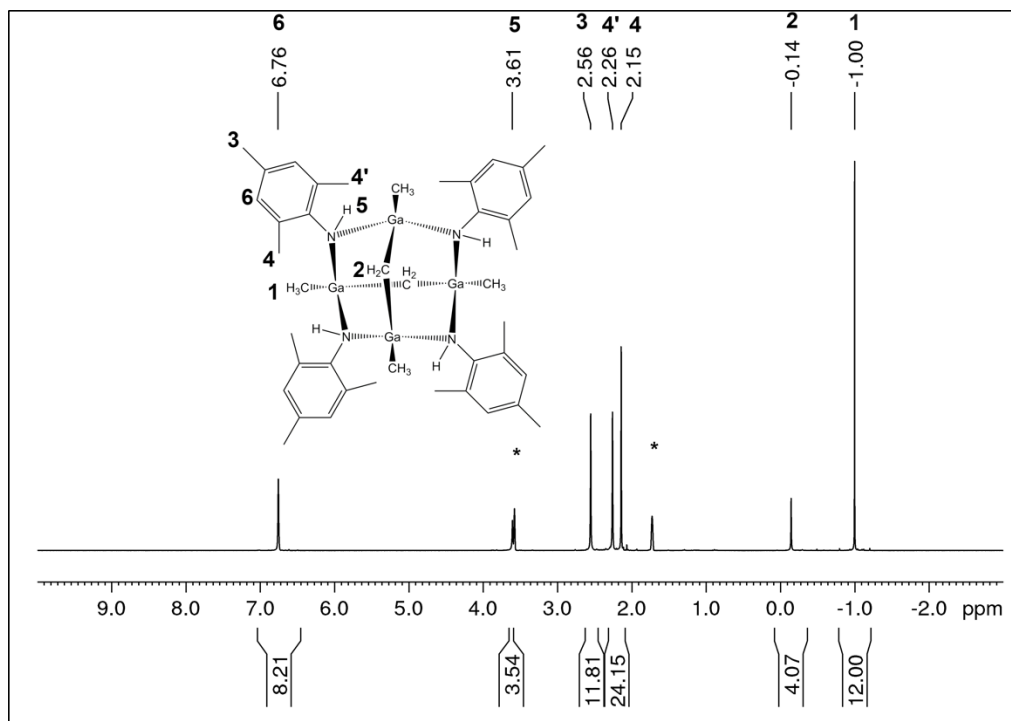
Figure S22. ^{1}H NMR spectrum (400 MHz, benzene-d_6 of complex $Ga_4(CH_3)_4(\mu_2\text{-}CH_2)_2(\mu_2\text{-}HNC_6H_2Me_3\text{-}2,4,6)_4$ (**6a**) at 26 °C.
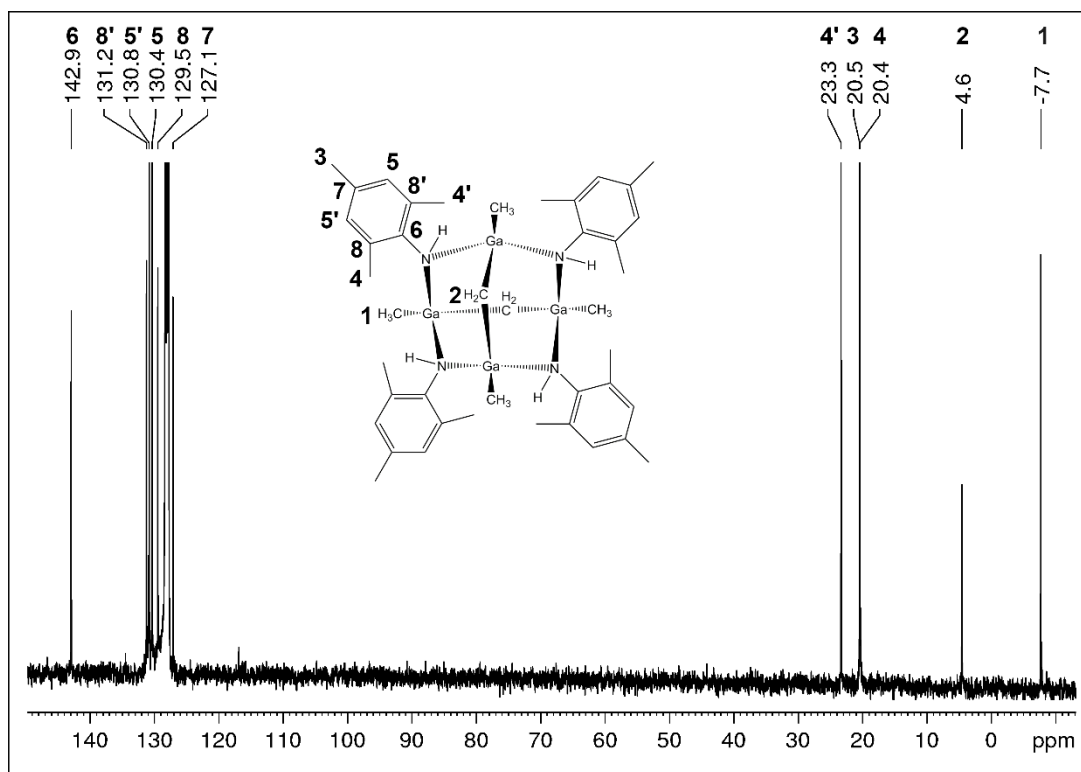
Figure S23. $^{13}C\{^1H\}$ NMR spectrum (100 MHz, benzene-$d_{6'}$ of complex Ga$_4$(CH$_3$)$_4$(μ_2-CH$_2$)$_2$(μ_2-HNC$_6$H$_2$Me$_3$-2,4,6)$_4$ (**6a**) at 26 °C.

Figure S24. ^1H NMR spectrum (400 MHz, benzene-$d_{6'}$ of complex Ga$_4$(CH$_3$)$_4$(μ_2-CH$_2$)$_2$(μ_2-HNC$_6$H$_3$Me$_2$-2,6)$_4$ (**6b**) at 26 °C.
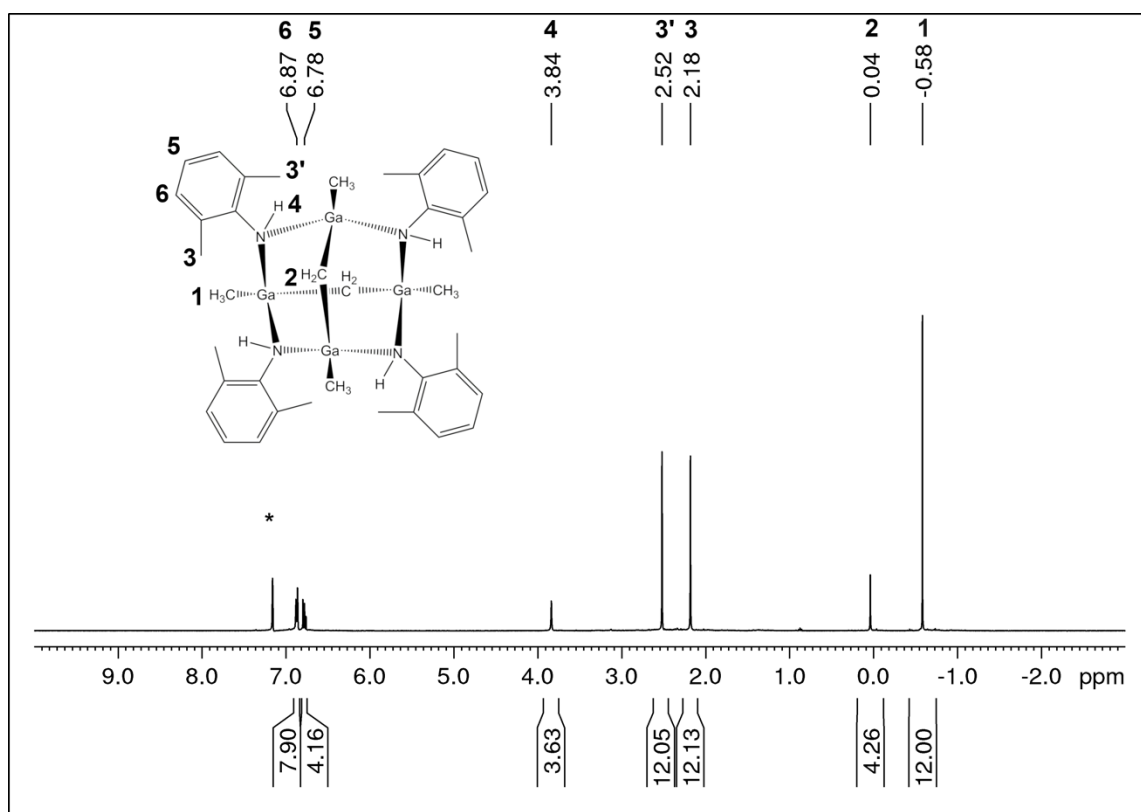
Figure S25. $^{13}C\{^1H\}$ NMR spectrum (100 MHz, benzene-d_6) of complex $Ga_4(CH_3)_4(\mu_2\text{-}CH_2)_2(\mu_2\text{-}HNC_6H_3Me_2\text{-}2,6)_4$ (**6b**) at 26 °C.
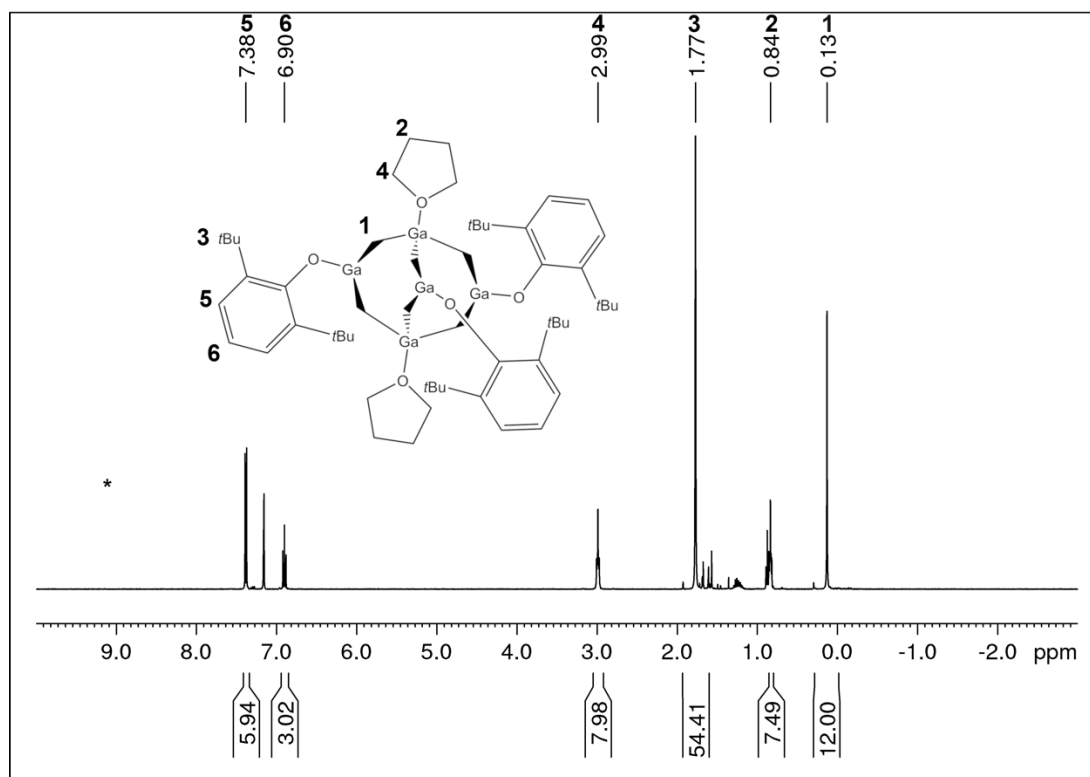
Figure S26. ^1H NMR spectrum (400 MHz, benzene-d_6) of complex $Ga_5(\mu_2\text{-}CH_2)_6(OC_6H_3tBu_2\text{-}2,6)_3(thf)_2$ (**7**) at 26 °C.
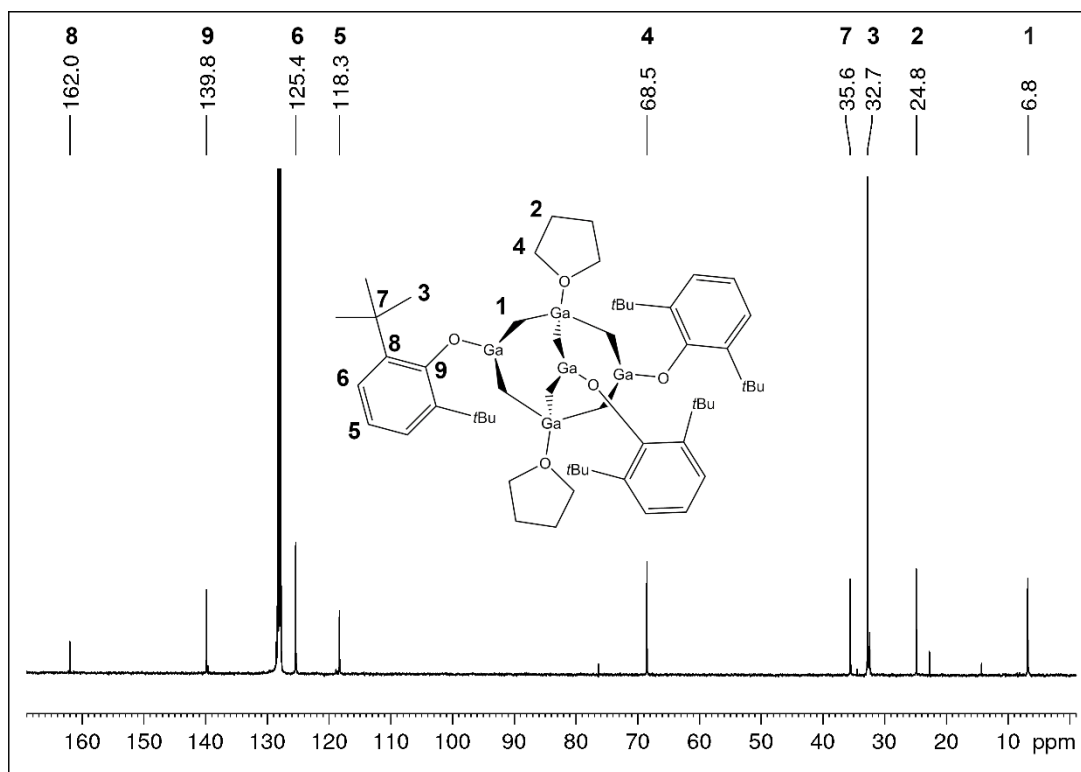
Figure S27. $^{13}C\{^1H\}$ NMR spectrum (100 MHz, benzene-d_6 of complex Ga$_5$(μ$_2$-CH$_2$)$_6$(OC$_6$H$_3$$tBu_2$-2,6)$_3(thf)_2$ (**7**) at 26 °C.
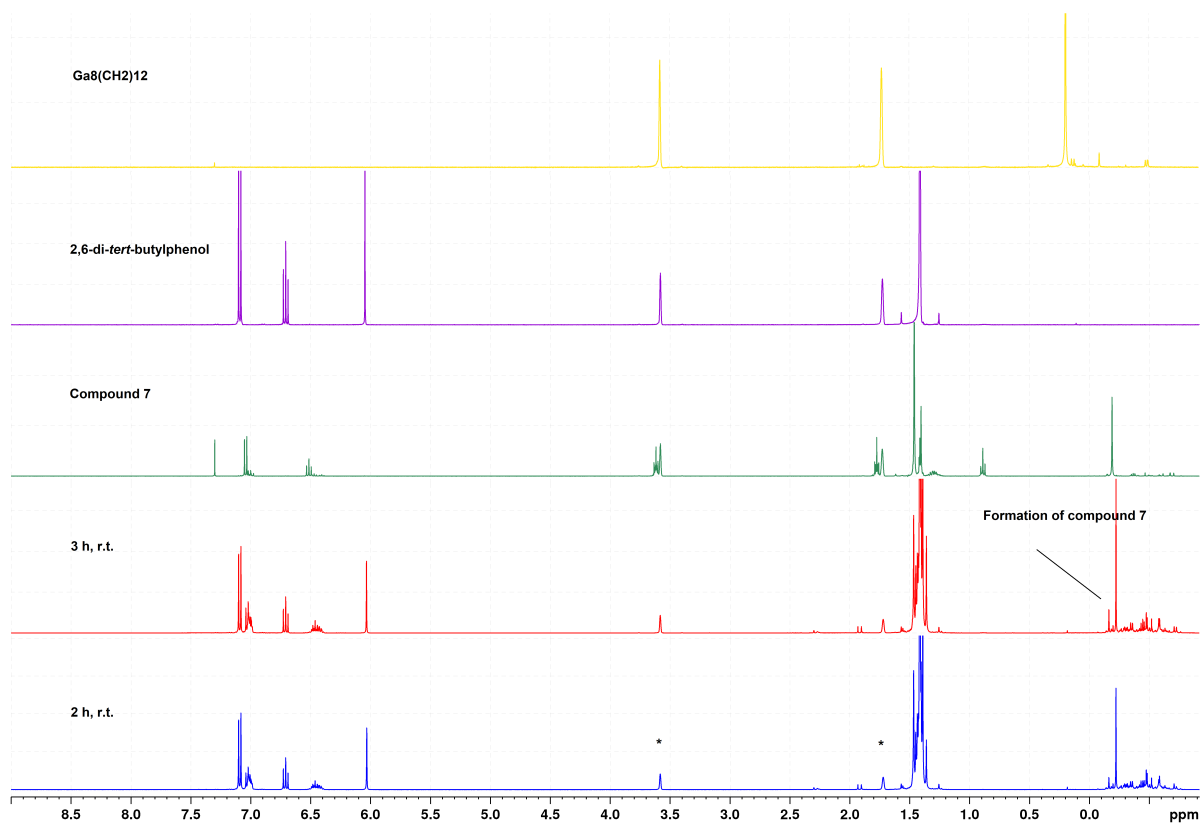
Figure S28. ^1H NMR spectra (400 MHz, THF-d_8) of the reaction of compound **1** with 2,6-di-*tert*-butylphenol at 26 °C, revealing the formation of complex **7**.
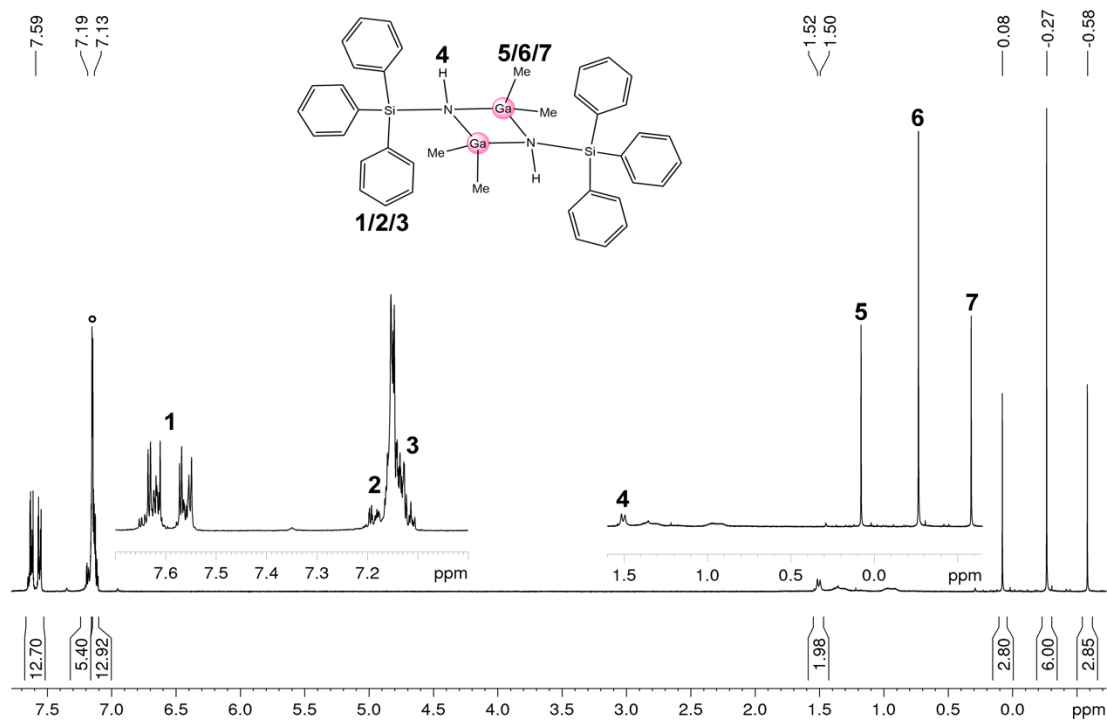
Figure S29. ^{1}H NMR spectrum (400 MHz) of [Me$_2$Ga(μ-HNSiPh$_3$)]$_2$ (**10**) in benzene-d$_6$ at 26 °C.
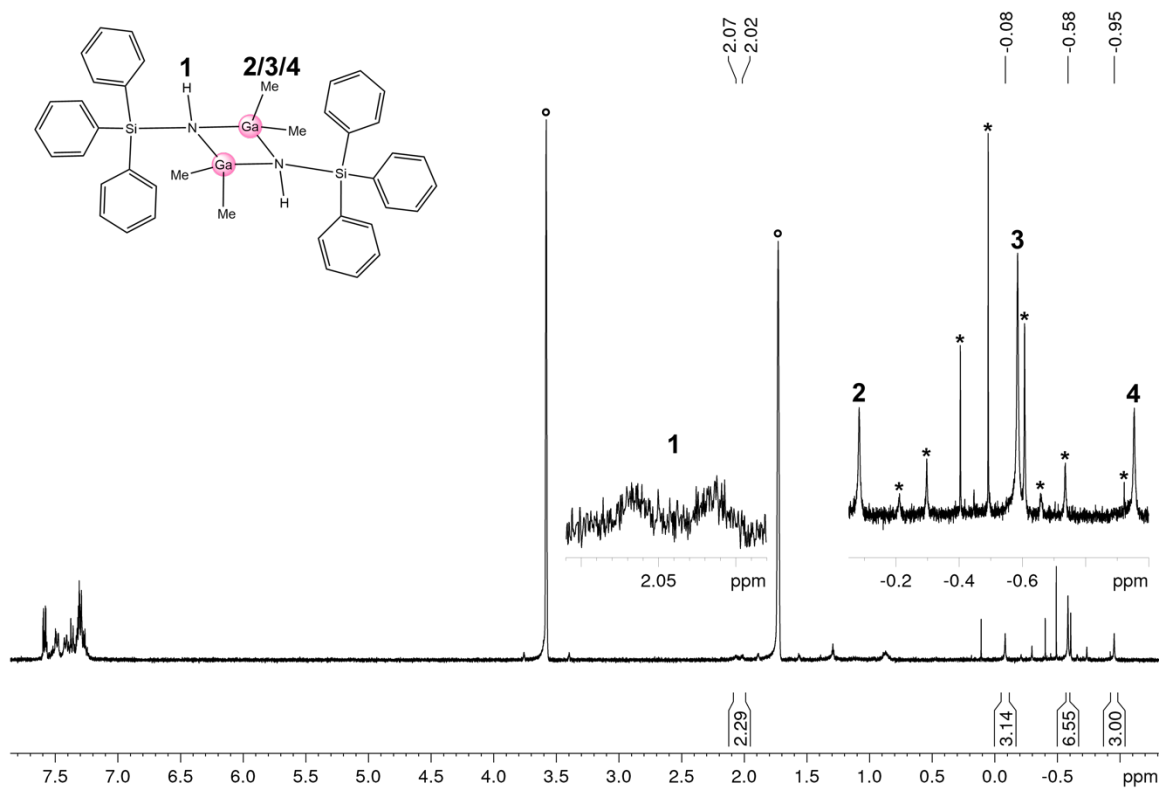
Figure S30. ^{1}H NMR spectrum (400 MHz) of [Me$_2$Ga(μ-HNSiPh$_3$)]$_2$ (**10**) in THF-d$_8$ at 26 °C (* unidentified side-products)

IR Spectra
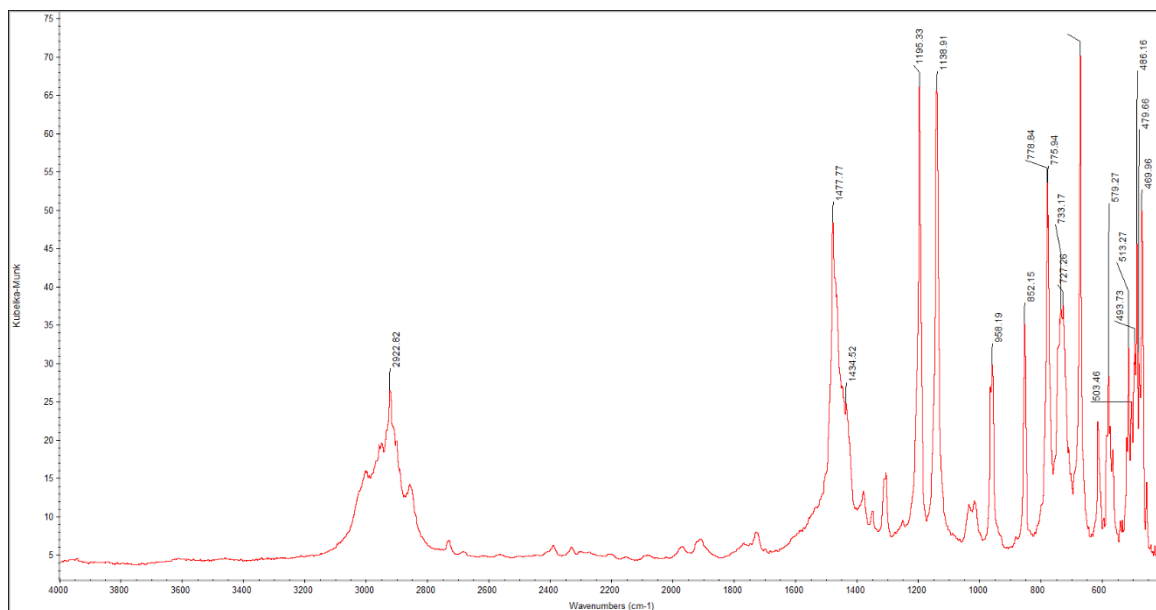
Figure S31. DRIFT spectrum of complex **4a**.
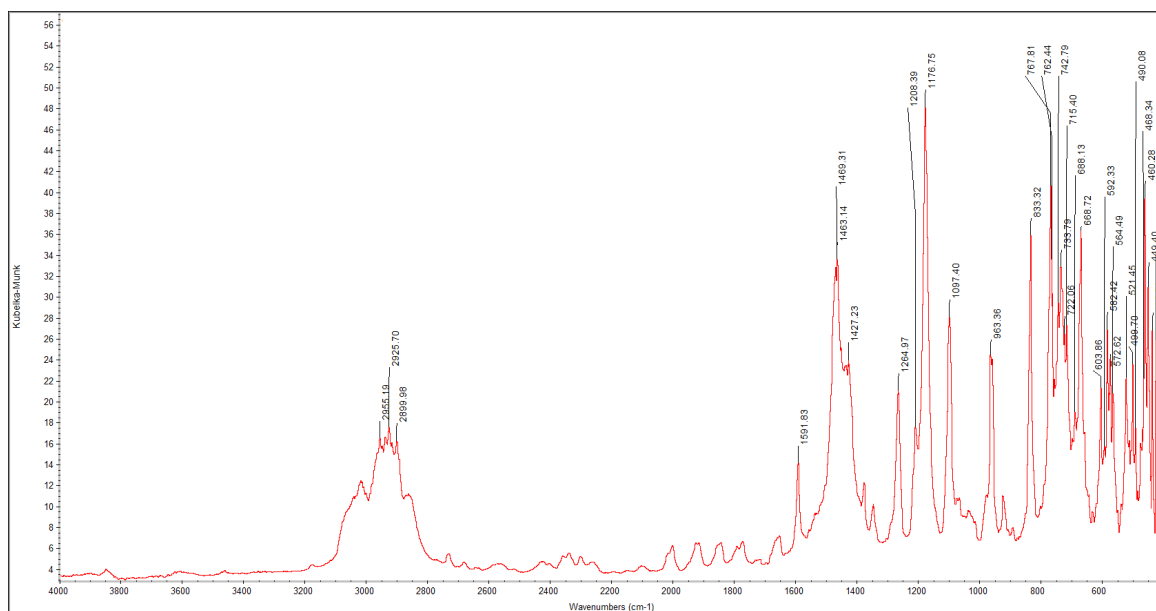
Figure S32. DRIFT spectrum of complex **4b**.
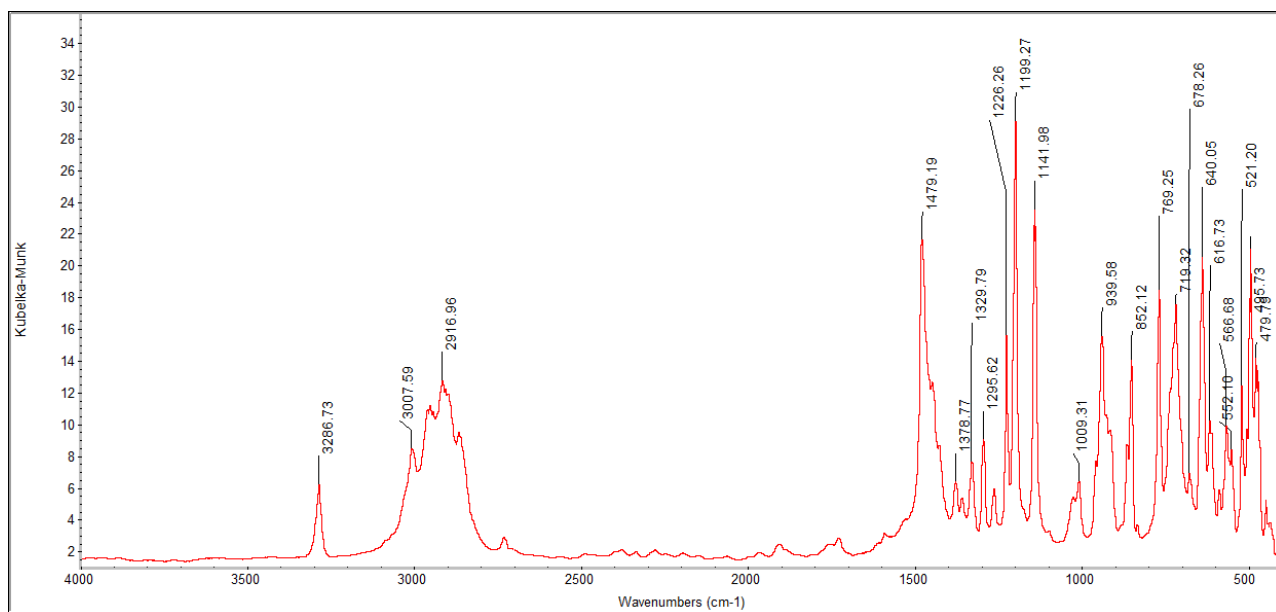
Figure S33. DRIFT spectrum of complex **6a.**
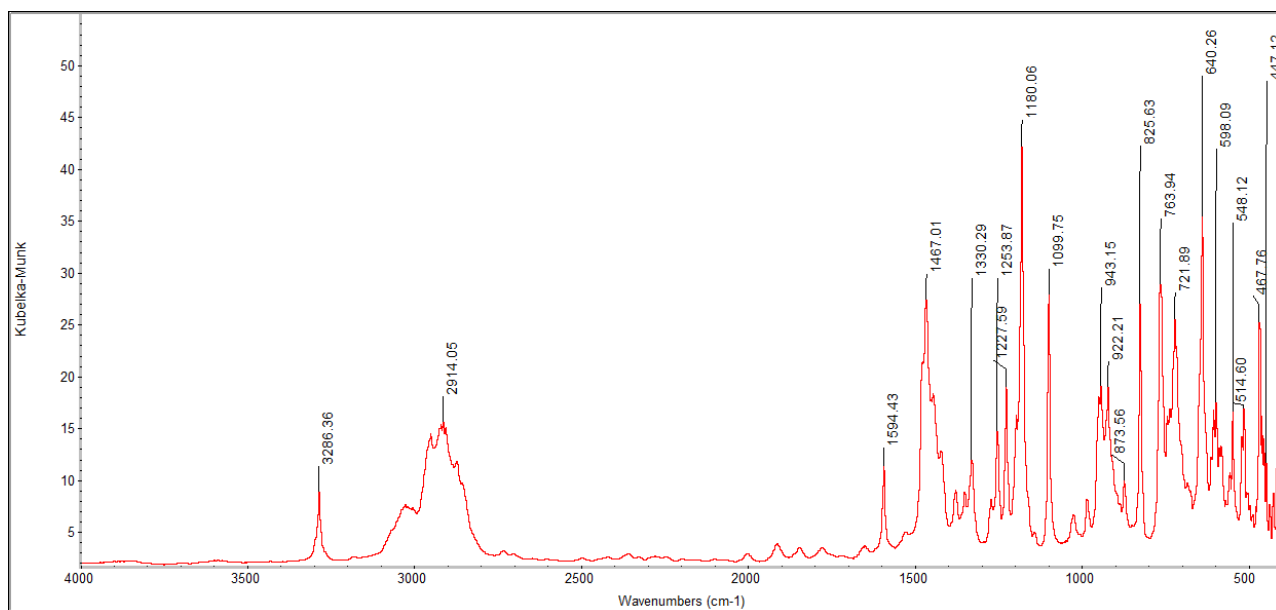
Figure S34. DRIFT spectrum of complex **6b.**
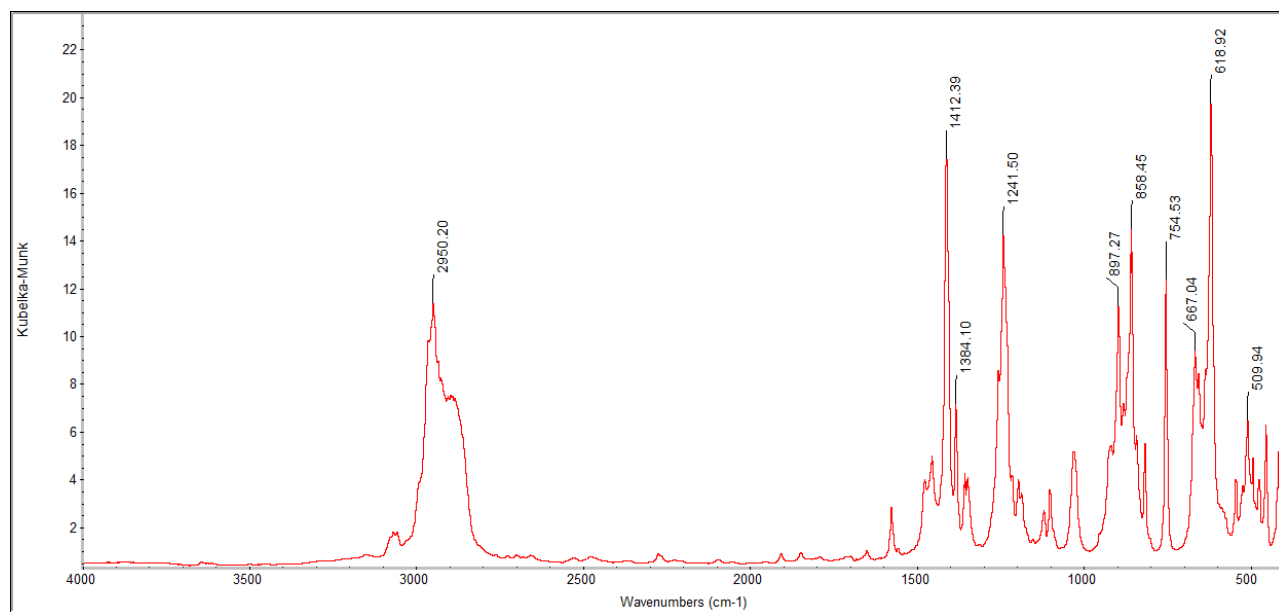
Figure S35. DRIFT spectrum of complex **7.**

Surface Organometallic Chemistry of Gallium Methylene $Ga_8(CH_2)_{12}$ on Mesoporous Silica

(Manuscript)

Journal Name

ARTICLE

Surface Organometallic Chemistry of Gallium Methylene Ga$_8$(CH$_2$)$_{12}$ on Mesoporous Silica

Georgios Spiridopoulos,[a] Yucang Liang[a] and Reiner Anwander *[a]

Gallium methylene Ga$_8$(CH$_2$)$_{12}$ was immobilized onto large-pore and small-pore mesoporous silica materials SBA-15$_{500}$ and MCM-41$_{500}$, thermally pretreated at 500 °C. For comparability reasons, trimethylgallium was employed as a grafting reagent. The hybrid materials Ga$_8$(CH$_2$)$_{12}$@SBA-15$_{500}$, GaMe$_3$@SBA-15$_{500}$, Ga$_8$(CH$_2$)$_{12}$@MCM-41$_{500}$ and GaMe$_3$@MCM-41$_{500}$ were characterized by ICP-OES, N$_2$ physisorption, elemental analysis, solid-state ^{1}H/^{13}C/^{29}Si NMR spectroscopy and diffuse reflectance infrared Fourier transform (DRIFT) spectroscopy. To gain further insight into potential surface species, the molecular compound Ga$_8$(CH$_2$)$_{12}$ was treated with excess (8 equivalents) of HOSi(OtBu)$_3$, which gave the dimeric species [GaMe$_2${OSi(OtBu)$_3$}]$_2$, being isolable also from the reaction of GaMe$_3$ with 1 equivalent of silanol. The hybrid materials revealed high metal contents and surface species with intact Ga–CH$_2$–Ga linkages as proposed by ^{1}H NMR spectroscopy the reactivity toward benzophenone.

Introduction

Since the discovery of the first transition-metal alkylidenes,[1] the interest in metal compounds with multiple bonded hydrocarbyl ligands has increased tremendously. The application of such alkylidene entailed unique chemistry of relevance both in natural product synthesis and industrial catalytic processes, such as, Fischer Tropsch[2] and olefination synthesis.[3-5] Given the plethora of transition-metal alkylidenes, it is noteworthy that there is only a limited number of main group metal derivatives. Not until the 1950s, Ziegler reported on the synthesis of [LiCH$_2$]$_n$ and [MgCH$_2$]$_n$ as pyrophoric powders.[7] Only recently, our group succeeded in the synthesis and full characterization of Ga$_8$(CH$_2$)$_{12}$ featuring the first molecular homoleptic main alkylidene complex.[8]

In parallel with alkylidene chemistry, surface organometallic chemistry (SOMC) developed into an important branch in field of organometallics.[9] Accordingly, the grafting of highly reactive (toward hydroxy functional groups) has generated novel heterogeneous catalysts with molecularly defined surface species, giving access to new catalytic transformations, such as Ziegler Natta depolymerization or alkane metathesis.[10] Especially, the immobilization of molecular complexes on periodic mesoporous silica[11, 12] allowed for the synthesis of nanostructured catalysts with a high loading of well-defined surface species. Potential advantages of organometallics grafted onto solid surfaces are the absence of extensive aggregation (clustering), relative stabilization of highly reactive surface species, and enhanced reactivity.[13-16] In terms of surface organogallium chemistry, GaR$_3$ (R = Me, iBu, CH$_2$SiMe$_3$) were immobilized on (meso)zeolites[17-23] or amorphous silica[24-26] generating gallium(III) surface species via release of alkane. When silica was used as a support material, the formation of silicon-methyl species was detected as well.[24] In addition, the grafting of gallium siloxides such as Ga[OSi(OtBu)$_3$]$_3$(thf) complexes on zeolite??? or silica was also investigated comprehensively.[27] Very recently, we investigated on the protonolysis of homoleptic gallium methylene Ga$_8$(CH$_2$)$_{12}$ with a series of phenols and anilines, resulting in cage-like structural motifs with bridging methylene groups (μ-CH$_2$) of the type [Ga$_4$(μ$_2$-CH$_2$)$_2$(CH$_3$)$_4$(μ$_2$-XR)$_4$] (X = O, HN; R = aryl).[28] Herein, the immobilization of gallium complexes Ga$_8$(CH$_2$)$_{12}$ and GaMe$_3$ on periodic mesoporous silica SBA-15$_{500}$ (large mesopores) and MCM-41$_{500}$ (small mesopores) in different solvents is reported leading to the proposal of new gallium surface species. In addition, the reactivity of gallium-modified hybrid materials toward benzophenone is investigated. Finally, the isolation of a potential model complex corroborates the uniqueness of the SOMC approach.

Results and Discussion

A large-pore mesoporous silica SBA-15^{29,30} and a small-pore mesoporous silica MCM-41[12] were selected as support materials, to assess the occurrence of any pore blocking effects. The silanol populations of the silicas activated at 500 °C and 10^{-3} mbar (labelled as SBA-15$_{500}$ and MCM-41$_{500}$) were determined

by the corresponding carbon content of silylated materials.[31] For MCM-41$_{500}$, a monodisperse spherical shape and hexagonal structure were confirmed by scanning electron microscopy (SEM) images and X-ray diffraction analysis (Figure S1 and S2, Supporting Information). Homoleptic Ga$_8$(CH$_2$)$_{12}$ (**1**)[8] and GaMe$_3$ (**2**) grafted onto SBA-15$_{500}$ and MCM-41$_{500}$ in different solvents (THF, *n*-hexane) to form hybrid materials (**H1-H5**, Scheme 1).

The parent and hybrid materials were characterized by DRIFT spectroscopy, ^{1}H NMR spectroscopy and N$_2$ physisorption. In addition, the Ga$_8$(CH$_2$)$_{12}$ was reacted with tris(*tert*-butoxy)silanol [HOSi(O*t*Bu)$_3$] as a model for terminal surface silanol groups. Finally, the reactivity of the gallium hybrid materials towards a carbonylic substrate was investigated.
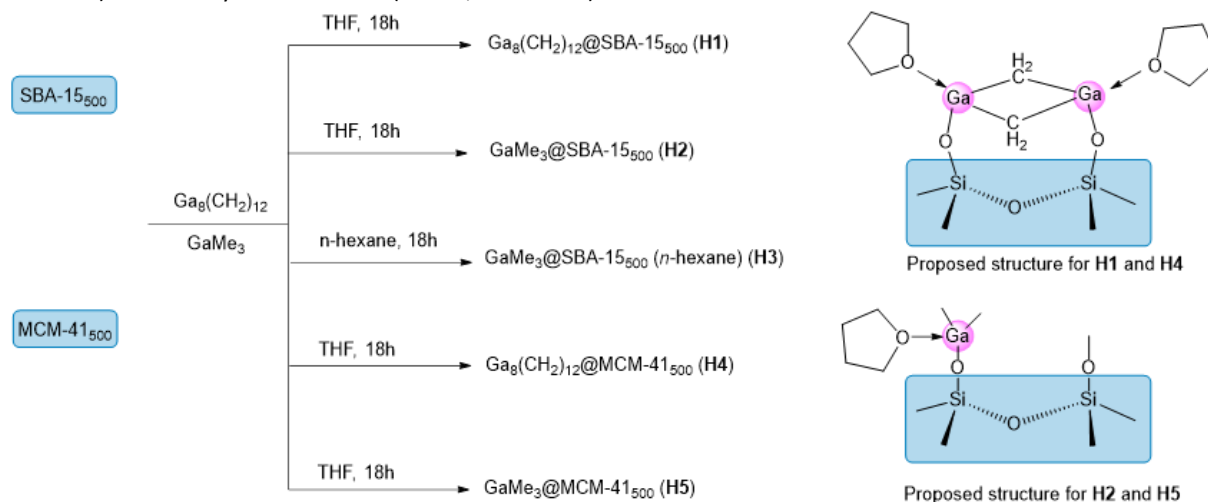
Scheme 1. Grafting of gallium complexes Ga$_8$(CH$_2$)$_{12}$ (**1**) and GaMe$_3$ (**2**) onto SBA-15$_{500}$ and MCM-41$_{500}$ parent materials and proposed surface species

DRIFT spectroscopy

The IR spectra of the parent materials SBA-15$_{500}$ and MCM-41$_{500}$ show the characteristic -O-H band (about 3742 cm^{-1}) from the isolated silanol group and Si-O-Si vibrations (1000~1200, 810, ~670-400 cm^{-1}) from the silica framework (Figure 1).[32] Upon grafting of compounds **1** or **2** and formation of hybrid materials **H1-H5**, the sharp band at about 3742 cm^{-1} almost completely disappeared, whereas a very weak absorption band assigned to inaccessible silanol groups is still observed (Figures 1 and S3). Moreover, a relatively broad and new band in the region of 3000 to 2850 cm^{-1} appeared. This corresponds to the asymmetric and symmetric stretching modes ν(C–H) of methyl and methylene groups bonded to the gallium centers, mainly species of type ≡SiO-GaMe$_x$. The IR spectra of Ga$_8$(CH$_2$)$_{12}$ (**1**) and GaMe$_3$ (**2**) derived grafted materials are difficult to distinguish, but the results are in good agreement with that of previously reported GaMe$_3$ immobilization on nonporous silica via gas-phase transfer.[24] Striking for hybrid materials **H1** and **H4** are the metal contents (ca. 15 wt.%) determined by the ICP-OES, which are much higher than the respective amount of carbon obtained by elemental analyses (Table 1). This can be explained by the existence of bi- and/or multimetallic surface species with bridged CH$_2$ group. Assuming the formation of surface species ≡SiO-GaMe$_2$ (monopodal) or ≡SiO-Ga(Me)-OSi≡ (bipodal) the molar ratio of C/Ga would correspond to 2 or 1, respectively, in the absence of donor solvent (Scheme 1 does not show any bipodally bound surface species). In line with the presence of multimetallic surface species for Ga$_8$(CH$_2$)$_{12}$-grafted materials are the comparatively low metal content of hybrid materials **H2** and **H5** derived from GaMe$_3$ (~8-9 wt.%). The high metal

content in material **H3** (~16%), obtained in *n*-hexane as a solvent might point to the formation of formation of digallium sites in a non-coordinating solvent, while the relatively low metal content in **H2** and **H5** suggest monometallic surface species.
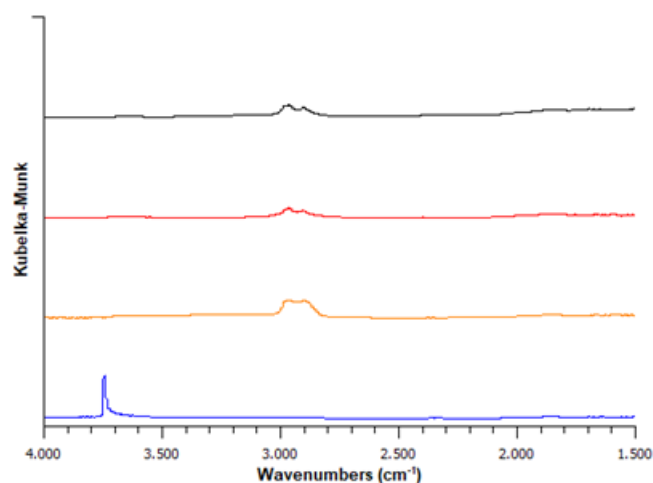
Figure 1. DRIFT spectra of support material SBA-15$_{500}$ (blue), Ga$_8$(CH$_2$)$_{12}$@SBA-15$_{500}$ (**H1**) (orange), GaMe$_3$@SBA-15$_{500}$ (**H2**) (red) and GaMe$_3$@SBA-15$_{500}$ (*n*-hexane, **H3**) (black) from bottom to top.

^{1}H-NMR Spectroscopy

Of primary interest was whether the reaction of Ga$_8$(CH$_2$)$_{12}$ (**1**) on the mesoporous silica materials would release methane during the grafting process. Accordingly and as a comparison,

the reaction of $Ga_8(CH_2)_{12}$ or $GaMe_3$ with SBA-15$_{500}$ was performed in THF-d_8 using molar ratios OH/Ga-CH$_2$ or OH/Ga-CH$_3$ of 1. As anticipated the ^{1}H NMR spectrum of the reaction of $GaMe_3$ with SBA-15$_{500}$ shows the evolution of methane (Figure S4). This is in agreement with the reactions of $GaMe_3$ with silica or $Ga(i\text{-Bu})_3$ with zeolite, respectively, which led to alkane elimination.[23,24] Crucially the reaction of $Ga_8(CH_2)_{12}$ (**1**) with SBA-15$_{500}$ under identical condition did not form methane even when the reaction continued for 4 days at ambient temperature (Figure S5). This reaction behavior is in good accordance with that of the protonolysis of **1** with phenols and anilines forming tetranuclear Ga_4 complexes with two intact bridging methylene groups in the core.[28] Therfore it could be hypothesized about the existence of bridging methylene groups on $Ga_8(CH_2)_{12}$-grafted SBA-15$_{500}$.
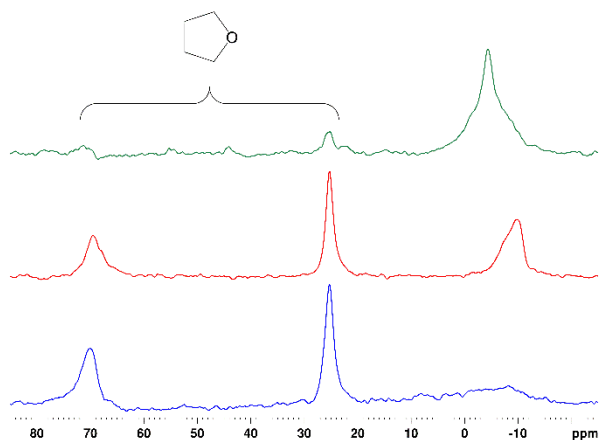
Figure 2. ^{13}C CP/MAS NMR spectra of $Ga_8(CH_2)_{12}$@SBA-15$_{500}$ (**H1**) (blue), $GaMe_3$@SBA-15$_{500}$ (**H2**) (red) and $GaMe_3$@SBA-15$_{500}$ (**H3**) (green) from bottom to top.
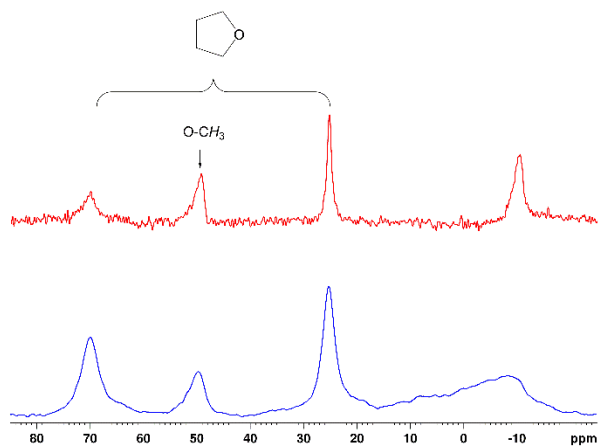
Figure 3. ^{13}C CP/MAS NMR spectra of $Ga_8(CH_2)_{12}$@MCM-41$_{500}$ (**H4**) (blue) and $GaMe_3$@MCM-41$_{500}$ (**H5**) (red) from bottom to top.

Solid-State NMR Spectroscopy

To verify the existence of methylene and methyl group in hybrid materials **H1**-**H5**, the ^{1}H MAS NMR spectra were measured. As

shown in Figures S6-10, ^{1}H signals for hybrid materials **H1** and **H4** appeared at 0.7 and 1.78 ppm, respectively, corresponding to Ga–CH_x group. For hybrid materials **H2** and **H5**, a sharp resonance at −0.5 ppm can be assigned to Ga–CH_3 groups, while **H3** shows a sharp signal at 0.9 ppm. The chemical shifts of molecular complexes (**?**) appeared in a similar range of −0.03 to −0.5 ppm.[33-35] The ^{13}C CP/MAS NMR spectra of **H1** and **H4** show broad peaks at −11.0 and −9.4 ppm, distinct from those of the $GaMe_3$-grafted materials with sharp peaks of the Ga–CH_3 units at −10.2 ppm (**H2**) and −11.0 ppm (**H5**) (Figures 2 and 3). The ^{13}C CP/MAS NMR spectrum of hybrid material **H3** shows a chemical shift at −4.7 ppm similar to other $GaMe_3$-grafted silica material.[24] For all hybrid materials **H1**-**H5**, two carbon signals attributed to THF were observed at 26 and 66 ppm, implying the coordination of THF with Ga center In addition, -OCH_3 groups could be detected, which originate from surfactant removal/extraction with HCl-acidified methanol. Moreover, the signal at −55 ppm in the ^{29}Si CP/MAS NMR spectrum of the hybrid material **H3** indicate the formation of ≡Si–Me groups. For comparison, a similar chemical shift of −62 ppm was reported for silica materials that were treated with different methylating agents.[36]

N$_2$ Physisorption

The specific surface areas of all materials were characterized using the Brunauer-Emmett-Teller (BET) method[37] and the pore diameters were determined using the Barrett-Joyner-Halenda (BJH) method.[38] The N_2-physisorption isotherms indicated the characteristic mesoporous structures for both activated parent materials SBA-15$_{500}$ and MCM-41$_{500}$. The type IV isotherm of the SBA-15$_{500}$ silica revealed a typical H1 hysteresis loop, while that of the MCM-41$_{500}$ sample features a reversible capillary loop (Figure 4, Figure 5). The specific BET surface area, pore volume and pore diameter are 887 m^2 g^{-1}, 0.96 cm^3 g^{-1} and 6.8 nm for SBA-15$_{500}$, 1228 m^{2}g^{-1}, 1.17 cm^3 g^{-1} and 2.5 nm for MCM-41$_{500}$, respectively (Table 1).
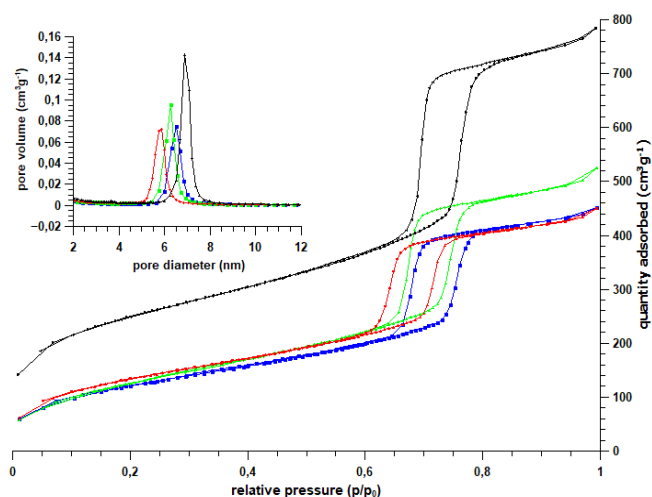
Figure 4. N_2 adsorption-desorption isotherms of parent material SBA-15$_{500}$ (black), $Ga_8(CH_2)_{12}$@SBA-15$_{500}$ (**H1**) (red), $GaMe_3$@SBA-15$_{500}$

(H2) (blue) and GaMe$_3$@SBA-15$_{500}$ (n-hexane) (H3) (green). Inset is the corresponding pore size distributions.

Table 1. Important Data of the Parent Silica Supports and Hybrid Materials **H1**-**H5**

material	$a_{BET}{}^a$ $(m^2 g^{-1})$	$V_{pore}{}^b$ $(cm^3 g^{-1})$	$d_{pore}{}^c$ (nm)	$c_{surfaceSiOH}{}^d$ $(mmol\ g^{-1})$	wt % metal
SBA-15$_{500}$	887	0.96	6.8	3.01	-
Ga$_8$(CH$_2$)$_{12}$@SBA-15$_{500}$ (**H1**)	501	0.39	5.0	-	14.86
GaMe$_3$@SBA-15$_{500}$ (**H2**)	455	0.27	5.7	-	9.15
GaMe$_3$@SBA-15$_{500}$(**H3**, *n*-hexane)	482	0.32	6.0	-	15.83
MCM-41$_{500}$	1228	1.17	2.5	2.05	-
Ga$_8$(CH$_2$)$_{12}$@MCM-41$_{500}$ (**H4**)	1010	0.26	1.9	-	14.99
GaMe$_3$@MCM-41$_{500}$ (**H5**)	899	0.28	2.1	-	7.88

[a] BET surface are calculated between p/p$_0$ 0.07 and 0.15. [b] BJH desorption cumulative pore volume between 4.0 and 10.0 nm for SBA-15$_{500}$ and 1.5 to 3.5 nm for MCM-41$_{500}$. [c] Maximum pore diameter from the BJH desorption branch. [d] Calculated according to published procedures.[20] [e] Metal content determined by ICP-OES.
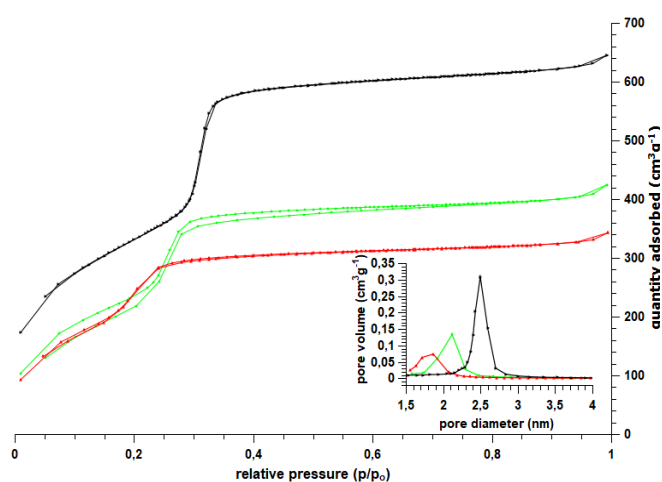
Figure 5. N$_2$ adsorption-desorption isotherms of the parent material MCM-41$_{500}$ (black), Ga$_8$(CH$_2$)$_{12}$@MCM-41$_{500}$ (**H4**) (red) and GaMe$_3$@MCM-41$_{500}$ (**H5**) (green). Inset is the corresponding pore size distributions.

For the hybrid materials **H1**-**H5**, prior to measurement, every sample was degassed for 12 h at 30 °C. The grafted materials H1-H5 are stable until 80 °C. Performing the grafting reaction of **1** in THF (involving an Ga$_8$(μ-CH$_2$)$_{12}$/Ga$_6$(μ-CH$_2$)$_9$ oligomer switch), affording **H1**, implied a drastic decrease of the specific BET surface area, pore size and pore volume what percentage???(Table 1), in agreement with the high gallium content found by ICP-OES analysis. For GaMe$_3$-grafted SBA-15$_{500}$ (**H2**), the specific BET surface area and pore volume were even significantly lower than those of **H1**, most likely due to the presence of larger amounts of donor ligand THF inside the pores. Note that pore size is bigger (h). When the reaction of GaMe$_3$ wth SBA-15$_{500}$ was conducted in hexane, the obtained **H3** shows a slightly increased specific BET surface area, pore volume and pore size as well as high Ga content compared to **H2**, due to the absence of THF. Similarly, when MCM-41$_{500}$ was used as the support for the grafting of **1** and **2** in THF, the hybrid materials **H4** and **H5** indicate a similar trend on surface area and pore volume as those of **H1** and **H2** (Table 1). However, the similar pore diameter of material **H4** and **H5** point considerable pore blockage in material **H4**. Overall, the distinct changes of surface area, pore volume and pore size as well as the different gallium contents dependent on the molecular size of the precursor, picture to some extent the surface Ga species. To further corroborate the formation of gallium surface species on silica, the preparation of molecular model complex has been pursued.

Molecular model of grafted gallium catalysts

The tris(*tert*-butoxy)siloxy ligand is routinely employed as a molecular model for silica surfaces by mimicking the grafting reaction on a molecular scale.[33,34,39-42] Accordingly, the treatment of homoleptic Ga$_8$(CH$_2$)$_{12}$ (**1**) with 8 equivalents of tris(*tert*-butoxy)silanol HOSi(OtBu)$_3$ led to the isolation of [GaMe$_2${OSi(O*t*Bu)$_3$}]$_2$ (**3**) (Scheme 2). Interestingly, the equimolar reaction of GaMe$_3$ (**2**) with tris(*tert*-butoxy)silanol also afforded the dimeric complex **3**.[33,34] The structural motif of **3** with the typical four-membered Ga$_2$O$_2$ ring was also observed in reactions of gallium complexes with aliphatic alcohols, phenols and amines.[43,44] Furthermore, the reactivity of molecular complexes **1** and **2** with silanols of the surface of silica indicates the formation of dimeric species in the hybrid material. The latter reaction was previously examined by Scott and co-workers.[24] Additionally, the formation of bridging methylene (−CH$_2$) units during the grafting reaction of **1** with SBA-15$_{500}$ and MCM-41$_{500}$ is suggested in this work by ^{1}H NMR spectroscopy, due to the evolution of no methane monitored
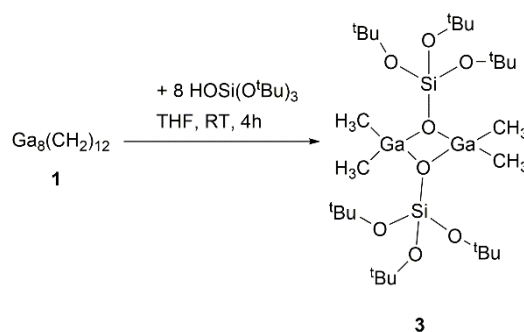
Scheme 2. Illustration of the reaction of molecular complex **1** with HOSi(OtBu)$_3$.

Reaction of the Hybrid Materials with Benzophenone

For hybrid materials **H1** and **H4**, the existence of surface methylene groups was further verified by their reactivity towards benzophenone in THF. As shown in Scheme 3, when the hybrid materials were exposed to benzophenone an methylenation reaction took place forming the corresponding 1,1-diphenylethylene. The reaction process in THF-d_8 was monitored by ^{1}H NMR spectroscopy. As can be seen in Figure S11 and S12, the ^{1}H NMR spectrum of the reaction at ambient temperature for 6 h shows only the presence of the starting materials. Changing the conditions to 80 °C for 16 h, the formation of 1,1-diphenylethylene could be clearly observed, confirming the occurrence of a methylene transfer for **H1** and **H4**. For comparison, the molecular complex $Ga_8(CH_2)_{12}$ (**1**) also reacted slowly with benzophenone at room temperature for 16 h to form 1,1-diphenylethylene (Figure S13). However, the amount of 1,1-diphenylethylene increased significantly at 60 °C for 2 h (Figure S14). Interestingly, the reaction of benzophenone with hybrid materials **H2** and **H5** at 80 °C for 21 h only resulted in the formation of methane (Figure S15 and S16), clearly corroborating the absence of a methylene transfer reaction.
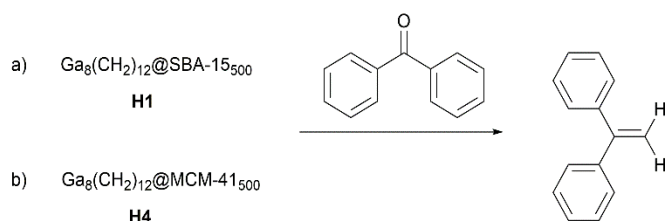
Scheme 3. Reactivity of hybrid materials **H1** and **H4** toward benzophenone.

Conclusions

Mesoporous silicas MCM-41$_{500}$ (pore diameter ca. 2.5 nm) and SBA-15$_{500}$ (pore diameter ca. 7 nm) are both suitable for the synthesis of gallium(III) hybrid materials via direct grafting reactions of homoleptic $Ga_8(CH_2)_{12}$. The resulting hybrid materials (pore diameter of 5 nm for SBA-15$_{500}$ and 1.9 nm for MCM-41$_{500}$) display metal contents of approximately 15%. The capability of these hybrid materials to engage in ketone olefination along with negative control reactions employing respective trimethylgallium-grafted silicas give clear evidence for intact methylene groups. Nevertheless, the methylenation efficiency of the hybrid materials is somewhat decreased compared to the molecular congener in the homogenous reaction. The analyses of the gallium-methylene grafted hybrid materials suggest that the surface species might involve digallium of the type [≡SiOGa(CH$_3$)(thf)(μ-CH$_2$)Ga(CH$_3$)(thf)(OSi≡].

Experimental Section

All operations regarding the organometallic precursors and the hybrid materials were performed under rigorous exclusion of air and water by using standard Schlenk, high-vacuum, and glovebox techniques (MBraun 200B; <0.1 ppm O$_2$, <0.1 ppm H$_2$O). Solvents were purified by using Grubbs-type columns (MBraun SPS, solvent purification system) and stored inside a glovebox. THF-d_8 was obtained from Sigma-Aldrich, stirred over NaK alloy for at least 24 h, and distilled before use. GaMe$_3$ was purchased from Dockweiler Chemicals and used as received. $Ga_8(CH_2)_{12}$ (**1**) was synthesized according to literature procedures. The NMR spectra were recorded by using J. Young valve NMR tubes on a Bruker AVII+400 spectrometer (^{1}H, 400.13 MHz; ^{13}C, 100.61 MHz). NMR chemical shifts are referenced to internal solvent resonances and reported in parts per million relative to tetramethylsilane (TMS). The solid-state NMR spectra were recorded on a Bruker Avance III HD 300 with MAS (magic angle spinning) technique at ambient temperature with samples packed in 3 mm ZrO$_2$ rotors at a rotation frequency of 5 or 8 kHz (^{1}H, 300.13 MHz; ^{13}C, 75.47 MHz; ^{29}Si, 59.62 MHz). Elemental analyses were performed on an Elementar Vario Micro Cube. IR spectra were recorded on a Thermo Fisher Scientific NICOLET 6700 FTIR spectrometer using a DRIFT chamber with dry KBr/sample mixture and KBr windows. The IR data were converted using the Kubelka-Munk refinement. The N$_2$-physisorption measurements were performed on a ASAP2020 volumetric adsorption apparatus from Micromeritics Instrument Corp. at 77 K (α_m (N$_2$, 77K) = 0.162 nm^2). All samples were degassed prior to analysis. In the case of the pure silica materials at 523 K for 4 h and for the hybrid materials at 313 K for 12 h to avoid degradation of the grafted gallium complexes. The Brunauer–Emmett–Teller (BET) specific surface area was calculated from nitrogen adsorption branch of the isotherm in the relative pressure range of 0.07–0.15 for the pure SiO$_2$ materials and the hybrid materials. The pore size distributions (*dV/dD*) were calculated from the nitrogen desorption branch using the Barrett–Joyner–Halenda (BJH) method.

Parent Material

SBA-15$_{500}$. The parent material was synthesized and activated according to literature procedure.[11] αBET 887 m^{2}g^{-1}, V$_{pore}$ 0.96 cm^{3}g^{-1}, and d$_{pore}$ 6.8 nm. DRIFTS: $\tilde{\nu}$ = 3743 (w, Si–OH), 3103 (vw), 1098 (vs), 1060 (vs), 818 (m), 467 (m), 446 (s), 426 (s) cm^{-1}.

MCM-41$_{500}$. Monodisperse mesoporous silica nanoparticles with MCM-41-like structure (MMSN-MCM-41) was prepared according to a slightly modified procedure described in the literature.[12] A typical process is as follows: cetyltrimethylammonium bromide (CTAB, 2.014 g) was dissolved in water (960 g) and a NaOH aqueous solution (2M, 8 mL) was added under stirring. The resulting solution was stirred at 65 °C for 1 h. Tetraethyl orthosilicate (TEOS, 10.017 g) was then added dropwise over 4 min and vigorously stirred at 65 °C for 2 h. After being cooled down to ambient temperature, the solid was collected by centrifugation at 2×10^4 rotations per minute for 5 min, and dried at 60 °C in the oven overnight to obtain as-synthesized MSN-MCM-41. Surfactant template CTAB was removed by stirring as-synthesized MSN-MCM-41 in a HCl-acidified methanol solution under reflux. The surfactant-free MSN-MCM-41 was dried at 60 °C in the oven, and then activated

at 500 °C for 4 h under high vacuum and stored in the glovebox under argon atmosphere as MCM-41$_{500}$ for further use.

Grafting Reactions

Ga$_8$(CH$_2$)$_{12}$@SBA-15$_{500}$ (H1): SBA-15$_{500}$ (200 mg, 0.617 mmol of SiOH) was suspended in 3 mL of THF, Ga$_8$(CH$_2$)$_{12}$ (448 mg, 0.617 mmol) dissolved in 3 mL of THF was then added under stirring. The suspension was stirred for 18 h at ambient temperature and then the hybrid material was separated via centrifugation and washed with THF (4 x 5 mL). The residual solvent was removed under reduced pressure for at least 48 h to yield 320 mg of Ga$_8$(CH$_2$)$_{12}$@SBA-15$_{500}$ (**H1**) as a colourless powder. The supernatant was filtered and dried under reduced pressure. From the THF extracts 366 mg of Ga$_8$(CH$_2$)$_{12}$ could be recovered. Elemental analysis found (%): Ga 14.86 (ICP-OES); C 11.94, H 1.99. α_{BET} 501 m^{2}g^{-1}, V_{pore} 0.38 cm^{3}g^{-1}, d_{pore} 5.1 nm. DRIFTS: $\widetilde{\nu}$ = 2959 (vw), 2901 (vw), 1460 (vw), 1367 (vw), 1346 (vw), 1219 (s), 1003 (s), 917 (vw), 825 (w) cm^{-1}.

GaMe$_3$@SBA-15$_{500}$ (H2): SBA-15$_{500}$ (200 mg, 0.617 mmol of SiOH) was suspended in 4 mL of THF, GaMe$_3$ (80 mg, 0.618 mmol) dissolved in 2 mL of THF was then added under stirring. The suspension was stirred for 18 h at ambient temperature and then the hybrid material was separated via centrifugation and washed with THF (3 x 5 mL). The residual solvent was removed under reduced pressure for at least 48 h to yield 274 mg of GaMe$_3$@SBA-15$_{500}$ (**H2**) as a colourless powder. Elemental analysis found (%): Ga 9.15 (ICP-OES); C 11.08, H 2.44. α_{BET} 455 m^{2}g^{-1}, V_{pore} 0.25 cm^{3}g^{-1}, d_{pore} 5.7 nm. DRIFTS: $\widetilde{\nu}$ = 2964 (vw), 2903 (s), 1461 (vw), 1100 (vs), 800 (w), 728 (w), 678 (vw), 589 (w) cm^{-1}.

GaMe$_3$@SBA-15$_{500}$ (H3): SBA-15$_{500}$ (200 mg, 0.617 mmol of SiOH) was suspended in 4mL of *n*-hexane, GaMe$_3$ (80 mg, 0.618 mmol) dissolved in 2 mL of *n*-hexane was added under stirring. The suspension was stirred for 18 h at ambient temperature and then the hybrid material was separated via centrifugation and washed with *n*-hexane (3 x 5 mL). The residual solvent was removed under reduced pressure for at least 48 h to yield 230 mg of GaMe$_3$@SBA-15$_{500}$ (**H3**) as a colourless powder. Elemental analysis found (%): Ga 15.83 (ICP-OES); C 7.39, H 1.80. α_{BET} 482 m^{2}g^{-1}, V_{pore} 0.30 cm^{3}g^{-1}, d_{pore} 6.0 nm. DRIFTS: $\widetilde{\nu}$ = 2964 (vw), 2900 (s), 1178 (s), 1018 (s), 801 (w), 744 (w), 602 (vw) cm^{-1}.

Ga$_8$(CH$_2$)$_{12}$@MCM-41$_{500}$ (H4): MCM-41$_{500}$ (230 mg, 0.472 mmol of SiOH) was suspended in 5 mL of THF. Ga$_8$(CH$_2$)$_{12}$ (342 mg, 0.472 mmol) dissolved in 4 mL of THF was then added under stirring. The suspension was stirred for 18 h at ambient temperature and then the hybrid material was separated via centrifugation and washed with THF (3 x 5 mL). The residual solvent was removed under reduced pressure for at least 48 h to yield 280 mg of Ga$_8$(CH$_2$)$_{12}$@MCM-41$_{500}$ (**H4**) as a colourless powder. Elemental analysis found (%): Ga 14.99 (ICP-OES); C 11.38, H 2.13. α_{BET} 1010 m^{2}g^{-1}, V_{pore} 0.44 cm^{3}g^{-1}, d_{pore} 1.9 nm. DRIFTS: $\widetilde{\nu}$ = 2954 (vw), 2900 (vw), 1234 (s), 1137 (s), 1012 (s), 830 (s), 1003 (s), 617 (s) cm^{-1}.

GaMe$_3$@MCM-41$_{500}$ (H5): MCM-41$_{500}$ (231 mg, 0.474 mmol of SiOH) was suspended in 5 mL of THF, GaMe$_3$ (54.4 mg, 0.474 mmol) was dissolved in 2 mL of THF was then added under stirring. After being stirred at ambient temperature for 18 h, the hybrid material was separated via centrifugation and washed with THF (3 x 5 mL). The residual solvent was removed under reduced pressure for at least 48 h to yield 278 mg of GaMe$_3$@MCM-41$_{500}$ (**H5**) as a colourless powder. Elemental analysis found (%): Ga 7.88 (ICP-OES); C 9.28, H 1.93. α_{BET} 899 m^{2}g^{-1}, V_{pore} 0.62 cm^{3}g^{-1}, d_{pore} 2.1 nm. DRIFTS: $\widetilde{\nu}$ = 2958 (vw), 2904 (vw), 1461 (s), 1181 (s), 1002 (s), 919 (w), 817 (s), 729 (w), 669 (w) cm^{-1}.

[GaMe$_2${OSi(O*t*Bu)$_3$}]$_2$ (3): Ga$_8$(CH$_2$)$_{12}$ (26.2 mg, 0.036 mmol) was dissolved in 0.3 mL of THF-d$_8$. (*t*BuO)$_3$SiOH (76.3 mg 0.289 mmol) was also dissolved in 0.3 mL of THF-d$_8$. After 1 d, the solution was filtered into a small vial. Colourless crystals could be obtained at −40 °C (60 % crystalline yield). The ^{1}H NMR spectrum and the XRD cell check is in accordance with the already published literature.[24]

Reactions with Benzophenone

a) Ga$_8$(CH$_2$)$_{12}$@SBA-15$_{500}$ (**H1**) (20 mg, 0.043 mmol of Ga) was suspended in 0.4 mL of THF-d$_8$ in a J. Young-valved tube, benzophenone (7.77 mg, 0.043 mmol) dissolved in 0.3 mL of THF-d$_8$ was then added. After being heated at 80 °C for 16 h, the ^{1}H NMR spectrum was recorded to monitor the formation of 1,1-diphenylethylene. ^{1}H NMR (THF-d$_8$, 400.16 MHz, 26 °C) δ 7.29 (10H, (*H*$_5$C$_6$)$_2$C=CH$_2$), 5.43 (2H, (H$_5$C$_6$)$_2$C=C*H*$_2$) ppm.

b) Ga$_8$(CH$_2$)$_{12}$@MCM-41$_{500}$ (**H4**) (20 mg, 0.043 mmol of Ga) was suspended in 0.4 mL of THF-d$_8$ in a J. Young-valved tube, benzophenone (7.77 mg, 0.043 mmol) dissolved in 0.3 mL of THF-d$_8$ was then added. After being heated at 80 °C for 16 h, the ^{1}H NMR spectrum was recorded to monitor the formation of 1,1-diphenylethylene. ^{1}H NMR (THF-d$_8$, 400.16 MHz, 26 °C) δ 7.29 (10H, (*H*$_5$C$_6$)$_2$C=CH$_2$), 5.43 (2H, (H$_5$C$_6$)$_2$C=C*H*$_2$) ppm.

Author Contributions

We strongly encourage authors to include author contributions and recommend using CRediT for standardised contribution descriptions. Please refer to our general author guidelines for more information about authorship.

Conflicts of interest

In accordance with our policy on Conflicts of interest please ensure that a conflicts of interest statement is included in your manuscript here. Please note that this statement is required for all submitted manuscripts. If no conflicts exist, please state that "There are no conflicts to declare".

Acknowledgements

Notes and references

‡ Footnotes relating to the main text should appear here. These might include comments relevant not central to the matter under discussion, limited experimental and spectral data, and crystallographic data.

§

§§

1. T. Takeda, *Modern Carbonyl Olefination: Methods and Applications*, *John Wiley & Sons*, 2006.
2. W. A. Herrmann, *Angew. Chem. Int. Ed. Engl*, 1982, **21**, 117-130.
3. Y. Chauvin, *Angew. Chem. Int. Ed.*, 2006, **45**, 3740-3747.
4. R. R. Schrock, *Acc. Chem. Res.*, 1979, **12**, 98-104.
5. N. Calderon, *Acc. Chem. Res.*, 1972, **5**, 127-132.
6.
7. K. Ziegler, K. Nagel and M. Patheiger, *Z. Anorg. Allg. Chem.*, 1955, **282**, 345-351.
8. M. Bonath, C. Maichle-Mössmer, P. Sirsch and R. Anwander, *Angew. Chem. Int. Ed.*, 2019, **58**, 8206-8210.
9. J. D. A. Pelletier and J.-M. Basset, *Acc. Chem. Res.*, 2016, **49**, 664-677.
10. J.-M. Basset, R. Psaro, D. Roberto and R. Ugo, *Modern surface organometallic chemistry*, John Wiley & Sons, 2009.
11. U. Bayer, Y. Liang and R. Anwander, *Inorg. Chem.*, 2020, **59**, 14605-14614.
12. D. R. Radu, C.-Y. Lai, K. Jeftinija, E. W. Rowe, S. Jeftinija and V. S. Y. Lin, *Journal of the American Chemical Society*, 2004, **126**, 13216-13217.
13. M. K. Samantaray, E. Pump, A. Bendjeriou-Sedjerari, V. D'Elia, J. D. A. Pelletier, M. Guidotti, R. Psaro and J.-M. Basset, *Chem. Soc. Rev.*, 2018, **47**, 8403-8437.
14. B. Cornils, W. A. Herrmann, M. Beller and R. Paciello, *Applied homogeneous catalysis with organometallic compounds: a comprehensive handbook in four volumes*, John Wiley & Sons, 2017.
15. Y. Liang and R. Anwander, *Dalton Transactions*, 2013, **42**, 12521-12545.
16. R. Anwander, *Chem. Mater.*, 2001, **13**, 4419-4438.
17. C. R. Bayense, J. H. C. van Hooff, J.W. de Haan, L.J.M. van de Ven and A.P.M. Kentgens, *Catal. Lett.,* 1993, **17**, 349-361.
18. U. Seidel, M. Koch, E. Brunner, B. Staudte and H. Pfeifer, *Microporous Mesoporous Mater.*, 2000, **35-36**, 341-347.
19. M. García-Sánchez, P. C. M. M. Magusin, E. J. M. Hensen, P. C. Thüne, X. Rozanska and R. A. van Santen, *J. Catal.,* 2003, **219**, 352–361.
20. E.J. M. Hensen, M. García-Sánchez, N. Rane, P. C. M. M. Magusin, P.-H. Liu, K.-J. Chao and R. A. van Santen, *Catal. Lett.*, 2005, **101**, 79-85.
21. V. B. Kazansky, I. R. Subbotina, R. A. van Santen and E. J. M. Hensen, *J. Catal.*, 2005, **233**, 351-358.
22. N. Rane, A. R. Overweg, V. B. Kazansky, R. A. van Santen and E. J. M. Hensen, *J. Catal.*, 2006, **239**, 478-485.
23. K. C. Szeto, A. Gallo, S. Hernández-Morejudo, U. Olsbye, A. De Mallmann, F. Lefebvre, R. M. Gauvin, L. Delevoye, S. L. Scott and M. Taoufik, *J. Phys. Chem. C,* 2015, **119**, 26611-26619.
24. Z. A. Taha, E. W. Deguns, S. Chattopadhyay and Susannah L. Scott, *Organometallics*, 2006, **25**, 1891-1899.
25. K. C. Szeto, Z. R. Jones, N. Merle, C. Rios, A. Gallo, F. Le Quemener, L. Delevoye, R. M. Gauvin, S. L. Scott and M. Taoufik, *ACS Catal.* 2018, **8**, 7566-7577.
26. A. Getsoian, U. Das, J. Camacho-Bunquin, G. Zhang, J. R. Gallagher, B. Hu, S. Cheah, J. A. Schaidle, D. A. Ruddy, J. E. Hensley, T. R. Krause, L. A. Curtiss, J. T. Miller and A. S. Hock, *Catal. Sci. Technol.*, 2016, **6**, 6339-6353.
27. a) J. P. Dombrowski, G. R. Johnson, A. T. Bell, T. D. Tilley, Dalton Trans. 2016, 45, 11025-11034; b) K. Searles, G. Siddiqi, O. V. Safonova and C. Copéret, *Chem. Sci.*, 2017, **8**, 2661-2666.
28. G. Spiridopoulos, C. Maichle-Mössmer and R. Anwander, *Chem. - Eur. J.*, 2021.
29. U. Bayer, Y. Liang and R. Anwander, *Inorg. Chem.*, 2020, DOI: 10.1021/acs.inorgchem.0c02502.
30. C.-T. Tsai, Y.-C. Pan, C.-C. Ting, S. Vetrivel, A. S. T. Chiang, G. T. K. Fey and H.-M. Kao, *Chem. Commun.*, 2009, DOI: 10.1039/B909680A, 5018-5020.
31. R. Anwander, I. Nagl, M. Widenmeyer, G. Engelhardt, O. Groeger, C. Palm and T. Röser, *The Journal of Physical Chemistry B*, 2000, **104**, 3532-3544.
32. Y. Liang, E. S. Erichsenb and R. Anwander, *Dalton Trans.*, 2013, **42**, 6922-6935.
33. N. Dettenrieder, H. M. Dietrich, C. Maichle-Mössmer and R. Anwander, *Chemistry – A European Journal*, 2016, **22**, 13189-13200.
34. K. Samedov, Y. Aksu and M. Driess, *ChemPlusChem*, 2012, **77**, 663-674.
35. S. D. Fleischman and S. L. Scott, *Journal of the American Chemical Society*, 2011, **133**, 4847-4855.
36. T. Tao and G. E. Maciel, *Journal of the American Chemical Society*, 2000, **122**, 3118-3126.
37. S. Brunauer, P. H. Emmett and E. Teller, *Journal of the American Chemical Society*, 1938, **60**, 309-319.
38. E. P. Barrett, L. G. Joyner and P. P. Halenda, *Journal of the American Chemical Society*, 1951, **73**, 373-380.
39. R. M. Gauvin, F. Buch, L. Delevoye and S. Harder, *Chemistry – A European Journal*, 2009, **15**, 4382-4393.
40. M. Zimmermann, N. Å. Frøystein, A. Fischbach, P. Sirsch, H. M. Dietrich, K. W. Törnroos, E. Herdtweck and R. Anwander, *Chemistry – A European Journal*, 2007, **13**, 8784-8800.
41. F. Blanc, C. Copéret, J. Thivolle-Cazat, J.-M. Basset, A. Lesage, L. Emsley, A. Sinha and R. R. Schrock, *Angew. Chem. Int. Ed.*, 2006, **45**, 1216-1220.
42. A. Fischbach, M. G. Klimpel, M. Widenmeyer, E. Herdtweck, W. Scherer and R. Anwander, *Angew. Chem. Int. Ed.*, 2004, **43**, 2234-2239.
43. C. J. Carmalt and S. J. King, *Coord. Chem. Rev.*, 2006, **250**, 682-709.
44. C. J. Carmalt, *Coord. Chem. Rev.*, 2001, **223**, 217-264.

Surface Organometallic Chemistry of Gallium Methylene $Ga_8(CH_2)_{12}$ on Mesoporous Silica.

Georgios Spiridopoulos, Yucang Liang and Reiner Anwander*

Institut für Anorganische Chemie, Universität Tübingen, Auf der Morgenstelle 18, 72076 Tübingen, Germany

Table of Contents

SEM images and PXRD patterns of the parent material MSN-MCM-41$_{500}$
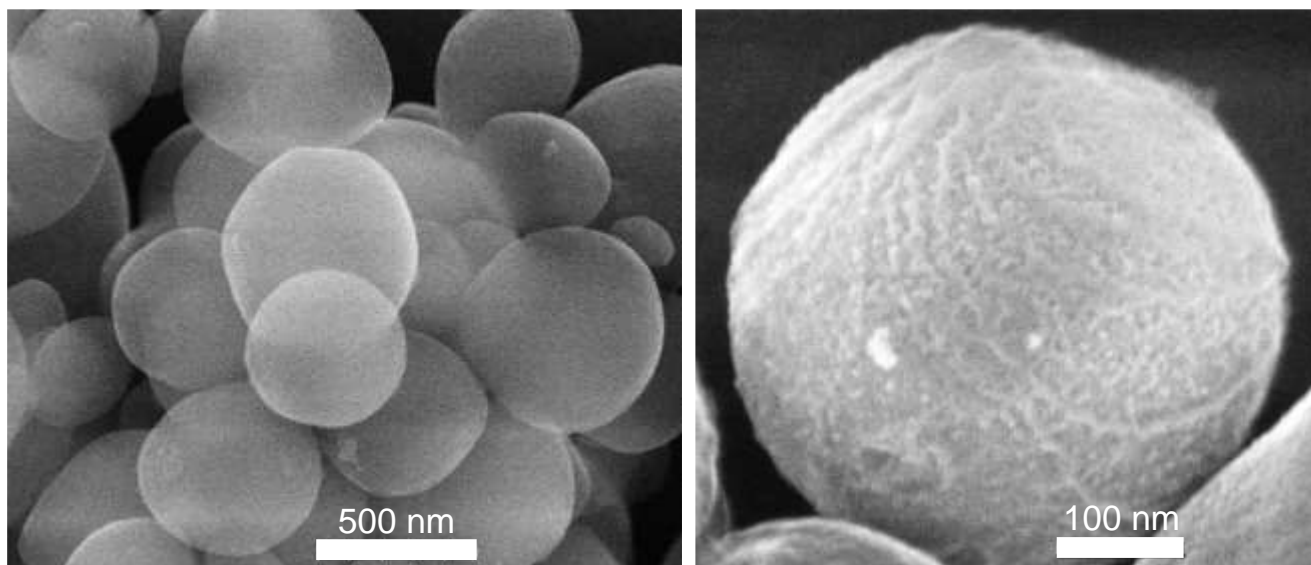
Figure S1. SEM images of MSN-MCM-41$_{500}$.
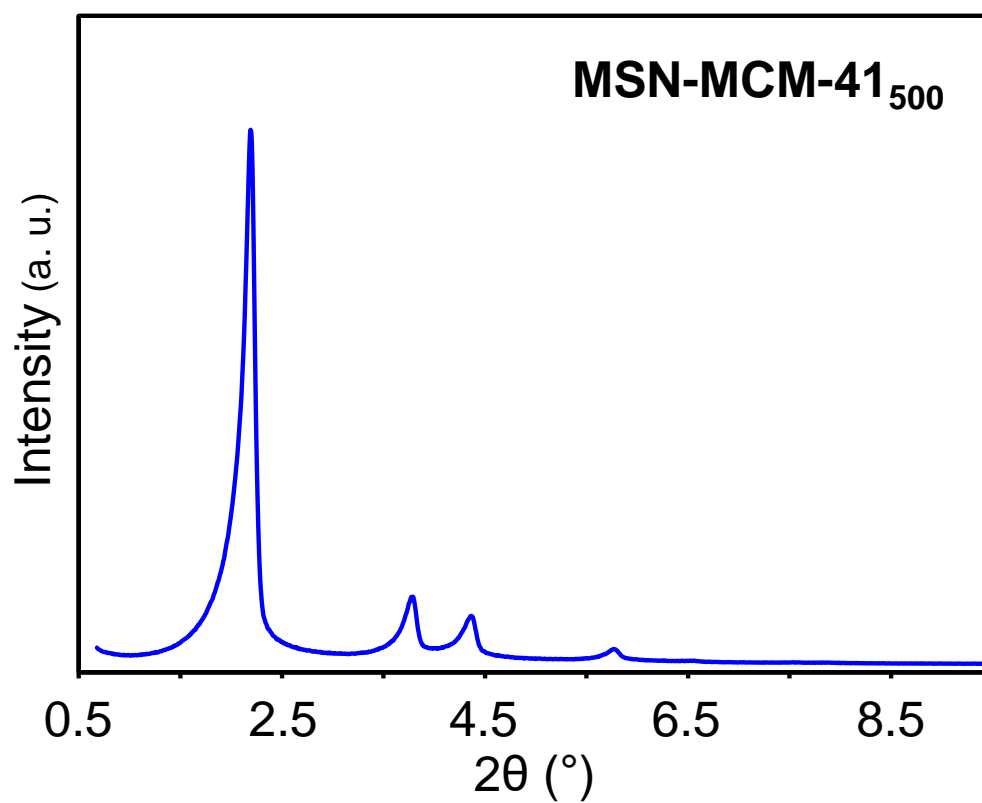
Figure S2. Low-angle PXRD pattern of MSN-MCM-41$_{500}$.

IR data
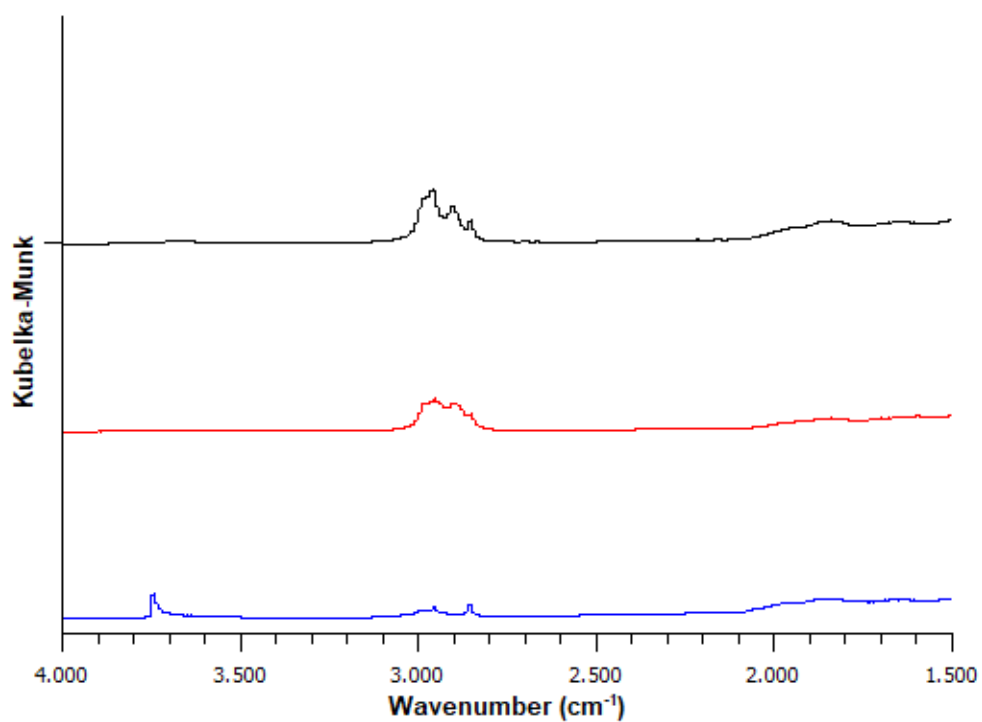
Figure S3. DRIFT spectra of support material MCM-41$_{5000}$ (blue), Ga$_8$(CH$_2$)$_{12}$@MCM-41$_{500}$ (**H4**) (red) and GaMe$_3$@MCM-41$_{500}$ (**H5**) (black) from bottom to top.

NMR Spectra
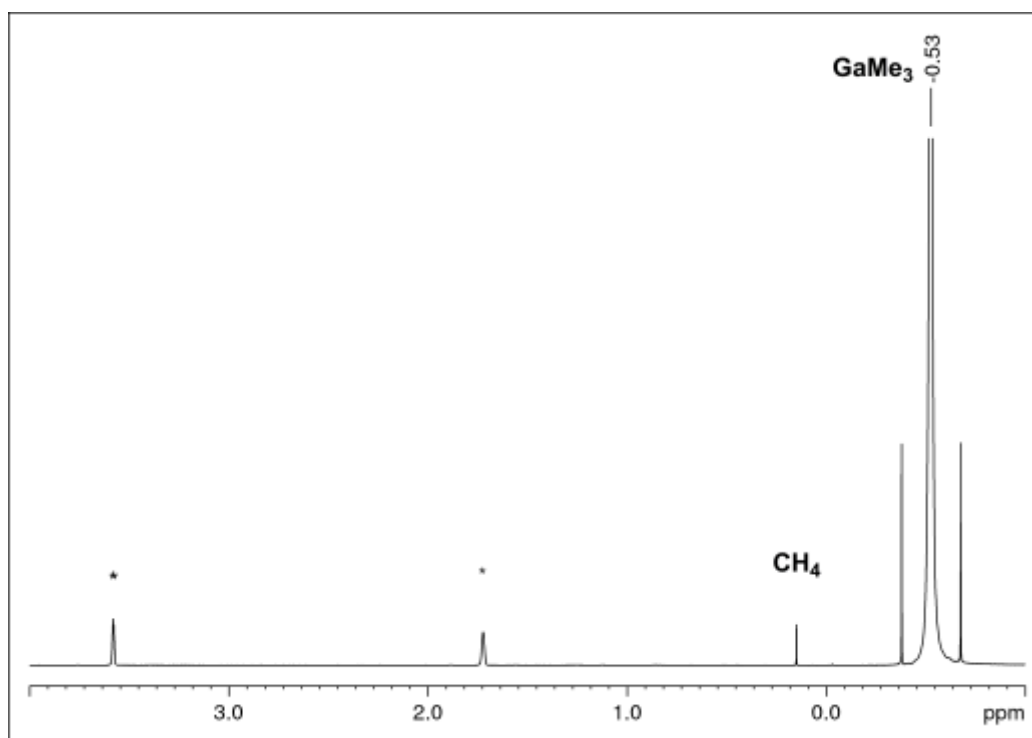
Figure S4. ^{1}H NMR spectrum of the grafting reaction of GaMe$_3$ (**2**) onto mesoporous SBA-15$_{500}$. (**A**).
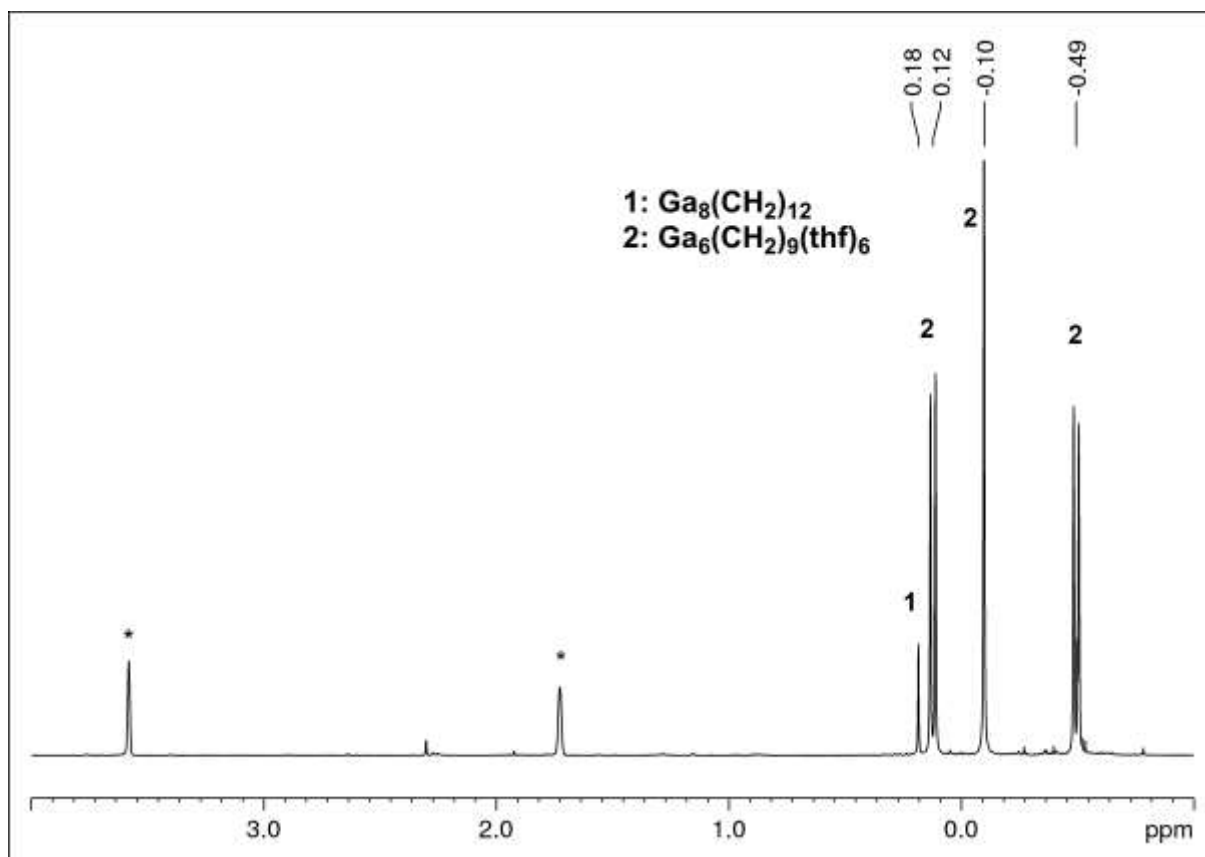
Figure S5. ^{1}H NMR grafting of Ga$_8$(CH$_2$)$_{12}$ onto mesoporous SBA-15$_{500}$ (**B**)
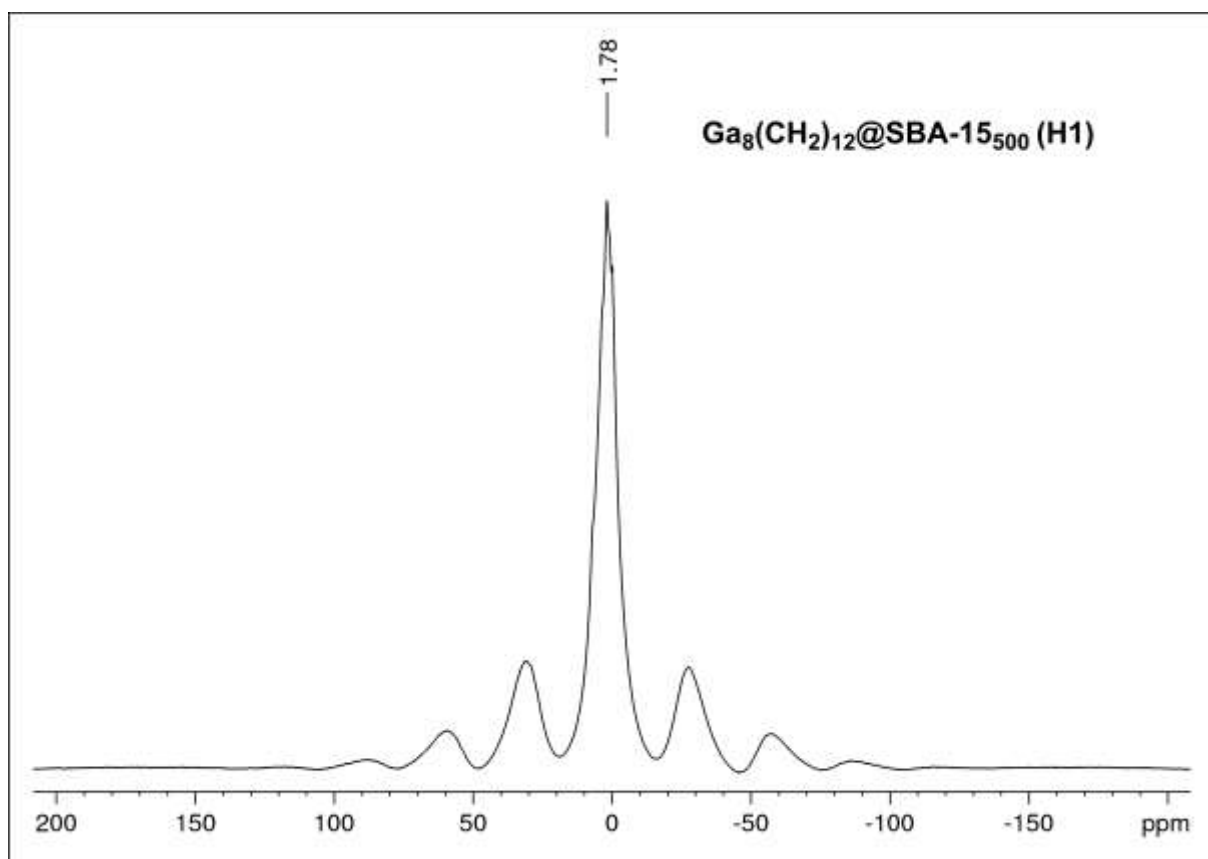
*Figure S6. ^{1}H MAS NMR of hybrid material **H1**.*
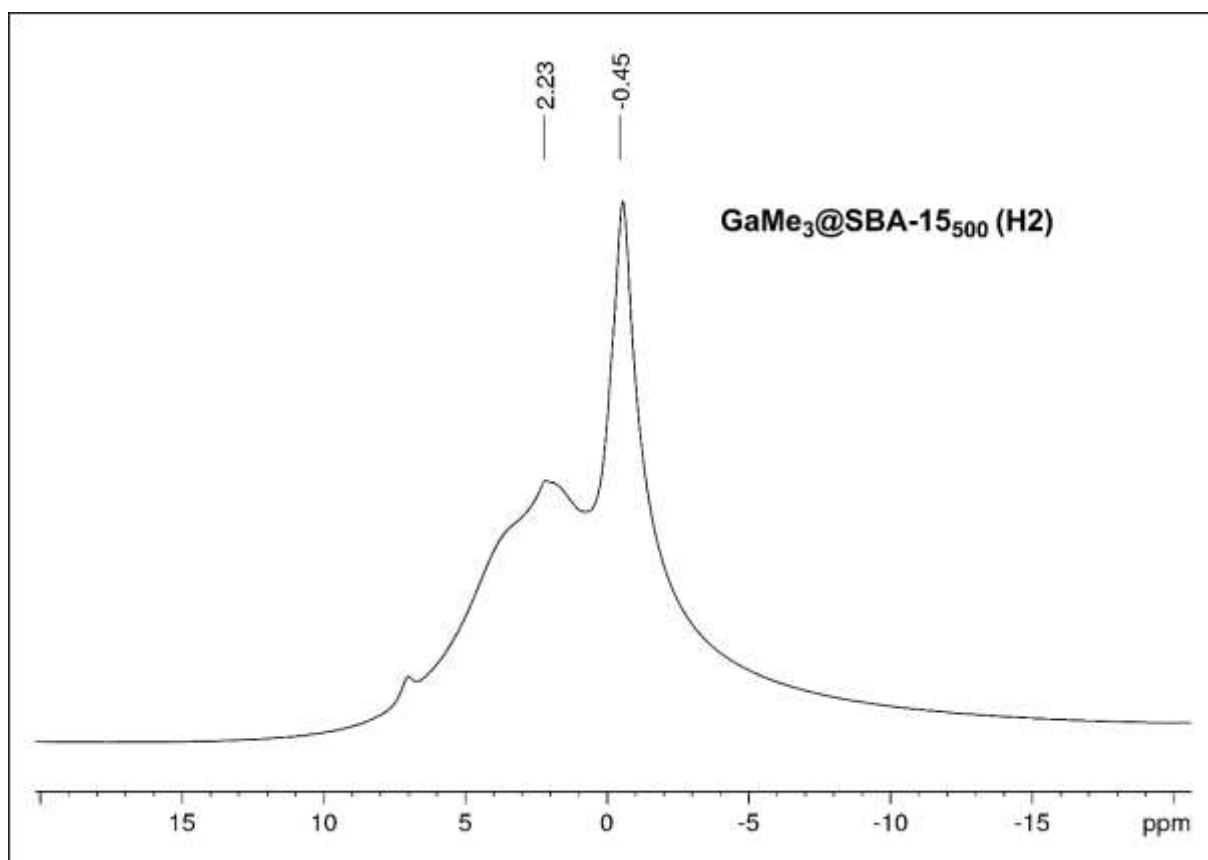
*Figure S7. ^{1}H MAS NMR of hybrid material **H2**.*
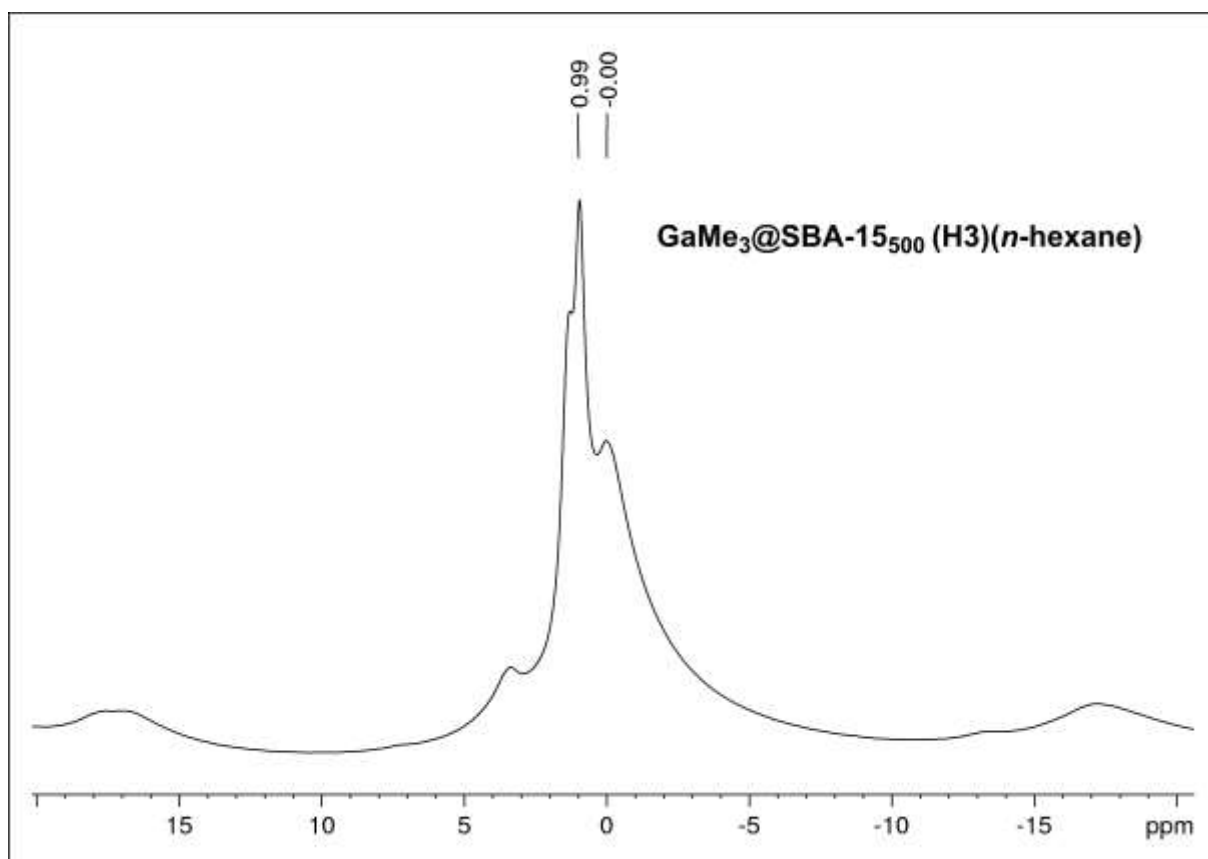
*Figure S8. ¹H MAS NMR of hybrid material **H3**.*
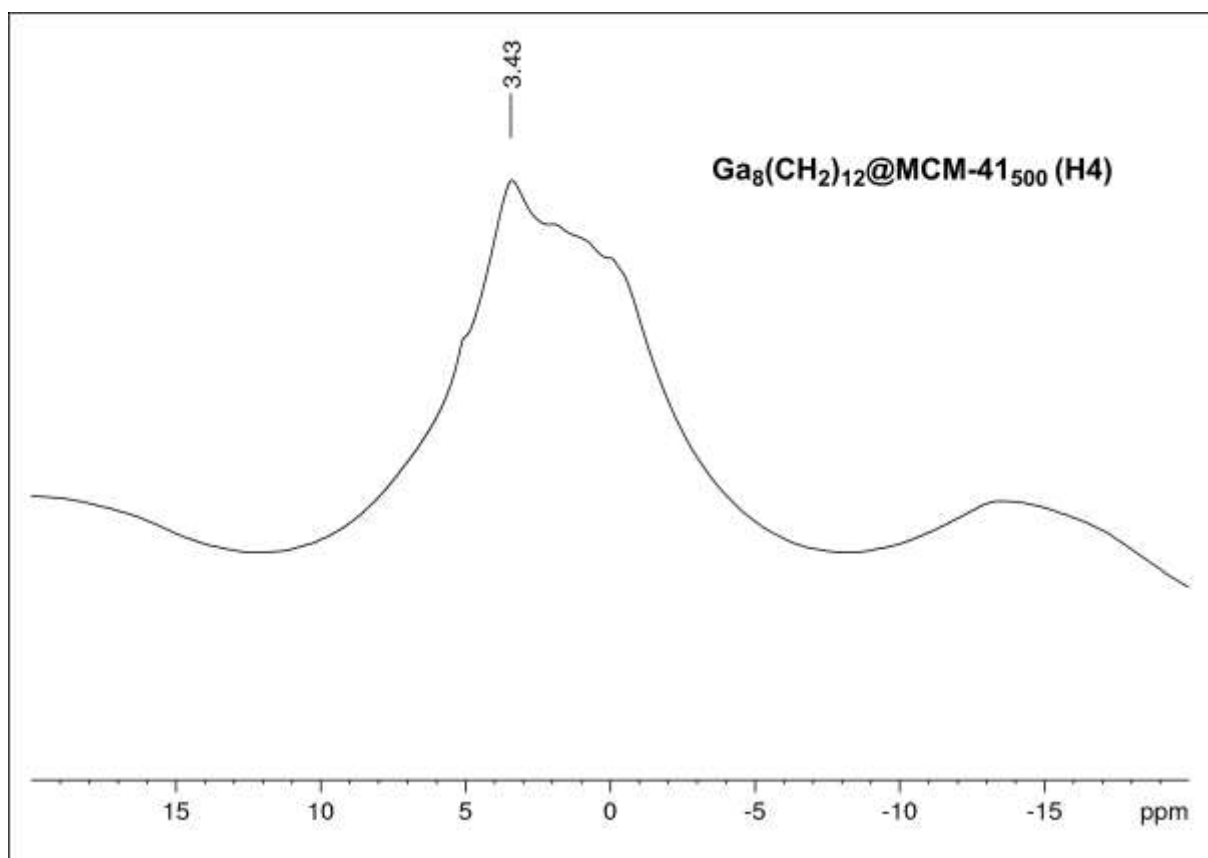
*Figure S9. ¹H MAS NMR of hybrid material **H4**.*
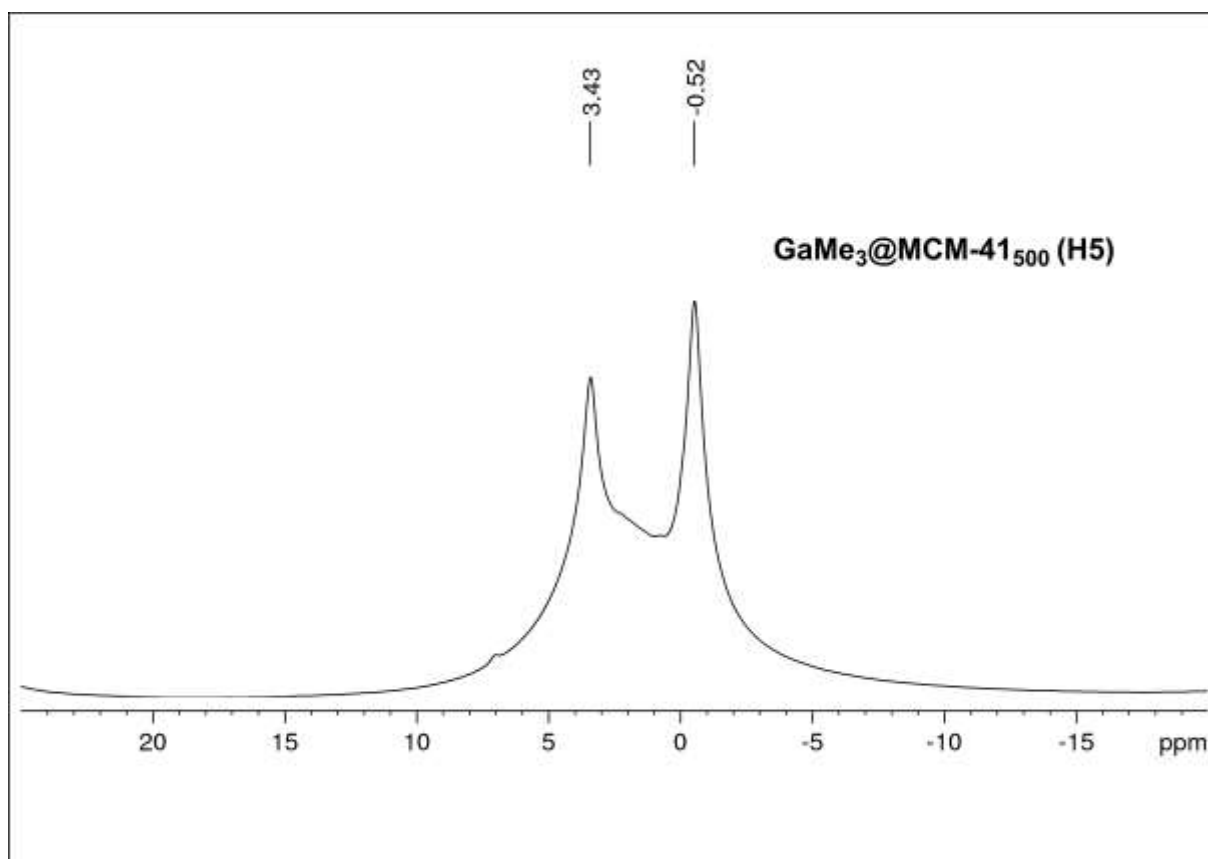
*Figure S10. ^1H MAS NMR of hybrid material **H5**.*
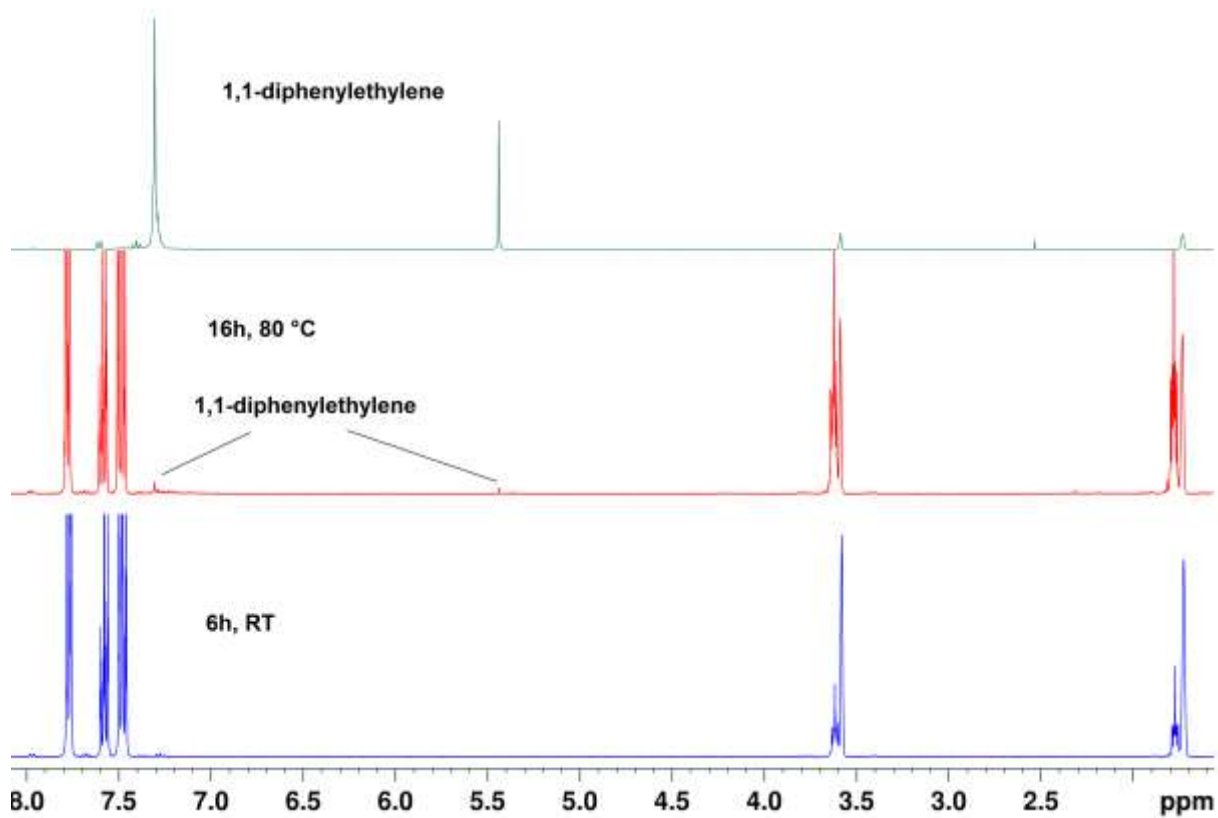
*Figure S11. ^1H NMR of hybrid material **H1** towards benzophenone.*
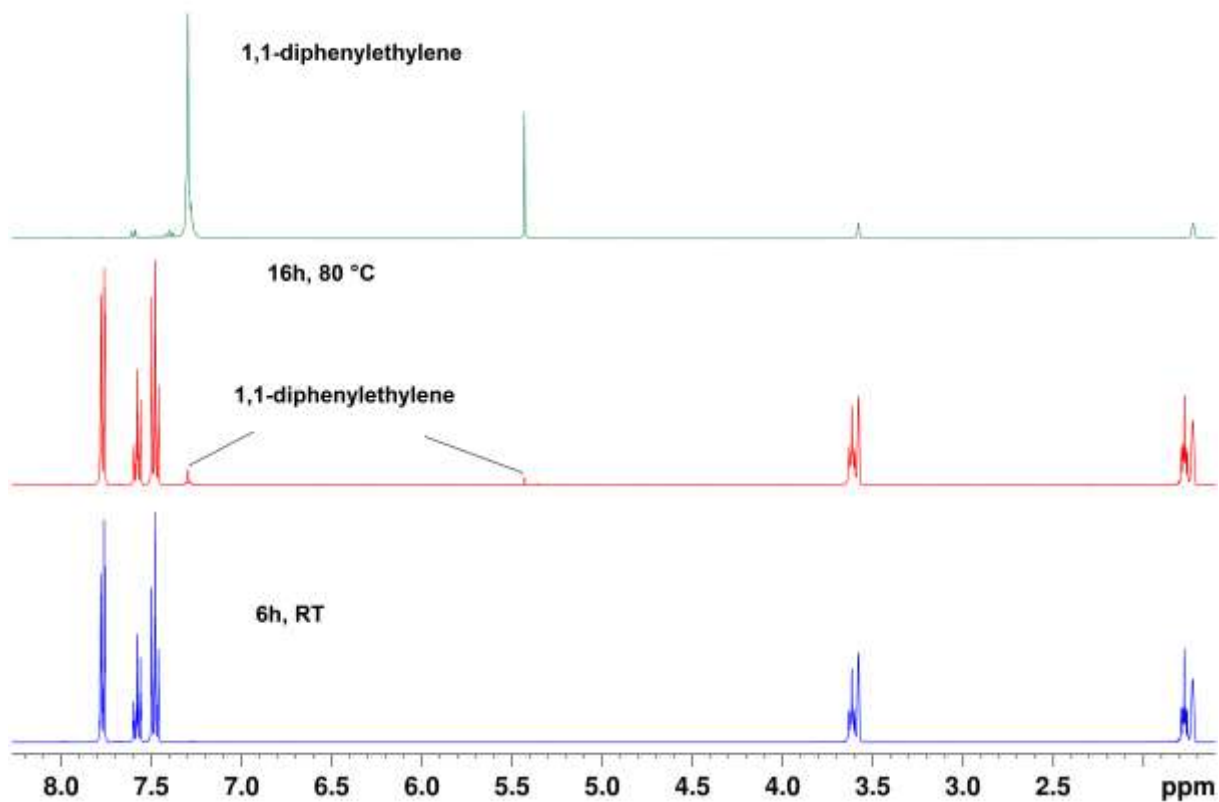
Figure S12. ^1H NMR spectra of hybrid material **H4** towards benzophenone
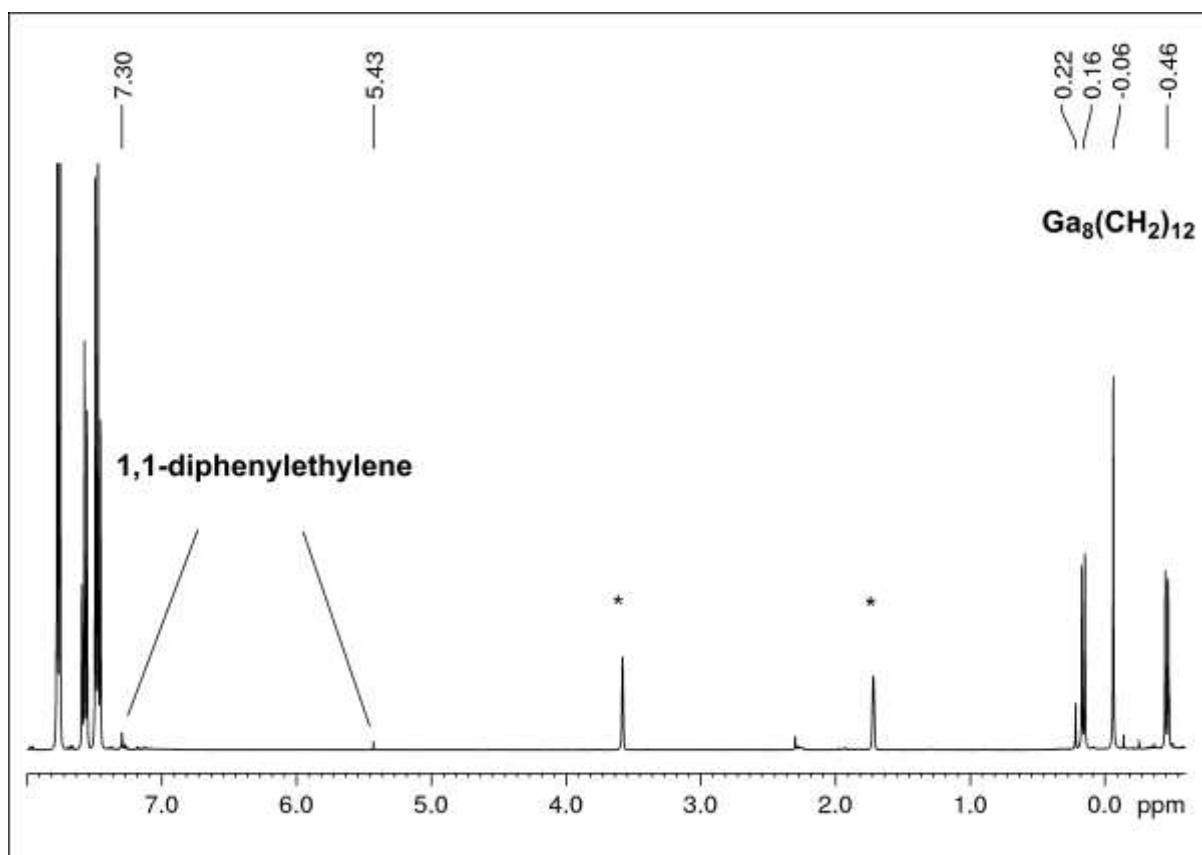
Figure S13. ^1H NMR of molecular $Ga_8(CH_2)_{12}$ with benzophenone (after 16 h at room temperature).
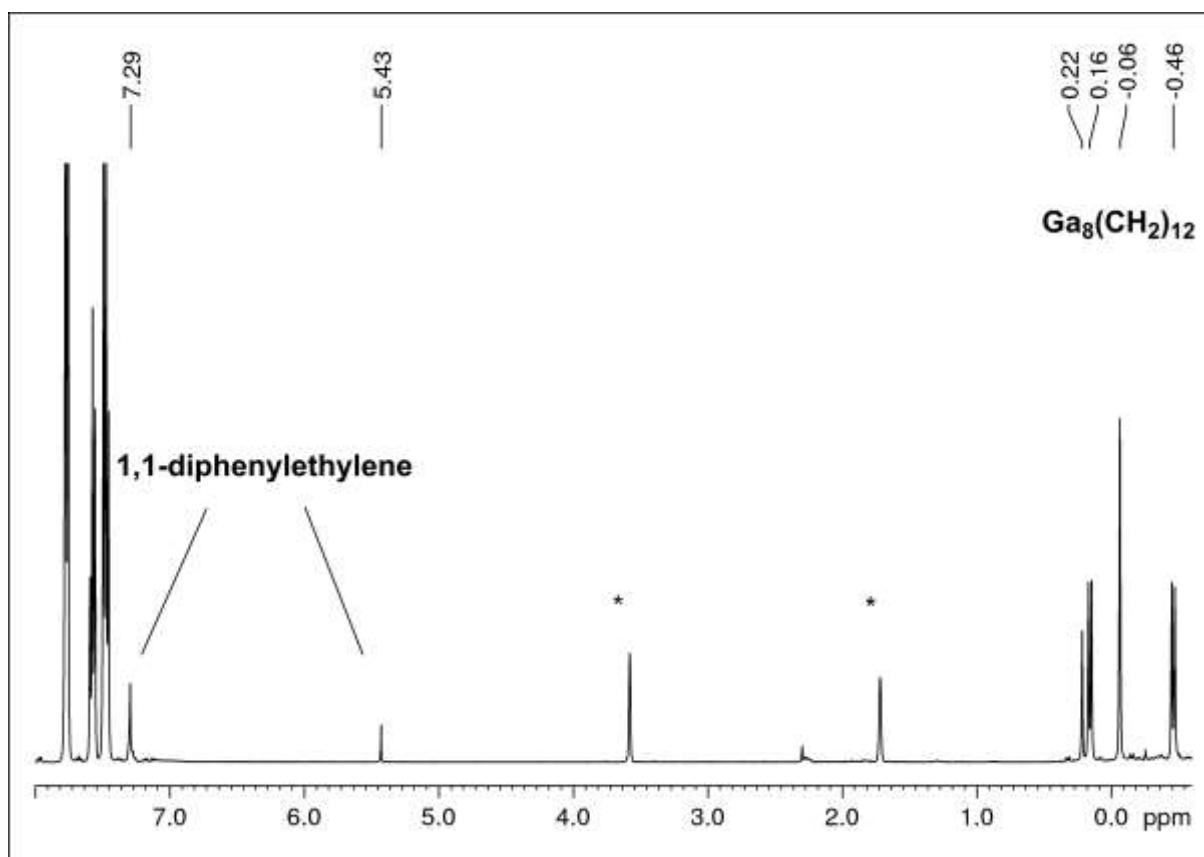
Figure S14. ¹H NMR of molecular Ga₈(CH₂)₁₂ with benzophenone (after 2 h at 60 °C).
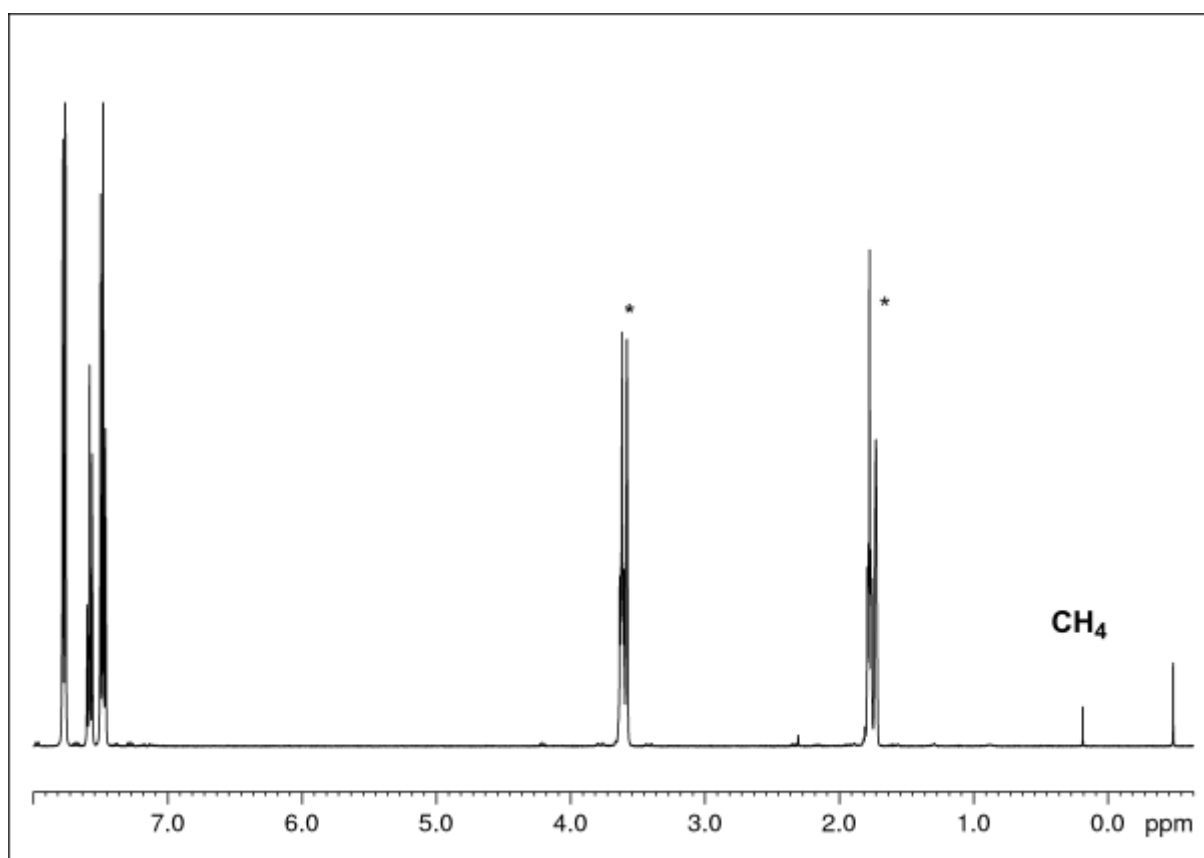
Figure S15. ¹H NMR of hybrid material H2 with benzophenone (21h at 80 °C)
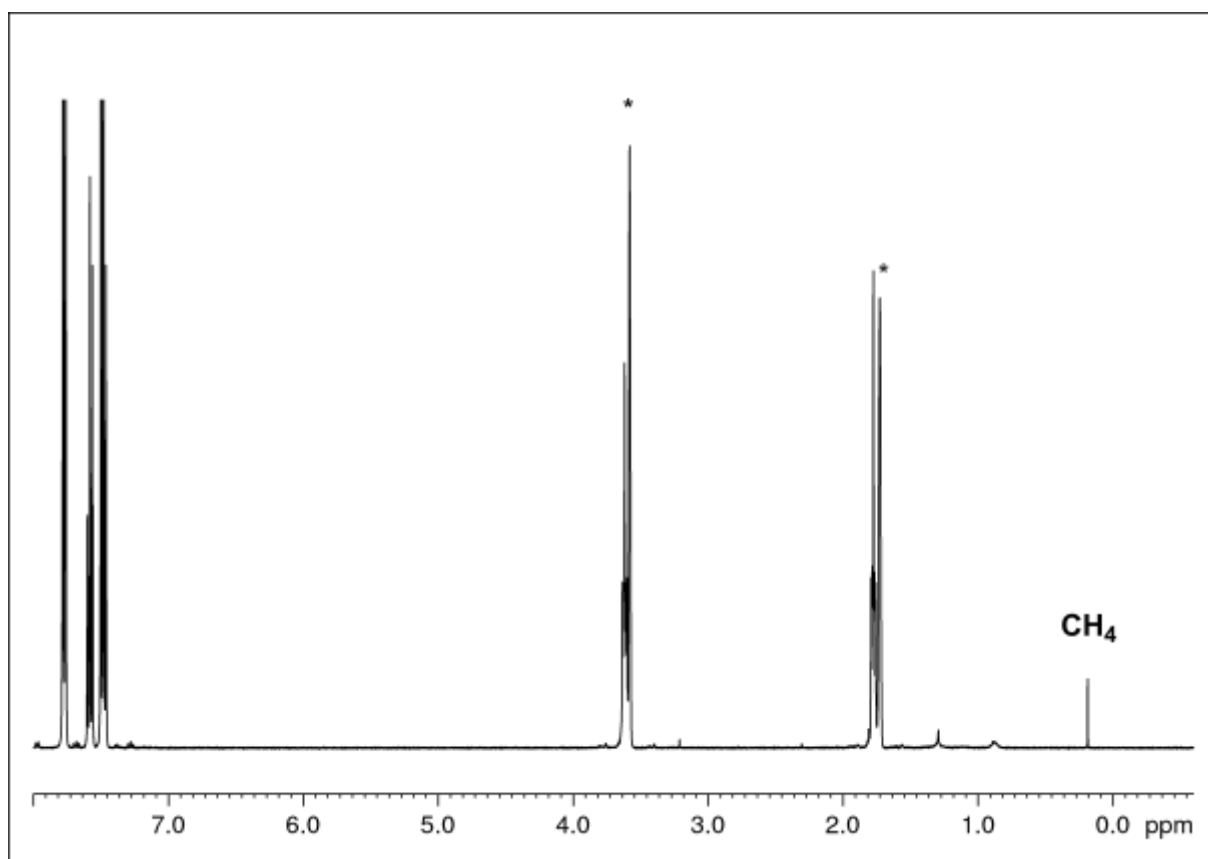
*Figure S16. ^{1}H NMR of hybrid material **H5** with benzophenone (21h at 80 °C)*
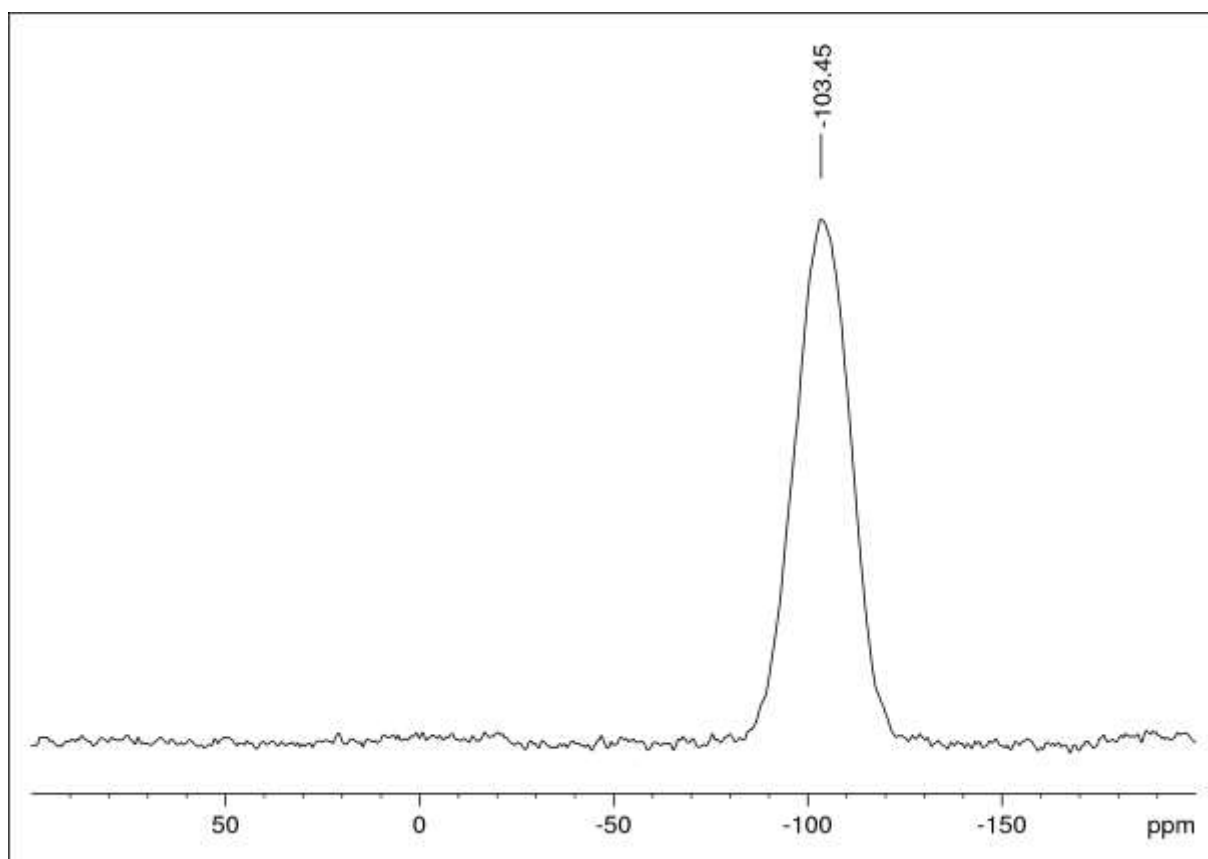
*Figure S17. ^{29}Si NMR of hybrid material **H1**.*
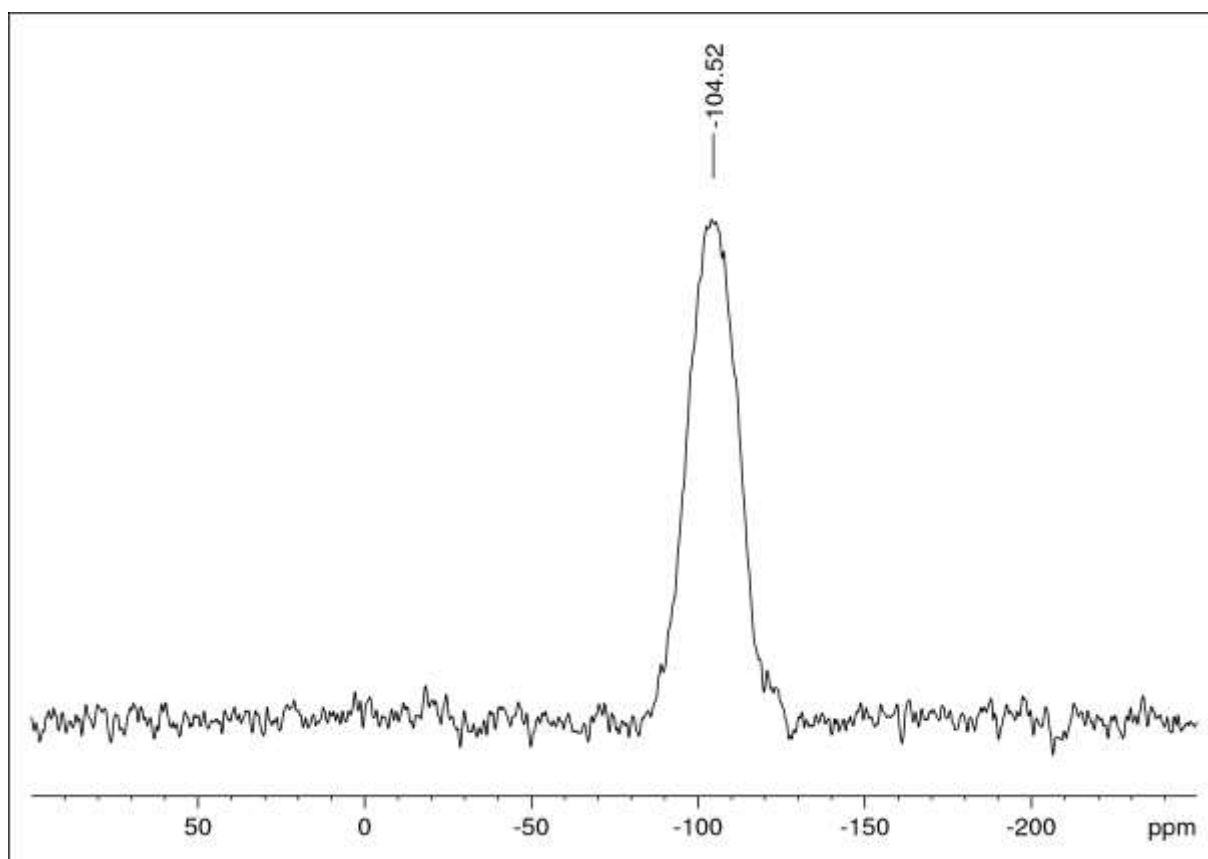
*Figure S18. ²⁹Si NMR of hybrid material **H2**.*
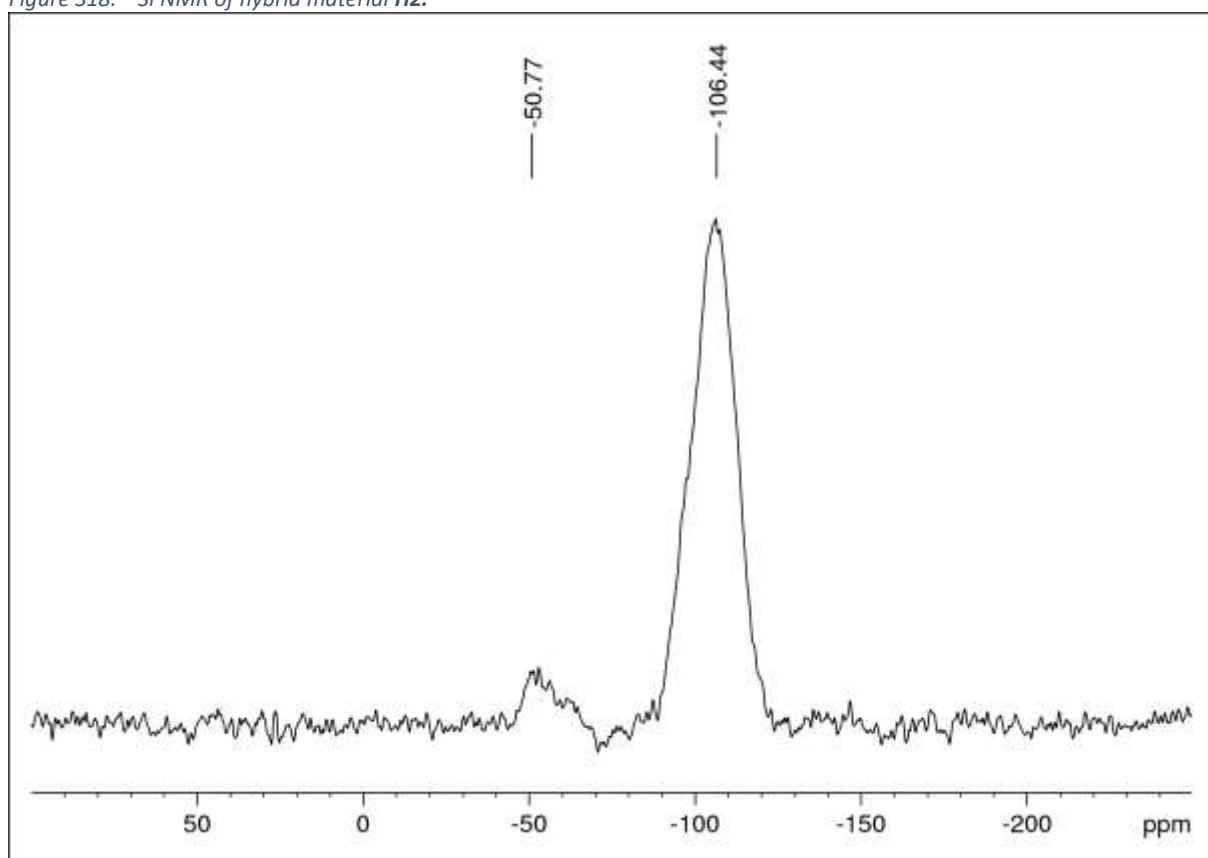
*Figure S19. ²⁹Si NMR of hybrid material **H3**.*
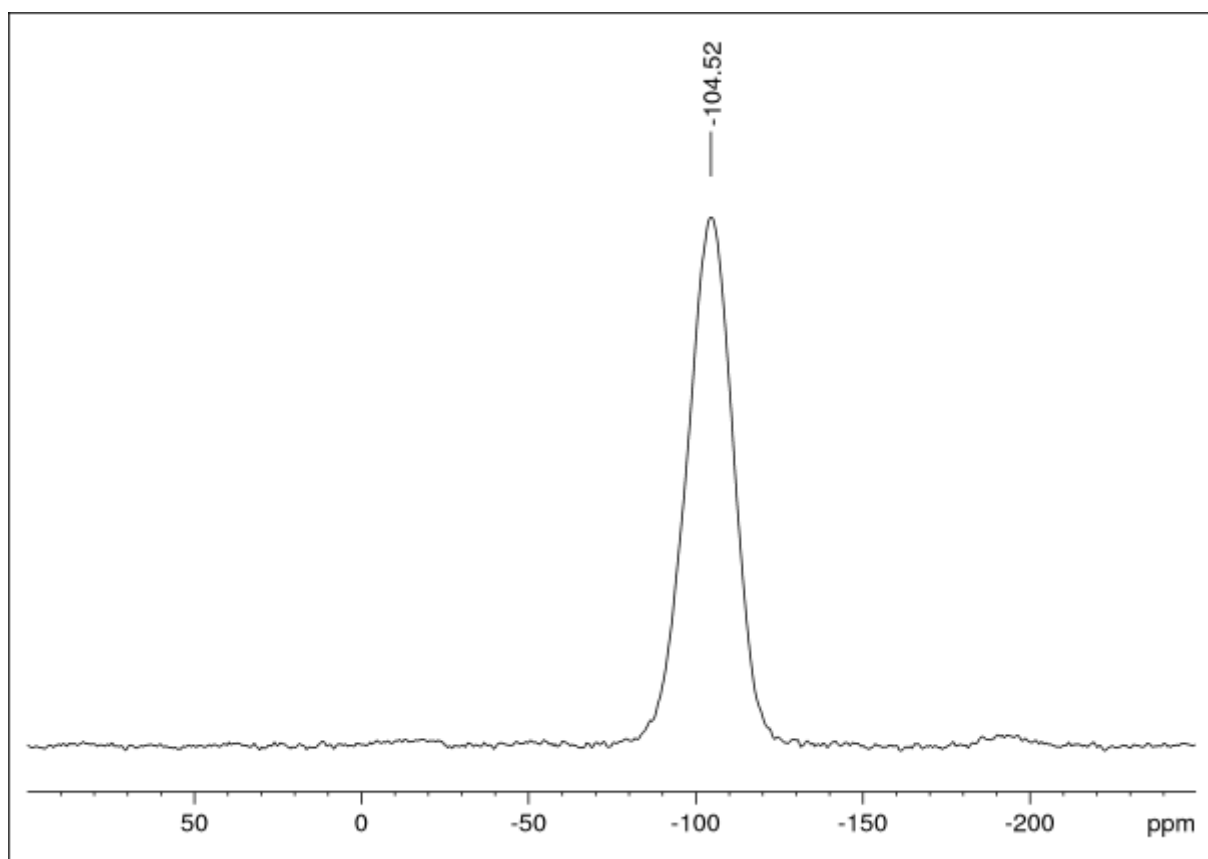
*Figure S20. ^{29}Si NMR of hybrid material **H4**.*
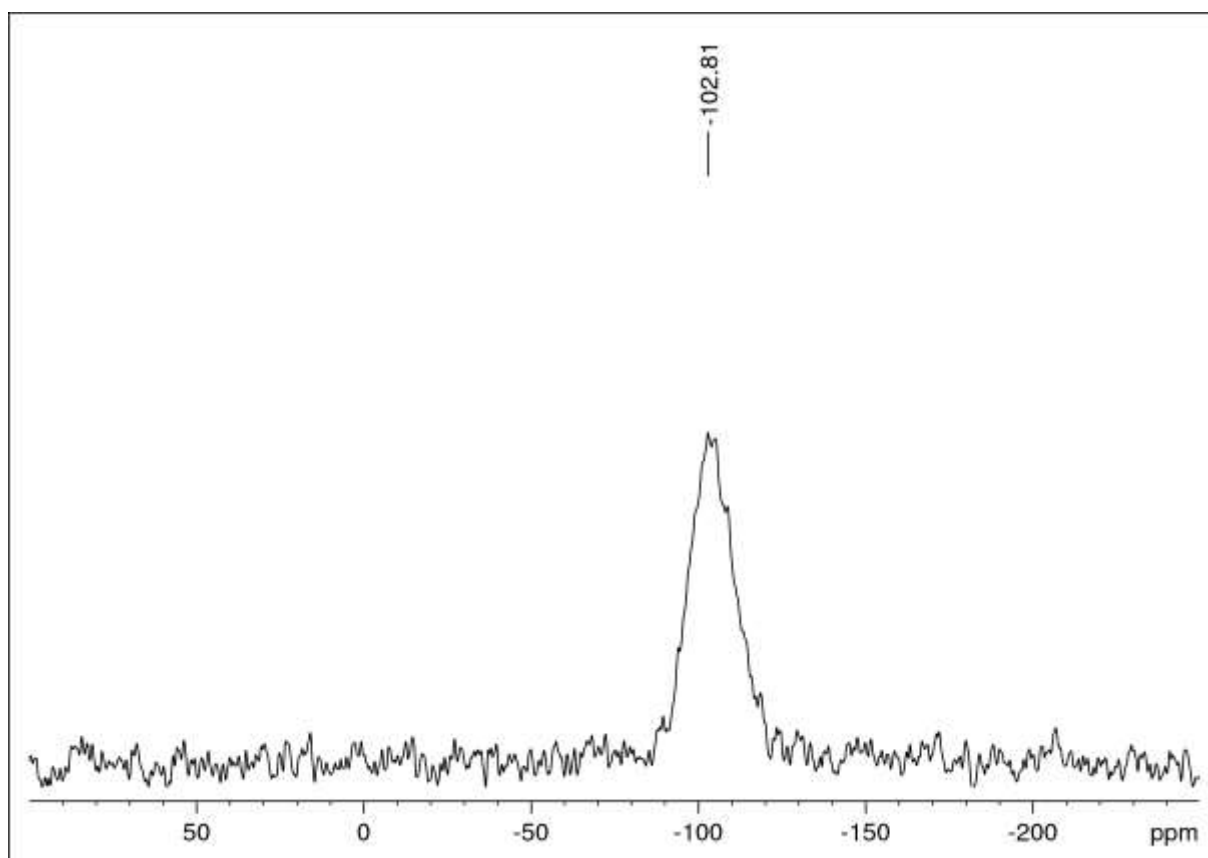
*Figure S21. ^{29}Si NMR of hybrid material **H5**.*